SOLVOTHERMAL LIQUEFACTION OF PEEL AND PULP OF *CITRUS LIMETTA* FRUITS AND ANALYSIS OF PRODUCTS

A Thesis submitted in partial fulfilment

of the requirements for the degree of

DOCTOR OF PHILOSOPHY

by

Sneha Acharya

(Roll No. 186107018)

DEPARTMENT OF CHEMICAL ENGINEERING

INDIAN INSTITUTE OF TECHNOLOGY GUWAHATI

ASSAM – 781039, INDIA

February 2024

Department of Chemical Engineering

Indian Institute of Technology Guwahati

Guwahati, Assam 781039

STATEMENT

I hereby declare that the content embodied in this thesis entitled **"Solvothermal Liquefaction of Peel and Pulp of *Citrus Limetta* Fruits and Analysis of Products"** is the result of investigations and experiments carried out by me at 210L, Non-Newtonian flow laboratory, Department of Chemical Engineering, Indian Institute of Technology Guwahati, India, under the guidance of Prof. Nanda Kishore. In keeping with the general practice of reporting scientific observations, due acknowledgments have been made wherever the work described is based on the findings of other investigators.

February, 2024 Sneha Acharya

Department of Chemical Engineering

Indian Institute of Technology Guwahati

Guwahati, Assam 781039

CERTIFICATE

It is certified that the work contained in this thesis entitled **"Solvothermal Liquefaction of Peel and Pulp of *Citrus Limetta* Fruits and Analysis of Products"** done by **Miss Sneha Acharya** (Roll No. 186107018) has been carried out under my supervision and this work has not been submitted elsewhere for a degree.

February, 2024

Dr. Nanda Kishore

Professor

Department of Chemical Engineering

Indian Institute of Technology Guwahati

Guwahati-781039

Assam, India

ACKNOWLEDGEMENTS

With great honor and deep appreciation, I extend my heartfelt gratitude and sincere thanks to my supervisor, Prof. Nanda Kishore. His invaluable guidance, scientific supervision, critical assessments, constant encouragement, patience and unwavering support have played a pivotal role in the success of this research endeavor

I am deeply indebted to the Chairman of my Doctoral Committee, Prof. Ramagopal V. S. Uppaluri and esteemed members of the Doctoral Committee, Prof. V. Prabu and Prof. N. Selvaraju for their invaluable perspectives and constructive feedback during the research evaluation. I extend my sincere appreciation to Prof. R. Prasanna Venkatesh and Prof. S. K. Majumder for generously sharing their time, expertise and insights during the Annual Progress Seminars, contributing immensely to my research.

I extend my heartfelt gratitude to the esteemed thesis examiners for their invaluable contributions to the evaluation of my thesis. I express sincere thanks to Prof. Phillip E. Savage from Chemical Engineering Department, Penn State University and Prof. Thallada Bhaskar from the Material Resource Efficiency Division, CSIR-Indian Institute of Petroleum, Dehradun. Their meticulous review, insightful comments, and valuable suggestions have significantly enhanced the quality and depth of my research work.

A special acknowledgment goes to Guwahati Biotech Park and the entire technical and office staff of the Department of Chemical Engineering, IIT Guwahati for their assistance.

I would like to thank my present lab mates (Gaffer, Praveen & Ashish), seniors (Dr. H. D Kawale & Dr. Kushagra Agrawal) and past lab mates for fostering a collaborative and conducive research environment. Their shared knowledge and camaraderie have been pivotal in overcoming challenges and achieving milestones.

I am profoundly grateful to my family for their selfless dedication and belief in my aspirations. I am truly fortunate to have such incredible pillars of support in my life. I extend my deepest appreciation to my relatives, friends and well-wishers for their emotional support, encouragement and understanding throughout this challenging journey.

Above all, I feel fortunate to have the blessings of the ***Almighty*** *upon me throughout this academic odyssey.*

Sneha Acharya

ABSTRACT

The contemporary demand for clean and sustainable renewable energy necessitates a shift towards leveraging versatile biomass resources for thermochemical conversion. Citrus fruits, notably sweet lime and scientifically recognized as *Citrus limetta* (CL), are widely consumed, generating substantial waste in the form of peel and pulp post-juice extraction. This dissertation addresses the disposal predicament by focusing on the liquefaction of these fruit wastes. This study employed less severe conditions of temperature (240-280 °C) and pressure (90-130 bar). Methanol, a high-polarity hydrogen-donor solvent, was chosen due to its efficacy in biomass hydrogenation, yielding biocrude and biochar with properties akin to traditional fossil fuels. Varying the biomass-to-solvent ratio resulted in a 12.5 wt. % biocrude yield from *Citrus limetta* peel at 240 °C, showcasing an increase compared to similar citrus fruit wastes. The generated biocrude boasted a notable energy density of 26.76 MJ kg^{-1} at a constant temperature of 260 °C and a 1:4 biomass-to-solvent ratio. GC-MS analysis revealed a higher area percentage of phenol derivatives in the biocrude, indicating the decomposition of the thermally stable lignin biopolymer during liquefaction. Co-liquefaction of *Citrus limetta* peel and pulp co-feed exhibited synergy, enhancing the biocrude yield to 13.47 wt. % at 240 °C and a 1:2 biomass-to-solvent ratio. The rise in temperature during co-liquefaction yielded a maximum higher heating value (HHV) of 27.6 MJ kg^{-1} at 280 °C, surpassing single feed liquefaction. GC-MS and proton nuclear magnetic resonance (^{1}H NMR) results confirmed a biocrude rich in aromatics, alkanes and aliphatics. Biochar energy densities in the range of 14.45 MJ kg^{-1} to 20.62 MJ kg^{-1} suggested its application as a source for thermochemical conversion. Additionally, Brunauer Emmett Teller (BET) results underscored the porous nature of solid biochar and its utility as low-cost adsorbents in soil remediation and catalysts for thermochemical conversion. Finally, in evaluating biocrude energy density, *Citrus limetta* pulp demonstrated higher efficiency than the peel under conditions of 280 °C and a biomass-to-solvent ratio of 1:4. In situations where separating pulp and peel would be impractical, co-liquefaction of *Citrus limetta* peel and pulp could possibly be recommended for optimal biofuel production.

CONTENTS

List of Figures

List of Tables

CHAPTER 1

INTRODUCTION

1.1 Background

Fruit processing sector boasts significant market potential owing to the high content of antioxidants, vitamins and polyphenols found in fruit products. Consequently, these industries generate substantial quantities of fruit peel, pomace and seed wastes. The Government of India's Agricultural statistics for 2021-22, based on the 3rd Advance Estimates, reported a total fruit production of 107.24 million tons in the country [1]. Citrus stands as one of the most crucial fruit crops globally, flourishing in tropical, subtropical and diverse climates to yield over 100 million tons annually [2]. Recognized for their nutritional richness, energy density and health benefits, citrus fruits are extensively utilized in the food industry, particularly for producing fresh juices and citrus-flavoured beverages [3]. The burgeoning consumer demand has led to a continuous rise in citrus production, resulting in substantial fruit waste annually, comprising peels, pulp and seeds, with peel waste constituting more than half of the wet fruit mass. Citrus pomace, the residual material from fruit processing, is a treasure trove of bioactive compounds like dietary fiber, carbohydrates, phenolic compounds, polysaccharides, phytochemicals, natural antioxidants and various other health-beneficial nutrients. Unfortunately, the vast amount of citrus pomace generated poses ecological challenges often being underutilized either as animal feed or discarded without proper processing [4]. In the global effort to combat food losses and waste, citrus fruit waste emerges as a sustainable solution for biorefinery, offering economic and industrial potential. Rich in essential oils, ascorbic acid, sugars, carotenoids, flavonoids, polyphenols and trace elements, citrus waste can be biologically converted into fuels and chemicals, such as bioethanol. These components find applications in pharmaceuticals, cosmetics, food supplements and as bio-sorbents [5]. Maximizing the reuse of by-products during citrus production is a central challenge for juice factories aiming to establish environment-friendly processes that recover and recycle value-added compounds from citrus waste. The incorporation of citrus by-products into a circular economy framework positions them as an excellent source of nutrients with sustainability at its core [6]. Evaluating these wastes opens avenues for their suitable utilization, thereby adding value to citrus processing waste and benefiting both the environment and industries.

1.2 Fossil fuels vs Renewable energy

Globalization and urbanization have taken a toll on our conventional sources of energy generation leading to their scarcity in contemporary times. The demand for fossil fuels and its derivatives have witnessed a rapid growth in the present times as energy has become an inseparable part of the daily life of human beings [7]. However, the depletion of fossil fuel reserves is a pressing global concern that has far-reaching implications for our energy security, environmental sustainability and economic stability. Fossil fuels, including coal, oil and natural gas have been the primary sources of energy for several decades, powering industries, transportation and households worldwide. However, their extraction and consumption have outpaced the natural replenishment rates, leading to a decline in accessible reserves. The extraction of fossil fuels from the Earth's crust is an inherently finite process, and as reserves are depleted, the remaining resources become more difficult and costlier to extract. This depletion not only poses challenges in meeting the growing energy demands of a rapidly urbanizing and globalized world but also contributes to environmental issues, such as climate change and air pollution [8]. The existing fuel technologies primarily in the transportation sector are mainly responsible for the greenhouse effect and global warming due to their harmful gaseous emissions. Moreover, rapid surging in the price of fossil fuel crude, gasoline, kerosene, naptha etc. has taken a toll on our economy and the growth of our country. So, the development of an energy efficient and economical fuel production process is necessary. With this comes the dire necessity to accelerate the transition to sustainable and renewable energy sources, improve energy efficiency and explore innovative technologies to reduce our dependence on finite fossil fuel reserves and mitigate their detrimental impacts on our planet. Renewable energy sources play a pivotal role in shifting towards an energy system that is more sustainable and characterized by reduced carbon emissions [9,10].

According to a report published by the International Energy Agency (IEA) the expansion of renewable capacity in the coming five years is anticipated to surpass previous expectations significantly. They have projected to grow by approximately 2400 GW from 2022 to 2027. This growth is equivalent to the total installed power capacity of China at present. It signifies an 85% acceleration compared to the previous five years and nearly 30% higher than the forecast provided in previous year's report. This revision represents a most substantial upward adjustment till date. During this forecast period, renewable energy sources have been projected to contribute to more than 90% of the global expansion in electricity

capacity. The significant upward revision in these projections can be attributed primarily to China, the European Union, the United States and India. These countries have been successful in implementing existing policies, regulatory measures and market reforms and they have also introduced new initiatives at a faster pace than anticipated, thereby responding to the energy crisis at hand [11]. At present, bioenergy represents approximately $1/10^{th}$ of the global total primary energy supply. Modern bioenergy plays a significant role as a renewable energy source, with its contribution to higher final energy demand across all sectors surpassing that of wind and solar PV combined by almost five times, even when excluding the traditional use of biomass. In recent times, there has been rapid growth in bioenergy utilization for electricity generation and transport biofuels, largely driven by increased policy support. Nevertheless, the heating sector continues to be the primary beneficiary of bioenergy, representing the largest share of its utilization. Biomass serves as a renewable energy resource obtained from various plant and algae-based materials. This diverse range of biomass sources encompasses crop wastes, such as agricultural residues left after harvesting, forest residues derived from forestry operations, purpose-grown grasses cultivated specifically for energy production, woody energy crops like fast growing trees or shrubs, microalgae that are rich in energy content, urban wood waste from construction or demolition activities and even food waste that can be repurposed for energy generation [12]. These biomass feedstocks provide a sustainable and abundant supply of organic matter which can be harnessed for a wide array of applications in the renewable energy sector. Biomass also demonstrates its versatility as a renewable energy source through its ability to be transformed into liquid transportation fuels that are commonly known as biofuels and are comparable to conventional fossil-based fuels like gasoline, jet fuel and diesel [13]. The advancements in bioenergy technologies facilitate the conversion of carbon present in biomass and waste streams into low-emission fuels suitable for various modes of transportation. Additionally, these technologies enable the production of bioproducts and renewable power, making biomass a valuable resource for multiple sustainable energy applications [14].

1.3 Biomass-a renewable energy resource

The increasing global population has led to a concerning surge in global energy demands. As a result, biomass has gained significant attention as an energy resource, with encouragement for its production in the form of energy crops. The potential for global energy generation from

virgin biomass is vast. It has been estimated that the carbon content of standing terrestrial biomass, which can be sustainably harvested and utilized as an energy resource, is approximately 100 times higher than the world's total annual energy consumption. The primary step in the growth of virgin biomass involves the capture of solar energy through photosynthesis, where carbon dioxide (CO_2) is transformed into organic compounds. This process enables the conversion of solar energy into fixed carbon within the biomass [15]. With few exceptions, the order of abundance of the major organic components in whole-plant samples of terrestrial biomass is celluloses, hemicelluloses, lignins and proteins. Alpha-cellulose, commonly referred to as cellulose, serves as the primary structural element and a major constituent in various biomass species. In trees, it typically accounts for approximately 40 to 50% of the dry weight. The lipid and protein fractions in plant biomass are generally present in lower percentages compared to the carbohydrate components. Lipids tend to have the lowest concentration, while proteins exhibit a slightly higher but still lower percentage than carbohydrates. The sulfur content in virgin and waste biomass can vary from very low levels to around 1% for primary biosolids [16]. The utilization of traditional biomass is favoured not only due to its abundant annual production and wide availability but also because of its carbon-neutral nature. This is due to the absorption of CO_2 by biomass during growth and its subsequent release into the atmosphere during combustion, resulting in a net-zero balance of CO_2 emissions. Fast-growing biomass exemplifies a renewable energy resource, particularly relevant given the ongoing crisis stemming from the excessive and unsustainable use of fossil fuels. The use of biomass as a biofuel has emerged as a prominent area of research in the scientific community, offering a means to mitigate forest fires by facilitating periodic cleaning of forest lands for biofuel production [17]. The heating value of biomass holds significant importance in biofuel studies, as biomass is utilized as a substitute for energy and fuel. The solid biomass exhibits a higher heating value (HHV) typically ranging from 15.6 to 20 MJ kg^{-1}, depending on the specific species. The carbon content of biomass plays a crucial role in determining its energy value, with higher carbon content indicating greater energy potential. In fact, the energy value of biomass is primarily derived from the chemical bonds within its organic components, which include carbon, hydrogen, oxygen and to a lesser extent nitrogen and sulfur. Carbon, being a key element, plays a fundamental role in determining the energy potential of biomass. When biomass is combusted or undergoes various thermochemical conversion processes to produce heat or biofuels, the energy released is a

result of breaking the chemical bonds between the atoms in the organic molecules. Carbon-carbon and carbon-hydrogen bonds contain significant energy. The higher the carbon content in the biomass, the more of these high-energy bonds are available for breaking, resulting in a greater release of energy during the combustion or conversion process. Furthermore, biomass with lower levels of oxygenation tends to possess a higher heating value, resembling characteristics of hydrocarbon fuels [18].

1.4 Biomass conversion pathways for energy generation

There have been several instances of direct utilization of biomass as a fuel or their conversion to liquid or gaseous fuels by use as feedstocks in various industries [19]. The conversion pathways of biomass for development of end products to be used as fuels have been illustrated in Figure 2.2.1 [20]. The biochemical conversion takes place by three processes viz. enzymatic hydrolysis, anaerobic digestion and fermentation [21]. Anaerobic digestion involves breaking down of the feedstock by micro-organisms to release heat along with CH_4, CO_2 and H_2S gases. This process requires a long time under particular hydrogen gas conditions. However, the accidental presence of certain anti-microbial compounds might lead to disturbances in digestion process. Therefore, it is essential to maintain the reactor fluid at constant circulation along with its temperature and pH [22]. The lignocellulosic biomass on being subjected to enzymatic hydrolysis get converted to sugars that is fermented and distilled to form cellulosic ethanol. The conversion pathway holds the advantage of being operated at low processing temperature with generation of highly selective products. However, their time-consuming pre-processing stages, processing duration etc. are the major setbacks associated with them [23]. Macroalgae *L. digitata* was reported to be used by Adams et al. [24] for ethanol fermentation and anaerobic digestion to produce CH_4. Biochemical conversion was used by Seabra et al. [25] for ethanol production and power generation from sugarcane bagasse in Brazil. Their motive being curbing down greenhouse gas (GHG) emissions by utilization of an environment-friendly fuel option. The physicochemical conversion of biomass involves extracting oils from diverse sources like sunflower, palm, hemp, flax, canola, rice bran, soybean, mustard, rapeseed and waste vegetable oils. These oils, known for their high viscosity, face limitations for direct use in diesel engines due to the presence of free fatty acids. An effective solution is to convert these feedstocks into biodiesel using catalyzed reactions like esterification or transesterification, yielding methyl ester and demonstrating pollution reduction benefits. The transesterification process involves the combination of

alcohol, catalyst and purification of methyl ester through steps like alcohol removal, glycerine neutralization and water washing [26].

Thermochemical conversion is a process that involves the transformation of biomass or other organic materials through the application of heat in the presence of limited or no oxygen. This process results in the production of various valuable products, including heat, biofuels and chemicals. Thermochemical conversion includes pyrolysis, combustion, hydrothermal processing and gasification. The direct burning of biomass in boilers to generate heat and power is referred to as combustion. Pyrolysis takes place at high temperature in oxygen devoid environment to decompose the biomass in order to form liquid, solid and gaseous products.

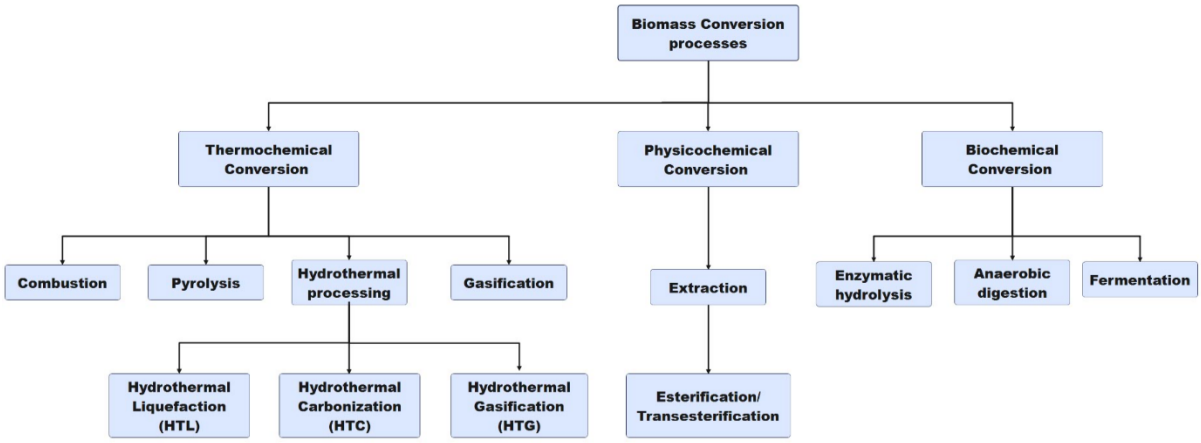

Figure 2.2.1 Classification of biomass conversion pathways [20].

Hydrothermal processing is the process of thermochemically converting wet biomass to solid and liquid products. On the basis of different temperature and pressure conditions they are cited as hydrothermal carbonization (HTC), hydrothermal liquefaction (HTL) and hydrothermal gasification (HTG) [27]. In thermochemical treatment of biomass, the nature of the reaction is completely chemical due to which the productivity is relatively higher. This type of reaction is completed in very less time with complete utilization of the biomass or waste. The products are also highly valuable and can be fractionated into several useful by-products. In fact, the basic aim behind the use of this conversion method for production of biofuel is development of hydrocarbon fuels from them rather than using them directly for energy supply [23]. The thermochemical methods of conversion of biomass are the most important as they do not require any feedstock pre-treatment unlike biochemical conversion

where lignin is removed from the lignocellulosic matrix by various pre-treatment techniques and thereby subjected to hydrolysis to produce sugars [23]. Thermochemical conversion can be classified into following types:

1.4.1 Combustion

This is a process, involving the rapid oxidation of biomass in the presence of oxygen to release heat energy. In the course of combustion, the carbon and hydrogen present in woody biomass undergo a reaction with oxygen, resulting in the formation of carbon dioxide and water vapor, accompanied by the release of heat [28]. Providing a precisely balanced chemical equation for the combustion of wood is challenging due to its composition being a mixture of various components. However, Demirbas et al. [29] proposed the following Equation 1.4.1 as a summarization of the process, where $C_{42}H_{60}O_{28}$ represents a generalized formula for woody biomass:

$$C_{42}H_{60}O_{28} + 43O_2 \rightarrow 42CO_2 + 30H_2O \quad (1.4.1)$$

The heat can be used directly for space heating, electricity generation or other industrial processes. For effective and complete combustion, it is necessary to achieve temperatures in the range of 800 to 1000 °C. Additionally, efficient mixing must occur within the combustion zone to guarantee the complete burnout of all combustion products. While combustion is generally adaptable to various biomass types, the efficiency of the process and the extent of biomass pre-processing needed are influenced by biomass quality, scale and technology employed. The properties of biomass that most impact combustion can be categorized as physical, chemical or thermal factors. Physical factors encompass feedstock density, porosity and internal surface area. Chemical factors involve parameters like higher heating value (HHV), elemental content and heating values related to pyrolysis and char. Lastly, thermal properties affecting combustion include specific heat, thermal conductivity and the influence of water content on emissivity, which is the relative ability of a surface to emit energy through radiation [30]. But, it is necessary that moisture content of feedstock be <50% for successful biomass combustion [31]. Thus, high moisture content biomass should be dried beforehand for an efficient combustion process. It also releases major environmental pollutants such as CH_4, CO along with NO_x and SO_x into the atmosphere when co-combusted with coal [32].

1.4.2 Gasification

It is the process of biomass conversion at high temperature (more than 700 °C) through partial oxidation and at atmospheric pressures [14]. The partial oxidation is carried out in existence of a gasification medium (such as steam, air, oxygen, CO_2 or a mixture of these compounds) to form a fuel gas called producer gas or syngas (comprising of CO_2, CO, CH_4, H_2 and N_2 in varying quantities). The gasification of solid fuel occurs within an air-sealed, enclosed chamber, maintained at a slight suction or pressure relative to ambient pressure. This gasification process involves four distinct stages as the fuel undergoes its transformation: (1) fuel drying, (2) combustion, (3) pyrolysis and (4) reduction. Biomass fuels typically contain moisture in the range of 5 to 35%. At temperatures exceeding 100 °C, the water is eliminated to dry the fuel and convert it into steam. In the combustion zone, the combustible elements of solid fuel are primarily carbon, hydrogen and oxygen. In complete combustion, carbon produces CO_2, while hydrogen yields water, often in the form of steam as depicted in Equations 1.4.2 and 1.4.3 respectively [33]. The combustion reaction is exothermic, resulting in a theoretical oxidation temperature of 1450 °C. The primary reactions involved are as follows [34].

$$C+O_2=CO_2 \quad (+393\ MJ/kmol) \tag{1.4.2}$$

$$2H_2+O_2=2H_2O\ (-242\ MJ/kmol) \tag{1.4.3}$$

The pyrolysis zone is where wood pyrolysis occurs, representing a complex process that remains incompletely understood. Below the temperature of 100 °C, only water is expelled. Within the range of 200–280 °C, there is the release of CO_2, acetic acid and water. The actual pyrolysis, unfolding between 280–500 °C, results in the generation of substantial amounts of tar and gases containing CO_2. In addition to light tars, there is also the formation of methyl alcohol. Between 500–700 °C, gas production is minimal and comprises hydrogen [34]. The primary pyrolysis reactions are outlined as follows in Equations 1.4.4 and 1.4.5 [35]:

$$C_6H_{10}O_5 \rightarrow C_xH_z + CO \quad (<0\ MJ/kmol) \tag{1.4.4}$$

$$C_6H_{10}O_5 \rightarrow C_nH_mO_y \quad (<0\ MJ/kmol) \tag{1.4.5}$$

In the reduction zone, several high temperature chemical reactions occur in the absence of oxygen. Assuming a gasification process employing biomass as a feedstock, the initial phase involves the thermochemical decomposition of lignocellulosic compounds, resulting in the

production of char and volatiles. The primary gasification reactions unfolding in the reduction zone have been outlined below in Equations 1.4.6, 1.4.7, 1.4.8 & 1.4.9 [36]:

$$\text{Boudouard reaction: } CO_2 + C = 2CO \quad (-172.6 \text{ MJ/kmol}) \tag{1.4.6}$$

$$\text{Water-gas reaction: } C + H_2O = CO + H_2 \quad (-131.4 \text{ MJ/kmol}) \tag{1.4.7}$$

$$\text{Water shift reaction: } CO_2 + H_2 = CO + H_2O \ (+41.2 \text{ MJ/kmol}) \tag{1.4.8}$$

$$\text{Methane production reaction: } C + 2H_2 = CH_4 \quad (+75 \text{ MJ/kmol}) \tag{1.4.9}$$

The principal reduction reactions, namely the Boudouard reaction and water-gas reaction, are endothermic processes with the capacity to lower gas temperature. Consequently, temperatures in the reduction zone typically range from 800 to 1000 °C. It is worth noting that a lower temperature in the reduction zone (below 700 °C) corresponds to a reduced calorific value of the gas [34]. The generated producer gas has a low-to-medium heating value and finds applications in industries for electricity and heat generation as well as in fuels and chemicals production [23].

1.4.3 Pyrolysis

In pyrolysis, biomass is decomposed thermally without oxygen (O_2). It occurs at moderate temperature (400-800 °C) and generates bio-oil, biochar and gases including syngas (CH_4, H_2, CO_2 and CO). The pyrolysis of biomass is a highly intricate process owing to the diversity, heterogeneity, and limited thermal stability of its components. The properties of feedstock applicable to pyrolysis depends on the composition of hemicellulose, cellulose, lignin, extractives and other inorganic materials. Despite synergistic effects, the pyrolysis of biomass generally produces products in line with the individual pyrolysis of its three constituent components. The analysis of these individual components serves as the foundation for predicting reaction pathways and identifying primary and secondary reactions. The sequence of these reactions, their rates and the resulting yields are influenced by factors like heating rate, temperature, pre-treatment, catalytic effects and more [37]. When the heating rate of pyrolysis is relatively slow, temperatures below 450 °C primarily produce biochar, while higher temperatures exceeding 800 °C, especially with rapid heating rates, result in the predominant formation of gases. At approximately 500 °C and with brief reaction times, the liquid product becomes the dominant output [28]. The residence time during pyrolysis also

effects the conversion of the solid product while vapour residence time determines its composition [38].

Cellulose, represented as $(C_6H_{12}O_5)_n$, constitutes the primary element of plant cell walls, featuring an arrangement of anhydroglucose units linked by glycoside bonds. Among all lignocellulosic components, the thermal decomposition of cellulose has been extensively investigated and is well-understood. The widely accepted Waterloo mechanism [39] delineates the reaction pathway, elucidating the expected products and outlining the influence of temperature and heating rate. Three primary competitive reactions are (i) fragmentation into hydroxyacetaldehyde, other carbonyls, acids and alcohols (ii) depolymerization into levoglucosan and other primary anhydrosugars and (iii) dehydration into char, gases and water. Dehydration prevails at lower temperatures (<350 °C) and slow heating rates. At higher temperatures, depolymerization and fragmentation take precedence. Depolymerization dominates between 300 and 450 °C, while fragmentation peaks around 600 °C. Nevertheless, inorganic species such as cations, bases, acids and salts can significantly influence these reactions [40]. The selectivity of cellulose for fragmentation and depolymerization can reach as high as 70–80 wt. % [41]. Hemicellulose serves to bind the cellulose microfibrils within the cell wall, exhibiting structural and compositional variation (predominantly xylan) and possessing lower thermal stability. Its decomposition mirrors that of cellulose: dehydration at lower temperatures (<280 °C) and depolymerization at elevated temperatures [42]. Dehydration results in anhydride fragments, water-soluble acids, char, gases and water, while depolymerization yields volatile organics, levoglucosan, other anhydrohexoses, levoglucosenone and furans [43]. Similar to cellulose, inorganic impurities induce fragmentation effects, with xylan being notably sensitive to cations due to its ion exchange sites. Lignin, the reinforcing element of the cell wall, primarily exists in woody biomass. It constitutes a polymer of hydroxy and methoxy substituted propyl phenol units [44]. The intricate structure varies among plant species, leading to diverse pyrolysis products (catechols, vanillins, aromatic carbohydrates). Dehydration prevails at lower temperatures (<500 °C), while higher temperatures foster the formation of a range of lignin monomers. Beyond 700 °C, these monomers undergo decomposition and enter the vapor phase. Lignin exhibits greater thermal stability than cellulose and hemicellulose, yielding more char and a higher proportion of aromatic compounds. In a pyrolysis reactor, biomass experiences the entire temperature spectrum and consequently, all the aforementioned reactions occur to some extent, influenced

by the heating rate of the biomass particle as a whole, as well as heat transfer and particle diameter [40].

Secondary reactions may transpire in the vapor phase or between the vapor and solid phases, predominantly forming gases. This often leads to a notable reduction in the desired oil yield [45]. Two pivotal secondary reactions in pyrolysis are cracking (>700 °C) and the water–gas shift reaction (<810 °C): $H_2O+CO \rightarrow H_2+CO_2$. However, these secondary reactions are constrained at temperatures below 650 °C, with residence times less than 2 sec for gases and vapors, particularly when char is promptly separated. These conditions align with the operational parameters in commercial pyrolysis. The overarching pyrolysis mechanism for biomass primarily hinges on cellulose pyrolysis, with similar outcomes observed for wood and other biomass species [39].

1.4.4 Hydrothermal processing

A lot of research has been conducted in this field; however, it has been reported that hydrothermal processing is advantageous in majority of aspects to pyrolysis. They are the most advantageous and promising technologies for production of renewables in a reaction medium such as water as well as other organic solvents. Wet biomass with more than 70 wt. % of moisture content can be directly fed to hydrothermal processing reactor without taking into account any pre-drying process at the expense of energy [27]. It has garnered attention as a potential route for converting various organic feedstocks including biomass, algae and organic waste into valuable products. Its ability to operate with wet feedstocks and its potential for producing biofuels and biochemicals align with the goals of sustainable resource utilization and waste reduction. Plant chemicals like resins, oils, phenolic compounds and phytosterols with significant value are extracted during the hydrothermal process at around 100 °C. When the temperature is increased to 200 °C under a 2 MPa pressure, biomass undergoes decomposition, yielding cellulose and hemicellulose decomposition products like furfural or 5-hydroxymethylfurfural. The next stage, occurring at 300–350 °C and under 12–18 MPa pressure, results in a bio-oil, which is a precursor to biofuel and a nonaqueous soluble organic phase. Finally, at 600–650 °C and under 30 MPa pressure, a gas product rich in methane is produced [46]. The chemical processes in hydrothermal processing are greatly affected by water as they are mostly chemical reactions in water. At the critical point (critical temperature, T_c = 373 °C and critical pressure, P_c = 22.1 MPa), vapour pressure curve of water

separating vapour and liquid phase ends. So, beyond this point water can undergo a change in its properties without any subsequent transition of phases [47]. Peterson et al. [48] in their research provided an overview of different hydrothermal processing techniques with reference to pressure vs temperature phase diagram of water as depicted in Fig 2.2.2. It is worth noting that hydrogen-donating solvents like alcohol, decalin and tetralin, in addition to subcritical and supercritical water, can be employed for biomass conversion. These hydrothermal techniques fall under the categories of carbonization, gasification and liquefaction [49]. Hydrothermal carbonization (HTC) is a thermochemical conversion process that transforms wet biomass or organic materials into a carbon-rich product known as hydrochar, through exposure to high temperatures and pressures in the presence of water. This process mimics the natural carbonization process that occurs over geological timescales, but it is accelerated to take place within hours to several days. Hydrothermal carbonization (HTC) requires a low temperature (≤200 °C) and saturated pressure (2-10 MPa) [50]. It is referred to as hydrous or wet pyrolysis under autogenous temperature and pressure conditions in subcritical water to undergo carbonization of biomass. It involves reducing the oxygen and hydrogen contents (expressed as O/C and H/C atomic ratios) through dehydration and decarboxylation. This process aims to enhance the carbon content of biomass, thereby increasing its calorific value [51]. The HTC process demonstrates the capability to generate nano and micro-sized carbon particles exhibiting diverse properties, including high energy value, chemical stability and thermal stability. The mechanism of hydrothermal carbonization encompasses hydrolysis, dehydration, decarboxylation, aromatization and condensation polymerization [52].

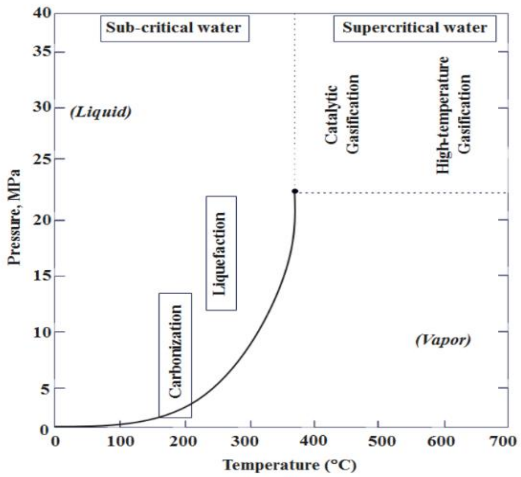

Figure 2.2.2. An overview of different hydrothermal processing techniques with reference to pressure vs temperature phase diagram of water [48].

Hydrothermal liquefaction (HTL) is a transformative process that harnesses heat and pressure to convert wet biomass or organic materials into liquid products. It occurs at around 200 and 370 °C temperature with 4-30 MPa pressure, just adequate for water to remain in the subcritical state (in liquid form). This unique environment triggers chemical reactions that cause the biomass to break down into its molecular components. As a result, we get liquid products known as "biocrude" or "bio-oil." These liquids are energy-dense and contain a mixture of useful organic compounds [53]. In the hydrothermal liquefaction process, both biomass and oxygen undergo rapid oxidation or mineralization, resulting in the formation of CO_2 or H_2O. Simultaneously, potentially harmful combustion by-products like NO_x are transformed into benign substances within the hydrothermal environment. At around 100 °C, water-soluble components dissolve, allowing for extraction. Hydrolysis takes place above 150 °C, leading to the decomposition of polymers such as cellulose and hemicellulose into oligomers and/or monomers. When subjected to approximately 200 °C and 1 MPa pressure, the biomass transforms into a sludge. The reactions occurring during hydrothermal liquefaction involve the hydrolysis and/or decomposition of larger biomass molecules into smaller ones [54]. Given that most resulting molecules are inherently unstable and reactive, they may undergo recombination with larger molecules. Additionally, a significant portion of the oxygen in the biomass is eliminated through dehydration or decarboxylation. This liquid output from liquefaction can then be used in multiple ways such as refining to produce renewable liquid fuels, such as substitutes for diesel or gasoline. These fuels have the advantage of being derived from renewable sources, reducing our reliance on fossil fuels [55]. This can be part of our efforts to sequester carbon by locking it into the liquid products, rather than letting it escape into the atmosphere as CO_2. The process of gasification proves to be a highly efficient thermochemical technique for converting biomass into gas products, including carbon monoxide (CO), hydrogen (H_2), carbon dioxide (CO_2), and methane (CH_4) [48]. Typically conducted within a temperature range of 400 to 700 °C, gasification aims to yield high amounts of methane or hydrogen. Under subcritical conditions (temperature: 225–265 °C, pressure: 2.9–5.6 MPa), facilitated by catalyst use, gasification becomes feasible [56]. Hydrothermal gasification (HTG) enables the nearly complete gasification of wet biomass without the need for pre-drying. The heating value of the resulting gas product is contingent upon the specific reaction conditions employed. HTG can be categorized into three primary regions based on temperature and pressure: Region 1 involves catalytic gasification (275–550

°C), region 2 entails supercritical gasification (374–700 °C) and region 3 encompasses high-temperature gasification (550–700 °C) [48].

1.5 Reaction mechanism of liquefaction

The reaction pathway of hydrothermal liquefaction has been depicted in Fig. 2.2.3 [53]. Biomass is a mixture of various composites like carbohydrates, lignin, proteins and lipids, their mechanisms and chemistry of reactions is also quite complex. HTL process comprises of three major steps which are depolymerization, decomposition and recombination that have been discussed in details in the following sub sections. Liquefaction decomposes and depolymerizes the biomass to highly reactive monomeric compounds which need to be further polymerized to liquid biocrude, gas and solid compounds. The long chain polymers comprising of structural entities such as hydrogen, oxygen and carbon are altered to hydrocarbons (short chain) by means of temperature and pressure changes during HTL processing. Water as a solvent causes recycling of the energy contents of the organic materials of biomass viz. cellulose, hemicellulose and lignin. The biopolymers of these organic materials help in development of the thermal stability of the biocrude and other products of this process [53].

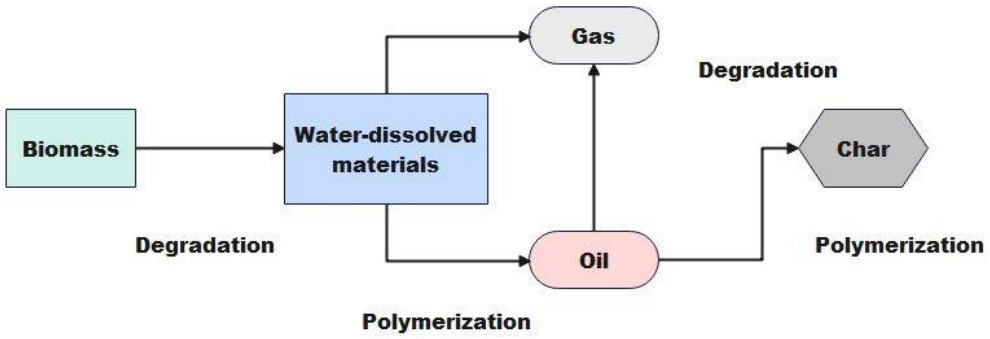

Figure 2.2.3 Reaction pathway of hydrothermal liquefaction [53].

1.5.1 Depolymerization of biomass

Liquefaction decomposes the lignocellulosic biomass material into monomer units by subsequent depolymerization. Biomass depolymerization entails the gradual dissolution of complex macro-molecules by leveraging their physical and chemical attributes. The inherent hemicellulose and cellulose biopolymers contribute positively to the biofuel's thermal stability. This depolymerization process effectively addresses the challenges inherent in

lignocellulosic biomass, which can resemble the properties of fossil fuels produced over geological time [57]. The pivotal factors of temperature and pressure induce structural changes in the elongated polymer chains containing hydrogen, oxygen and carbon resulting in the formation of shorter hydrocarbon chains. Furthermore, the energy content of the organic materials is regenerated in the presence of water. The yield of liquid product is increased by this process [14]. Biocrude yield within 33.5-83 wt. % by HTL of different microalgae species have been reported [58]. The biocrude produced has less content of oxygen as the carbon content of biomass is completely utilized.

1.5.2 Decomposition of biomass

In this stage, a sequence of chemical changes occur including the expulsion of a water molecule (dehydration), the removal of a CO_2 molecule (decarboxylation) and the extraction of amino acid content (deamination). Dehydration and decarboxylation work together to eliminate oxygen from the biomass in the form of H_2O and CO_2 respectively. Complex biomass molecules are broken down through hydrolysis forming polar oligomers and monomers. Under elevated temperatures and pressure, water disassembles the hydrogen-bonded structure of cellulose leading to the creation of glucose monomers. Fructose being more reactive than glucose undergoes rapid degradation producing a multitude of products through various reactions including isomerization, hydrolysis, dehydration, reverse-aldol fragmentation, rearrangement and recombination reactions. Most of these degradation byproducts such as polar organic compounds, furfurals, glycoaldehydes, phenols and organic acids exhibit high solubility in water [59].

1.5.3 Recombination and repolymerization

In this phase a reversal of the initial processing steps occurs due to the absence of hydrogen compounds. When an adequate amount of hydrogen is present in the organic matrix during the liquefaction process, the free radicals are controlled resulting in the formation of stable molecular weight species. However, under circumstances where hydrogen is limited or the concentration of free radicals becomes exceedingly high the fragments either combine or reassemble leading to the creation of large, high molecular weight char compounds often referred to as coke formation. The reactive fragment undergoes recombination and repolymerization due to excessively large concentration of free radicals and unavailability of

hydrogen compound. The fragments thus form char compounds having higher molecular weight [60].

Although the liquid biocrude obtained as a product of liquefaction is not suitable for direct use in vehicles, it can be utilized for co-refining in existing refinery facilities. Catalytic upgrading in metal-carbon catalysts led to efficient hydrogenation of biocrude that increased its energy density and lowered the viscosity and water content to produce a transparent product with colourless or light yellow appearance [61]. Karagoz et al. [62] performed HTL of pine wood sawdust at a temperature of 280 °C for reaction time of 15 min in a 200 ml TaS-02-HC type autoclave reactor and reported 96% conversion of biomass during HTL at 280 °C temperature for 15 min. Wet algal feedstock are composed of proteins, carbohydrates, lipids and algae nans which require a uniform particle size for HTL processing for reduction of difficulties associated with supplying slurry to the reactor [53]. Macroalgae *Enteromorpha prolifera* was used as feedstock by Zhou et al. [63] for biocrude production by HTL with water in a batch reactor at 220-320 °C with 30 min duration of reaction time to obtain a maximum yield of 23 wt. % of biocrude having HHV of 28-30 MJ kg^{-1}.

1.6 Energy from fruit waste

Waste generation from food processing industries has been a matter of concern from the environmental, economic and social point of view. Understanding of the food supply chain network, it can be realized that this type of wastage is more prevalent during the consumption and manufacturing stages. This makes their effective disposal an important issue to be looked upon by emerging waste management technology developers [64,65]. Recently, several waste management strategies have been implemented to look into this matter. Hydrothermal liquefaction (HTL) of food wastes [66,67] and more particularly fruit wastes [68–73] have been developing recently, but the pace is quite slow for that. Anouti et al. [69] explored the physical and chemical characteristics of biocrude derived from HTL of blackcurrant pomace. These biocrude characterized by their black viscous nature and commendable heating values were subjected to standard normalized tests. The obtained results were compared against the specifications mandated for commercialized biofuels and conventional fuels. HTL of castor residue, including stem and leaves, was conducted at temperatures of 260, 280 and 300 °C and residence times of 15, 30, 60 and 90 min. Exploration of the impact of temperature and residence time on product distribution revealed a maximum biocrude yield of approximately

15.8 wt. % at 300 °C for 60 min. Major compounds identified through gas chromatography mass spectrometry (GC-MS) analysis included phenols and their derivatives, aromatic hydrocarbons, N-containing compounds and acids [74]. HTL of fresh lemon peels were carried out to produce biocrude oil. Optimization using response surface methodology considered parameters such as temperature, reaction time and feedstock concentration. The highest oil yield, approximately 18 wt. % was achieved under optimized conditions at 336 °C, 50 min and a 9.6 wt. % feedstock loading. GC-MS analysis identified numerous ketones in the biocrude, with fewer fatty acids, nitrogen and oxygen-containing compounds [72].

Citrus fruits are widely consumed and very popular during the summer season in the Indian sub-continent due to the nutrition as well as the refreshment they provide. Sweet lime, commonly known as Mosambi and scientifically as *Citrus limetta* (CL) [75,76] is consumed for its juice, thereby, generating lots of wastage in the form of peel and pulp (after juice extraction). This fruit waste is extensively available after juice extraction and goes as a waste which is disposed of without any value addition to it. The state of the art establishes that researchers have been using CL peel as an adsorbent for heavy metals removal [77] and methylene blue dye [78] from water. Besides, the biochar obtained from these peels have also been used as an adsorbent for removal of lead from battery manufacturing industrial effluent [79]. Biodiesel production from CL seed oil by simple transesterification process [80] and pyrolysis of such citrus fruits [81,82] has paved the path for their utilization in other thermochemical conversion processes. Moreover, none of these studies deal with the liquefaction and extensive product analysis of CL fruit waste. This motivated this research and to decide upon the novelty of this work to investigate the liquefaction of CL fruit waste (both pulp and peel) in a hydrogen-donor solvent and thorough characterization of the products obtained.

The process of liquefaction is predominated by a number of parameters such as the type of feedstock used, biomass-to-solvent ratio, the process employed whether it is a batch type or continuous process, its temperature, pressure and residence time [55]. However, amongst these parameters temperature proved to be the most influential factor as it was evident from the quality and quantity of the final product [83]. In liquefaction's depolymerization phase, when the temperature surpasses the bond cessation activation energy, it occurs significantly, leading to a rise in free radical concentration and consequently accelerating repolymerization [55]. Numerous studies have documented that elevated

temperatures during liquefaction enhance the extraction of hydrocarbons and nitrogenates into biocrude from the feedstock, while the opposite effect is observed for oxygenates [84]. The amount of biocrude and biochar generated is reportedly controlled by the biomass-to-solvent ratio, according to research carried out by several groups of academicians. To achieve the optimal quantity of biocrude with high energy efficiency and calorific value, it is crucial to carefully adjust this ratio [53]. The alterations of the biomass-to-solvent ratio during the feedstock loading process into the reactor can be determined by observing changes in both the solvent and biomass components. Compared to changing the biomass component, studies show that changing the biomass-to-solvent ratio through changes in the solvent has a considerable influence on the production of biocrude. The yield of biocrude was somewhat decreased by switching the biomass technique to changing biomass method, which might be relatable to the considerable amounts of lower fractions of molecular weight that were produced but lost throughout the drying and evaporation stages. Nevertheless, a rise in the yield of biochar was noted, suggesting an inadequate conversion of organic components in the biomass to liquid products in a situation of solvent deficiency. The variations in the reaction pressure can be attributed to the way in which the biomass-to-solvent ratio is regulated, resulting in the observed differences [85]. Therefore, variation in reaction parameters have been studied herein. Co-liquefaction entails mixing one or more feedstocks to carry out the liquefaction process. It has the benefit of streamlining the processing and improving process efficiency [86]. It is undeniable that investigations of liquefaction with a single biomass have certain limitations in terms of their applicability. Additionally, it is also impossible to have year-round access to specific feedstocks with the appropriate compositions and energy contents to meet the demands of continuous energy production [87]. Due to the heterogeneous content in compositional characteristics of the feedstock combination (biomass) in co-liquefaction, there is potential for enhancing the physico-chemical properties and yield of the resulting biocrude [88]. The biocrude produced by the liquefaction of certain biomasses have higher concentrations of unfavourable components like oxygen and nitrogen, which lowers the quality of the product. Therefore, liquefaction of these biomasses in conjunction with other acceptable feedstocks might serve to address these problems [89]. Literature studies have reported that the co-liquefaction process increased the quality of the biocrude as evident from their GC-MS analysis. As a consequence, the level of fatty acid molecules was substantially uplifted whereas the quantity of nitrogen-containing heterocyclic compounds in biocrude

dramatically decreased [90]. Additionally, it could result in a decrease in the expenses related to the logistics and gathering of huge amounts of a single biomass.

Based on the knowledge gaps on research of biomass (especially food waste) and their liquefaction approaches, the objectives of this thesis have been established. This thesis work depicted the solvothermal liquefaction of *Citrus limetta* fruit wastes (both pulp and peel) at variable biomass-to-solvent ratios and temperatures followed by their co-liquefaction. Their products have been analyzed for their yield along with the investigation of their physico-chemical properties and energy content. Additionally, other characterization techniques such as nuclear magnetic resonance (NMR) spectroscopy, gas chromatography mass spectrometry (GC-MS) and Fourier transform infrared (FTIR) spectroscopy of the biocrude have been used for determination of the functional groups, molecular identity and structure of molecules respectively. Further for the solid product, field emission scanning electron microscope (FESEM), X-ray diffraction (XRD), Brunauer-Emmett-Teller (BET) and thermo gravimetric analysis (TGA) studies have been done to determine their surface morphology, crystalline nature, porous nature depicting adsorption capability and thermal stability respectively. Besides their ultimate analysis along with energy content determination have been done to investigate their applications as a fuel source.

1.7 Organization of thesis

This thesis deals with the management and valorization of wastes from *Citrus limetta* fruits (peel and pulp) by their solvothermal liquefaction and extensive product analysis. The dissertation is structured into the following chapters:

- Chapter 1 depicts the background of selection of fruit wastes as feedstock for this research, comparison of the current status of fossil fuels and renewable energy utilization, biomass, various biomass conversion pathways for energy generation. Further, this chapter presents the reaction mechanism of liquefaction of biomass, possibilities of harnessing energy from fruit wastes by solvothermal liquefaction.
- Chapter 2 covers literature review on different modes of liquefaction and the effects of operating parameters on liquefaction along with the description of the products obtained from liquefaction.
- Chapter 3 presents the motivation of the research for the thesis work, moving up to the objectives of the thesis on the basis of the literature review done in Chapter 2. This

thesis has four objectives where objectives 1 and 2 deal with solvothermal liquefaction of *Citrus limetta* fruits at variable biomass-to-solvent ratios and temperatures, while objectives 3 and 4 deal with the co-liquefaction of pulp and peel of *Citrus limetta* fruits.

- Chapter 4 explores the materials and methods employed for carrying out the experimental work of this thesis. Further, the techniques for characterization of the products obtained have also been presented here.
- Chapter 5 delves into the results and discussion arising from the research presented in this thesis.
- Chapter 6 discusses conclusions and future scope. It provides overarching conclusion of the thesis, accompanied by prospects for future research in this field.

1.8 Summary of the chapter

This chapter encapsulates the primary focus areas and objectives of the thesis, which are:

- Impact of globalization and urbanization that have strained conventional energy sources posing serious threat to energy security, the environment and the economy has been discussed.
- Need for transition to renewables, particularly bioenergy which has become imperative for reduced carbon emissions and fossil fuel independence has been pointed out.
- The versatility of biomass as an energy resource highlighting its various conversion pathways, each with its advantages and challenges have been demonstrated here.
- Utilization of thermochemical conversion technologies particularly hydrothermal liquefaction (HTL) to transform biomass along with an explanation of its reaction mechanism has been provided.
- Exploration of *Citrus limetta* waste liquefaction and co-liquefaction in a hydrogen-donor solvent for biofuel production, with variation of temperature and various parameters crucial for product quality and yield was mentioned.
- Declaration of the aim to bridge knowledge gaps in biomass liquefaction approaches has been portrayed.
- Finally, chapter wise organization of the dissertation has been presented.

CHAPTER 2

LITERATURE REVIEW

2.1 Various modes of liquefaction

Different liquefaction modes refer to various methods or approaches used to transform solid biomass into liquid biofuels or bio-oils. These modes involve distinct techniques, conditions, and mechanisms for breaking down the complex biomass structure and converting it into more usable liquid forms. Each of these modes offers distinct advantages and challenges making them suitable for different types of biomass feedstocks and end product requirements.

2.1.1 Solvent liquefaction

In this approach, solvents are used to dissolve and break down biomass into liquid products. This method can enhance the yield and quality of the resulting biocrude. Solvents wield a significant influence on liquefaction reactions. The main role of any solvent in liquefaction is to decompose raw biomass significantly and provide active hydrogen [91]. Solvent liquefaction procedure has garnered significant interest due to its ability to operate under moderate temperatures, eliminating the need for high pressures or drying procedures. For instance, the use of supercritical alcohol, as opposed to water has proven successful in converting low-rank coal into liquid oil [92]. Several studies have examined the solvolysis liquefaction of biomass, showcasing the effective role of organic solvents in reducing the viscosity of heavy oil derived from biomass liquefaction [93]. In light of economic and environmental considerations, solvents of industrial interest are often those derived from biomass itself, such as alcohols and ketones, or even water [94]. Solvolysis stands out as a highly utilized conversion method within the realm of thermal liquefaction due to its comparatively lower process temperatures when contrasted with the pyrolysis approach. This characteristic helps avert the creation of tar compounds arising from the interlinking of hydrocarbon and aromatic compounds [95]. In solvolysis, biomass undergoes depolymerization while in the presence of organic reagents, culminating in the creation of valuable chemicals [96]. The majority of biomass waste comprises cellulose, hemicellulose, lignin and starch, each exhibiting varying levels of reactivity during the liquefaction process. Broadly speaking, when subjected to hydrothermal conditions, hemicellulose and starch exhibit swifter reactions compared to cellulose while all of these components are more reactive than lignin. Consequently, a higher presence of cellulose, hemicellulose and starch

within biomass corresponds to increased bitumen production. The use of hydrogen-donor solvents has the advantage of giving higher overall conversions to produce liquids and gases and producing bitumen-like heavy bio-oils that are amenable to upgrading to distillate fuels via hydro-cracking [97]. Hydrogen-donor solvents showed significant improvement not only in conversion and product distribution to liquid but also on the quality of biocrude due to the improvement of hydrogenation and hydrocracking reactions with inhibition of polycondensation. These abilities were also much higher than with gaseous hydrogen as the hydrogen donor. This was due to the low strength bonding in tetralin C-H compared to hydrogen gas H-H bond. In terms of its composition, the biocrude produced contained more fully saturated hydrocarbons but less esters and alkenes when using hydrogen donor compare to non-hydrogen-donor solvents [98]. Numerous previous investigations have delved into the solvolysis of biomass using diverse solvents. Yan et al. [99] meticulously explored the liquefaction of sawdust's molecular structure, considering factors such as temperature, reaction time, hydrogen pressure and solvent type. Yip et al. [100] embarked on bamboo liquefaction employing varied solvents, including phenol, ethylene glycol and ethylene carbonate. Similarly, the liquefaction of pinewood in the presence of distinct solvents (water, acetone and ethanol) was conducted within a temperature range of 250–450 °C by Liu and Zhang [101]. Kunaver et al. [102] delved into the liquefaction of various southern European hardwoods and softwoods, utilizing glycerol and diethylene glycol. Yamada and Ono [103] reported on cellulose liquefaction utilizing ethylene glycol in conjunction with hydrochloric acid. The resultant products held potential as fundamental materials for functional polymers and various chemical products. Neavel [104] reported that in tetralin at 400 °C, coal was converted to benzene-soluble products with vitrinite becoming almost completely soluble in pyridine. Hydrogen transfer from tetralin increased exponentially with increased conversion of the coal to benzene-soluble material. Abdel-Baset et al. [105] investigated tetralin extraction for sixty-eight coal samples and found linear equations to predict the liquefaction behavior and help the feedstocks selection. The thermal liquefaction of white birch wood and filter pulp was explored using water and methanol vapor at 2 MPa pressure in a flow-through reactor [106]. Demirbas [95] delved into the delignification of wood and agricultural materials through glycerol or alkaline glycerol, both in aqueous and non-aqueous environments, aimed at pulp production. Cemek et al. [107] explored the liquefaction of verbascum stalk using supercritical fluid extraction, resulting in distinct benzene and ethyl ether soluble fractions.

Significant progress was achieved in the depolymerization of Kraft and organosolv-derived lignin using KOH in supercritical methanol or ethanol. This study was conducted using a rapidly heated batch microreactor, with model compound investigations corroborating that the primary depolymerization pathway involves the solvolysis of ether linkages [108].

Hazelnut shell decomposition using ethanol, acetone and their combinations under sub/supercritical conditions had been examined by Demirkaya et. al [109] to obtain 44.2 wt. % of biocrude at 300 °C when employing a 50/50 mixture of ethanol and acetone (v/v). Polyhydric alcohols sourced from renewable origins such as ethylene glycol derived from bioethanol and glycerol (that is a by-product of biodiesel manufacturing) were used for liquefaction of walnut shells (possessing around 35 wt. % of lignin) to obtain 85 wt. % of liquefaction yield at 200 °C temperature [110]. Oil palm empty fruit bunches (EFB) fibers were liquefied using a range of solvents (acetone, ethylene glycol, ethanol and toluene) to obtain liquid products having higher heating value (HHV) as high as approximately 29.42 MJ kg^{-1} and leading to the formation of ketones, aldehydes, phenolic and alcoholic compounds [111]. Tetralin demonstrated its merit as an optimal solvent, enhancing the efficacy of the EFB liquefaction process and effectively inhibiting the creation of char. The solid remnants obtained post-liquefaction underwent thermal activation with certain samples showcasing notable CO_2 adsorption capability in comparison to activated carbons [112]. The presence of ethanol solvent and elevated temperatures significantly lead to the substantial transformation of sugarcane bagasse into products, resulting in heightened total conversion rates. Their findings suggested that both solvents and reaction temperature exert an impact on the attributes of biocrude and char [91].

2.1.2 Co-liquefaction

Co-liquefaction of biomasses refers to a synergistic process in which two or more different types of biomass materials are simultaneously subjected to liquefaction. This process aims to harness the combined properties and characteristics of these biomasses to produce valuable products, such as biofuels and biochemicals. The co-liquefaction approach capitalizes on the unique composition and reactivity of various biomasses when they are treated together. This can lead to enhanced conversion rates, improved product yields and a more efficient utilization of resources compared to individual liquefaction processes. Key factors influencing the success of co-liquefaction include the selection of compatible biomasses, the optimization of

process conditions (such as temperature, pressure and solvent) and the choice of catalysts or additives. Research in co-liquefaction is ongoing to explore optimal biomass combinations and process parameters. By understanding the synergies between different biomasses, researchers and engineers aim to develop efficient and sustainable pathways for producing bio-based fuels and chemicals, contributing to the advancement of renewable energy and the reduction of carbon emissions. The application of solvothermal co-liquefaction prevents the creation of water-soluble products and fosters improved interplay between intermediates during the liquefaction procedure. This interaction with free radicals results in heightened bio-oil formation [113]. The co-liquefaction approach in presence of solvents proves to be the most efficient means of converting biomass into diverse chemicals and high-quality crude bio-oil [114]. It generates significant functional groups throughout the procedure [115]. The co-liquefaction of various feedstocks holds promise for augmenting oil yield, managing product distribution and effectively utilizing a wide range of available biomass waste resources [116].

Co-liquefaction stands as an effective procedure for gathering hydrogen and carbon, as well as redistributing other elements like nitrogen and oxygen into different products, including water-based and gas-based ones. This makes co-liquefaction a practical and straightforward method for generating liquid hydrocarbons from a blend of plastic waste and lignocellulosic materials [117]. The primary objective of blending plastics with biomass is to enhance the quality of biocrude. Plastics, being rich in hydrogen, act as valuable hydrogen donors during the co-liquefaction process [118]. The co-processing of lignocellulose and microalgae alongside plastic waste through co-liquefaction has revealed synergistic effects that enhance biocrude yields during liquefaction. It has been observed that the presence of highly reactive biomass decomposition products can reduce the thermal stability of polyethylene (PE) and accelerate its thermal degradation at lower temperatures. In turn, PE can serve as a hydrogen source during biomass liquefaction [119]. Co-liquefaction of PE with *Spirulina* was observed to decrease the oxygen content in the resulting biocrude products. Furthermore, previous studies have demonstrated that co-liquefaction of Vietnamese *Ulva intestinalis* with PE led to biocrude with reduced nitrogen levels and an increased higher heating value (HHV), thereby improving overall fuel properties. Importantly, the presence of plastics was found to facilitate the conversion of biomass into biocrude [120]. The biocrude obtained from the co-liquefaction of *Spirulina* microalgae and high-density polyethylene (HDPE) exhibited increased carbon (C) and hydrogen (H) content but a decreased oxygen (O)

content. This resulted in a higher calorific value, measured at 48.35 MJ kg^{-1} [119]. The co-liquefaction of rice straw (RS) and linear low-density polyethylene wastes (LLDPE) using supercritical methanol was investigated across a temperature spectrum spanning from 240 to 340 °C for durations ranging from 0 to 2 h. Elevated temperatures led to increased degradation of LLDPE, consequently yielding more oil. However, it is noteworthy that higher temperatures did not result in higher hydrocarbon content within the oil. The optimal conditions for producing high quality oil were determined to be at 300 °C for 1.5 h, where a 33.05 wt. % oil yield was achieved, containing 70.91% hydrocarbons [10]. The increase in bio-oil yield during the co-liquefaction process can be attributed to its ability to impede the formation of gases and water while promoting interactions between free radicals and intermediate products. This, in turn leads to an augmentation in biocrude production [113].

The biocrude yield achieved from the individual liquefaction of feedstocks were relatively low and the resultant biocrude contained a high proportion of heavy fractions, which wasn't ideal for combustion. However, when rice straw or sawdust was co-liquefied with municipal sewage sludge (MSS), it led to the production of biocrude with superior properties and increased yields. Through this co-processing, the biocrude yields were significantly enhanced, rising from the original 22.74 % to 26.73 % (which were the yields from the individual feedstock liquefaction) to over 32 % when using the optimal mixing ratios of feedstocks. Importantly, the content of heavy fractions within the biocrude was notably reduced [121]. Under the ideal reaction conditions (270 °C, 30 min, peanut residue: cattle manure ratio of 3:1), the co-liquefaction yielded an overall biocrude mass fraction of 23.5 % and a biochar mass fraction of 18.5 %. The biocrude produced reached its highest calorific value at 31.74 MJ kg^{-1}. During the co-liquefaction process, it was observed that Maillard and Mannich reactions occurred. Notably, the experimental biochar yield exceeded the calculated values and attributed to higher carbon and nitrogen content, signifying a synergistic effect in biochar formation. Throughout the co-liquefaction process, nitrogen present in the biocrude was translocated to the biochar. This transference enhanced the biocrude's quality and bolstered its utilization efficiency [122]. Co-liquefaction involving high protein microalgae and high carbohydrate sweet potato waste led to a reduction in nitrogen content, an increase in ester content and enhanced energy recovery within the biocrude [123]. The co-liquefaction of microalgae and rice husk led to an augmentation in biocrude yield while concurrently reducing the acidity and nitrogen content within the biocrude [124]. The intense reaction conditions

were mitigated, and the deoxygenation of biocrude was enhanced following the co-liquefaction of both micro and macro-algae [125]. Furthermore, the co-liquefaction of spent coffee grounds and lignocellulosic feedstocks led to a decrease in viscosity and a reduction in relative molecular mass of biocrude [116]. Hydrothermal co-liquefaction of *Spirulina platensis* and lemon peel at 280–350 °C, 10–60 min residence time and various blending ratios was systematically investigated using response surface methodology. The highest biocrude yield, reaching 26 wt. %, was attained at 336 °C and 35 min with a *Spirulina platensis*/lemon peel mass ratio of 4:1. The results indicated that the biocrude yield increased with higher microalgae content in the blending, while the influence of temperature and time was contingent on other parameters [68]. The co-liquefaction of tomato, carrot and broccoli wastes in a 1:1:1 ratio at temperatures ranging from 280 to 360 °C resulted in a biocrude yield of 5-15 wt. % within a 40 min reaction time. Peak HHV at 33.05 MJ kg^{-1} was achieved at 280 °C and 40 min reaction time. Similarly, a combination of orange and banana peels in a 1:1 ratio produced a biocrude yield of 4-12 wt. % under the same temperature range and reaction time [126]. The biocrude derived from a combination of municipal sewage sludge (MSS) and lignocellulosic biomass primarily consisted of esters and phenols characterized by lower boiling points (degradation temperatures) compared to those obtained from individual feedstocks, which typically contained higher fractions of heavy bio-oils. These synergistic effects were likely attributed to interactions between the intermediate products of MSS and those generated from biomass during the processing phase [121]. Certain studies have indeed noted that co-liquefaction could increase the yield and modify the characteristics of the resultant biocrude. However, the precise mechanisms behind the synergistic effects of combining these biomass sources are not yet fully comprehended. From an economic standpoint, co-liquefaction offers an added advantage by significantly reducing the logistical expenses linked to the collection and transportation of biomass to a central processing facility. Biomass is typically bulky, has a low energy density and its availability can vary seasonally. This can make it challenging to amass a sufficient quantity of a single biomass type within a particular region, which may otherwise be necessary to render overall production economically viable [127].

2.2 Effects of operating parameters on liquefaction

The processing of biomass by liquefaction can take place in both batch type and continuous type process. In batch process the feedstock can be fed to the reactor in batches and then the

reaction can be proceeded. However, continuous feeding to reactors is to be done by a slurry pump in a continuous process. Liquefaction of biomass is carried out in presence of water or other solvents at 280-370 °C temperature and 10-25 MPa pressure [53] at certain residence time to produce liquid biocrude as well as some solid char like product. The final output of the liquefaction process depends on biomass loading, temperature, reaction time, pressure, solvent type, catalyst type, reaction atmosphere, heating rate and extraction process.

2.2.1 Biomass-to-solvent ratio

The concept of biomass-to-solvent ratio, often referred to as the feed ratio, can be understood differently depending on the type of liquefaction process. Several researchers have examined the biomass-to-solvent ratio because it has a significant impact on biocrude and biochar yields. In batch HTL processes involving lignocellulosic biomass, it is typically expressed as the biomass-to-water ratio. However, in continuous hydrothermal liquefaction (HTL) systems where a pre-treated concentrated slurry is continuously fed into the processing unit, it is more commonly described as the solid concentration, often denoted in weight percentage (wt. %) or mass fraction, or as the reactor loading. Water is considered to be a crucial solvent for HTL of biomass due to its wide range of applications. It serves as both a solvent and a reactant for hydrolyzing proteins and carbohydrates in biomass. Since, biomass naturally contains varying amounts of water, it is important to consider the overall biomass-to-water content [128]. Qu et al. [129] studied HTL of *Cunninghamia lanceolata* with varying biomass-to-water (B/W) ratios and found that increasing this ratio led to a reduction in biocrude yields. They also noted that smaller B/W ratios resulted in higher biocrude yields, but using water as a solvent increased energy requirement and raised the cost of downstream wastewater treatment. Hence, it is imperative to fine-tune the ideal biomass-to-solvent ratio for each experiment. This ratio should be determined based on factors such as the feedstock type, operational conditions and the capacity of the liquefaction unit. This calibration process aims to achieve the highest possible biocrude yield while maintaining reasonable energy consumption. Akhtar et al. [130] conducted a study on the liquefaction of empty palm fruit bunches at 270 °C and 1.0 M K_2CO_3 for varying feed ratios, expressed as the biomass-to-water ratio, ranging from 1/10 to 8/10 g mL^{-1}. Their findings indicated that raising the feed ratio from 1/10 to 2/10 g mL^{-1} resulted in higher conversion and liquid yield. However, when the feed concentration was further increased there was a notable decline in both biomass conversion and product yield. In a microalgae-water liquefaction reaction, a small reduction in biocrude yield from 44.2 to 42

wt. % was noticed when the biomass to solvent ratio was raised from 0.075 to 1 [131]. Similar trends of diminishing biocrude yield with increasing biomass concentration have been observed in several other studies [129,132,133]. In scenarios where the feed concentration is high, the limited presence of the aqueous solvent poses challenges in dissolving the biomass effectively. The inadequate ability of the solvent to dissolve the biomass results in reduced degradation, leading to lower conversion rates and yields. In highly concentrated feedstocks, unconverted biomass must contend with other intermediate hydrolysis reactions for access to water, which results in elevated intermediate concentrations in both the aqueous phase and biocrude. This heightened concentration of intermediates increases the likelihood of repolymerization reactions, consequently leading to a greater formation of solid residues [133]. Furthermore, an excessive quantity of solid material in relation to the available water can restrict the accessibility of water for solvolysis and the hydration process. This limitation ultimately leads to inadequate and incomplete degradation of the lignocellulosic biomass, resulting in the retention of unconverted solid residues [134]. In the liquefaction of lignocellulosic biomass (pine wood) in supercritical ethanol the effect of biomass-to-solvent ratio on conversion and products yields were examined at 345 °C, 30 min of residence time and an initial N_2 pressure of 5 MPa. Marginal increase in biomass conversion upto 85 % was found with increase in biomass-to-solvent ratio. However, this was limited upto a certain extent only as further increase in this ratio resulted in significant decrease of conversion due to adhesion of wet biomass powder (ethanol absorbed) to the surface of inner walls of reactor. This biomass-to-solvent ratio failed to significantly impact the chemical composition of biocrude and biochar [135]. Therefore, to achieve the optimal quantity of biocrude with high energy efficiency and calorific value, it is crucial to carefully adjust this ratio [53].

2.2.2 Temperature

Temperature is a key factor that liquefaction process is dependent on. Though typical operation range of temperature is reported within 200-375 °C, this can be varied between the subcritical to supercritical range of the solvent used with dependence on biomass type and nature of catalysts employed [23]. Temperature improves fragmentation and lignocellulosic fraction cleavage and has a considerable effect on product yield. It is imperative to overcome the energy barrier and use sufficient activation energy for biomass breakup to achieve higher concentrations of free radicals. Biomass liquefaction is usually endothermic at low temperatures and becomes exothermic at high temperatures [136]. As a result, biocrude yield

increases with temperature and reaches a point where a further rise in temperature suppresses liquefaction. Reduced biocrude yield could also be due to the dominating secondary decomposition and Boudouard gas reactions [137] along with the recombination effects of high concentrations of free radicals into char. Several studies at subcritical conditions have also reported enhancement in yield of biocrude with reaction temperature rise, which could be accredited to the variation in chemical component composition of the biomass especially lignin decomposition that occurs at 280-300 °C temperature [114,138,139]. This increase occurs upto a certain limit of temperature after which opposing behaviour is observed in the biocrude yield which might possibly be due to biocrude cracking and repolymerization reactions to produce light gas species and char respectively [138]. The oxygen content decreases and HHV increases due to rise in reaction temperature [114]. The primary function of temperature is to surpass the energy barrier between raw biomass and intermediates, facilitating the progression of the process by supplying adequate potential energy for breaking chemical bonds. Initially, elevating the temperature enhances the endothermic phase in the HTL process by providing the necessary activation energy for bond disruption. During this phase, numerous unstable entities, primarily free radicals and fragmented compounds, are generated. With further temperature increase, these excited radicals undergo repolymerization by establishing new chemical bonds and releasing energy, ultimately rendering HTL an exothermic process [136].

The biocrude yield from microalgae HTL of *Tetraselmis sp.* and *Spirulina sp.* increased by 24 wt. % and 9 wt. % respectively with temperature rise from 300 to 350 °C [140,141]. At a temperature of 325 °C, the use of methanol as a solvent for liquefying natural rubber resulted in the highest yield of 79 wt. %. This was attributed to the faster rate of thermal cracking of the feedstock that occurred under these high temperature conditions [83]. Sun et al. [142] investigated *Paulownia sp.* biomass using a HTL reactor with hot compressed water at 300 °C. They found that as the temperature increased, the biocrude yield also increased. However, at higher temperatures, there was a noticeable decrease in biocrude production. Chunbao and Lancaster [134] conducted experiments using HTL reactor to process paper pulp/sludge powder at various temperatures ranging from 250 to 380 °C. They observed that the highest biocrude yield, reaching 60 wt. %, was achieved at lower temperatures. However, at higher temperatures in the range of 350 to 380 °C, there was a substantial reduction in biocrude yield, down to 24 wt. %. Zhang et al. [72] conducted research on the HTL of fresh

lemon peel. Their findings indicated that at a temperature of 336 °C, with a residence time of 50 min and a feedstock loading of 9.6 wt. %, they achieved biocrude yields of approximately 18 wt.%. Minowa et al. [143] conducted a study on the degradation of microcrystalline cellulose in the presence of hot compressed water. Their observations revealed that as the temperature was raised from 200 °C to 240 °C, all the hydrolysis products, including glucose and oligomers, exhibited water-soluble characteristics. Beyond 240 °C, non-glucose products began to form. During this process, primary products such as char, oil and gas also emerged. The decomposition of cellulose notably accelerated between 240 and 270 °C, leading to complete dissociation of cellulose and the highest glucose yield was observed at 260 °C. With further temperature elevation, the yield of the oil fraction increased, reaching its peak at 300 °C. However, as the temperature surpassed 300 °C, the oil yield declined, while the production of char and gases started to rise. Mathanker et al. [144] conducted a comprehensive study to investigate the impact of temperature on the liquefaction of corn stover and found that increasing the temperature from 250 °C (resulting in a heavy oil yield of 22.2 wt. %) to 300 °C (yielding 27.2 wt. %) led to a notable increase in heavy oil production, while simultaneously minimizing the solid char yield. However, a significant decline in oil yield was observed as the temperature continued to rise, reaching the supercritical point of water at 375 °C (yielding 14.3 wt. %). Khampuang et al. [145] investigated the influence of temperature on the liquefaction of corncobs using supercritical ethanol. They maintained a reaction time of 60 min and an initial H_2 pressure of 4 MPa. Their results indicated that the oil yield exhibited a gradual increase, starting at 300 °C (33.9 wt. %) and peaking at 340 °C (38.6 wt. %). However, a significant decline in oil yield was observed at 360 °C (27.3 wt. %).

2.2.3 Pressure

Pressure of the system has to be monitored effectively during liquefaction of biomass for both supercritical and subcritical conditions as it maintains a single-phase media beyond critical conditions. Achieving a single-phase liquefaction is essential to prevent excessive energy requirements associated with the phase transition of solvents [146]. Operating HTL above the solvent medium's critical pressure is thermodynamically favorable for promoting specific reaction pathways that lead to the production of biocrude or gas. This elevated pressure helps regulate the rates of hydrolysis and biomass dissolution. Furthermore, pressure enhances the density of the solvent, facilitating its penetration into the large biomass molecules, causing them to break down into smaller, more manageable compounds. Once supercritical conditions

are attained during HTL, variations in pressure have a minimal impact on biocrude and gas yields. This is mainly because pressure has a limited influence on water quality within the supercritical region [134]. Moreover, the increase in solvent pressure in this region caused the C-C bonds in the biomass to prevent their breakage by caging effect. Thus rise of pressure lead to decrease in biocrude yield and favoured the conversion of biomass to gases by means of free radical reactions [71]. In the supercritical phase, it's worth noting that the impact of pressure on the hydrolysis reaction kinetics is relatively modest. Even when applying pressures in the range of 30 to 40 MPa, the effect on the rate of hydrolysis may not be significant [147]. However, what does change notably is the selectivity of the cellobiose hydrolysis reaction. For instance, elevating the pressure above the critical point leads to a reduction in the rate of glucose isomerization to fructose and an increase in retro-aldol condensation of glucose. Conversely, lowering the pressure promotes the formation of 5-hydroxy methyl furfural (HMF) and the hydrolysis of oligosaccharides [148].

HTL of microalgae *Kirchneriella sp.* reported decrease in yield from 45.5 % at 9 MPa to 43.3 % at 25 MPa initial pressure [149]. In a study conducted by Chan et al. [150], they examined the HTL of palm empty fruit bunch, palm mesocarp fiber and palm kernel shells under different conditions, including pressure ranging from 25 to 35 MPa, residence times of 30 to 240 min and temperatures between 330 and 390 °C. Their findings demonstrated that the highest biocrude production was achieved at a pressure of 25 MPa and a temperature of 390 °C. Mathanker et al. [144] found that pressure had no impact on oil yield in the supercritical region of water (374 °C). However, when the initial pressure was raised from 2 to 4 MPa at 300 °C, there was an increase in the biocrude yield from 21 wt. % to 27 wt. %. Ogi et al. [151] noted that as the initial pressure was raised from 0.5 to 4 MPa, the biocrude yield increased from 6 to 20 wt. %. However, they also observed that any further increase in pressure up to 10 MPa at 350 °C had a negligible effect on biocrude yield. It was observed that pressure has minimal to negligible effects on the production of crude oil and gas. However, it does have a slight influence on the overall biocrude yield. In fact, it plays a more substantial role in determining the energy efficiency of the HTL process [152].

2.2.4 Residence time

Residence time, sometimes referred to as retention time, is the duration for which the reactor is held at the desired temperature, excluding the time taken for heating and cooling. Residence

time duration is a critical operational parameter that influences both the yield and properties of the resulting product, including solid residue. The maximum allowable residence time is determined by various factors including the biomass type, composition, catalysts used and other operating conditions [153]. Employing a lower heating rate extends the time needed to reach the final temperature. This prolonged heating period allows for enhanced biomass conversion and oil production, thereby decreasing the requirement for an extended residence time. Likewise, within the critical temperature range and in the presence of alkalis, hydrolysis occurs more rapidly reducing the necessity for an extended residence time [128]. In liquefaction reactions the residence time has a critical value at which oil yield is maximum. This time duration effects the overall biomass conversion and composition of the products formed. A long residence time in liquefaction leads to a high biocrude yield which holds good for even biomass with high lignin content [138].

Several works have provided evidence on the role of higher residence time on higher yield of biocrude due to larger biomass degradation to product phase. Biocrude yield rose from 41.63% to 45.5% with rise in 15 to 30 min for residence time [21,149]. In a supercritical process, short residence time led to enhanced degradation of biomass due to speed up of hydrolysis and decomposition [154]. However, after a certain limit this biocrude yield decreased due to ensuing polymerization and condensation of oil molecules that are energy dense and mixed with the intermediates forming tar-like heavy substances that resulted in biochar formation [149]. Xu and Etcheverry [155] found that residence time influenced the cracking of liquid products leading to the formation of gases and solid residues through processes such as condensation, crystallization and re-polymerization of the liquid products. They investigated jack pine powder in an HTL reactor at varying residence times, ranging from 20 to 40 min and found that the biocrude yield increased steadily up to 40 min. Li et al. [156] observed that residence time is closely linked to temperature and the liquefaction reaction of rice stalk biomass at different temperature ranges led to varying residence times. They noted that the yields of liquid, gas and solid residues exhibited initial increase at lower temperatures and were influenced by residence time, especially at higher temperatures. Additionally, at lower temperatures and shorter residence times the decomposition of solid residue was only partial resulting in lower conversion rates. It has been suggested that as temperature and residence time increases, there is a decrease in the yield of solid residue due to ongoing cracking and repolymerization reactions [157]. Valdez et al. [158] investigated

Nannochloropsis sp. by HTL at varying residence times, ranging from 10 to 90 min. Their findings indicated that the optimal residence time for achieving the maximum biocrude yield was 10 min. In liquefaction of empty fruit bunch and palm mesocarp fiber, it was observed that the highest biocrude yield was obtained at 120 min, while palm kernel shell yielded the maximum biocrude at 240 min [150]. Xu et al. [134] carried out an HTL process on secondary pulp/paper sludge at 280 °C without a catalyst, with retention times ranging from 15 to 120 min. They noted a rise in heavy oil yield with longer retention times facilitating the dehydration of carbohydrates and formic/acetic acids from the water-soluble organics, thereby contributing to the heavy oil mass fraction.

In contrast to the aforementioned results, several other studies advocated for longer retention times, suggesting that they are more advantageous for enhancing yield. Yang et al. [159] investigated the liquefaction of birch powder using methanol as solvent under supercritical conditions for residence times ranging from 10 to 480 min. They observed that as the residence time increased, the conversion and yield of gases, heavy oil and water-soluble organics all increased. Yim et al. [160] investigated how residence time influenced the relative yield of biocrude when using metal oxide catalysts at a temperature of 390 °C. The increase in residence time from 15 min to 60 min led to an increase in the relative yield of biocrude. This suggested that the breakdown of C–C bonds in the biomass resulted in dehydration, decomposition and the recombination of fragments that contributed to the biocrude. However, further extension of the residence time beyond 60 min and up to 960 min led to a decrease in the relative biocrude yield. This decrease was primarily due to the cracking of biocrude into low molecular weight gaseous products and the repolymerization of intermediates into solid char. Wang et al. [132] carried out HTL of *L. cubeba seeds* for varying durations (30–120 min). Initially, the biocrude yield showed an increase, rising from 53.5% at 30 min to 56.9% at 60 min. However, a further extension of the residence time had a detrimental effect on the biocrude yield due to increased cracking and polymerization reactions. The yield of solid residue on the other hand exhibited little sensitivity to this time, decreasing from 15.3% at 30 min to 13.2% at 60 min. However, it is important to note that there is no universally accepted optimal residence time as this parameter varies depending on other process conditions. A brief residence time might result in incomplete biomass decomposition, while an excessively prolonged residence time could encourage repolymerization and carbonization as well as the

cracking of oil and organic compounds into char and gas. Simultaneously, this could also lead to higher operational costs.

2.2.5 Solvent

Solvents play a significant role in liquefaction of biomass and can significantly influence the resulting product yields. Liquefaction necessitates the utilization of solvents capable of efficiently transforming biomass into high energy density fuels with the desired composition. Product yield has been observed to rise with increase in solvent dosage due to increase in free radical concentration of the solvent acting on the biomass molecules resulting in cracking and liquefaction. But excessive amount of solvents further increased the free radical concentration to promote secondary reactions such as cyclization, polymerization and isomerization that increased the yield of residue [161].

Water is often regarded as one of the environmental friendly solvents due to its capacity, in both subcritical and supercritical states to extract valuable products from biomass during the liquefaction process [162]. Above its critical point at 374 °C and 22 MPa, water lacks phase boundaries, rendering it an exceptional solvent. In this state, water exhibits remarkable diffusion and mass transfer properties due to its low viscosity and strong miscibility. Below the supercritical condition lies the subcritical region with intermediate temperatures, which facilitates initial hydrolysis and radical reactions by creating a reservoir of H^+ and OH^- ions [163]. During HTL, water serves a triple role functioning as a solvent, reactant and catalyst in both its dissociated and natural states.

At subcritical and supercritical state alcoholic solvents such as ethanol and methanol having low critical temperature, pressure and low dielectric constant lead to better liquefaction owing to higher dissolving tendencies of organic hemicellulose, cellulose and lignin [164]. Acetone, methanol, ethanol, 2-propanol, n-hexane and n-heptane are among the frequently employed solvents in the HTL process. They have been frequently utilized in conjunction with water as co-solvents. Numerous investigations have been dedicated to comprehending and refining the solvent-to-water ratio to enhance both product quantity and quality. Ogi et al. [165] examined various solvents including acetone, propanol, butanol, methyl ethyl ketone and ethyl acetate for the liquefaction process. They discovered that when an acetone-water mixture was used, it resulted in heavy oil with reduced viscosity. Minami et al. [166] highlighted the advantages of utilizing supercritical methanol (temperature = 239 °C, pressure

= 8.1 MPa) in combination with water as a co-solvent for the liquefaction of beech wood. Methanol, with lower critical temperatures and pressures compared to water has the effect of reducing the liquefaction operating conditions. Methanol exhibits a decrease in its dielectric constant from 32 under ambient conditions to 7 at its critical point, enabling it to dissolve various non-polar organic substances and inorganic gases. Furthermore, the study noted that water played a crucial role in the decomposition of lignin and hemicelluloses. Therefore, a mixture of 10 vol% water and 90 vol% methanol was found to be effective for decomposition and liquefaction. Yan et al. [167] observed that methanol proved effective in breaking down cellulose and hemicellulose, while more efficient lignin degradation occurred when water was used as the sole solvent, as water played a role in the hydrolysis of cellulose and hemicellulose components, resulting in ketone formation through cyclization reactions and facilitating esterification reactions in the presence of methanol.

Other organic solvents have been explored for various feedstocks beyond pure lignocellulosic materials, including microalgae and sewage sludge. A renewable solvent such as supercritical ethanol which acted as an effective hydrogen donor was used for biomass liquefaction of microalgae, this solvent was in fact responsible for transfer of hydride from its α-hydrogen. Singh et al. [168] focused their research work on a comparative analysis of the effects of alcoholic solvents on macro algae *Ulva fasciata* HTL yield. Liquefaction with CH_3OH and C_2H_5OH were found to produce 44% and 40% of biocrude yield in contrast to 11% with water solvent. Alcoholic solvents that acted as hydrogen donors lead to increase in aliphatic compounds in biocrude and aided in conversion of the acids in it to corresponding ethyl and methyl esters. Durak and Aysu [169] investigated HTL of *Onopordum heteracanthum* stalks using various solvents, including methanol, ethanol and acetone in the presence of KOH and $ZnCl_2$. Their study examined the impact of different temperatures (250, 270 and 290 °C) in an autoclave without the use of a catalyst on the yield and properties of biocrude. The utilization of ethanol and methanol as HTL solvents revealed more moderate reaction conditions owing to their lower critical points. Moreover, ethanol and methanol, with their lower dielectric constants, facilitated the dissolution of high-molecular-weight products during the process [170]. Cheng et al. [171] examined the HTL of pine sawdust using water, methanol and ethanol as solvents. Their findings indicated that compressed hot water resulted in a 40 wt. % biocrude yield, whereas methanol and ethanol produced lower yields of 23 wt. % and 26 wt. %, respectively. Wang et al. [172] investigated the HTL of pinewood using

ethanol as the solvent. Their results revealed a biocrude yield of 30.8 wt. % and a solid residue yield of 28.9 wt. %. They further emphasized that the choice of solvent not only influenced conversion yields but also significantly impacted the composition of liquid products. In their study, 2,4,5,7-tetramethyl-phenanthrene and bis(2-ethylhexyl) phthalate were identified as the predominant compounds in the liquid products when supercritical CO_2 was employed, while 2-methyl-naphthalene was highlighted as a favorable compound when water was used as the solvent. Furthermore, the utilization of solvent combinations has also been explored by several researchers.

The potential advantages of co-solvent systems over individual solvents were examined by Cheng et al. [173] in their investigation of the HTL of pine sawdust. They proposed that co-solvent systems, specifically those composed of a 50/50 w/w ratio of water to alcohol (either methanol or ethanol), could yield as much as 65 wt. % of biocrude. Likewise, Yu et al. [170] conducted a study on the impact of co-solvents in the HTL of *Tertiolecta* biomass and found that a biocrude yield of 64 wt. % could be attained using a co-solvent mixture consisting of 40/60 v/v ethanol/water. Nevertheless, it was crucial to note that the selection of an appropriate and promising solvent system remained contingent upon the specific biomass feedstock and operational conditions.

2.2.6 Catalyst type

The incorporation of catalysts in liquefaction processes aimed to enhance process efficiency by minimizing the production of char and tar. It also initiated biomass degradation and accelerated the process impeding secondary reactions like repolymerization and cracking resulting from lignin decomposition [47]. This activation of reaction kinetics reduced the reliance on pressure, temperature and retention time. Numerous investigations into catalytic HTL of biomass have linked the increased biocrude yield to pivotal factors engendered through catalyst incorporation. While there is no set standard for selecting catalysts, they notably influence the yield, composition and proportions of resulting products. The selection of a catalyst is determined by factors such as the biomass characteristics, composition and the desired final product distribution. Lignocellulosic biomass is composed of hemicellulose, cellulose and lignin, the polymers of which are held tight by glycosidic bonds. These bonds on breakage resulted in organic acids which showed tremendous rise in presence of alkali catalysts. Lignin was also seen to depict cleavage in alkali catalysts at hydrothermal

conditions. However, this fact was not always true as there existed difference in feedstock composition.

Xu and Etcheverry [155] examined the effects of FeS and $FeSO_4$ catalysts during the HTL of Jack pine powder. They noted that catalysts effectively diminished solid residue formation while concurrently boosting the biocrude yield. The type of catalyst influenced the physico-chemical properties and yield of biocrude. Due to increase in H/C ratio and minimization of content of hetero-atom in the biocrude there was a significant rise in its calorific value and decrease in NO_x and SO_x emissions [174]. Matsui et al. [175] conducted research on liquefaction of microalgae with iron catalyst. Tetralin solvent was used to increase the yield of biocrude from 52.3 to 66.9 wt. % at 350 °C, 5MPa pressure of hydrogen and $Fe(CO)_5$-S catalyst. The use of $FeSO_4$ and FeS catalysts were favourable in sewage sludge and woody biomass liquefaction as they showed the tendency to improvise transfer of hydrogen from hydrogen donor. Both alkali metal hydroxides and carbonates have been observed to significantly enhance biomass degradation in an aqueous environment, leading to increased liquid product yields [128]. Alkali salts played a pivotal role in mitigating char and tar formation while enhancing product yield through the acceleration of the water-gas shift reaction. They offered an economical solution for hydrothermal technologies. Their operational mechanism involved the generation of esters through a decarboxylation reaction between the hydroxyl groups present in biomass and the formate ions within alkali carbonates. This initiated a sequence of reactions encompassing dehydration, deoxygenation, decarboxylation and the dehydrogenation of micellar-like fragments into smaller constituents. Subsequently, these underwent a cyclic process of rearrangements involving cyclization, polymerization and condensation [44].

Alkali salts catalysts, such as Na_2CO_3 or KOH, which have been classified as homogeneous catalysts, were found to cause an increase in biocrude yield while decrease in solid residue formation during HTL of microalgae [176]. Additionally, the inclusion of alkali salts in the hydrothermal environment elevated pH levels, effectively reducing dehydration reactions that typically resulted in the formation of unstable unsaturated compounds [177]. Shuping et al. [178] investigated *Dunaliella tertiolecta* cake in an HTL reactor with 5% Na_2CO_3 catalysts and observed a significant increase in biocrude yield by 25.8 wt. %. Zhang et al. [179] conducted research on the HTL of *Spirulina platensis*, employing K_2CO_3 and KOH catalysts within a temperature range of 240–300 °C and a residence time of 35 min. Their

findings indicated that KOH had a more favourable impact on biocrude yield compared to K_2CO_3. Khampuang et al. [145] examined the impact of NaOH (10 wt. %) and KOH (10 wt. %) on the liquefaction of corncobs in a 100% ethanol solvent. The findings revealed a significant rise in biocrude yield, increasing from 38.6 wt. % (without a catalyst) to 50.5 wt. % (in presence of NaOH) and 55.6 wt. % (in presence of KOH). This highlighted the effectiveness of alkali catalysts for hydrothermal liquefaction in alcohol solvents as well. Among alkali catalysts, K_2CO_3 stood out as the most efficient in boosting biocrude yield within the ideal temperature range of 280–350 °C. It contributed to an increase in biocrude yield, mitigated char formation and notably enhanced the oil's quality by raising carbon content and lowering oxygen content, resulting in a higher value of HHV. The presence of an alkaline medium altered the way biomass reacted and facilitated the breakdown of intramolecular interactions in glucoside bonds within the biomass. This, in turn, lowered the activation energy required for complex reactions and diminished the thermal stability of stable chemical structures [180]. Additionally, it disrupted the physical barriers within the biomass, leading to the absorption of the solvent into the biomass. This resulted in a more extensive separation between the structural connections within cellulose and lignin, thereby increasing the surface area accessible to the internal structure and promoting enhanced degradation [181]. Therefore, when employed in appropriate concentrations, alkali catalysts offered significant benefits to the HTL process and contributed to enhancement of biocrude yield.

Castello et al. [182] conducted research on the HTL of three distinct biomass sources (*Miscanthus*, *Spirulina* microalga, and primary sewage sludge) using $NiMo/Al_2O_3$ catalysts under different temperature and pressure conditions. Their findings highlighted the potential of sewage sludge biocrude, which exhibited a higher degree of promise. This biocrude contained straight-chain hydrocarbons within the diesel range and showed effective reduction in heteroatom content, even with minimal hydrotreatment. Tekin [183] conducted research on the HTL of olive seeds, varying the temperatures and residence times while employing a mussel shell catalyst known for its high CaO content. The results indicated that the inclusion of the catalyst resulted in higher yields of biocrude and increased conversion rates. Metal oxide catalysts exhibited two noteworthy characteristics, their relatively lower surface area and sensitivity to water could have a negative impact on their effectiveness but their exceptional hydration and dehydration capabilities made them a preferred choice. Zeolite-based catalysts, particularly those supported by zeolite, enhanced hydrocarbon yields and

decreased the presence of oxygenated compounds due to their larger surface area, pore size and improved water tolerance [184]. Furthermore, zeolite catalysts with varying silica-to-alumina ratios were employed to facilitate the conversion of bio-polymers into biocrude during the HTL process [162]. Meanwhile, catalysts supported by carbon enhanced biocrude properties by increasing surface area, reducing non-condensable gas production and enhancing catalyst recovery rates [171].

When dealing with wet feedstocks like algae and microalgae, a broad range of both homogeneous and heterogeneous catalysts found widespread application [185]. Homogeneous and heterogeneous catalysts both lead to enhancement of liquefaction reaction rates. But homogeneous catalysts were more effective in biocrude yield enhancement as well as char reduction. Utilization of homogeneous catalysts offered several advantages, including a reduction in solid residue production, an increase in biocrude yield and enhancement of biocrude quality. However, the recovery of homogeneous catalysts is costly and involved energy-intensive separation processes. Heterogeneous catalysts often consisted of rare metals like Pt, Ni and Pd. Given the scarcity of these metals, attention has been shifted towards metallic oxides as alternatives [186]. He et al. [187] investigated the HTL of *Chlorella* microalgae using five different catalysts (Pt/C, Pd/C, Ru/C, Pt/C, Pd/C and a newly synthesized CoNiMoW/γ-Al_2O_3). Their findings revealed that Pt/C catalyst resulted in the highest yield and energy recovery for the upgraded oil, albeit with lower elemental composition and heating value. In contrast, Pd/C catalyst lead to the highest HHV but resulted in the lowest yield and energy recovery for the modified oil, accompanied by increased yields of CH_4 and C_2H_6. Zhang et al. [188] investigated how the addition of both homogeneous catalysts (HCOOH, KOH) and a heterogeneous catalyst (FeS) influenced the liquefaction of secondary pulp/paper mill sludge at 300 °C for 20 min. The catalyst's reactivity in terms of biocrude yield, followed the order: HCOOH (34.4 wt.%) > KOH (31.2 wt.%) > FeS (27.7 wt.%) > non-catalytic (24.9 wt.%). However, there were no significant differences observed in the elemental analysis and higher heating value of the oil obtained in the presence of different catalysts. The choice of catalyst held significant importance in the HTL process. Both homogeneous and heterogeneous catalysts have proven effective in enhancing the yield and quality of biocrude when appropriately employed. Nanocatalysts, particularly those utilizing Ni, have been explored due to their ability to enhance biocrude production at lower temperatures, a development that could facilitate the commercialization of HTL [189]. To

address the cost associated with reductive noble metal catalysts like Pt and Ru, efforts have been made to explore the use of a CuZnAl catalyst. This catalyst has been observed to have the capability to transform furfural into cyclopentanone through hydrogenation and hydrogenolysis processes. Furthermore, the activity of these catalysts could be adjusted by modifying the composition of Cu or Zn oxide and they could be recycled through reactivation in a hydrogen gas environment [190]. For industrial purposes, carbonaceous materials like carbon nanotubes (CNTs) supported on activated carbon were advantageous. These materials offered a substantial surface area and the ability to recycle precious metals making them well-suited for the task [191].To ensure the longevity of catalysts during hydrothermal processes, it is crucial to use catalysts that exhibited excellent hydrothermal stability.

2.3 Description of the products

The products obtained by biomass liquefaction are biocrude, gases and solid residues. Their physical and chemical properties undergo variation as per the type of feedstock and also the conditions employed for their production. Biocrude constitutes of enormous compounds which are evident from their gas chromatography analysis. The liquid portion is collected by a suitable solvent to obtain two phases, one is the oil phase while the other is the aqueous phase. Brown et al. [192] degraded constituents such as carbohydrates, proteins, lipids and algae nans in microalgae to produce a dark, viscous and energy-dense liquid product called biocrude. Its energy content was around 75-90% of that of petroleum fuel. However, the large content of nitrogen in microalgae biocrude leads to NO_x emissions from them upon combustion [193]. The aqueous phase of the liquid product had abundance of organic matter and nutrients so that it found its use as a source of carbon for heterotrophic strains. Around 20% of organics present in the feedstock originally was yielded as gases in HTL, with CO_2 being the major gaseous product along with H_2. Since most of the oxygen removal from the biocrude occurred by decarboxylation rather than decarbonylation, the CO concentration was less in the gaseous product [194]. The solid residue fraction obtained as a product of HTL of microalgae had lower amounts of hydrogen, nitrogen and sulfur [14]. Solid yields less than 10% were reported by most researchers [176]. The nutrient content of solid residues made them useful as soil conditioners. They could also act as feedstock for pyrolysis or gasification for energy rich products formation. Studies in these fields and their applications have been gaining importance in recent times.

2.3.1 Biocrude

The biocrude/bio-oil or heavy oil obtained through the liquefaction process is a dark, highly viscous liquid characterized by a high carbon, low oxygen content and an overall elevated HHV value (25 to 40 MJ kg^{-1}) [128]. The chemical makeup of biocrude is influenced by various liquefaction reaction conditions like temperature, solvent, solvent polarity, reaction time and the gas used as a reaction atmosphere. However, the biomass composition entering the liquefaction process has the most substantial impact. Biocrude constitutes a complex mixture of numerous compounds with varying molecular weights. While GC-MS analysis provides a partial characterization of these oils, many heavy compounds do not elute into the column, remaining uncharacterized. It comprises of a complex blend of chemical compounds, encompassing ketones, aldehydes, phenolics, phenyl derivatives, fatty acids, esters, fatty acid alkyl esters, alcohols, polyols, unsaturated hydrocarbons, saturated hydrocarbons and a fraction of nitrogenous compounds like amines and amides [195]. Garcia Alba et al. [194] presented the elemental composition (in mass fraction) of biocrude from *Desmodesmus* sp. at 375 °C and 5 min reaction time. N: 6.3%, C: 74.5%, H: 8.6% and O: 10.5% was obtained in biocrude. With a substantially lower oxygen content compared to original microalgae cells (33.9%), its higher heating value (HHV) reached 35.4 MJ kg^{-1}. Ye et al. [153] explored swine manure HTL produced biocrude, noting a broader distillation temperature range than diesel and gasoline with a gross heating value of 36.41 MJ kg^{-1}, acidity at 5.02 and viscosity at 2.78 cP. Distillate fractions contained mainly esters, alkanes and alkenes showing greater stability than products from traditional liquefaction or pyrolysis. Run et al. [156] investigated rice stalk HTL, revealing kinematic viscosity (5.63 mm^2 s^{-1}) and 2.2% moisture content. Biocrude properties depended on feedstock and HTL conditions, but potential upgrades could make it commercially viable. Pedersen et al. [196] conducted fractional distillation of HTL-derived biocrude yielding six distillate fractions and a residue. The lighter distillate fraction contained light oxygenates, offering potential for chemical production. A ketone mixture obtained could serve as a precursor for liquid transport fuels. Biocrude versatility extended to producing high-value fuels like jet fuel, gasoline, diesel and hydrogen-rich gas. Tzanetis et al. [197] devised a method involving hydrotreatment to reduce oxygen content, producing a range of fuels and a waste aqueous stream. Fractional distillation isolated individual fractions, with recirculated H_2 rich gas aiding the upgrading process. Beyond fuels, biocrude holds promise for synthesizing various industrial chemicals as well [198].

2.3.2 Aqueous phase

In batch processes, the aqueous phase is a secondary product, while in continuous operations, it emerges as a side stream of process water. Around 25% to 50% of the carbon in biomass can be directed to the aqueous phase [199], emphasizing the necessity for techniques and methodologies to decipher its properties and composition. The management of the aqueous phase extracted post liquefaction is crucial due to its elevated organic matter and nutrient content [176]. It is primarily composed of low molecular weight organic acids, polyols, a substantial fraction of phenolic compounds and ketones, along with a minor amount of sugar. The dominant fraction, acids, contributes to 40%–50% of the aqueous phase weight, constituting a blend of acetic acid, lactic acid, glycolic acid, propionic acid, formic acid, butanoic acid, pentenoic acid and butenedioic acid. Alcohols and polyols encompass methanol, glycol, ethylene glycol, propylene glycol, catechol, glycerol, D-glucitol, xylitol and ribitol [200]. The substantial volume of the aqueous phase generated in HTL raised concerns about economic efficiency and utilization. Recirculating the aqueous phase as a solvent in continuous operations or for subsequent HTL runs in a batch cycle could enhance its utilization, benefiting bio-oil and char yield and quality. This approach reduced the need for water treatment and conserved fresh water. Studies, like Zhu et al. [201] reported increased bio-oil yield from 34.9% to 38.4% after recirculation in barley straw HTL. This enhancement was linked to the presence of organic compounds in the aqueous phase, expediting the overall breakdown of biomass. Biller et al. [202] explored the impact of recirculating the aqueous phase during the HTL of dry distillers' grain with K_2CO_3. They noted a rise in bio-oil yield from 44.3% to 60% after the initial recirculation, along with an increase in solid residue yield from 1.2% to 14% after the seventh recirculation run. Another intriguing method, aside from straightforward recycling into the culture medium, involved gasifying this phase under supercritical conditions to generate a hydrogen-rich fuel gas. Following this procedure, the aim was for most nutrients to ideally remain dissolved in the resulting aqueous phase, enabling their recycling back to the growth step [14]. Many studies suggested other possible options such as the catalytic cracking of the aqueous phase product to obtain valuable chemicals such as olefins and aromatic hydrocarbons such as benzene, toluene and xylene. Miyata et al. [203] developed a method to separate the light water-soluble fraction (by freeze drying) and heavy water-soluble fraction (by water removal) and conducted catalytic cracking on separated fractions, producing an olefins plus BTX yield of 49% and 14%, respectively. Even though

there is a lot of potential, more knowledge is needed before one can aptly implement the aqueous phase.

2.3.3 Gases

Gas is another by-product derived from the liquefaction process. Owing to the process's suboptimal gas composition and the prioritization of biocrude, gas is typically either not analyzed or amalgamated with other products [204]. Typically, the gas fraction constituted 5–15 wt. % (in between 250–375 °C) of the overall product distribution from liquefaction [133]. Gas yields were notably increased at temperatures near and above the critical point of water. About 20% of the initial organics in microalgae feedstock were typically found in the gaseous fraction [192,193]. The primary gas product of liquefaction was CO_2, followed by H_2. CO_2 and CO primarily resulted from the breakdown of oxygen-containing groups in lignocellulosic biomass through decarboxylation and decarbonylation reactions. CH_4 was generated by the decomposition of a methoxy group, while other short-chain hydrocarbons (C_2–C_3) were formed during the cracking of long-chain hydrocarbons and aromatics [135]. Many authors noted a decrease in CO_2 concentration beyond the critical point of water, accompanied by an increase in small hydrocarbons (CH_4 and C_2). The limited presence of CO in the literature suggested that oxygen removal in liquefaction was primarily through decarboxylation or that CO readily reacted to form CO_2 and H_2 via the water-gas shift reaction, particularly in the presence of salts from the growth medium [205]. Alba et al. [194] explored microalgae liquefaction across temperatures from 175 to 450 °C. They found minimal gas yield around 200 °C (negligible) and 15% at 300 °C. As the temperature exceeded 375 °C, the gas yield notably increased to 24% and reached 47.4% at 450 °C, while other product fractions decreased. They suggested that the generated CO_2 could be redirected to the microalgae production system and the H_2 might be utilized for additional hydrotreating of the produced biocrude. Consequently, this fraction presented an appealing prospect from a biorefinery integration perspective. At 350 °C, Brown et al. [192] reported the gas composition as follows: 662 mmol mol^{-1} CO_2, 297 mmol mol^{-1} H_2 and trace amounts of CH_4, N_2, C_2H_4 and C_2H_6. Moreover, extending retention time at subcritical and supercritical temperatures led to a rise in gas yield. This increase in the gas fraction could be attributed to enhanced cracking of oil and char. While researchers have examined gas quantification and composition in lab-scale models, there is limited data on the gas phase's feasibility and potential for large-scale

operations. Future studies could explore variations in gas yield and composition during scaling operations and methods to enhance light hydrocarbon fractions in obtained gases [128].

2.3.4 Biochar

The solid by-product obtained through liquefaction is referred to as solid residue, residue, char or biochar. The biochar yield is highly dependent on the biomass type and composition, varying from approximately 5% to 60% by weight. Biomass rich in lignin generally yielded more biochar compared to those with higher cellulose and hemicellulose content [200,206]. The yield and chemical composition of biochar were significantly influenced by process parameters such as temperature, pressure, retention time, biomass-to-solvent ratio and the type and concentration of the catalyst. Biochar is characterized by high carbon (C) and hydrogen (H) content, low oxygen (O) content and a high HHV in comparison to biomass [207]. For solid residue derived from lignocellulosic biomass, the carbon content ranged from 55% to 78% by weight, hydrogen content ranged from 4% to 6% by weight and oxygen content ranged from 15% to 35% by weight. Additionally, it was observed that the nitrogen percentage was higher in solid residue compared to biomass [208]. Jena et al. [209] provided an elemental composition of the solid residue obtained from HTL of *Spirulina platensis* at 350 °C and 60 min of reaction time: 11.82% carbon (C), 1.81% hydrogen (H), 1.41% nitrogen (N) and 0.61% sulfur (S). These solid residues likely contained nutrients, making them appealing as a soil amendment. Demirbas et al. [210] explored the impact of lignin content on oil and char yield, revealing that biomass with a high lignin content (41–48 wt. %) generated a solid residue in the range of 40–50 wt. %. In contrast, biomass with a low lignin content (14–27 wt. %, cellulose: 45–50 wt. %) yielded a solid residue in the range of 21–26 wt. %.

The biochar produced through liquefaction exhibited promising qualities, making it suitable for applications in the energy sector as feedstock for subsequent thermochemical processes, such as pyrolysis or gasification, for soil enhancement and as an adsorbent. Notably, the biochar demonstrated high hydrophobicity, facilitating easy handling and storage by resisting humidity effectively [211]. While the biochar could have positive effects on soil fertility, its potential negative impact on plant growth necessitated pre-treatment [212]. The biochar's mineral and organic contents, which vary based on biomass sources, might include a high C:N ratio and low mineral N, or vice versa, along with other minerals. Investigating the biochar's interaction with fertilizer was crucial to ensure proper plant growth without

leaving behind excess nitrogen that could release toxic chemicals [213]. The biochar also served as an effective adsorbent for eliminating pollutants such as heavy metals and organic substances from flue gas, water and wastewater. In a study by Liu et al. [207], the characteristics of biochar derived from HTL of pinewood and rice husks were examined to assess their potential for lead removal from an aqueous solution. The biochar exhibited more irregular surfaces and developed oxygen-containing functional groups. The maximum lead adsorption capacity was found to be 2.40 to 4.25 mg/g for rice husks and pinewood biochar, respectively. While biochar boasted high energy density and superior qualities compared to biomass for various applications, leveraging it with current technology requires additional quality work to ensure compliance with environmental standards and a more comprehensive understanding of its life cycle assessment.

2.4 Summary of the chapter

This chapter presented a detailed overview of the literature related to the objectives of this thesis work. They have been summarized below:

- A detailed account of various modes of liquefaction along with the impact of various operational parameters on it was provided.
- A detailed portrayal of the products derived from the liquefaction process has been described here.

CHAPTER 3

MOTIVATION & OBJECTIVES

3.1 Research motivation

The motivation of this research has been based on the broad area of waste management of organic biomass wastes by means of renewable techniques for energy generation. The focus has been on fruit wastes from *Citrus limetta* processing industries after juice extraction as they are required to be managed efficiently instead of disposing them of without any value addition. The current state of research demonstrates the utilization of cost-effective, biodegradable and readily accessible *Citrus limetta* fruit wastes mostly as a biosorbent and biodiesel. Instances of their application in various thermochemical conversion processes with detailed analysis of the products have been limited and needs to be explored. This research addresses the pressing issue of waste disposal in fruit processing industries by delving into the liquefaction of such fruit residues. To enhance both yield and product quality, a rarely used high-polarity hydrogen-donor solvent has been employed here. The consequences of different operational limits on the quantity and quality of products obtained by liquefaction and co-liquefaction, owing to changes that they bring about has been selected to be the area of concern for the authors as very few research works have been found on them till date. Notably, the experiments conducted here have deviated from the typically stringent conditions of high temperature and high pressure associated with liquefaction, opting for milder conditions. Moreover, the co-liquefaction of fruit wastes, an underexplored area, was investigated, holding potential benefits for total waste disposal of fruit juice processing industries. This research thus strives to contribute novel insights and solutions to the multifaceted challenges in biofuel production and waste management.

3.2 Objectives of the research

Based on the knowledge gaps on research of *Citrus limetta* fruit waste biomass and their liquefaction approaches and a thorough review of the literature, the objectives of this thesis work have been established. They are categorized as follows:

1. Solvothermal liquefaction of *Citrus limetta* fruit wastes at variable biomass-to-solvent ratios.

2. Solvothermal liquefaction of *Citrus limetta* fruit wastes at variable temperatures and biomass-to-solvent ratios.
3. Solvothermal co-liquefaction of *Citrus limetta* fruit wastes at variable biomass-to-solvent ratios.
4. Solvothermal co-liquefaction of *Citrus limetta* fruit wastes at variable temperatures and biomass-to-solvent ratios.

These objectives have been accomplished followed by an extensive characterization of the liquid and solid products obtained, thereby accessing their potentiality for future applications as biofuels in comparison to conventional fossil fuels.

CHAPTER 4

MATERIALS & METHODS

4.1 Materials

Sweet lime or *Citrus limetta* wastes (peel and juice extracted pulp) were collected from a juice shop within the academic complex of IIT Guwahati, Assam, Bharat campus. The collected pulp sample was further vacuum filtered to remove any remaining juice from it, while the peel was used as it is. The solvent methanol (CH_3OH) that was used was a reagent grade chemical (Make: Merck).

4.2 Characterization of biomass

Information on the proximate and ultimate analysis of biomass is crucial for understanding its potential as a renewable energy source and for assessing its suitability for various applications in its thermochemical conversion. It also helps in optimizing the design of biomass conversion processes and identify strategies for enhancing the efficiency and environmental performance of these technologies [214]. Therefore, the proximate analysis of *Citrus limetta* pulp (CLPU) and *Citrus limetta* peel (CLPE) biomass (as received basis) to investigate its moisture content (MC), ash content, volatile matter (VM) and fixed carbon (FC) content was carried out as per ASTM standards ASTM E871-82, ASTM E872-82 and ASTM D1102-84 respectively [215]. The determination of moisture content involved assessing the weight loss of the sample under precisely controlled conditions of temperature, time and atmosphere, considering sample weight and equipment specifications. Following the ASTM E871-82 standard method [216], 50 g of the sample was placed in a pre-weighed container and placed within a hot air oven (Make: Relitech) maintained at 103 °C for a duration of 16 h. Subsequently, the sample was removed, dried in a desiccator and weighed. The sample was then returned to the oven for an additional 2 h duration at the same temperature. These steps were iterated until the total weight change between consecutive weighings varied by less than 0.2%, at which point the final weight was recorded. The moisture content in the sample was calculated using the following formula as shown in Equation 4.2.1:

$$\text{Moisture content, wt. \%} = \left[\frac{(W_i - W_f)}{(W_i - W_c)}\right] \times 100 \qquad (4.2.1)$$

where, W_c = container weight, g, W_i = initial weight, g & W_f = final weight, g.

The determination of volatile matter involves assessing the weight loss resulting from heating the sample under rigorously controlled conditions. The ASTM E872-82 [217] standard method was employed, wherein a crucible was weighed and loaded with 1 g of the sample. The crucible with the sample was then placed in a muffle furnace (Make: Ikon Instruments Pvt. Ltd.) set at 950 ± 20 °C. The furnace was maintained at 950 °C for precisely 7 min, after which the crucible was removed and cooled in a desiccator. The final weight of the crucible with the sample was recorded to the nearest 0.1 mg. Subsequently, the following formula as depicted in Equation 4.2.2 and 4.2.3 were utilized for the calculations:

$$\text{Weight loss, \%} = 100 \times \left[\frac{(W_i - W_f)}{(W_i - W_c)}\right] = A \qquad (4.2.2)$$

where, W_c = weight of crucible & cover, g, W_i = initial weight, g and W_f = final weight, g.

$$\text{Volatile matter in analysis sample, \%} = A - B \qquad (4.2.3)$$

where, A = weight loss, % and B = moisture, %.

The determination of ash content in the sample is derived as the percentage of residue remaining after dry oxidation (580-600 °C), providing a measure of the mineral content and other inorganic matter present. The standard method ASTM D1102-84 [218] was applied for this procedure. An empty crucible and cover were ignited in a muffle furnace (Make: Ikon Instruments Pvt. Ltd.) at 600 °C and subsequently cooled in a desiccator. Subsequently, 2 g of the test sample was placed in the crucible and subjected to heating in a hot air oven (Make: Relitech) at 100 to 105 °C. After an hour, it was removed, cooled in a desiccator and weighed. These drying and weighing steps were repeated until the weight remained constant within 0.1 mg. The weight of the oven-dry test specimen was determined by subtracting the weight of the crucible from the weight of the crucible plus the sample. Following this, the crucible was placed in the muffle furnace and ignited until all the carbon was eliminated, reaching the final ignition temperature of 600 °C for a duration of 6 h. Finally, the weight of the crucible was recorded after cooling in a desiccator. The ash content was calculated using the following formula as given in Equation 4.2.4:

$$\text{Ash content, wt. \%} = \left(\frac{W_1}{W_2}\right) \times 100 \qquad (4.2.4)$$

where, W_1 = weight of ash, g and W_2 = weight of oven-dry sample, g.

Ultimate analysis of the biomass in CHNS elemental analyzer (Model: EuroEA3000, Make: Euro Vector, Italy), the schematic of which has been illustrated in Figure 4.2.1, provided its mass % of elemental composition. CHNS elemental analyzers offers a rapid method for determining carbon, hydrogen, nitrogen and sulfur in organic matrices and various materials. The system employs 'Pressurized Oxygen Injection System' (TurboFlash Combustion Technology), allowing independent programming of oxygen volume and pressure. This technology provides comprehensive flexibility and control over the combustion process. Elemental analysis is facilitated using the Callidus SW software, enabling both full automation and manual adjustments through the instrument keypad. Callidus manages analytical parameters, data integration and reprocessing. In the combustion process, conducted in a furnace at 1000 °C, C is transformed into CO_2, H_2 into H_2O, N into N_2 gas/oxides of N and S into SO_2. If other elements like Cl are present, they are also converted to combustion products, such as HCl. Various absorbents are employed to eliminate these additional combustion products, along with some principal elements (e.g. S), if determination of these elements is unnecessary. The combustion products, carried by an inert carrier gas like He are directed over heated (approximately 600 °C) high-purity Cu situated either at the base of the combustion chamber or in a separate furnace. This Cu serves to eliminate any unconsumed O_2 from the initial combustion and convert oxides of N to N_2 gas. The gases then pass through absorbent traps to retain only CO_2, H_2O, N_2 and SO_2. Detection of the gases can be achieved through various methods, including GC separation followed by quantification using thermal conductivity detection. Calibration for each element requires the use of high-purity compound such as benzoic acid. For this process a pure and contaminant-free sample weighing 4-5 mg was taken.

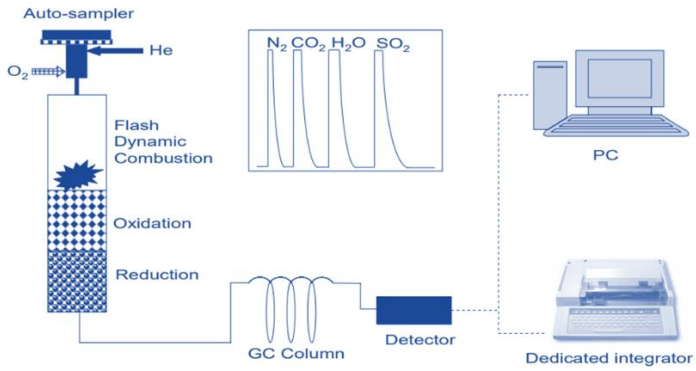

Figure 4.2.1 Schematic diagram of CHNS elemental analyzer [219].

The sample was introduced from the Autosampler into the reactor, accompanied by synchronized injection of pressurized oxygen provided by TurboFlash for optimal combustion. Gases such as NO_x, CO_2, H_2O, SO_2/SO_3 resulted from the combustion stage. The reduction step eliminated excess oxygen, converting the gas mixture into N_2, CO_2, H_2O and SO_2. The gases are time-separated by a GC column in less than 5 min with peaks detected by TCD. The oxygen percentage in the biomass was found by deducting the C, H, N and S content in mass % from 100, i.e., O (mass %) = 100 – (C mass % + H mass % + N mass % + S mass %) [219].

The energy content of biomass which is typically expressed as its calorific value or higher heating value (HHV), represents the amount of energy that can be extracted from the biomass by burning or other thermal processes. It aids in identifying whether the biomass is efficient for energy production. Thus, to determine the higher heating value (HHV) of the biomass, filtrate, remaining methanol solvent, biochar and biocrude a bomb calorimeter set-up manufactured by HAMCO Instruments Pvt. Ltd. in Bharat was used. Its schematic diagram has been depicted in Figure 4.2.2. A bomb calorimeter comprises of several component parts.

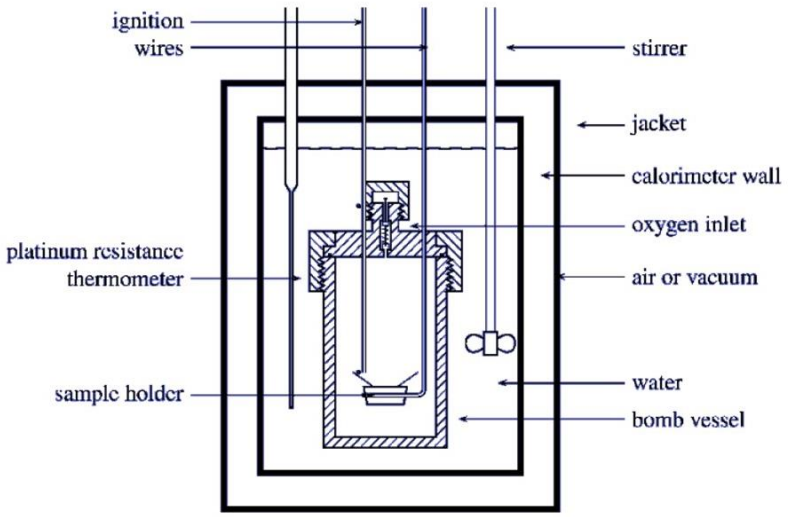

Figure 4.2.2 Schematic diagram of bomb calorimeter [220].

The outermost section is a cylindrical stainless-steel vessel known as the bomb, where the combustion of solid or liquid fuel occurs. The bomb is equipped with a lid to ensure that the bomb is air tight, thus, preventing leakage of any combustion gas. The lid includes spacing for two stainless steel electrodes and an oxygen valve, which supplies oxygen for combustion.

The bomb is positioned within a calorimeter surrounded by a water and air jacket to minimize heat losses caused by radiation. Within the calorimeter, there is a Beckmann's thermometer capable of reading temperature differences to 1/100th of a degree. For the test, 1 g of powdered sample was taken and the calorimeter was filled with 2l water. The sample was then placed in a stainless-steel crucible. Surrounding the sample is iron fuse wire, connected to the lower end of the two electrodes. These electrodes extend through the base of the bomb and link the fuse wire to an electric circuit. The fuel can be ignited by closing the electric circuit. The bomb was connected to an O_2 cylinder and O_2 was introduced into the bomb through the valve until the pressure gauge indicated a pressure of 26 kg/cm^2. Ignition of the fuel was initiated by passing a current through the fuse wire. The temperatures of both the bomb and the water started to rise and readings on the thermometer were recorded. Once the temperature exhibited a steady rate of decline, readings were taken at regular intervals for an additional 5 min and the final rise in temperature was noted. Thereafter, the following formula shown in Equation 4.2.5 was used to calculate the HHV of the sample:

$$\text{HHV, MJ/kg} = \frac{\Delta T \times W - (CV_t + CV_w)}{M} \times 4.184 \times 10^{-3} \quad (4.2.5)$$

where, ΔT = rise in temperature, °C

W = water equivalent, cal/°C

CV_t = calorific value of thread, cal

CV_w = calorific value of wire, cal

M = Mass of the sample, g.

4.3 Experimental procedure of solvothermal liquefaction and co-liquefaction of *Citrus limetta* at variable temperatures and biomass-to-solvent ratios

Liquefaction of CLPU and CLPE waste biomass was done in a batch stirred autoclave reactor (Make: Lelesil, Bharat) of 500 ml volume, the schematic diagram of which has been shown in Figure 4.3.1. CLPU biomass along with solvent i.e., CH_3OH was fed to reactor at 1:2, 1:3 and 1:4 biomass-to-solvent ratios. These biomass-to-solvent ratios were selected on the basis of changing biomass weight method where the amount of biomass was changed in each case while fixing the amount of solvent. The batches of co-liquefaction experiments of CLPE and CLPU were also processed in the same reactor. The feed ratio of both the biomasses were

chosen based on average weight ratio of peel waste and pulp waste obtained after extraction of juice from 10 individual samples of *Citrus limetta* fruit. This attempt was made to obtain a normalized feed ratio of the biomasses to be co-liquefied as the wastes from each fruit generally varies in weight depending on its size and weight. In this way the peel to pulp feed ratio was calculated to be 1.2 and the biomasses were taken in this ratio on weight basis for each experimental run. Thereafter, the reactor was positioned within the furnace possessing 15-20 °C min^{-1} heating rate. Then the reactor was closed properly and the fittings were checked and tightened to ensure that no leakage occurred during the reaction. At first, 20 bar of N_2 was purged through the reactor and leak tests were performed to identify any leakage that might exist in reactor fittings and hamper with the results obtained. Thereafter, the N_2 gas was totally released from the reactor prior to starting of furnace heating. The desirable reactor temperature was set to 260 °C for the study where variation of biomass-to-solvent ratio was done at a fixed temperature condition. While for variable temperature study it was set between 240 °C and 280 °C respectively at variable biomass-to-solvent ratios of 1:2, 1:3 and 1:4 while stirring speed of the rotor to 200 rpm to begin the reaction. The system pressure was allowed to escalate freely until the temperature of the reaction was achieved. The reactor was held for 30 min residence time at the reaction temperature. It was observed that the pressure within the reactor during the reaction time remained within 90-130 bar. The selected reaction conditions were specific to equipment specifications and literature review [66,68,85,221] and were finalized on the basis of test runs in the lab-scale set up. The furnace was switched off at the end of residence time and then the reactor was quenched immediately by an ice water circulating pump to reduce the reactor temperature by 80-100 °C in 5 min. Further, the cooling process was continued until the reactor temperature dropped to room temperature.

The products inside the reactor were a mixture of semi-viscous liquid and solid char that were extracted as per procedure adapted from literature [135,222,223]. They were subjected to filtration with a Whatman 40 filter paper using a vacuum pump until all the liquid had been separated from solid residue. This filtrate was analyzed for its physical properties and HHV and then stored separately for solvent extraction. Meanwhile, the reactor interior and the stirrer were washed with 40 ml of acetone to remove any sticky or greasy product being attached to them. This was collected and stored in a separate sample bottle. The filter paper having the solid residue was further subjected to Soxhlet extraction using acetone to remove any greasy viscous substance stuck to them. The remaining acetone after extraction was also stored along

with the acetone that had been used for washing for further processing. The solid residue termed as biochar was dried at 103 °C in a hot air oven for 3 h and stored properly for further characterization. Thereafter, the filtrate was taken in a pear-shaped round bottom flask and evaporation at 60 °C in a vacuum rotary evaporator under reduced pressure to remove the unreacted methanol solvent from it in a separate collection flask was carried out.

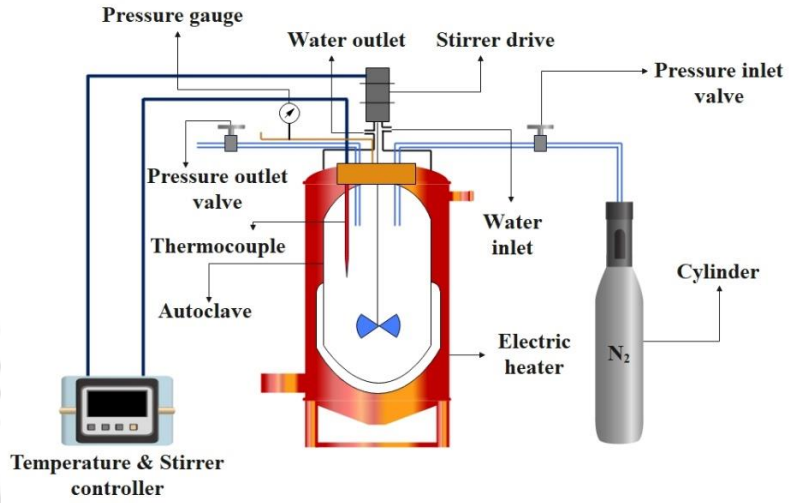

Figure 4.3.1 Schematic diagram of batch stirred autoclave reactor set up.

This was termed as remaining methanol solvent (MSR). The volume of the MSR was recorded and it was stored for further analysis. After methanol solvent removal, some dark and viscous liquid could be seen to be remaining in the round bottom flask. Now, the acetone that had been used for reactor washing as well as that obtained from Soxhlet extraction were further added to this flask and evaporation of the solution was done to remove the acetone and aqueous part of the product liquid to get a highly viscous and sticky bitumen-like product that was termed as 'biocrude' and was stored for characterization [224–227]. However, it was possible that some light hydrocarbons might have evaporated during the solvent and water removal from the biocrude. The same reaction procedure was repeated using CLPE biomass and co-liquefaction feed of CLPE and CLPU at 1:2, 1:3 and 1:4 biomass-to-solvent ratios and 240-280 °C temperature conditions and the products were collected and stored for further characterization. Further regarding the selection of these parameters, the primary aim was to conduct the liquefaction and co-liquefaction at moderate temperature and pressure conditions. On rising the temperature beyond 280°C, the corresponding pressure in the reactor shoots up and therefore it was aimed to conduct these experiments at moderate pressure of <120-130atm. However, as discussed in subsequent sections, success in obtaining optimum results at

selected moderate parameters was possible, especially on comparing the results of this research with the literature ones. The yield of the filtrate and biochar obtained in wt. %, was the ratio of the product found to that of the raw feed material as well as solvent. The total yield of the gaseous products and losses incurred through solvent retrieval were termed collectively as 'yield of others', that was found by difference [228]. However, the yield of the biocrude obtained in wt. % was the ratio of biocrude obtained after solvent separation to that of the raw feedstock used. The formula for calculation of the same has been provided in Equations 4.3.1 to 4.3.4 below:

$$\text{Yield of filtrate, wt.\%} = \frac{\text{Mass of liquid product from liquefaction}}{\text{Mass of raw feed biomass + Mass of solvent}} \times 100 \quad (4.3.1)$$

$$\text{Yield of biochar, wt.\%} = \frac{\text{Mass of solid product from liquefaction}}{\text{Mass of raw feed biomass + Mass of solvent}} \times 100 \quad (4.3.2)$$

$$\text{Yield of others}^{*}\text{, wt.\%} = 100 - (\text{Yield of filtrate, wt.\%} + \text{Yield of biochar, wt.\%}) \quad (4.3.3)$$

$$\text{Yield of biocrude, wt.\%} = \frac{\text{Mass of biocrude obtained after solvent separation}}{\text{Mass of raw feed biomass}} \times 100 \quad (4.3.4)$$

'*' corresponds to the total yield of the gaseous products and losses incurred through solvent retrieval.

4.4 Characterization of products

Parameters related to fuel and physico-chemical characteristics such as density, viscosity and higher heating value (HHV) hold significant importance in a variety of industries, including transportation, chemical and energy sectors. These characteristics help to determine the performance and suitability of fuels and chemicals for various applications [229]. Therefore, they were determined for the filtrate as well as the subsequent MSR. The density was measured by a 10 ml pycnometer at ambient temperature conditions while the viscosity by an Ostwald's viscometer. The solvent removal in a rotary evaporator (Model: Rotavapor, R 300, Make: Buchi, Switzerland) was done to obtain MSR and biocrude. The rotary evaporator (schematic presented in Figure 4.4.1) facilitates swift single-stage distillation without subjecting the product to excessive stress. The process revolves around the evaporation and condensation of solvents within a rotating evaporating flask under vacuum conditions. Distillation under vacuum proves more efficient and gentler on the product. The product undergoes heating in the evaporating flask via the heating bath. The rotary drive unit ensures even rotation of the evaporating flask, enhancing the liquid's surface area, leading to an

accelerated evaporation rate. This rotational motion also promotes continuous mixing of the product, preventing localized overheating and delayed evaporation. The vapor travels from the evaporating flask through the vapor duct into the cooling section (cooling condenser). In this area, the thermal energy of the vapor is transferred to the coolant fluid, causing the vapor to re-condense. The resulting solvent is collected in the receiving flask, ready for reuse or proper disposal. The distillation capacity is contingent upon factors such as the temperature of the heating bath, pressure in the evaporating flask, rotation speed of the evaporating flask and size of the evaporating flask. To ensure optimal distillation, it is crucial to maintain a temperature difference of at least 40 °C between the coolant and the heating bath. The temperature of the rising vapor should ideally be midway between the temperature of the heating bath and the coolant temperature. For achieving optimal distillation conditions, it is essential to eliminate the energy absorbed by the solvent from the heating bath in the condenser. To accomplish this, the recommended settings were followed, coolant temperature at 20 °C, vapor temperature at 40 °C and heating bath temperature at 60 °C [230].

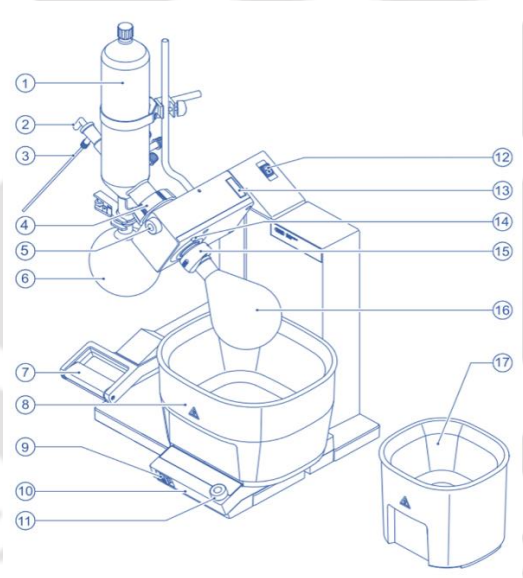

Figure 4.4.1 Schematic diagram of rotary evaporator where 1. Condenser, 2. Glass stopcock, 3. Solvent back feed, 4. Flange nut, 5. Control knob for rotation speed, 6. Receiving flask, 7. Handle for height adjustment, 8. Heating Bath, 9. On/Off master switch for heating bath, 10. Heating Bath Base, 11. Control knob for heating bath temperature setting, 12. On/Off master switch for Rotavapor, 13. Button for angle adjustment, 14. Locking button for rotary drive unit, 15. Combi-clip, 16. Evaporating flask and 17. Heating Bath [230].

The degradation pattern of biomass as well as biochar was found by thermo gravimetric analysis (TGA) trailed by their differential thermogravimetry (DTG). TGA measures the weight loss of a material as a function of temperature or time, under controlled heating conditions. DTG is an extension of TGA that measures the rate of weight loss as a function of temperature, allowing for the identification of different stages of decomposition and the determination of kinetic parameters. TGA involves gradually elevating the temperature of a material within a furnace while measuring its weight using an analytical balance positioned outside the furnace. Mass loss is observed in TGA when a volatile component is released during a thermal event. While chemical processes like combustion lead to mass loss, physical changes such as melting do not. The weight of the sample is graphed against temperature or time to highlight material thermal transitions, such as the loss of solvents and plasticizers in polymers, dehydration in inorganic materials and eventual material disintegration. The TGA instrument comprises a microbalance for measuring the specimen's weight, a furnace and a purified gas system to supply the gas required for TGA experiments. The furnace and data collection (temperature vs. weight) are monitored and controlled using a computer. As the sample's mass changes, the balance generates a corresponding electrical signal. Consequently, the thermal curve is represented on the y-axis, with this electrical signal converted into mass or mass loss [231]. Figure 4.4.2 provides a schematic diagram of a thermogravimetric analysis setup. The TGA equipment (Model: TG 209 F1 Libra, Make: Netzsch, Germany) was used within 25 °C to 900 °C range of temperature with 10 °C min^{-1} heating rate with N_2 gas purging to obtain volatility and thermal stability of the biomass sample. This made it possible to evaluate the biomass's volatile properties and potential for thermal stability.

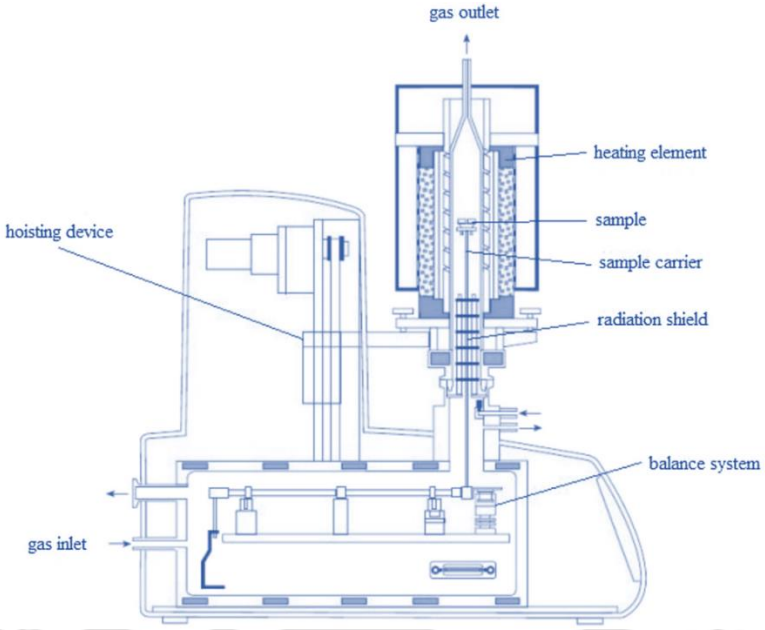

Figure 4.4.2 Schematic diagram of TGA apparatus [231].

The primary chemical bonds and functional groups present in biocrude were examined using Fourier transform infrared (FTIR) spectroscopy. In the FTIR instrument, an interferometer system is utilized, consisting of a source, beam-splitter, moving mirror, fixed mirror and detector. The radiation from the source travels to the beam-splitter, where it is split into two parts. One half travels to a moving mirror, while the other half travels to a fixed mirror. The moving mirror oscillates back and forth at a constant velocity, introducing an optical path difference (δ) as the two reflected beams are recombined at the beam-splitter. This results in constructive and destructive interference, creating an interference pattern. The interference intensity, plotted against the optical path difference is known as an interferogram. The interferogram then passes from the beam-splitter to the sample, where some energy is absorbed and some is transmitted. The transmitted portion reaches the detector. The received interferogram is converted into a spectrum using Fourier transform, transforming the intensity versus optical path difference into an infrared spectrum with intensity versus wavenumber. Attenuated total reflectance (ATR) method was used in this instrument where diamond crystal is used as a sampler. ATR has revolutionized solid and liquid sample analyses in recent years, offering advantages such as requiring no sample preparation and providing good spectral reproducibility. This method relies on total internal reflection, measuring changes occurring in a totally internally reflected infrared beam upon contact with the sample. An infrared beam is directed onto an optically dense crystal with a high refractive index at a specific angle,

creating an evanescent wave that extends beyond the crystal surface into the sample held in contact with the crystal. The evanescent wave, protruding only a few microns beyond the crystal surface and into the sample, may be absorbed or alter the sample. The attenuated energy from each evanescent wave is returned to the IR beam, which exits the opposite end of the crystal and is directed to the detector, generating an infrared spectrum. For ATR analysis, the sample must be in direct contact with the ATR crystal and the refractive index of the crystal must be significantly greater than that of the sample. ATR crystals typically have refractive index values between 2.38 and 4.01, while most solids and liquids have lower refractive indices. The experimental factors affecting the final spectrum include the refractive indices of the ATR crystal and the sample, wavelength of the IR beam, angle of incidence of the IR beam, depth of penetration, number of reflections, quality of the sample contact with the ATR crystal and ATR crystal characteristics [232]. The schematic diagram of FTIR equipment (Model: IRAffinity-1, Make: Shimadzu, Japan) was shown in Figure 4.4.3. It utilized the Shimadzu IR solutions 1.5 software to produce 30 scan spectra with a resolution of 4 cm^{-1} and a wavenumber range of 400–4000 cm^{-1}. It was feasible to recognize certain chemical compounds and molecular structures, as well as to learn more about the chemical characteristics and behaviour of a material, by analyzing the FTIR spectrum.

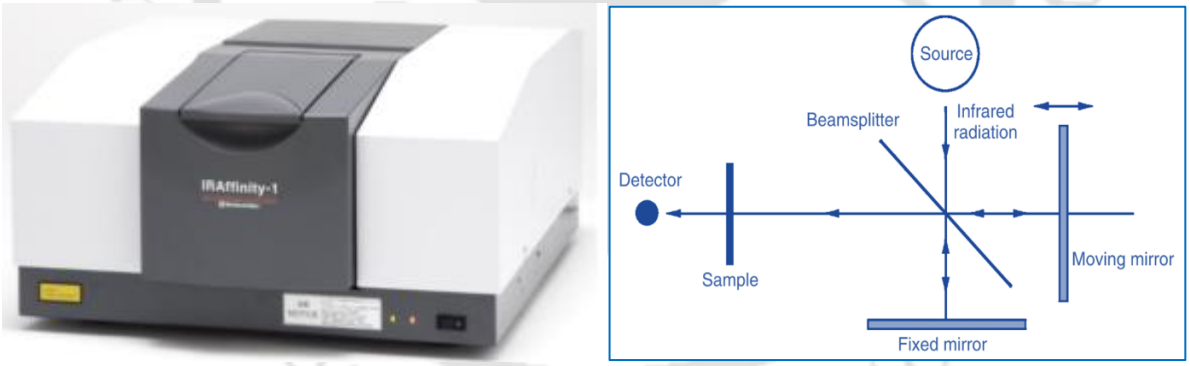

Figure 4.4.3 Schematic diagram of FTIR spectrometer [233].

The molecular structure, dynamics and interactions of chemical compounds were studied in depth using proton nuclear magnetic resonance spectroscopy (^{1}H NMR). The NMR instrument (schematic shown in Figure. 4.4.4) comprises a sample holder, NMR magnet, probe, sweep generator, radio frequency transmitter & receiver and readout systems. Radio waves serve as the energy source in NMR. Radiation in the radiofrequency region of the electromagnetic spectrum, known as RF radiation possesses long wavelengths, resulting in

low frequency and energy. Biocrude dissolved in a solvent such as $CdCl_3$, is placed in a magnetic field. A radio frequency generator then irradiates the biocrude sample with a short pulse of radiation inducing resonance. When the nuclei return to their lower energy state, the detector measures the released energy, recording a spectrum. Protons in different environments absorb radio frequency radiations at distinct frequencies making them distinguishable by NMR. The frequency at which a particular proton absorbs is determined by its electronic environment. The NMR spectrometer employs a narrow range of frequencies to achieve the resonance of all protons. Only nuclei containing odd mass numbers, such as ^1H, produces NMR signals. NMR allows for the mapping of the carbon and hydrogen framework of an organic molecule. An NMR spectrum plots the intensity of a signal against its chemical shift, measured in parts per million (ppm). The common scale for chemical shifts is called the δ (delta) scale [234]. A chemical shift expresses absorptions as a fraction of the NMR operating frequency, rendering it independent of the spectrometer used to record a spectrum. A 600MHz NMR equipment (Make: Bruker, USA) for 16 number of scans for proton was used to do the ^1H NMR. The results of this investigation matched up with those from the FTIR spectrum.

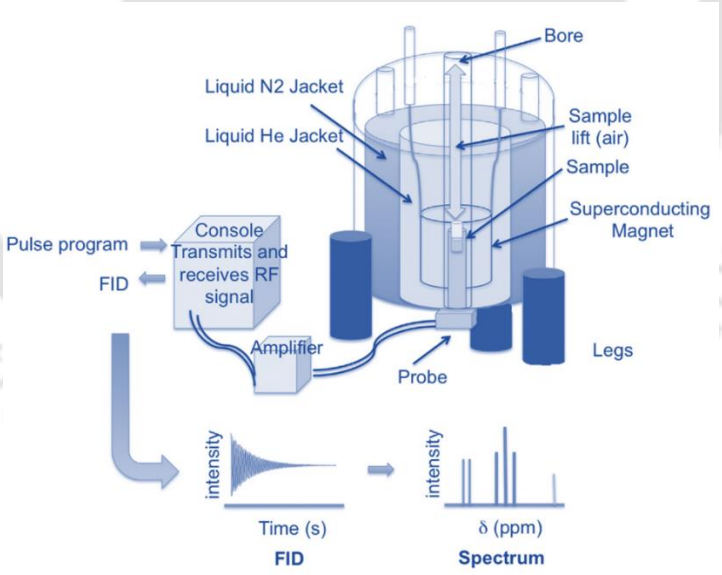

Figure 4.4.4 Schematic diagram of NMR spectrometer [235].

The components of biocrude were identified and measured using the gas chromatography mass spectrometry (GC-MS) method. This method combines the capabilities of gas chromatography for separation with the sensitivity and selectivity of mass spectrometry for detection. GC process (schematic diagram shown in Figure 4.4.5 a) involves passing a

mixture through a long capillary column coated with a liquid (the liquid stationary phase) in a gas stream causing the components to separate and elute from the column. In a basic GC instrument, emerging components are detected, either by burning them in a flame (popularly using a flame ionization detector, FID) or passing them to the atmosphere through another detector. Detected components are recorded as peaks on a gas chromatogram, with information about their identity inferred from peak area, height and retention time. In stark contrast, a mass spectrometer is generally less effective with mixtures. When a single substance is introduced, its mass spectrum is obtained through various ionization methods, facilitating positive identification or confirmation of its molecular structure. However, if a mixture is analyzed in the MS (schematic diagram shown in Figure 4.4.5 b), the resulting mass spectrum becomes a complex summation of all components, posing challenges for positive identification. GC/MS instrument is capable of separating, positively identifying and quantifying complex mixtures, provided they could be vaporized (schematic diagram shown in Figure 4.4.5 c). The mobile phase carrying mixture components along a gas chromatographic column is a gas, typically He. This gas flows at or near atmospheric pressure at a rate of generally 0.5 to 3.0 mL min^{-1} and exits the capillary column into the ion source of the mass spectrometer. In GC/MS systems, ion sources typically operate at about 2 x 10^{-5} Torr with 1.0 mL min^{-1} He for electron ionization to about 3 x 10^{-4} Torr for chemical ionization. The significant pressure change between the chromatographic column's end and the ion source causes the gas to expand to a flow equivalent to several liters per minute. Hence, large pumps are needed to remove the excess gas and maintain vacuum inside the source near the optimum for ionization. As each mixture component elutes and enters the ion source, it is ionized either by an electron beam (electron ionization) or by a reagent gas (chemical ionization). The resulting ions are analyzed by the mass spectrometer to produce a mass spectrum. For capillary GC, separated mixture components elute in a short time interval, often just a few seconds. Consequently, the concentration of any one component in the ion source is not constant while its mass spectrum is obtained. It starts from zero, rises rapidly to a maximum and then drops rapidly back to zero. At the end of a GC/MS run, all data are stored in the computer in the form of a mass spectrum for every scan conducted for a sample [236].

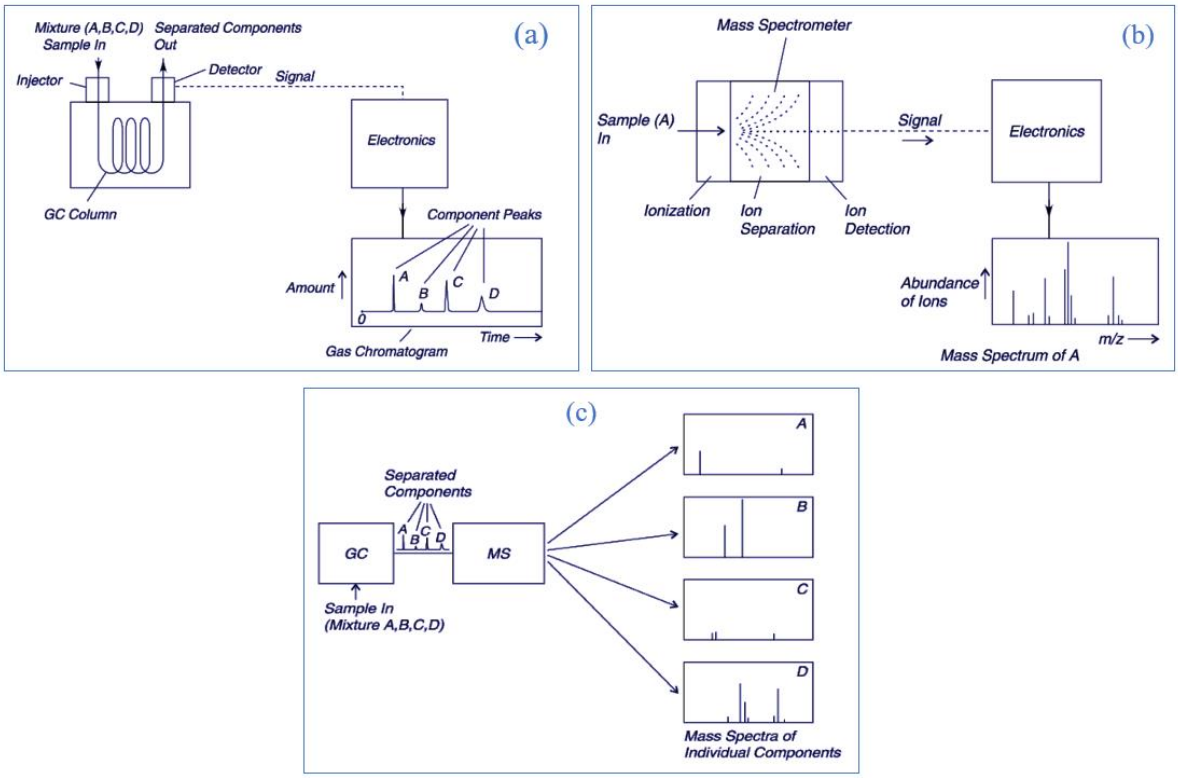

Figure 4.4.5 Schematic diagram of (a) gas chromatograph showing an injection of a mixture onto a GC column, their separation, detection and display (gas chromatogram), (b) mass spectrometer where after inserting a sample (A) it is ionized, the ions are separated according to their m/z value and identified, (c) GC/MS combination [236].

It offers thorough details on the chemical makeup of a sample and is a very sensitive technology with the capacity to find minute quantities of substances in intricate matrices. A GC-MS apparatus of make Perkin Elmer and model Clarus 680 GC/600C MS with a capillary column arrangement measuring 60 m in length and a film coating of 250 m was employed. The column was equipped with a split type injector system having a 10:1 split specific ratio and 280 °C temperature. The use of a carrier gas with a purity of 99.95% He and rate of flow 1ml min^{-1} was made. The oven temperature of GC was first set at 40 °C for duration 2 min, then it was raised to 140 °C at a rate of 10 °C per min for 2 min. Finally, the ramp was lowered to 7 °C per min to reach 300 °C and maintained there for 5 min. The National Institute of Standards and Technology (NIST) 2014 MS library was referred to detect the compounds present in the biocrude.

X-ray-diffraction (XRD) can provide valuable insights into the physical properties and behaviour of a material, such as its chemical composition and crystallography. A diffractometer utilizes a single-wavelength X-ray beam to investigate polycrystalline specimens. By continuously varying the incident angle of the X-ray beam, a diffraction intensity spectrum versus the angle between the incident and diffraction beams is recorded. Diffractometry allows for the identification of crystal structure and quality by analyzing and comparing the spectrum with a database. The primary function of a diffractometer is to detect X-ray diffraction from materials and record the diffraction intensity across a range of diffraction angles (2θ). Figure 4.4.6 illustrated the schematic diagram of an X-ray diffractometer, consisting of the X-ray source, specimen and detector. In the diffractometer setup, an X-ray beam generated by an X-ray tube passes through specialized slits, known as Soller slits, which collimate the X-ray beam. These slits prevent beam divergence in the direction perpendicular to the figure plane. The divergent X-ray beam then strikes the specimen, typically a flat plate supported by a specimen table. The diffracted X-ray beam converges at receiving slits before entering a detector. To improve data quality, the diffracted X-ray beam passes through a monochromatic filter or monochromator before reaching the detector. This filter, commonly placed in the diffracted beam path, helps suppress wavelengths other than Kα radiation and reduce background radiation originating within the specimen. A graphite crystal monochromator, designed to diffract a single wavelength based on Bragg's Law, is commonly used. Relative movements among the X-ray tube, specimen and the detector ensure the recording of diffraction intensity over a range of 2θ. It is crucial to note that the θ angle is not the angle between the incident beam and the specimen surface, rather, it is the angle between the incident beam and the crystallographic plane that generates diffraction. X-ray diffraction relies on wave interference where scattered waves superimpose resulting in constructive or destructive interference. For every atom in a crystal arranged in a periodic manner, diffraction from different planes of atoms produces a pattern containing information about the atomic arrangement within the crystal. The diffraction intensity depends on collective scattering by all atoms in the crystal and X-ray beams incident on a crystalline solid will be diffracted by crystallographic planes following Bragg's Law as shown in Equation 4.4.1:

$$n\lambda = 2d \sin\theta \tag{4.4.1}$$

where, λ = wavelength and d = spacing between two planes.

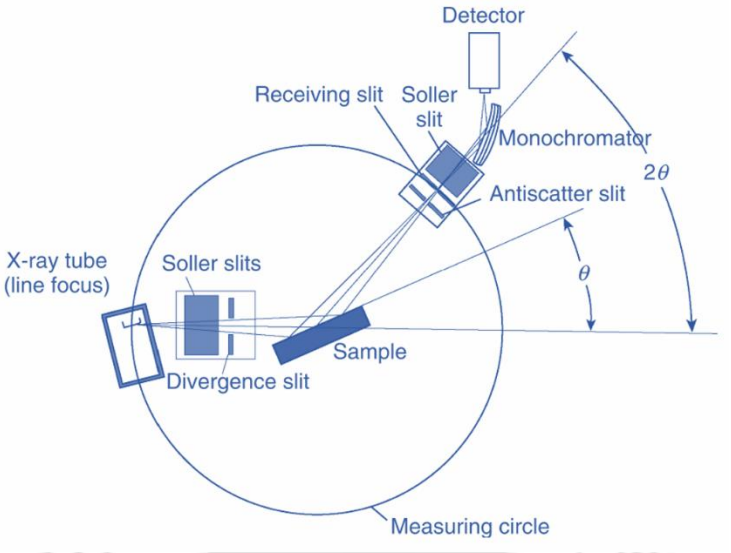

Figure 4.4.6 Schematic diagram of X-ray diffractometer [232].

While the X-ray diffractometer was initially designed for examining powder samples, it is commonly used for examining samples of crystalline aggregates other than powder, including polycrystalline solid samples and liquids [232]. This analysis was conducted using a Rigaku XRD equipment made in Japan to define the crystalline and amorphous characteristics of both biomass and biochar. The analysis was carried out over 10º-90º values of 2θ by X-ray radiation, Cu-K-α.

Field emission scanning electron microscope (FESEM), is a powerful imaging technique used to visualize the surface and internal structure of materials at very high resolution. It can provide detailed information about the morphology, topography and microstructure of both biomass and biochar samples. FESEM is a type of microscope (schematic diagram shown in Figure. 4.4.7) that operates with electrons, particles carrying a negative charge, as opposed to light. The primary distinction between the Scanning Electron Microscope (SEM) and FESEM lies in the emitter type. Unlike thermionic emitters for SEM, which have relatively low brightness and encounter issues such as cathode material evaporation and thermal drift during operation, field emission emitters minimize these problems. FESEM delivers a cleaner image with fewer electrostatic distortions and boasts a spatial resolution of < 2nm, significantly better (3 to 6 times) than SEM [237]. Operating as a high vacuum system, in the FESEM process electrons are scanned over the object in a zig-zag pattern, allowing for the visualization of very small topographic details on the surface of entire or fractioned objects.

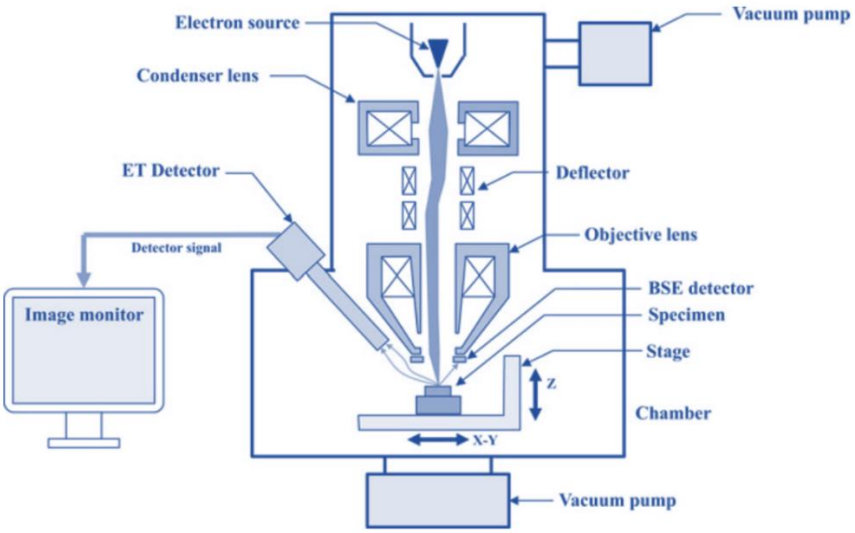

Figure 4.4.7 Schematic diagram of field emission scanning electron microscope [237].

The primary electrons liberated from the field emission source, are accelerated in a high electrical field gradient within the high vacuum column. These primary electrons are then focused and deflected by electronic lenses to generate a narrow scan beam directed at the object. Upon impact, secondary electrons are emitted from each spot on the object and their angle and velocity are indicative of the object's surface structure. A detector captures these secondary electrons producing an electronic signal. This signal is amplified and transformed into a video scan-image visible on a monitor or a digital image that can be saved and further processed. FESEM yields high-quality, low-voltage images while minimizing electrical charging of samples [232]. The images of the samples were captured using a Gemini model (Make: Zeiss, Germany) FESEM for 2KX, 5KX and 10KX magnification along with JSM-7610F model FESEM manufactured by JEOL, Japan, at 1KX magnification.

The surface area, pore size and pore volume of the biochar were measured using the Brunauer Emmett Teller (BET) and Barrett Joyner Halenda (BJH) techniques (Model: Tri-Star-II equipment, Make: Micro-metrics Company, USA) the schematic of which has been presented in Figure 4.4.8 (a). The Brunauer Emmett Teller (BET) method, developed by Stephen Brunauer, Paul Emmett and Edward Teller, is widely regarded as one of the most effective techniques for surface area analysis. This approach relies on the principles of adsorption and desorption. In the BET analysis process as depicted in Figure 4.4.8 (b), a partial vacuum is created to induce adsorption between the sample and liquid nitrogen (as the interaction between the solid and gaseous phases is weak, the surface is cooled with liquid

nitrogen to facilitate detectable adsorption). Following the formation of adsorption monolayers, the sample is extracted from the nitrogen atmosphere and heated, causing the adsorbed nitrogen to be released from the material (desorption) and its quantity is quantified. The collected data is presented in the form of isotherms, which are graphs depicting the amount of nitrogen adsorbed as a function of relative pressure at a constant temperature. These isotherms are categorized into five types and information derived is instrumental in determining the surface area of the sample [238]. For non-porous materials, the desorption curve traces the adsorption curve. In contrast, mesoporous and macroporous materials exhibit a hysteresis loop where the desorption curve does not retrace the adsorption curve resulting in a broad loop. This phenomenon corresponds to capillary condensation of the adsorbate in the multilayer and pore-filling region. The shapes of hysteresis loops are indicative of different pore shapes. The BET Equation describes the relationship between the volume adsorbed at a given partial pressure and the volume adsorbed at monolayer coverage. Nitrogen (N_2) adsorption and desorption experiments were carried out at a temperature of 77 K. Before initiating the experiment, the samples were accurately weighed and positioned in separate pre-treatment vacuum cells at 180 °C for 5 h to eliminate any residual moisture in them. The N_2 adsorption experiment commenced with the determination of the dead volume, followed by gas adsorption-desorption at a bath temperature of 77 K maintaining liquid nitrogen circulation.

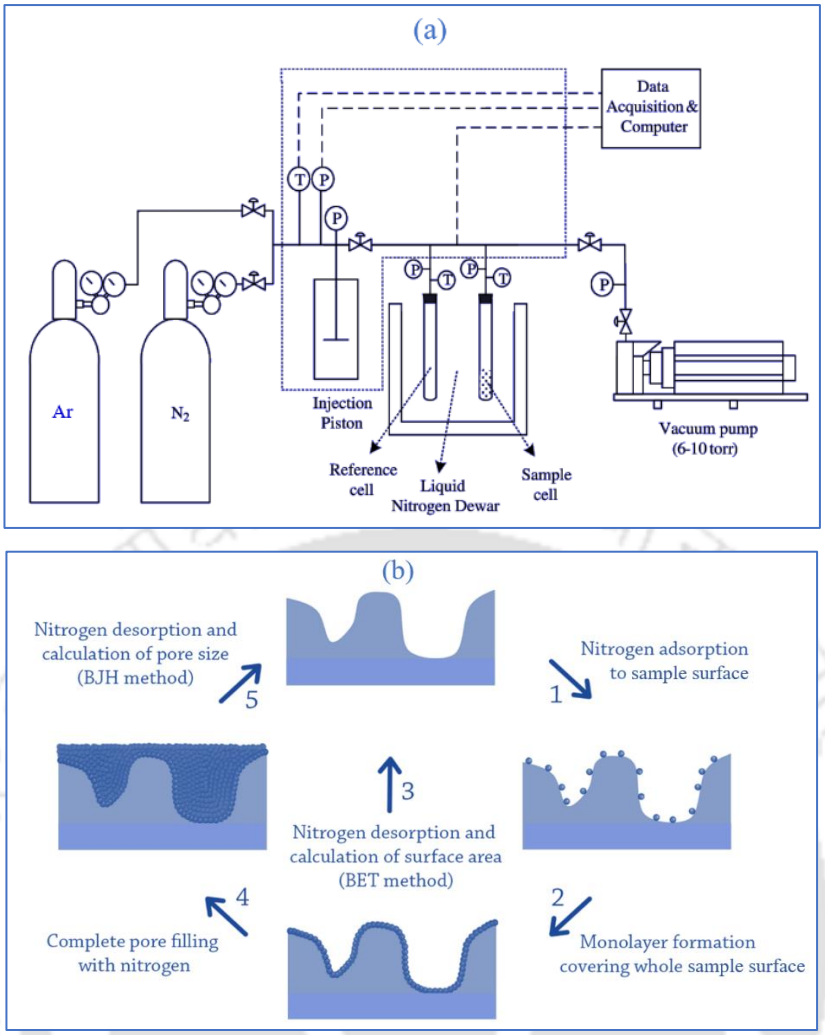

Figure 4.4.8 (a) Schematic diagram of BET apparatus [239], (b) Principles underlying the BET and BJH methods [238].

The BET equation [240] (Equation 4.4.2) for calculating surface area is expressed as:

$$SA_{BET}(m^2/g) = \frac{V_m NA}{VW} \quad (4.4.2)$$

where, V_m = volume adsorbed at monolayer coverage

N = Avogadro constant (6.022×10^{23} mol^{-1})

A = Effective cross-sectional area of one adsorbate molecule, in square meters (0.162 nm^2 for nitrogen)

V = volume occupied by 1 mole of the adsorbate gas at STP allowing for minor departures from the ideal, in millilitres.

The Barrett Joyner Halenda (BJH) method, based on the Barrett Joyner Halenda principle, is employed for the determination of porosity, specifically pore size. Similar to the BET method, this approach utilizes nitrogen gas to undergo adsorption on the sample as illustrated in Figure 4.4.8 (b). However, the BJH method extends the process, allowing gas to condensate within the sample pores as the pressure increases. In the BJH method, the pressure is systematically increased until a saturation point is reached, indicating that all pores within the sample are filled with liquid. Subsequently, the condensate gas undergoes evaporation and the desorption data is calculated. This data is then correlated to the pore size through the utilization of a modified Kelvin equation, often referred to as the Kelvin model of pore filling [239]. Kelvin equation [240] (Equation 4.4.3) relates equilibrium vapor pressure of a liquid contained in a capillary (P) to equilibrium pressure of same liquid over a free surface (P_o):

$$\ln \frac{P}{P_0} = \frac{-2\gamma V_{liq} \cos\theta}{rRT} \quad (4.4.3)$$

where, γ = surface tension of liquid nitrogen

θ = contact angle (usually zero for liquid nitrogen)

V_{liq} = the molar volume of liquid nitrogen

r = radius of pore

R = gas constant.

4.5 Summary of the Chapter

This chapter elaborates the materials and methodology employed for this thesis work. They have been presented below:

- A detailed account of the materials employed for both liquefaction and co-liquefaction has been provided.
- The characterization techniques employed for biomass analysis has been explained.
- A vivid description of the experimental procedure followed during liquefaction and co-liquefaction studies have been given.
- Various techniques used for characterization of liquefaction and co-liquefaction products has been presented.

CHAPTER 5

RESULTS & DISCUSSION

5.1 Characterization of feedstock material

The proximate analysis of CLPU and CLPE (as received basis) along with their HHV had been depicted in Table 5.1.1. Both biomasses had a high MC of >20 wt. % as they were directly used for liquefaction without any prior drying or heat treatment. Both CLPU and CLPE had high VM content of 61.33 wt. % and 66.35 wt. % respectively which was actually an affirmative indication from the biocrude yield point of view as biomasses with high VM get devolatilized easily along with production of less amount of char [82]. The amount of inorganic compounds present in the biomass was detected by its ash content. In both the biomasses the ash content was almost similar to other fruit wastes (pomace and peels) [82,241,242]. The FC content of CLPU was less than 10.5 wt. % indicating that the biochar yield would be less than that of biocrude. Both the biomasses had HHV values that were in close conformity with other lignocellulosic biomasses [8,243] and fruit wastes [69,82,241]. The ultimate analysis of CLPU showed 43.16 wt. % of elemental carbon composition which was comparable to 38.51 wt. % of similar citrus biomass waste [241]. The hydrogen content was also in range with other lignocellulosic biomasses. H/C ratio of CLPU and CLPE was 1.568 and 1.772 respectively and was consistent with similar fruit waste biomasses [69,82,241]. However, O/C ratio of 0.855 and 0.873 for CLPU and CLPE respectively was slightly lower compared to other similar biomass [82,241], which added value to CLPU and CLPE for utilizing them as a source for production of biocrude.

Table 5.1.1 Proximate and ultimate analysis of biomass samples and their HHV.

Biomass feedstock	Proximate Analysis, wt. %				HHV, MJ kg^{-1}
	MC	Ash	VM	FC[a]	
CLPU	23.20	5.26	61.33	10.22	15.88
CLPE	24.57	6.18	66.35	2.89	13.81

Ultimate Analysis, wt. %							
Biomass feedstock	C	H	N	S	O[b]	H/C	O/C
CLPU	43.16	5.64	2.02	-	49.19	1.568	0.855
CLPE	42.60	6.29	1.56	-	49.56	1.772	0.873

[a, b] calculated by difference

Thermo gravimetric analysis (TGA) and differential thermogravimetry (DTG) curves of CLPU and CLPE biomass were shown in Figure 5.1.1. Within temperature range of 30 to 100 °C, water molecules adsorbed on the surface of both the biomass samples as well as those bound within the inner cells underwent dehydration to cause weight loss from 10-20 wt. % that was common to other lignocellulosic biomass samples. The hemicellulose volatilization was observed in between 200 to 400 °C with maximum weight loss at approximately around 300-350 °C [8]. Firstly, the decomposition of less thermally stable volatile compounds occurred leading to the breakage of their chemical bonds. In between 350 to 400 °C overlapping between the cellulose and hemicellulose decomposition took place [244]. The loss of lignin content in CLPE was apparent from a long devolatilization tail at 440 °C temperature. A groove between 220 and 330 °C in the DTG profile indicated degradation of hemicellulose and cellulose. A small groove at around 500 °C had been a proof of lignin degradation [245]. These plots were in agreement to studies conducted on similar citrus fruit wastes [82].

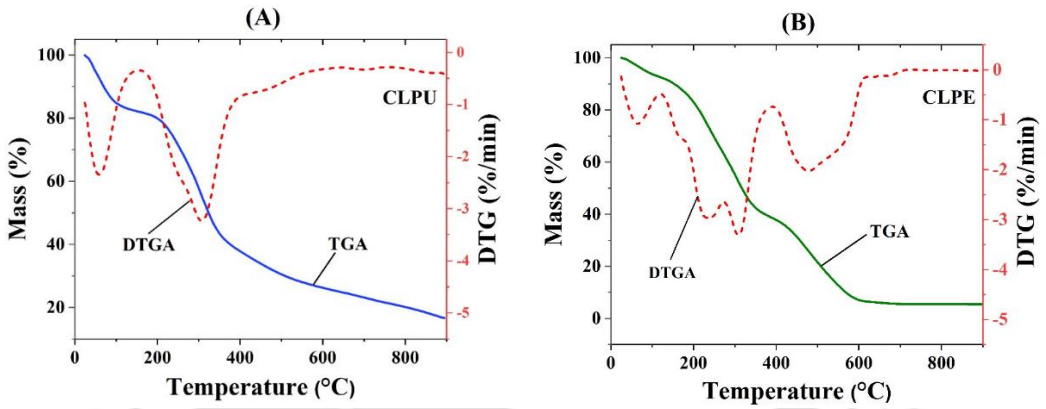

Figure 5.1.1 Thermo gravimetric analysis and differential thermo gravimetry plot of (A) CLPU and (B) CLPE biomass.

Figure 5.1.2 presented the TGA and DTG curves for *Citrus limetta* peel and pulp co-feed biomass (CLPE-PU) showing the degradation pattern for cellulose, hemicellulose and lignin. Upto 100 °C weight loss occurred due to water molecules that were physically adsorbed in the biomass sample. Both hemicellulose and cellulose decomposition was observed in 200-340 °C temperature range [246] with maximum weight loss at around 306 °C. Weight loss above 380 °C indicated loss of lignin from sample and this was observed to continue by DTG depression peak at 663 °C [245].

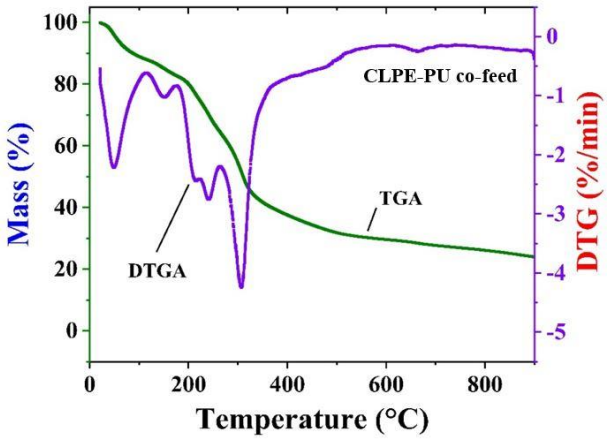

Figure 5.1.2 Thermogravimetric analysis (TGA) and differential thermogravimetry (DTGA) plot of *Citrus limetta* peel and pulp biomass co-feed.

5.2 Solvothermal liquefaction of pulp and peel of *Citrus limetta* fruits at variable biomass-to-solvent ratios

5.2.1 Product yield

Figure 5.2.1 illustrated yield of filtrate (wt. %), biochar (wt. %) and yield of others (wt. %) found from liquefaction of both pulp (CLPU) (Figure 5.2.1A) and peel (CLPE) (Figure 5.2.1B) of *Citrus limetta* biomasses by liquefaction in hydrogen-donor methanol solvent at 260 °C temperature, residence time of 30 min and 1:2, 1:3 and 1:4 biomass-to-solvent ratios respectively. It was observed that the variations in biomass-to-solvent ratios led to the variation in product yield from liquefaction. For CLPU biomass, the highest yield of filtrate was obtained at 1:4 ratio. Similar trends were observed with CLPE biomass as well. However, biochar yield was found to be decreasing for both biomasses with decreasing biomass-to-solvent ratios. This was an indication of the better conversion of organics in the biomass to liquid products under a solvent-rich environment. This low biochar yield might also be considered to be a characteristic of the fruit waste biomass being used. The yield of dark and highly viscous biocrude was found to be increasing with decrease in biomass-to-solvent ratio for both biomasses as depicted in Table A1 and Figure A1 of Annexure. A maximum biocrude yield of 7.88 wt. % and 12.5 wt. % was obtained with CLPU and CLPE biomasses respectively. The reason behind this could be the reaction of the hydrogen-donor methanol solvent with the reaction intermediates produced from liquefaction of CLPE biomass, thereby enhancing the biocrude yield from it. It may be noted that the biocrude yield obtained in this

work was higher than that reported in literature on liquefaction of other citrus fruit wastes at wherein the yield was reported as 7.53 wt. % [68].

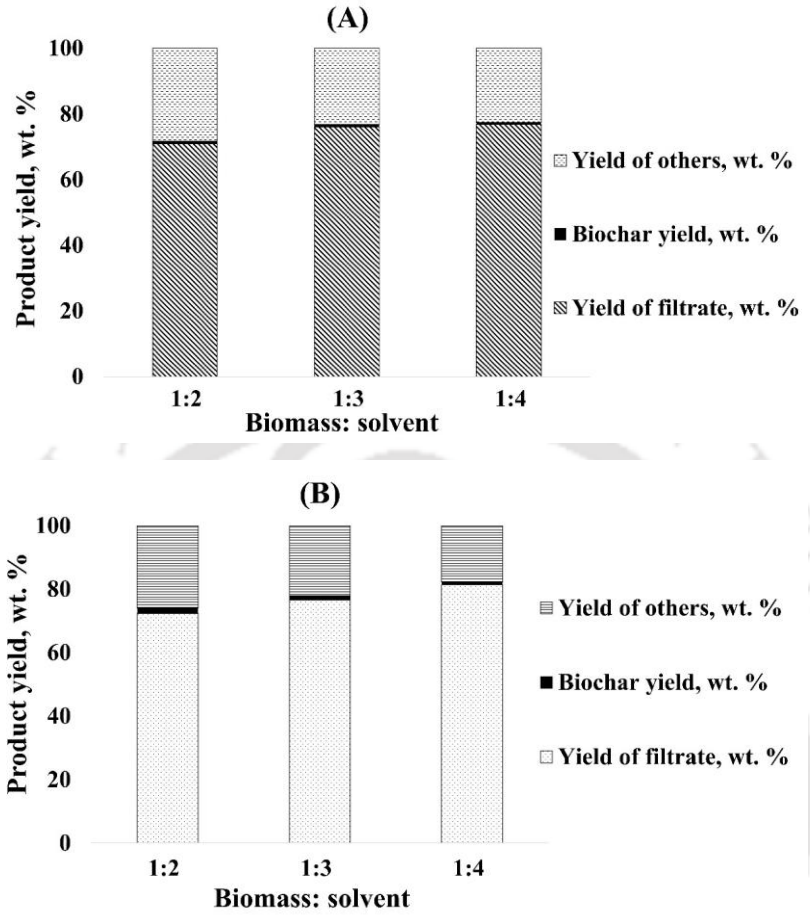

Figure 5.2.1 Product yield from liquefaction of (A) CLPU and (B) CLPE biomass with hydrogen-donor solvent methanol at 260 °C and 1:2, 1:3 and 1:4 biomass-to-solvent ratios.

Nonetheless, it becomes difficult to draw a general conclusion regarding the optimum biomass-to-solvent ratio to generate maximum biocrude yield because several other important reaction parameters such as operating temperature, reactor volume, residence time, pressure, feedstock type, cooling and heating rates, particle size etc. influence the biocrude yield to a large extent [85]. The pressure of the system that reached about 100 bar played a significant part in the product yield from liquefaction. The reason being the increase in pressure led to the increase of solvent density in the supercritical state allowing better penetration of solvent into the biomass aiding in its decomposition to extract the disintegrated products into the liquid phase [247]**.** The high pressure system also inhibited vaporization to allow compounds to be in the liquid state [85].

5.2.2 Analysis of liquid products

5.2.2.1 Physical and fuel analysis

The physical characteristics and HHV of the filtrate and remaining methanol solvent (MSR) after evaporation of this filtrate, obtained from liquefaction of CLPU and CLPE at 260 °C with hydrogen-donor methanol solvent at 1:2, 1:3 and 1:4 biomass-to-solvent ratios were investigated and have been listed in Table 5.2.1. The density of CLPU filtrate was decreasing with decreasing biomass-to-solvent ratio and the comparable trend was detected in the situation of CLPE filtrate. The density values of filtrates obtained by liquefaction of CLPU were slightly higher than those obtained by CLPE liquefaction regardless of biomass-to-solvent ratio values. Similarly, the density values of recovered methanol by evaporation of crude, i.e., MSR of CLPU were slightly higher than those of CLPE irrespective of solvent ratios. On the other hand, the density values of MSRs (both from filtrates of CLPU and CLPE liquefaction) were substantially higher than that of pure solvent. This indicated that some of the lighter hydrocarbons of filtrates and/or methanol soluble components of filtrates obtained by liquefaction of CLPU and CLPE were transferred to the MSR during evaporation process; thus, cannot be reused as solvent but may be used as lighter fuel fraction.

Table 5.2.1 Physical characteristics of filtrate and MSR after liquefaction of CLPU and CLPE at 260 °C and different biomass-to-solvent ratios.

Product	1:2	1:3	1:4
Density, g mL^{-1}			
CLPU (Filtrate)	0.872	0.861	0.844
CLPU (MSR)	0.824	0.847	0.822
CLPE (Filtrate)	0.860	0.851	0.841
CLPE (MSR)	0.819	0.826	0.816
Density of pure reagent grade methanol, g mL^{-1} = 0.782			
Viscosity, mPa.s			
CLPU (Filtrate)	1.182	1.178	1.038
CLPU (MSR)	0.899	1.074	0.913
CLPE (Filtrate)	1.155	1.142	1.040
CLPE (MSR)	0.938	0.918	0.883
Viscosity of pure reagent grade methanol, mPa.s = 0.677			

	HHV, MJ kg^{-1}		
CLPU (Filtrate)	18.40	14.89	16.09
CLPU (MSR)	16	15.89	17.69
CLPE (Filtrate)	15.16	16.23	17.19
CLPE (MSR)	17.58	17.36	17.41
HHV of pure reagent grade methanol, MJ kg^{-1}= 19.62			

The viscosity of CLPU filtrate was found to decrease with decreasing biomass-to-solvent ratio; and the same was the case for CLPE filtrate with each biomass-to-solvent ratio. The viscosity of MSRs were substantially lower than the filtrates of both CLPU and CLPE liquefaction. Whereas, the viscosity of MSRs of both CLPU and CLPE liquefaction were much higher compared to that of pure methanol solvent. Thus, it was again clear that MSR possessed same lighter fuel fractions and/or methanol soluble components of liquefaction products in them and cannot be reused as solvent. In other words, the filtrate contained some lighter hydrocarbons where vapor pressures are close to that of pure methanol solvent. The HHV of filtrate of CLPE liquefaction was found to rise with decrease in biomass-to-solvent ratio whereas mixed trends were found in the case of CLPU filtrate. The HHV of MSR of both CLPU and CLPE liquefaction was found to be higher than either filtrate except in the case of CLPU with 1:2 ratio. This may be attributed to increased penetration of solvent into the biomass, during initial period of liquefaction, with increasing biomass-to-solvent ratio [85].

Table 5.2.2 Fuel potential of biocrude and biochar obtained by liquefaction at 260 °C and different biomass-to-solvent ratios.

	HHV of biocrude, MJ kg^{-1}			HHV of biochar, MJ kg^{-1}		
Biomass feedstock	1:2	1:3	1:4	1:2	1:3	1:4
CLPU	26.36	26.7	26.76	16.98	16.46	16
CLPE	24.91	24.2	23.7	14.94	15.55	16.5

On the other hand, the HHV of biocrude was found to be almost constant (or only marginally increasing) in the case of CLPU whereas the opposite was true for CLPE with respect to the decreasing biomass-to-solvent ratio. However, for a fixed value of biomass-to-solvent ratio, the HHV of CLPU biocrude was higher than that of CLPE (Table 5.2.2, Table A3, Figure A3, Table A4 and Figure A4 of Annexure). The HHV values of the biocrude was

comparable to those obtained from other lignocellulosic biomasses. The probable reasons for HHV trends might be that in comparison to biomass, the biocrude had a higher content of carbon while lower content of oxygen, resulting in HHV rise. The dehydration, decarboxylation and decarbonylation reactions occurring during liquefaction were the key factors behind the decline in oxygen content in biocrude. Moreover, rise in hydrogen content occurred due to generation of active hydrogen by supercritical methanol and its integration in the biocrude [53]. Nonetheless, the biomass-to-solvent ratio should be adjusted with utmost care to get optimum yield of biocrude with optimum heating value [85,248]. But it was worth noting that these HHV values were still higher than the corresponding raw biomasses.

5.2.2.2 Chemical analysis

Henceforth, the products obtained from liquefaction of CLPU at 260 °C and 1:2, 1:3 and 1:4 biomass-to-solvent ratios have been denoted as CLPU 260_2, CLPU 260_3 and CLPU 260_4 respectively. Similarly, the products from CLPE at similar biomass-to-solvent ratios have been denoted as CLPE 260_2, CLPE 260_3 and CLPE 260_4 respectively. The FTIR spectra of the biocrude has been depicted in Figure 5.2.2 and gave an account of the functional groups present in them. The broad peaks in the spectra in between 3200-3400 cm^{-1} corresponded to phenolic compounds owing to the presence of O-H stretching vibration of hydroxyl groups [249]. The absorption peaks in 3000-2800 cm^{-1} and 1460-1350 cm^{-1} range, corresponding to C-H stretching vibration might have occurred due to methyl and methylene groups and indicated the possibility of presence of long chain alkanes [155,250]. The absorption peaks in between 1800-1586 cm^{-1} indicated C=O stretching vibration in carboxylic acids, esters, ketones and aldehydes group [251]. C-O stretching and O-H bending of primary, secondary, tertiary alcohols, ester, phenol and ether were evident from peak at around 1020 cm^{-1} [252]. In addition to these, the peaks in 800-740 cm^{-1} range specified the presence of single, polycyclic and substituted aromatic groups [170]. Although, the functional groups were almost similar in the FTIR spectra of both biomasses, the slight increase in the intensity of peaks owing to C-H stretching while decrease in intensities of O-H, C-O and C=O peaks in biocrude of CLPU put forward the decline in oxygen groups. This was evident from the higher HHV of the biocrude obtained from CLPU in comparison to CLPE.

The molecular composition of biocrude from liquefaction of CLPU and CLPE were examined by GC-MS analysis. The compounds corresponding to the major peaks were

identified from NIST library as portrayed in Table 5.2.3. Major compounds were seen to be lying within range of C_2 to C_{38} groups. Table 5.2.4 depicted that biocrude mainly consisted of esters, fatty acids, phenols, alcohols, ketones, hydrocarbons and N-containing compounds as already evident from their FTIR (Figure 5.2.2). The presence of esters could be credited to the breakdown of hemicellulose and cellulose [253]. The methylated esters designated the contribution of hydrogen-donor methanol in liquefaction by esterification/methanolysis [254]. However, the biocrude composition was also highly dependent on the operation conditions and type of feedstock being used [255]. Biocrude obtained from liquefaction of microalgae was generally high in N & O containing compounds along with fatty acids which was contrary to low N-containing compounds in this case. The same has been found and reported in liquefaction studies with other citrus fruit wastes and rendered this biocrude as fruitful for further upgrading as well as downstream applications [72]. The breakage of benzoylether and β-aryl bonds in lignin led to its decomposition and formation of phenolic compounds in biocrude [62]. Low content of phenols indicated the less harmful and noxious nature of the biocrude. The hydrolysis of lipids in the feedstock promoted by the in-situ hydrogen donation by methanol [223] led to the formation of long chain hydrocarbons in them [72].

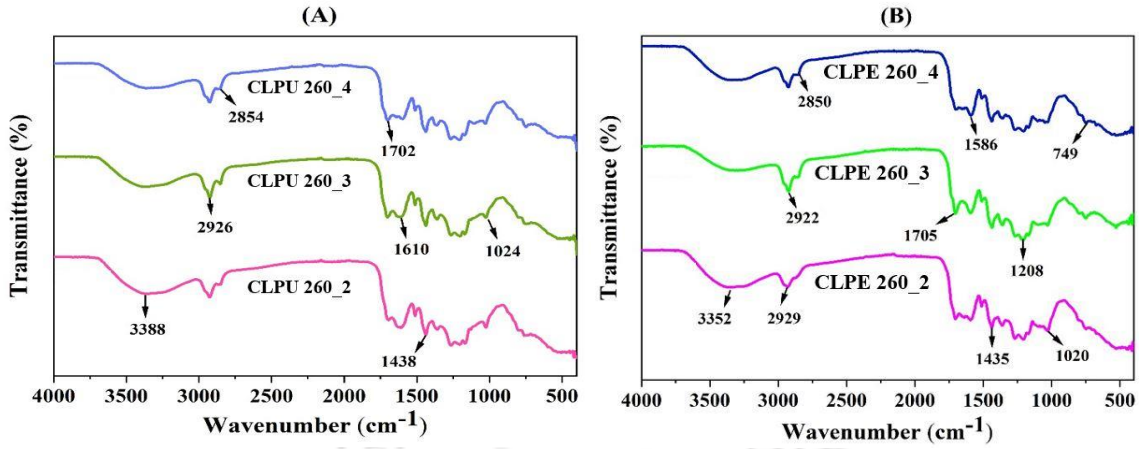

Figure 5.2.2 FTIR spectra of (A) CLPU and (B) CLPE biocrude at different biomass-to-solvent ratios.

The high temperature solvent environment led to the dehydration of hemicellulose and aided the formation of ketones as seen in the GC-MS. Meanwhile, compounds of higher aromatic content were formed from the dehydration and aromatization of cellulose and hemicellulose structural units [256]. These results were comparable to literature that signified high share of

hydrocarbons and esters with low N-containing compounds and phenols in liquefaction biocrude [251,257,258]. However, due to instrument limitations, GC-MS was able to give only partial information about the probable chemical compounds in the biocrude. Such as the identification of some high boiling point compounds remained absent because of temperature limit of the GC-MS. Similarly, compounds with low boiling point also remained unaccounted for due to their losses during biocrude separation.

The confirmation of the functional groups and assignments by means of chemical shift in ppm was obtained by proton NMR technique as presented in Figure 5.2.3 [259]. ^{1}H NMR of the biocrude from liquefaction of CLPU and CLPE presented peaks at chemical shift of 7.26 ppm which corresponded to chloroform-D solvent used in the analysis. However, the peak at 0 ppm could be considered as a standard for tetramethylsilane (TMS) that is default in NMR systems [260]. Aliphatic protons attached to carbon atoms (alkanes) were evident in peaks between 0-1.5 ppm [261]. This indicated the fatty acids and hydrocarbons in the biocrude and was consistent with the GC-MS results discussed above. Peaks between 1.5-3 ppm indicated the presence of aliphatic protons attached to unsaturated heteroatom or carbon [262]. While, the peaks at 3-4.5 ppm corresponded to protons bonded to carbon of ethers, alcohols and esters [245]. The consumption of methanol in the liquefaction reaction boosted the alcoholic and esters compounds formation which was verified from the FTIR spectra of the biocrude from both biomasses. A low proton distribution in between 4.5-6 ppm was an indication of weak carbohydrate and methoxy functionality [248].

Table 5.2.3 Major compounds identified through GC-MS analysis of biocrude obtained from liquefaction of CLPU and CLPE at different biomass-to-solvent ratios.

Compounds	Molecular formula	Chemical class	CLPU 260_2		CLPU 260_3		CLPU 260_4		CLPE 260_2		CLPE 260_3		CLPE 260_4	
			RT (min)	Area (%)	RT (min)	Area (%)	RT (min)	Area (%)	RT (min)	Area (%)	RT (min)	Area (%)	RT (min)	Area (%)
Ethanamine	C_2H_7N	Amines, Aliphatic	8.133	4.332	-	-	-	-	-	-	-	-	-	-
Furan, 2-methoxy-	$C_5H_6O_2$	Alkyl aryl ethers	8.629	23.989	-	-	6.909	8.073	-	-	6.914	8.778	6.909	10.356
Cyclobutanecarboxylic acid	$C_5H_8O_2$	Organic acid	-	-	-	-	-	-	-	-	-	-	-	-
Cyclopentane-1,2-diol	$C_5H_{10}O_2$	Cyclopentalnols	-	-	-	-	-	-	-	-	5.279	8.021	-	-
Ethanol, pentamethyl-	$C_7H_{16}O$	Alcohol	9.469	12.891	7.664	9.320	7.669	5.163	-	-	7.669	5.814	-	-
2-azetidinone, 3,3,4,4-tetramethyl-	$C_7H_{13}NO$	Ketone	-	-	-	-	5.289	11.319	-	-	-	-	-	-
Azetidine, 2,2,3,3-tetramethyl-	$C_7H_{15}N$	Amine	-	-	-	-	-	-	-	-	-	-	5.279	8.903

3-methyl-2-(2-oxopropyl) furan	$C_8H_{10}O_2$	Heteroatomic compounds	-	-	5.013	4.232	-	-	15.122	4.282	-	-	-	-
5-hepten-2-amine, n,6-dimethyl-	$C_9H_{19}N$	Amine	-	-	-	-	5.013	7.379	-	-	-	-	-	-
2-octanol, 2,6-dimethyl-	$C_{10}H_{22}O$	Fatty alcohols	-	-	-	-	-	-	-	-	-	-	7.674	7.021
2-octene, 4-ethyl-	$C_{10}H_{20}$	Unsaturated aliphatic hydrocarbons	10.574	0.293	-	-	-	-	-	-	-	-	-	-
Benzaldehyde, 4-(1-methylethyl)-	$C_{10}H_{12}O$	Aromatic monoterpenoids	-	-	-	-	-	-	-	-	32.401	1.374	-	-
2-ethylmethcathinone	$C_{12}H_{17}NO$	Alkyl-phenylketones	8.023	2.047	-	-	-	-	-	-	-	-	-	-
Bicyclo[4.1.0]heptane, 7-pentyl-	$C_{12}H_{22}$	Polycyclic hydrocarbons	31.813	0.363	-	-	-	-	-	-	-	-	-	-
4-hydroxyphenyl-4-methyl-2-pentanone	$C_{12}H_{16}O_2$	Ketone	41.417	0.393	-	-	-	-	-	-	-	-	-	-

Undecanoic acid, 10-methyl-, methyl ester	$C_{13}H_{26}O_2$	FAME	-	-	-	-	28.898	2.189	-	-	-	-	-	-
Methyl 11-methyl-dodecanoate	$C_{14}H_{28}O_2$	Fatty acid methyl esters (FAME)	-	-	-	-	-	-	-	-	-	-	28.898	1.892
4-tert-octylphenol	$C_{14}H_{22}O$	Phenol	38.511	0.349	-	-	-	-	-	-	-	-	-	-
7,11-hexadecadienal	$C_{16}H_{28}O$	Fatty aldehydes	-	-	-	-	-	-	-	-	31.315	1.752	-	-
1-pentadecene, 2-methyl-	$C_{16}H_{32}$	Branched unsaturated hydrocarbons	-	-	-	-	-	-	-	-	-	-	5.013	7.326
1-nonylcycloheptane	$C_{16}H_{32}$	Polycyclic hydrocarbons	31.733	0.601	-	-	-	-	-	-	-	-	-	-
(1s,15s)-bicyclo[13.1.0]hexadecan-2-one	$C_{16}H_{28}O$	Ketones	-	-	31.289	1.123	-	-	-	-	-	-	-	-

Orcinyl di-angelate	$C_{17}H_{20}O_4$	Ester	-	-	6.904	13.229	-	-	-	-	-	-	-	-
9,12-hexadecadienoic acid, methyl ester	$C_{17}H_{30}O_2$	Fatty acid methyl esters	-	-	-	-	-	-	-	-	-	-	31.289	1.706
6-octadecenoic acid	$C_{18}H_{34}O_2$	Fatty acid (Petroselinic)	-	-	-	-	-	-	12.496	2.631	-	-	-	-
Hexestrol TMS derivative	$C_{18}H_{22}O_2$	Phenol	41.627	0.401	-	-	-	-	-	-	-	-	-	-
Methyl 9,10-octadecadienoate	$C_{19}H_{34}O_2$	Fatty Acid Ester	-	-	-	-	31.219	1.670	-	-	-	-	-	-
11,14-octadecadienoic acid, methyl ester	$C_{19}H_{34}O_2$	Fatty acid methyl esters (FAME)	31.658	0.5	-	-	-	-	-	-	-	-	-	-
11,14-octadecadienoic acid, methyl ester	$C_{19}H_{34}O_2$	Fatty acid methyl esters	-	-	-	-	-	-	-	-	31.245	1.254	31.224	1.671
Butyl 9-hexadecenoate	$C_{20}H_{38}O_2$	Fatty acid esters	-	-	-	-	-	-	-	-	5.013	6.108	-	-

Methyl 9-eicosenoate	$C_{21}H_{40}O_2$	Fatty acid methyl esters	-	-	-	-	31.294	2.107	-	-	-	-	31.349	1.326
I-propyl 11,12-methylene-octadecanoate	$C_{22}H_{42}O_2$	Lipid derivative	-	-	-	-	-	-	13.532	3.803	-	-	-	-
Methyl 11-docosenoate	$C_{23}H_{44}O_2$	Fatty acid ester	-	-	-	-	31.354	1.743	-	-	-	-	-	-
2,6,10,14-tetramethyl-7-(3-methylpent-4-enylidene) pentadecane	$C_{25}H_{48}$	Alkyne	-	-	-	-	-	-	10.866	3.935	-	-	-	-
Hexacosyl acetate	$C_{28}H_{56}O_2$	Long chain fatty acid	-	-	-	-	-	-	20.380	3.303	-	-	-	-
Heptacosanoic acid, 25-methyl-, methyl ester	$C_{29}H_{58}O_2$	Fatty acid methyl esters (FAME)	29.267	0.637	28.893	1.005	-	-	-	-	-	-	-	-
(Z)-decyl icos-9-enoate	$C_{30}H_{58}O_2$	Wax monoesters	-	-	-	-	-	-	16.978	3.297	-	-	-	-

9-octadecenoic acid (z)-, octadecyl ester	$C_{36}H_{70}O_2$	Fatty acid methyl esters (FAME)	-	-	-	-	-	-	16.798	5.1992	-	-	-	-
Z,z-6,28-heptatriactontadien-2-one	$C_{37}H_{70}O$	Long chain ketone	-	-	31.219	1.117	-	-	14.237	4.667	-	-	-	-
Oleic acid, eicosyl ester	$C_{38}H_{74}O_2$	Wax monoesters	-	-	-	-	-	-	15.358	6.640	-	-	-	-

Table 5.2.4 Percentage distribution of major compounds in biocrude from liquefaction of CLPU and CPLE at 260 °C and 1:2, 1:3 & 1:4 biomass-to-solvent ratios on the basis of GC-MS results.

Class	CLPU 260_2 (Area %)	CLPU 260_3 (Area %)	CLPU 260_4 (Area %)	CLPE 260_2 (Area %)	CLPE 260_3 (Area %)	CLPE 260_4 (Area %)
Ester/Acid	1.137	14.234	7.709	21.063	7.362	5.269
Alcohol	12.891	9.32	5.163	-	13.835	7.021
Amine	4.332	-	7.379	-	-	8.903
Alkane	0.964	-	-	3.935	-	-
Phenol	0.75	-	-	-	-	-
Aliphatic	0.293	-	-	-	-	-
Ether	23.989	-	8.073	-	8.778	10.356
Ketone/ Aldehyde	2.44	2.24	11.319	4.667	1.752	
Aromatic	-	-	-	-	1.374	-
Other	-	4.232	-	8.085	-	7.326

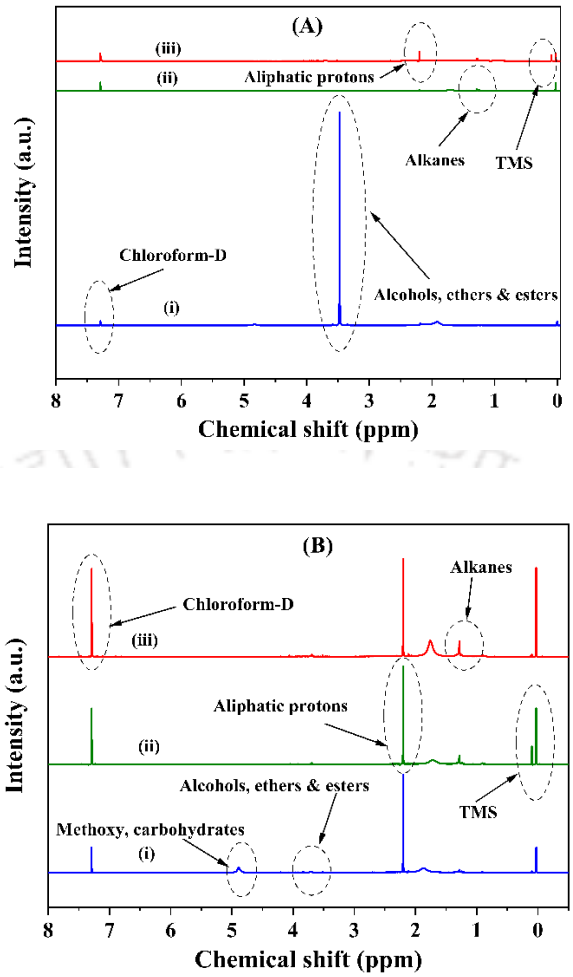

Figure 5.2.3 ^{1}H NMR of biocrude samples from liquefaction at 260 °C and 1:2, 1:3 & 1:4 biomass-to-solvent ratios where (A (i)-(iii)) CLPU 260_2, CLPU 260_3, CLPU 260_4 respectively and (B (i)-(iii)) CLPE 260_2, CLPE 260_3, CLPE 260_4 respectively.

5.2.3 Analysis of biochar

Figure 5.2.4 showed TGA and DTG plots of biochar from liquefaction of CLPU and CLPE at all three biomass-to-solvent ratios mixed together which were denoted as CLPU 260 and CLPE 260 respectively. The moisture loss from bio-molecules and changes in lipid structure were indicated by the mass loss in the temperature range of 40-200 °C. Decomposition of carbohydrates was evident in between 200-400 °C. However, above 400 °C the mass loss pointed towards complete decomposition and oxidation of organic matter [263]. The highest weight loss rate of biochar obtained from liquefaction in methanol was observed at 350-357 °C, suggesting that complete degradation of cellulose and hemicellulose in CLPU and CLPE had not occurred. The TGA curves of the biochar indicated their high thermal stability [264].

The HHV of the biochar as shown in Table 5.2.2, Table A3, Figure A3, Table A4 and Figure A4 of Annexure indicated a maximum at 16.98 MJ kg^{-1} for biochar from CLPU. While, it ranged between 14.94-16.5 MJ kg^{-1} for CLPE biochar. To be specific, the HHV of CLPU biochar was marginally decreasing with increasing biomass-to-solvent ratio and the opposite was true for the case of CLPE biochar. Nevertheless, the HHV of CLPU biochar was higher than that of CLPE biochar for any fixed biomass-to-solvent ratio.

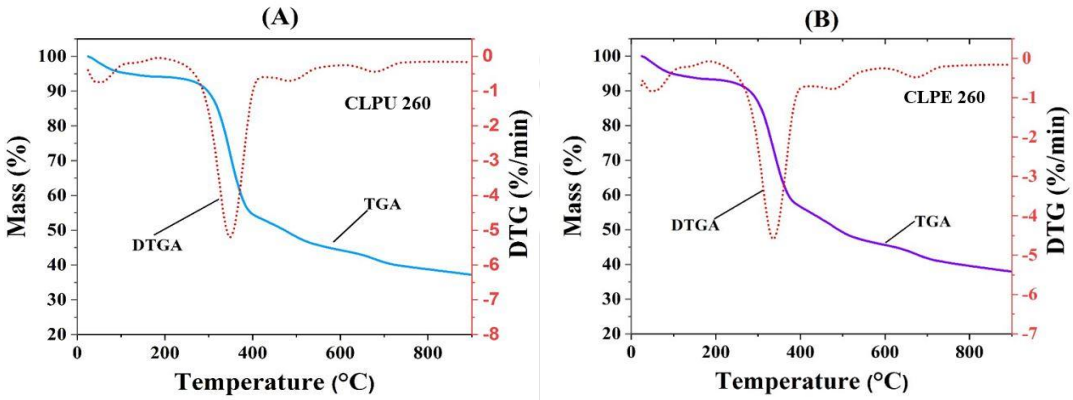

Figure 5.2.4 Thermo gravimetric analysis (TGA) and differential thermo gravimetry (DTG) plot of (A) CLPU and (B) CLPE biochar.

These values signified their ability to be used as a potential feedstock in bio-refineries [245]. Their porous structure verified their applications in wastewater bioremediation, soil treatment and as catalyst for biomass conversion [251,265–267].

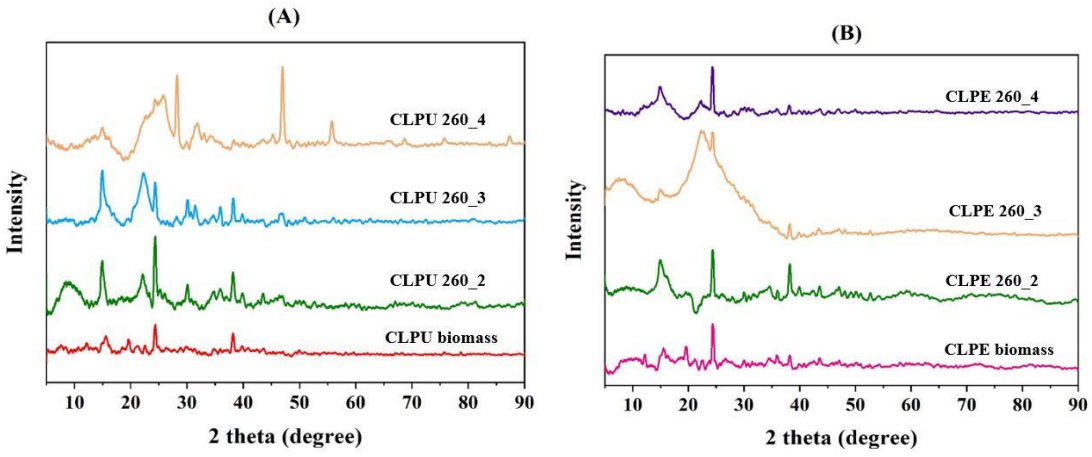

Figure 5.2.5 X-ray diffractrogram of (A) CLPU and (B) CLPE biomass and biochar obtained by liquefaction at different biomass-to-solvent ratios.

The powder X-ray diffraction (XRD) technique was utilized to find out the crystallinity of the biomass and dry biochar samples by taking into account the changes in crystalline structure of cellulose by interruption of hydrogen bonding of cellulose chains occurring due to liquefaction [268]. Figure 5.2.5 illustrated the XRD pattern for the CLPU and CLPE biomasses along with their corresponding liquefaction biochar obtained at 1:2, 1:3 and 1:4 biomass-to-solvent ratios. The XRD pattern of both CLPU and CLPE biomass showed two discrete peaks for cellulose at $2\theta = 15°$ and 22° [269,270]. The presence of peaks at $2\theta = 24°$ and 26° showed cellulose and lignin breakdown in the process and implied turbostratic and amorphous carbon [74]. These carbon peaks signified biochar formation by cellulose and lignin decomposition during liquefaction [271]. The biomass structure was composed of multifaceted compounds but despite of their breakdown due to thermochemical conversion processes to produce biochar, the biochar samples retained their crystalline nature partially which was visible from their XRD plots [245,272].

The surface morphology of the CLPU and CLPE biomasses along with their corresponding mixed biochar obtained at all three biomass-to-solvent ratios have been studied by FESEM (at (i) 2KX, (ii) 5KX and (iii) 10KX resolutions) as depicted in Figure 5.2.6. It was evident from the images that the biomass was a lumpy, dense solid matrix having fibrous structure. However, after liquefaction the changes in the surface were visible from the images of the biochar. Due to cellulose and hemicellulose decomposition, the structure of the cell was broken leading to development of cracks on the surface with certain pores over them [273]. Certain agglomerations were observed on the biochar surface owing to cross-linking instigated by the dehydration between hemicellulose and cellulose molecules. The mineral residues from biomass liquefaction were apparent from the magnified FESEM images showing small particle deposits on the biochar surface [274].

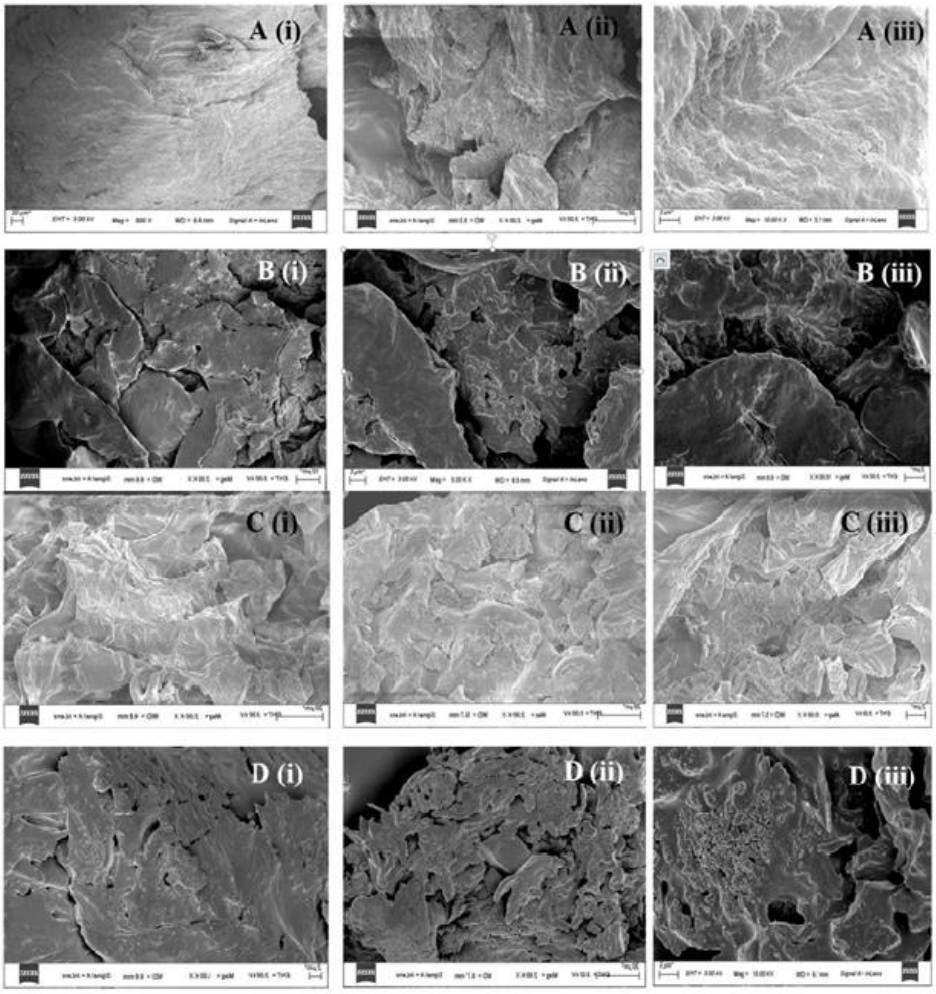

Figure 5.2.6 A(i), A(ii) & A(iii): FESEM images of CLPU biomass; B(i), B(ii) & B(iii): FESEM images of biochar obtained by liquefaction of CLPU biomass; C(i), C(ii) & C(iii): FESEM images of CLPE biomass; and D(i), D(ii) & D(iii): FESEM images of biochar obtained by liquefaction of CLPE biomass (at (i) 2KX, (ii) 5KX and (iii) 10KX resolutions each).

5.2.4 Summary

The significant outcomes of this objective where solvothermal liquefaction of *Citrus limetta* pulp and peel had been carried out at 260 °C temperature and 1:2, 1:3 & 1:4 biomass-to-solvent ratios have been summarized below:

- This research successfully addressed the pressing need for waste management by employing liquefaction on fruit wastes (pulp and peel) of *Citrus limetta* in a hydrogen-donor methanol solvent.

- The highly volatile nature of *Citrus limetta* peel contributed to a remarkable biocrude yield, reaching a maximum of 12.5 wt. % at 1:2 biomass-to-solvent ratio, surpassing similar processes with other citrus fruit waste biomasses documented in the literature.
- From an energy content perspective, the highest HHV of biocrude was observed for *Citrus limetta* pulp biomass, specifically 26.76 MJ kg^{-1} at biomass-to-solvent ratio of 1:4.
- GC-MS analysis revealed the presence of esters in the biocrude, a result of the esterification of the hydrogen-donor methanol solvent.
- The biocrude exhibited compounds with higher aromatic content, attributed to the dehydration and aromatization of cellulose and hemicellulose.
- Biochar derived from *Citrus limetta* pulp biomass demonstrated high thermal stability, with a maximum HHV of 16.98 MJ kg^{-1}, showcasing potential use in bio-refineries.

5.3 Solvothermal liquefaction of pulp and peel of *Citrus limetta* fruits at variable temperatures and biomass-to-solvent ratios

5.3.1 Analysis of product yield

The yield analysis of the products from liquefaction of *Citrus limetta* pulp (CLPE) and peel (CLPU) have been depicted in Figure 5.3.1 (A) & (B) respectively. Variations have been observed in these yield results due to temperature variations at different biomass-to-solvent ratio values. The percentage yield of filtrate from both biomasses have been observed to be rising with the rise in temperature from 240 °C to 280 °C at biomass-to-solvent ratio ratios viz. 1:2, 1:3 and 1:4. The highest output of filtrate in terms of its yield was noted at 280 °C and 1:4 biomass-to-solvent ratio. Simultaneously, the biochar yield was found to be gradually decreasing with rise in temperature with least value reported at 280 °C indicating higher conversion rate at this temperature. The yield of the immensely viscous and dark coloured biocrude obtained after solvent removal from the liquefaction filtrate was calculated and it was found that for CLPE biocrude at biomass-to-solvent ratio of 1:2 the rise in temperature from 240 °C to 260 °C led to increase in yield from 11.71 wt. % to 12.5 wt. % [275], however a decrease in yield to 10 wt. % was observed with further increase of temperature to 280 °C. The reason for this could be that when the reaction temperature is increased, polymers tend to break down and transform into a liquid phase rich in oil [276]. However, it has been observed that if the temperature exceeds a certain threshold, there may be a slight reduction in the

amount of liquid produced, which could be attributed to the secondary degradation of both biocrude and organic compounds in aqueous phase [277]. In fact, higher biocrude yields were found from liquefaction biocrude at 240 °C rather than at higher temperatures for both.

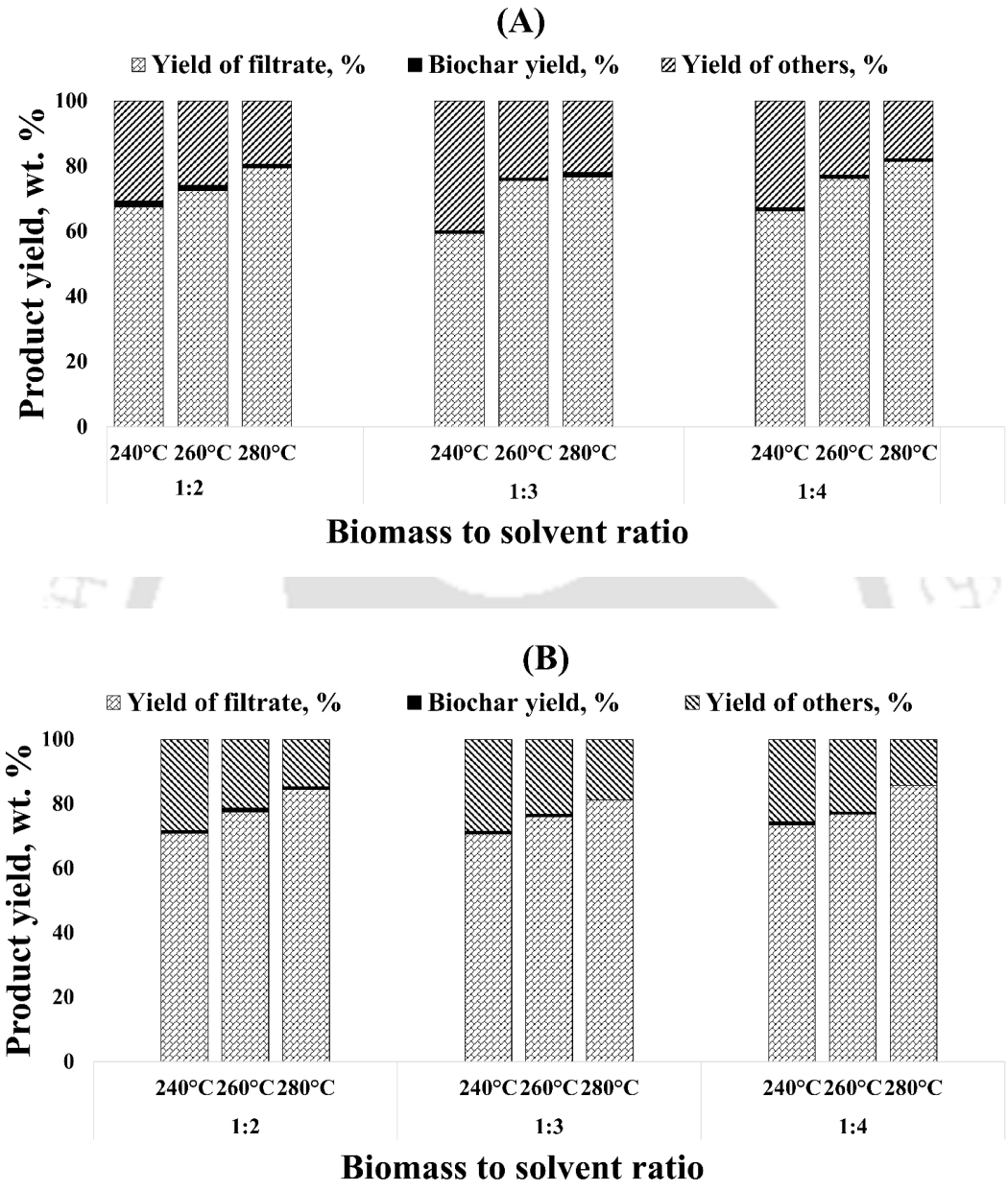

Figure 5.3.1 (A) Product yield variation from CLPE and (B) CLPU biomass liquefaction at 240 °C, 260 °C and 280 °C temperature and varying biomass-to-solvent ratio.

It was found that 12.5 wt. % at 240 °C and 1:3 biomass-to-solvent ratio of CLPE was the maximum among the results obtained at the temperature variations in this work for both biomasses and was comparable to same yield obtained at 1:2 biomass-to-solvent ratio but at

slightly higher temperature of 260 °C. In comparison to the hydrothermal liquefaction of citrus fruit wastes in which Zhang et al. [68] claimed to produce a 7.53 wt. % yield at 315 °C and 35 min residence time, the biocrude yield produced here was greater. Additionally, these results were obtained at less severe temperature conditions, which added to the significance of this findings. The alteration of biomass-to-solvent ratio by changing biomass method as in this case has less significant effects on the biocrude yield. Despite efforts to determine the ideal biomass-to-solvent ratio for maximum biocrude yield, it remains challenging to come to a definitive conclusion. This is due to the fact that various other critical reaction variables, including operating pressure, volume of reactor, time of residence for reaction, type of feedstock, cooling and heating rates, particle size, etc., have a substantial impact on biocrude yield [85].

5.3.2 Analysis of products in liquid form

5.3.2.1 Physical and fuel characterization

The notations of CLPE 240, CLPE 260, CLPE 280, CLPU 240, CLPU 260 and CLPU 280 indicate products (filtrate, MSR, biocrude and biochar) produced by liquefaction of peel of *Citrus limetta* at 240 °C, *Citrus limetta* peel at 260 °C, *Citrus limetta* peel at 280 °C, *Citrus limetta* pulp at 240 °C, *Citrus limetta* pulp at 260 °C and *Citrus limetta* pulp at 280 °C respectively. The analysis of the physical and fuel characteristics of CLPE and CLPU biomass liquefaction products between 240 °C to 280 °C for 1:2, 1:3 and 1:4 biomass-to-solvent ratios have been summarized in Table 5.3.1. Across all biomass-to-solvent ratios and temperatures, it was discovered that the densities and viscosities of the filtrates and the residual methanol solvent (MSR) were significantly larger than those of the pure methanol solvent used in the experiment. This observation strongly suggested that methanol soluble components and/or lighter hydrocarbons from the liquefaction of both biomasses were transferred to the MSR as a result of solvent evaporation in the rotary evaporator. Furthermore, these values exhibited a decreasing trend as the biomass-to-solvent ratio decreased for both biomasses with the exception of MSR at 260 °C and 1:2 biomass-to-solvent ratio. As temperature for liquefaction rose from 240 °C to 280 °C, the filtrates and MSRs density gave mixed trends for both.

Table 5.3.1 Fuel and physical characteristic properties of products (filtrate & MSR) via liquefaction specific to CLPE and CLPU at 240 °C, 260 °C and 280 °C and varying biomass-to-solvent ratios.

Product	1:2	1:3	1:4
		Density, g mL^{-1}	
CLPE 240 (Filtrate)	0.863	0.855	0.84
CLPE 240 (MSR)	0.821	0.818	0.817
CLPE 260 (Filtrate)	0.860	0.851	0.841
CLPE 260 (MSR)	0.819	0.826	0.816
CLPE 280 (Filtrate)	0.867	0.846	0.841
CLPE 280 (MSR)	0.826	0.84	0.838
CLPU 240 (Filtrate)	0.864	0.855	0.846
CLPU 240 (MSR)	0.82	0.821	0.819
CLPU 260 (Filtrate)	0.872	0.861	0.844
CLPU 260 (MSR)	0.824	0.847	0.822
CLPU 280 (Filtrate)	0.871	0.865	0.85
CLPU 280 (MSR)	0.955	0.832	0.83
Density, Methanol (pure reagent), g mL^{-1} = 0.782			
		Viscosity, mPa.s	
CLPE 240 (Filtrate)	1.205	1.155	1.016
CLPE 240 (MSR)	0.846	0.843	0.848
CLPE 260 (Filtrate)	1.155	1.142	1.040
CLPE 260 (MSR)	0.938	0.918	0.883
CLPE 280 (Filtrate)	1.191	1.105	1.054
CLPE 280 (MSR)	1.011	1.016	1.052
CLPU 240 (Filtrate)	1.238	1.136	1.055
CLPU 240 (MSR)	0.881	0.852	0.831
CLPU 260 (Filtrate)	1.182	1.178	1.038
CLPU 260 (MSR)	0.899	1.074	0.913
CLPU 280 (Filtrate)	1.209	1.123	1.072
CLPU 280 (MSR)	1.25	0.907	0.892
Viscosity, Methanol (pure reagent), mPa.s = 0.677			

	HHV, MJ kg^{-1}		
CLPE 240 (Filtrate)	14.55	14.96	15.22
CLPE 240 (MSR)	16.27	19.05	19.54
CLPE 260 (Filtrate)	15.16	16.23	17.19
CLPE 260 (MSR)	17.58	17.36	17.41
CLPE 280 (Filtrate)	15.36	12.21	14.95
CLPE 280 (MSR)	15.82	14.77	16.86
CLPU 240 (Filtrate)	12.87	13.89	14.35
CLPU 240 (MSR)	16.75	17.35	17.41
CLPU 260 (Filtrate)	18.40	14.89	16.09
CLPU 260 (MSR)	16	15.89	17.69
CLPU 280 (Filtrate)	14.34	13.52	10.75
CLPU 280 (MSR)	16.19	16.72	15.1
HHV, Methanol (pure reagent), MJ kg^{-1}= 19.62			

In fact, the viscosity of the MSR exhibited a substantial increase with higher liquefaction temperatures for both biomasses except for a minor decrease for CLPU from 260 °C to 280 °C. However, the viscosity of the filtrates showed mixed trends. HHV of MSR was found to be greater than that of the filtrates for both CLPE and CLPU biomasses except for CLPU at 1:2 biomass-to-solvent ratio. This could be explained by the solvent's higher penetration into biomass whilst the starting liquefaction phase, which is influenced by the biomass-to-solvent ratio [85]. As the temperature increased from 240 °C to 260 °C, HHV of the filtrates were observed to rise for both CLPE and CLPU biomasses, however, the opposite was observed for further rise in temperature to 280 °C except for CLPE at 1:2 biomass-to-solvent ratio. HHV specific to biocrude (Table 5.3.2) obtained in this study from the liquefaction of CLPE and CLPU biomass were found to be between 21.65 MJ kg^{-1} and 27.18 MJ kg^{-1}, in comparison to the HHV of 13.81 and 15.88 MJ kg^{-1} of CLPE and CLPU biomass feedstock, respectively [275]. The considerably higher energy values of the biocrude, as compared to the feedstock, could be attributed to the enhanced energy densification resulting from the liquefaction in methanol solvent [277]. The findings obtained were consistent with literature reports on other lignocellulosic biomasses [144]. Based on the results, it could be inferred that the liquid products obtained from the liquefaction of both biomasses could be utilized as valuable fuels for heat generation. The HHV of the biocrude showed upsurge with temperature rise from 240

°C to 280 °C at all biomass-to-solvent ratios, except for the 1:2 biomass-to-solvent ratio from 260 °C to 280 °C. At 280 °C and a 1:4 biomass-to-solvent ratio, CLPU liquefaction biocrude produced a maximum HHV of 27.18 MJ kg^{-1}, which was greater than its value at 240 and 260 °C [275]. This relatively high HHV could be attributed to the higher carbon content and lower oxygen content resulting from dehydration, decarbonylation and decarboxylation reactions during liquefaction [277]. Another potential explanation for the observed trend is the rise in hydrogen content brought on by the production of active H_2 by CH_3OH in its supercritical state and its incorporation into biocrude. For both CLPE and CLPU biomasses, it was discovered that at 240 °C, the HHV of the biocrude initially increased and subsequently decreased with a decline in the biomass-to-solvent ratio. Hence, careful adjustment of the biomass-to-solvent ratio has to be done in order to obtain optimum heating values of the biocrude [85].

Table 5.3.2 Fuel potential of biocrude and biochar from liquefaction of CLPE and CLPU at 240 °C, 260°C and 280 °C temperature and changing biomass-to-solvent ratios.

	HHV of biocrude, MJ kg^{-1}			HHV of biochar, MJ kg^{-1}		
Feedstock	1:2	1:3	1:4	1:2	1:3	1:4
CLPE 240	23.02	23.82	21.65	14.65	15.71	16.28
CLPE 260	24.91	24.2	23.7	14.94	15.55	16.5
CLPE 280	22.83	26.72	25.58	17.27	17.19	19.07
CLPU 240	22.36	23.63	22.73	15.32	15.6	15.43
CLPU 260	26.36	26.7	26.76	16.98	16.46	16
CLPU 280	26.36	26.7	27.18	24.65	20.62	16.58

5.3.2.2 Chemical characterization

To make sure the quality of the biocrude fulfils the required standards its chemical characterization is required. It provides valuable information about the quality, properties and potential applications of this renewable energy source. An assessment of the qualitative changes in the composition of samples obtained through different processing conditions was conducted using FTIR analysis [277]. The FTIR spectra corresponding to biocrude from CLPE and CLPU liquefaction between 240 °C and 280 °C, respectively, with biomass-to-solvent ratios of 1:2, 1:3 and 1:4 has provided information on various functional groups specific to the biocrude by their corresponding % transmittance peaks at different

wavenumbers as depicted in Figure 5.3.2 and it depicts their mutual resemblance. The notations of CLPE 240_2, CLPE 240_3, CLPE 240_4, CLPE 260_2, CLPE 260_3, CLPE 260_4 and CLPE 280_2, CLPE 280_3, CLPE 280_4 indicated biocrude found via liquefaction of peel of *Citrus limetta* at 240 °C, 260 °C and 280 °C with biomass-to-solvent ratios of 1:2, 1:3 & 1:4 respectively. Similarly, it was also applicable to *Citrus limetta* pulp biomass too.

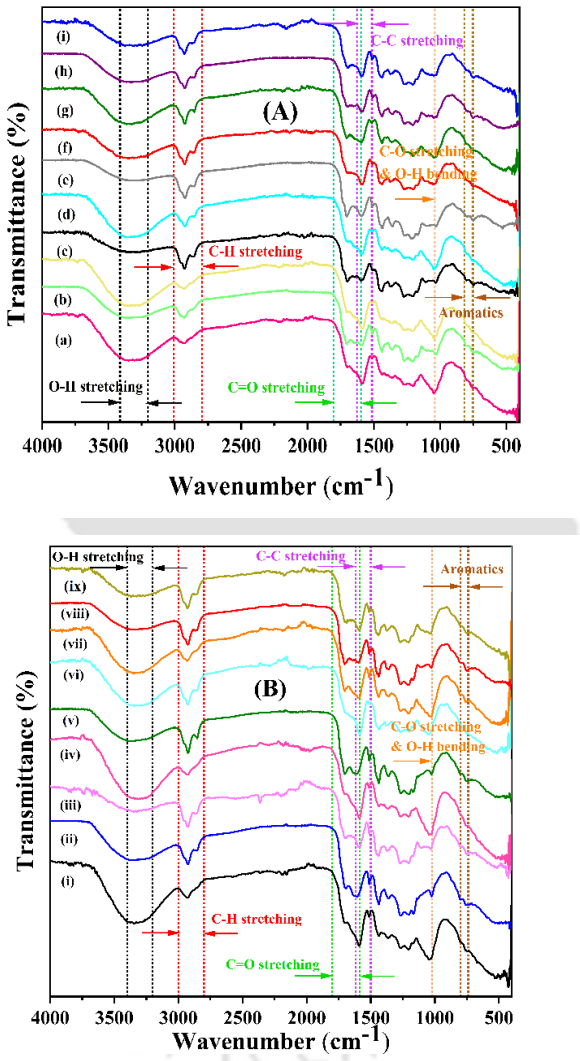

Figure 5.3.2 Biocrude FTIR spectra from liquefaction of (A) CLPE where (a) CLPE 240_2 (b) CLPE 260_2 (c) CLPE 280_2 (d) CLPE 240_3 (e) CLPE 260_3 (f) CLPE 280_3 (g) CLPE 240_4 (h) CLPE 260_4 (i) CLPE 280_4 and (B) CLPU where (i) CLPU 240_2 (ii) CLPU 260_2 (iii) CLPU 280_2 (iv) CLPU 240_3 (v) CLPU 260_3 (vi) CLPU 280_3 (vii) CLPU 240_4 (viii) CLPU 260_4 (ix) CLPU 280_4.

The presence of vibrations caused by the stretching of hydroxyl O-H groups between 3200 and 3400 cm^{-1} wavenumbers for both biomasses has been clearly seen here [278]. The evidence of the occurrence of methyl and methylene groups indicating towards long chain alkanes has been supported by visible points of peaks in 3000-2802 cm^{-1} and 1460-1351 cm^{-1} wavelength for C-H absorption in the spectra [250]. The abundance of species that contain aliphatic chains is demonstrated by the relatively high intensity of these modes for high temperature biocrude obtained from CLPE. The sharp absorption peaks within the range of 1800-1586 cm^{-1} were assigned to the vibrational stretching phenomenon of the C=O bond in mainly esters, carboxylic acids, ketones and aldehydes. Given the chemical characteristics of both the treated feedstock and the liquefaction medium comprising of alcohol, the presence of esters is an expected outcome [277]. Absorption peaks between 1500-1620 cm^{-1} confirmed the presence of aromatic C-C stretching vibrations. A peak around 1020 cm^{-1} indicated the presence of C-O and O-H stretching and bending vibrations respectively in primary, secondary and tertiary alcohols along with phenol, ether and esters. These peaks were less sharp at high temperatures for CLPE biocrude indicating the deterioration of oxygen groups in them due to high temperature conditions. Peak points within 800-741 cm^{-1} region demonstrated the existence of single, polycyclic and replaced groups in aromatic compounds. The qualitative composition of the obtained biocrude appears to be minimally affected by the variation in biomass-to-solvent ratios, as evidenced by the close similarity of the collected spectra.

Figure 5.3.3 provided the NMR analysis of biocrude from both biomasses which gave information on their chemical structure. On the basis of chemical shift with reference to literature [279], the functional groups were assigned to them. The chloroform-D solvent employed in NMR investigations caused a chemical shift, as demonstrated by the peak point at 7.26 ppm. Peak at 0 ppm represented the default tetramethylsilane (TMS) standard [215].

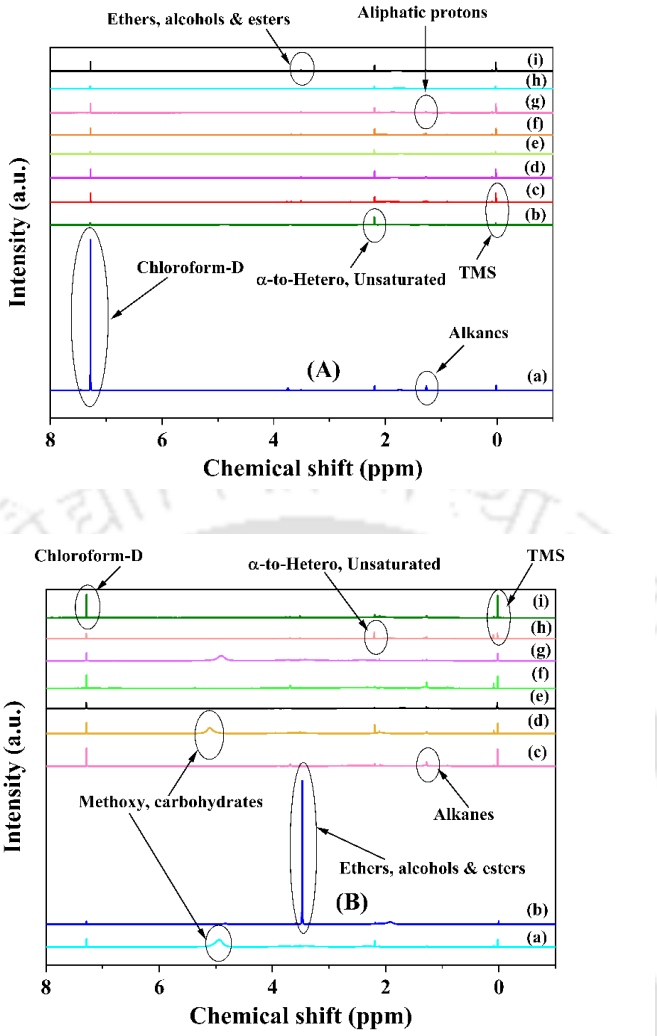

Figure 5.3.3 ^{1}H NMR showing chemical shift in ppm for biocrude from liquefaction of (A) CLPE where (a) CLPE 240_2 (b) CLPE 260_2 (c) CLPE 280_2 (d) CLPE 240_3 (e) CLPE 260_3 (f) CLPE 280_3 (g) CLPE 240_4 (h) CLPE 260_4 (i) CLPE 280_4 and (B) CLPU where (a) CLPU 240_2 (b) CLPU 260_2 (c) CLPU 280_2 (d) CLPU 240_3 (e) CLPU 260_3 (f) CLPU 280_3 (g) CLPU 240_4 (h) CLPU 260_4 (i) CLPU 280_4.

Peaks at 0 to 1.5 ppm implied the presence of aliphatic connection of proton to the carbon atoms of alkanes [280]. The occurrence of fatty acids and alkanes in both CLPE and CLPU biocrude that resulted from the decomposition of feedstock may be responsible for the alkane content [281]. The α-heteroatom/unsaturated functional groups were represented by chemical shift in 1.5 to 3 ppm range. This was an indication of generation of large number of nitrogenous and oxygenated compounds from feed [279]. The peaks within the range of 3 to 4.5 ppm showed protons attached to C atoms in alcohols, esters and ethers [245]. Alcoholic

and ester compound synthesis increased as a result of the use of methanol in the liquefaction process. This was verified by investigating the spectra of FTIR of the biocrude that was produced using both biomasses. At 240 °C, small peaks were observed for CLPU within the 4.4 to 6 ppm range. However, these peaks were not present at 280 °C, suggesting that the occurrence of protons associated with methoxy/carbohydrate functional groups in biocrude reduced significantly at higher temperatures. This observation indicated that a substantial amount of carbohydrates underwent conversion at the higher temperature [282]. Commonly, aldehydes and acidic protons are responsible for the proton signals in the 8.5–10 ppm range. However, none of the biocrude analyzed exhibited proton signals in this region. Nevertheless, FTIR spectrum analysis of the biocrude portrayed incidence of C=O functional groups, which could be attributed to carbonyl groups, esters, amides and ketones [283].

A list of exemplary compounds from GC-MS results were compiled based on their fitting to the NIST library above a certain threshold level in Table 5.3.3. GC-MS analysis of the obtained biocrude at different temperatures was carried out for identification of probable chemical compounds in them. While several compounds were identified, only those with relatively higher peak areas were included. It was worth mentioning that due to the high molecular weights and boiling point distributions of the biocrude, as well as the limitations of the GC-MS instrument's temperature range, only a fraction of the products resulting from liquefaction were identifiable. Additionally, some low boiling point compounds could potentially be masked by solvent peaks or lost during the solvent evaporation process used for biocrude recovery. The majority of the components in biocrude produced via liquefaction of CLPE and CLPU between 240 and 280 °C fell into the C_5 to C_{18} group range. which was consistent with earlier liquefaction experiments for the same biomasses at 260 °C [275]. Table 5.3.4 provided an area % distribution of major compounds in biocrude as obtained from their GC-MS results However, with variations of biomass as well as temperature it was observed that the relative area percentages of these compounds against their retention times in the column started to change and become more prominent. Due to the depolymerization of the lignin or cellulose present in the biomasses, the biocrude produced from both biomasses had a higher amount of phenolic derivative chemicals [283]. The biocrude, in fact, contained a greater proportion of aliphatic structural elements, as well as substituted phenol and aromatic compounds. Previous literature have reported that the production of phenols from glucose during liquefaction involves a process wherein glucose is first converted to furan and then to

phenols by rearrangement reactions [284]. At the highest processing temperature of 280 °C, the presence of higher area % of phenol derivatives suggested that lignin, which is known to be the most thermally stable biopolymer, underwent more extensive decomposition during the liquefaction process [285]. The production of esters was likely due to the decomposition of cellulose and hemicellulose in the biomass and this production was enhanced in the presence of alcoholic solvents. Methanol's presence in the liquefaction reaction showed that it underwent alkylation and esterification reactions with the intermediates from the liquefied biomass [286]. Cyclic ketones and furan derivatives were found in the biocrude, which pointed to the breakdown of polysaccharides including cellulose and hemicellulose. It was likely that under the liquefaction conditions, polysaccharides underwent depolymerization into smaller monosaccharides [277]. Furthermore, the identification of N-containing heterocycles in the liquefaction products might have indicated the manifestation of Maillard reaction amid amino acids and carbohydrates, which are thermodynamically preferred at temperatures above 180 °C [287]. However, the identification of low N-containing compounds in the present investigation is consistent with the information found in the literature about the liquefaction of specific citrus wastes [72]. The decreased O_2 amount in the biocrude from liquefaction might be attributed to the removal of H_2O through dehydration and CO_2 through decarboxylation processes. It is possible that this deoxygenation prompted the hydrocarbon production of biocrude [288]. The analysis of the liquid biocrude indicated its potentiality and implementation as an alternative fuel source but obviously only after their processing through suitable upgrading technologies.

Table 5.3.3 Major compounds obtained via GC-MS study of liquefaction biocrude of CLPE and CLPU at 240 °C and 280 °C temperature.

Compounds	Molecular formula	Chemical class	CLPE 240		CLPE 280		CLPU 240		CLPU 280	
			RT (min)	Area (%)	RT (min)	Area (%)	RT (min)	Area (%)	RT (min)	Area (%)
Aziridine, 2-methyl-2-(2,2,4,4-tetramethylpentyl)-	$C_{12}H_{25}N$	Aziridines	7.018	5.294	-	-	-	-	-	-
3-methyl-2-(2-oxopropyl) furan	$C_8H_{10}O_2$	Heteroaromatic compounds/Furan	-	-	7.018	3.755	-	-	-	-
Cyclohexanol, 4-methyl-	$C_7H_{14}O$	Alcohol	-	-	-	-	7.018	6.341	-	-
1-cyclohexyl-2-propen-1-ol	$C_9H_{16}O$	Secondary alcohols	-	-	-	-	-	-	7.018	3.869
2-(1-methylcyclopentyloxy)-tetrahydropyran	$C_{11}H_{20}O_2$	Oxanes/ Hexic cyclic ether ring	7.133	3.144	-	-	-	-	7.138	2.502
6,6-dimethyl-1,3-heptadien-5-ol	$C_9H_{16}O$	Secondary alcohol	-	-	7.133	2.160	-	-	-	-
Cyclopentane, methyl-	C_6H_{12}	Cycloalkanes	7.314	20.864	7.314	17.637	7.314	25.449	7.314	22.637
Cyclopentanone, 2-(1-methylpropyl)-	$C_9H_{16}O$	Cyclic ketones/Cyclo oxegenates	8.084	1.035	8.084	0.739	8.084	0.684	-	-
Furan, 2-methoxy-	$C_5H_6O_2$	Alkyl aryl ethers	10.975	8.254	10.975	5.931	10.985	8.015	10.980	7.926

2-octanol, 2,6-dimethyl-	$C_{10}H_{22}O$	Tertiary alcohols	12.090	3.640	12.090	2.563	-	-	12.095	3.038
4-pyridinol	C_5H_5NO	Hydroxypyridines	18.208	0.544	-	-	-	-	-	-
4(1h)-pyridone	C_5H_5NO	Pyridine	-	-	-	-	18.248	0.622	-	-
Catechol	$C_6H_6O_2$	Phenol/Phenolics	20.639	0.540	-	-	20.679	0.358	20.664	0.451
2-amino-3-hydroxypyridine	$C_5H_6N_2O$	Aminopyridines and derivatives	-	-	-	-	-	-	22.320	0.479
Alpha.-d-xylofuranoside, methyl	$C_6H_{12}O_5$	Glycoside	24.425	0.582	-	-	-	-	-	-
Phenol, 2,6-dimethoxy-	$C_8H_{10}O_3$	Phenol	-	-	-	-	-	-	24.841	0.355
Cyclohexanone, 4-methoxy-	$C_7H_{12}O_2$	Cyclic ketones	24.931	0.758	-	-	-	-	-	-
2h-pyran-3,4,5-triol, tetrahydro-2-methoxy-6-methyl-	$C_7H_{14}O_6$	Pyranoid	-	-	-	-	24.971	0.392	-	-
D-galactitol, 1-o-octyl-	$C_{14}H_{30}O_6$	Alcohol	25.221	0.673	-	-	-	-	-	-
Arsenous acid, tris(trimethylsilyl) ester	$C_9H_{27}AsO_3Si_3$	Arsenic ester	33.734	0.605	36.025	0.675	34.184	0.809	36.305	0.436
1,2-dimethoxy-4-(1-methoxy-1-propenyl)benzene	$C_{12}H_{16}O_3$	Methoxy benzene	34.124	0.769	-	-	-	-	-	-
4-tert-octylphenol, tms derivative	$C_{14}H_{22}O$	Phenol	34.374	0.561	35.055	0.531	34.009	0.359	36.775	1.095
Tetradecanoic acid, 10,13-dimethyl-, methyl ester	$C_{17}H_{34}O_2$	Fatty acid methyl ester	-	-	34.374	3.730	-	-	-	-

4-(4-hydroxyphenyl)-4-methyl-2-pentanone, tms derivative	$C_{12}H_{16}O_2$	Phenylpropanes	-	-	35.330	0.536	-	-	-	-
Hexadecanoic acid, methyl ester	$C_{17}H_{34}O_2$	FAME	-	-	-	-	-	-	34.434	1.616
Benzestrol, 2tms derivative	$C_{26}H_{42}O_2Si_2$	TMS derivative	-	-	35.795	0.605	38.686	0.387	-	-
1,e-11,z-13-octadecatriene	$C_{18}H_{32}$	Alkatrienes	-	-	36.650	4.235	-	-	-	--
4-hydroxyphenyllactic acid, ethyl ester, di-tms	$C_{17}H_{30}O_4Si_2$	TMS derivative	36.655	1.662	-	-	-	-	-	-
Hexestrol, 2tms derivative	$C_{18}H_{22}O_2$	Phenol	-	-	36.695	1.604	34.264	0.352	36.730	1.629
Thymol, tms derivative	$C_{10}H_{14}O$	Phenol	-	-	36.760	3.477	34.444	1.070	-	-
2,4-dihydroxyacetophenone, 2tms derivative	$C_{14}H_{24}O_3Si_2$	Ketone	-	-	-	-	36.855	0.583	-	-
4-tert-amylphenol, tms derivative	$C_{11}H_{16}O$	Aromatic hydrocarbon/Phenyl propanes	-	-	-	-	-	-	38.591	0.383
Cyclotrisiloxane, hexamethyl-	$C_6H_{18}O_3Si_3$	Column bleeding, Chemical	-	-	36.955	0.632	36.735	1.029	36.830	1.132

Table 5.3.4 Percentage distribution of major compounds in biocrude via liquefaction of CLPE and CLPU between 240 °C and 280 °C based on GC-MS results.

Compound Class	CLPE 240 (Area %)	CLPE 260 (Area %)	CLPE 280 (Area %)	CLPU 240 (Area %)	CLPU 260 (Area %)	CLPU 280 (Area %)
Acid & Ester	0.605	21.063	4.405	0.809	7.709	2.052
Alcohol	4.313	7.021	4.723	6.341	5.163	6.907
Phenol	1.101	-	5.612	2.139	0.75	3.53
Alkane	20.864	3.935	18.173	25.449	0.964	22.637
Alkene	-	-	4.235	-	-	-
Ether	11.398	8.778	5.931	8.015	8.073	10.428
Ketone/Aldehyde	1.793	4.667	0.739	1.267	11.319	-
Aromatic	0.769	-	3.755		-	0.383
Nitrogen containing	5.838	-	-	0.622	-	0.479
Other	2.244	8.085	1.237	1.988	7.379	1.132

5.3.3 Characterization of solid products

The HHV of biochars obtained from the liquefaction of CLPE and CLPU exhibited an increasing trend with the rise in temperature from 240 °C to 280 °C as shown in Table 5.3.2. This observation was consistent with findings reported in the literature [144]. The biochars obtained from both biomasses showed HHV values ranging from 14.65 to 24.65 MJ kg^{-1}, with the highest HHV of 24.65 MJ kg^{-1} observed for CLPU at a biomass-to-solvent ratio of 1:2 at 280 °C. The reduction in the biochar's initial mass as well as the removal of low energy volatiles through hydrolysis, decarboxylation and dehydration processes may be responsible for the rise in carbon content of the material [289].

TGA & DTG analysis figures corresponding to biochars attained via liquefaction of CLPE and CLPU at temperatures of 240 °C and 280 °C have been depicted in Figure 5.3.4 (A) & (B) respectively. The initial decomposition temperature, extent of weight loss and rate of weight loss could provide information on the compositional and structural changes that occurred during the liquefaction process, as well as the thermal stability of the biochar. These plots could be useful in understanding the properties and characteristics of biochar as a product of biomass liquefaction [265]. They demonstrated that the biochar exhibited a higher initial decomposition temperature compared to the raw biomass. This suggested that liquefaction had induced both compositional and structural modifications in the biomass. The moisture removal from acidic functional groups, which took place across a number of phases, may be responsible for the weight loss that happened during the liquefaction process. The first stage comprised the elimination of water, while the second stage entailed the degradation of hemicelluloses. The third step included cellulose breakdown, while the fourth stage involved the breakdown of the lignin structure. The thermal analysis of biochar revealed weight loss in 40-200 °C that attributed to the removal of moisture from them. In the 280–500 °C temperature range, cellulose breakdown was first noticed followed by hemicellulose.

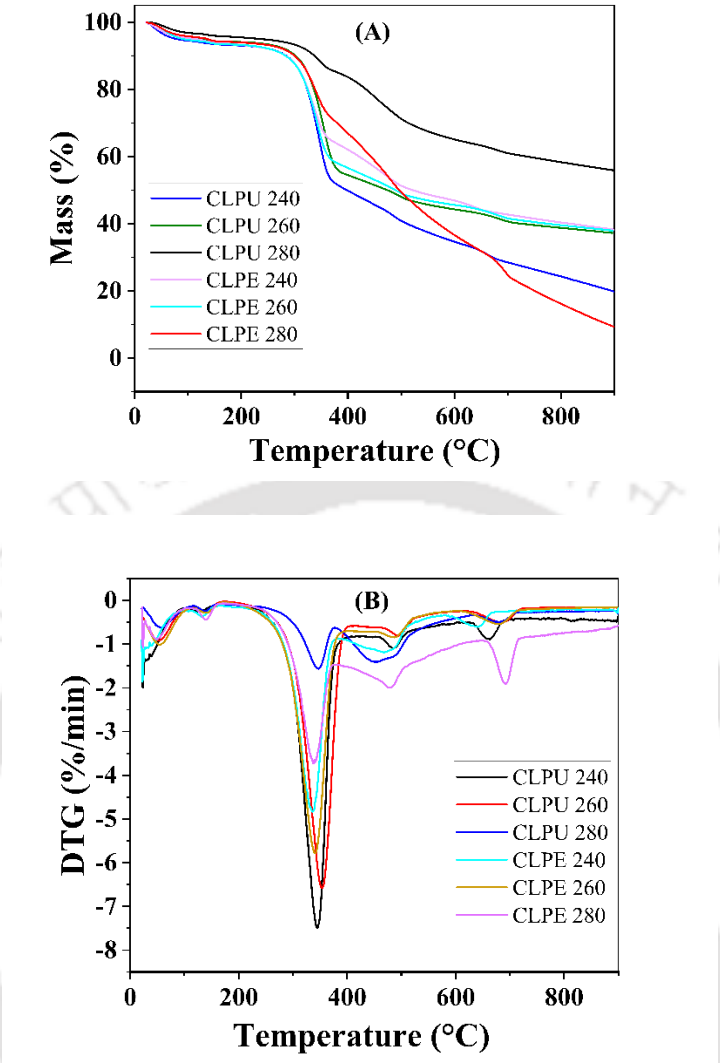

Figure 5.3.4 (A) Thermo-gravimetric-analysis (TGA) and (B) Differential-thermo-gravimetry (DTG) plot corresponding to CLPE & CLPU biochar between 240 °C and 280 °C.

Additionally, the study found that mass loss over 600 °C temperature specified complete oxidation and degradation of organic components with low boiling and melting points, leaving only carbon residue [290]. The highest weight loss rate was obtained at 340-350 °C and indicated that complete decomposition of cellulose and hemicellulose of both biomasses in liquefaction have not occurred [264]. It was evident from the corresponding TGA and DTG plots for CLPU biochar at 280 °C that it possessed higher thermal stability in comparison to biochar at 240 °C owing to the occurrence of an insignificant weight loss derivative in its case. But similar conclusion could not be drawn from biochar obtained at 280 °C from CLPE

biomass. This could be due to the difference in composition of these biomasses. Table 5.3.5 provided the ultimate analysis of the biochars from liquefaction of CLPE and CLPU at temperatures of 240 °C to 280 °C. It was observed that with rise in temperature from 240 °C to 260 °C H/C ratio of both CLPE and CLPU biochar was decreasing which might have been due to initial removal of hydrogen from biomass during liquefaction.

Table 5.3.5 Ultimate analysis of biochars from CLPE and CLPU liquefaction at 240 °C, 260°C and 280 °C.

	Ultimate analysis, wt. %						
Biochar	C	H	N	S	O[a]	H/C	O/C
CLPE 240	47.16	6.17	2.06	-	44.61	1.570	0.710
CLPE 260	59.96	4.77	2.21	-	33.06	0.955	0.414
CLPE 280	62.59	5.93	2.08	-	29.4	1.137	0.352
CLPU 240	50.09	5.83	1.9	-	42.18	1.397	0.632
CLPU 260	50.92	4.26	2.13	-	42.69	1.004	0.629
CLPU 280	51.62	6.17	1.77	-	40.44	1.434	0.588

[a] calculated by difference

However, for further rise in temperature from 260 °C to 280 °C, the increase in H/C ratio indicated occurrence of hydrogenating reaction at high temperature during its liquefaction. O/C ratio for both biochars on the other hand was found to be decreasing with temperature rise thereby giving a clear sign of substantial oxygen removal from them during liquefaction at high temperatures [291].

The impact of liquefaction on cellulose crystalline structure, resulting in disruptions of cellulose chain hydrogen bonding, was assessed using powder XRD analysis. This technique was employed to study the crystalline characteristics of dry samples of biochar and to investigate any fluctuations or changes in their crystalline structure [292]. Figure 5.3.5 represented the XRD patterns of both CLPE and CLPU biochars between temperatures of 240 and 280 °C. The diffractrogram patterns of all biochars exhibited similarities, although slight differences were observed. Diffraction related peaks were compared to a database by the Joint Committee on Powder Diffraction Standards (JCPDS). XRD patterns of CLPU & CLPE biochars revealed two peaks at $2\theta = 15°$ and 22°, which pointed to presence of cellulose in both [293]. According to JCPDS No. 00-003-0192, these peaks were due to cellulose pattern.

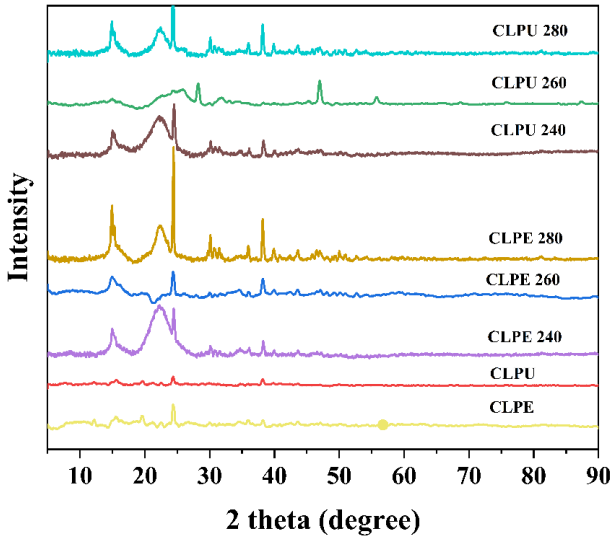

Figure 5.3.5 X-ray diffractogram of CLPE and CLPU biomass and their biochars from liquefaction between 240 °C to 280 °C.

Peak values viz. 2θ = 24° and 26° having JCPDS No. 00-003-0192 in the XRD pattern showed that cellulose and lignin were broken down during the liquefaction process. These peaks also indicated the presence of turbostratic and amorphous carbon, suggesting the formation of biochar through the breakdown of biomass components due to liquefaction [74]. In fact, the presence of these peaks indicated that the biomass underwent partial decomposition, while the cellulose component retained some of its crystalline nature, demonstrating its thermal stability to a certain extent [294]. However, it was observed that subsequent heating to high temperature of 280 °C did not cause the peak positions of XRD plots of biochar to change noticeably, but it did lead to sharper and more symmetrical peaks.

The adsorption/desorption isotherms of nitrogen at 77K and the surface parameters of biochars obtained from the liquefaction of CLPE and CLPU between 240 °C and 280 °C have been illustrated in the Figure 5.3.6 and summarized in the Table 5.3.6, respectively. The presence of a hysteresis loop in the nitrogen adsorption/desorption isotherms, as shown in the Figure 5.3.6, indicated a Type IV isotherm as per the classification of IUPAC [295]. This suggested that the biochars predominantly possessed mesoporous carbon with some traces of microporous solids and that multilayer formation occurred at low pressure after monolayer coverage [296]. The diameter size of the pores, as confirmed by the Table 5.3.5, lay between 2-50 nm, which is in the mesopore range according to the IUPAC classification of pore sizes

[295]. Literature suggested that the characteristic mesoporous structure of biochars conferred favourable attributes for adsorbing not only large sized dye molecules and emerging contaminants, but also heavy metals [297,298]. The surface areas of the biochars in this study were found to be consistent with those reported in contemporary studies on biomass liquefaction [295,299,300]. The comparatively low surface area and pore volume measurements could be explained by potential pore blockage brought on by the organic materials present in the biochars [301].

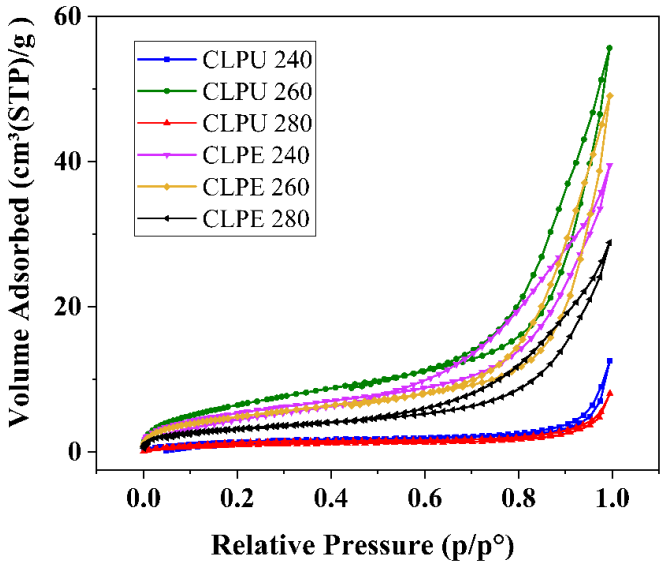

Figure 5.3.6 Adsorption and desorption isotherms for N_2 at 77K for biochars found via liquefaction of CLPE and CLPU biochars at 240 °C, 260°C and 280 °C.

Table 5.3.6 Surface parameters of biochars via liquefaction of CLPE and CLPU at 240 °C, 260 °C and 280 °C.

Biochar	Surface morphology		
	Surface area, $m^2\ g^{-1}$	Avg. size of pore / diameter, nm	Total volume of pore (P/P_o = 0.99), $cm^3\ g^{-1}$
CLPE 240	20.11	11.74	0.059
CLPE 260	18.11	16	0.073
CLPE 280	11.62	14.86	0.043
CLPU 240	5.42	12.87	0.018
CLPU 260	25.08	13.27	0.083
CLPU 280	3.57	12.69	0.011

The surface morphology, structure and topography of the biochar material as studied by FESEM analysis (at 600X and 1KX magnification) has been shown in Figure 5.3.7 and Figure 5.3.8. As reported in previous studies the biomasses CLPE and CLPU possessed a lumpy and fibrous dense solid structure [275] that was evidently disrupted by liquefaction in methanol at varying temperatures to a rough and porous structure. The observed changes in morphology might be pertained to the various chemical reactions that ensued during the process of liquefaction [299]. The biochars for both biomasses at 240 °C showed somewhat fibrous structure adhered with some particle deposits along with the presence of small pores. These deposits came from the mineral residues after their liquefaction [74]. The biochar surface also exhibited agglomerations that could be attributed to cross-linking triggered by the dehydration reaction between hemicellulose and cellulose molecules. However, upon closer examination, the biochars obtained at 280 °C revealed the presence of numerous cavities and pores with varying sizes and irregular shapes on their surfaces.

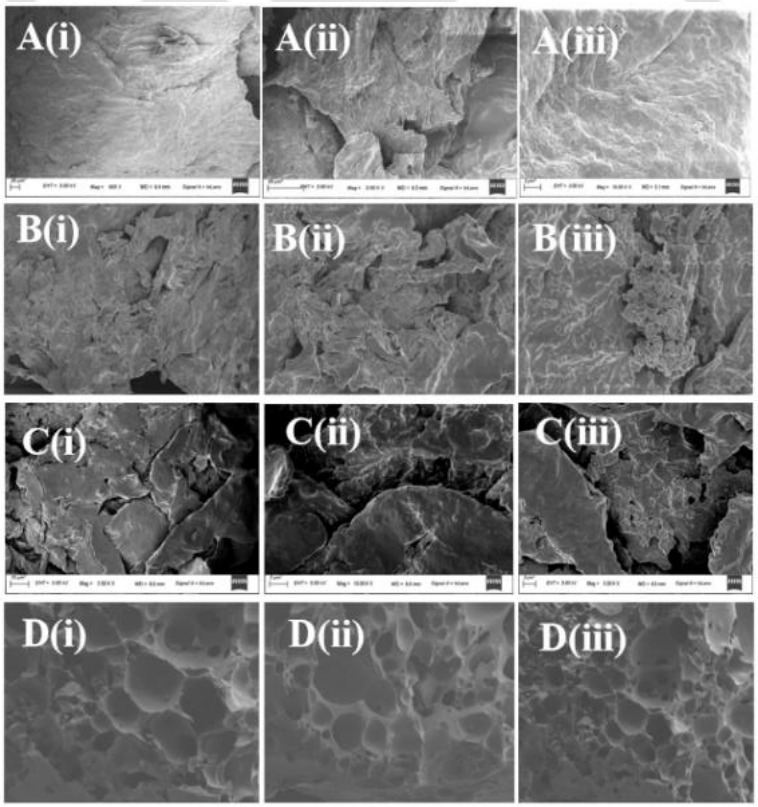

Figure 5.3.7 A(i), A(ii) & A(iii): FESEM images of CLPU biomass; B(i), B(ii) & B(iii), C(i), C(ii) & C(iii) and D(i), D(ii) & D(iii): FESEM images of biochar obtained by liquefaction of CLPU biomass at 240 °C, 260 °C and 280 °C ((i) 2KX, (ii) 5KX and (iii) 10KX resolutions each).

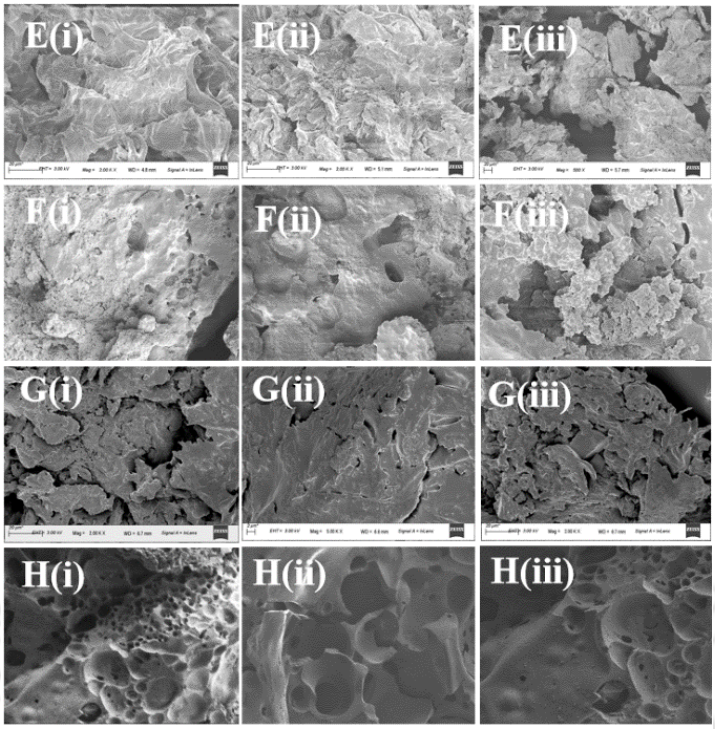

Figure 5.3.8 E(i), E(ii) & E(iii): FESEM images of CLPE biomass; F(i), F(ii) & F(iii), G(i), G(ii) & G(iii) and H(i), H(ii) & H(iii): FESEM images of biochar obtained by liquefaction of CLPE biomass at 240 °C, 260 °C and 280 °C ((i) 2KX, (ii) 5KX and (iii) 10KX resolutions each).

This occurrence could be linked to the decomposition of cellulose and hemicellulose during the process of liquefaction at higher temperature, leading to disruptions in the cell structure and the formation of cracks and pores on the surface [295]. These characterization results clearly indicated the suitability of biochars to be used as a solid fuel source as well as an adsorbent for soil and water remediation.

5.3.4 Summary

The findings from this objective where solvothermal liquefaction of *Citrus limetta* pulp and peel had been carried out at variable temperature between 240 °C to 280 °C and variable biomass-to-solvent ratios of 1:2, 1:3 and 1:4 have been summarized below:

- The highest biocrude yield of 12.5 wt. % for *Citrus limetta* peel biomass occurred at 240 °C and 1:3 biomass-to-solvent ratio.
- Enhanced energy densification was observed, with a maximum higher heating value (HHV) of 27.18 MJ kg^{-1}, obtained from pulp liquefaction of *Citrus limetta* biocrude at 280 °C and a 1:4 biomass-to-solvent ratio.

- Major compounds identified in biocrude through GC-MS included phenols (more significant at 280 °C), alcohols, alkanes, ketones, ethers, esters and fatty acid methyl esters, suggesting their potential use as biofuel.
- High HHV of biochar between 14.65 MJ kg^{-1} to 24.65 MJ kg^{-1} suggested the potential implementation of biochar as a solid fuel source.

5.4 Solvothermal co-liquefaction of pulp and peel of *Citrus limetta* fruits at variable biomass-to-solvent ratios

5.4.1 Product yield analysis

From Figure 5.4.1 we can observe the filtrate (wt. %) and biochar (wt. %) yield as well as yield of others obtained from solvothermal co-liquefaction of *Citrus limetta* peel (CLPE) and pulp (CLPU) biomasses at 1.2 co-feed ratio in methanol at 260 °C temperature and varying biomass-to-solvent ratios of 1:2, 1:3 and 1:4. The variation in product yield with biomass-to-solvent ratios depicted highest filtrate yield at 1:4 biomass-to-solvent ratio for co-liquefaction of peel and pulp, which was similar to filtrate yield trends from individual peel and pulp biomasses as reported in Subsection 5.2.1 of this thesis. As a probable characteristic of the fruit waste biomass and in consistency with biochar yield from single feed liquefaction of CLPE and CLPU biomasses, the yield of biochar from their co-liquefaction was also found to be quite low. This yield in a solvent-rich environment was found to be decreasing with decline in biomass-to-solvent ratios just like from individual biomass runs indicating maximum conversion of biomass organics to liquid biocrude. The biocrude obtained from co-liquefaction of CLPE and CLPU was analyzed for its yield in wt. % basis with reference to the raw feedstock for co-liquefaction as shown in Table A2 and Figure A2 of Annexure. This yield was observed to decline with diminution in biomass-to-solvent ratio which was just opposite to the case of individual peel and pulp biomass liquefaction as depicted in Subsection 5.2.1. In fact, the maximum biocrude yield from co-liquefaction was found to be 11.25 wt. % which was slightly lower than the maximum yield for CLPE liquefaction (12.5 wt. %) while higher than CLPU liquefaction (7.88 wt. %) at the same biomass-to-solvent ratio and temperature 260 °C. The difference in yield from co-liquefaction in comparison to individual feedstock liquefaction might have presumably occurred due to intermixing of like constituents of lignocellulosic biomass viz. hemicellulose, cellulose and lignin amongst themselves [121]. This would possibly have resulted in higher cracking and repolymerization by conversion of

most of the organic matters into gaseous and solid phases, respectively, thereby reducing biocrude yield from them [302]. The biocrude yield reported from co-liquefaction in this work was comparable and higher (for certain biomass co-feed ratio) than hydrothermal co-liquefaction of citrus fruit waste with microalgae [68]. However, it may be noted that apart from biomass-to-solvent ratio, several other decisive factors such as biomass co-feed ratio, operating temperature, pressure, feedstock type, residence time, reactor volume, particle size, cooling and heating rates etc. effect the yield of biocrude to get optimum results [53,85].

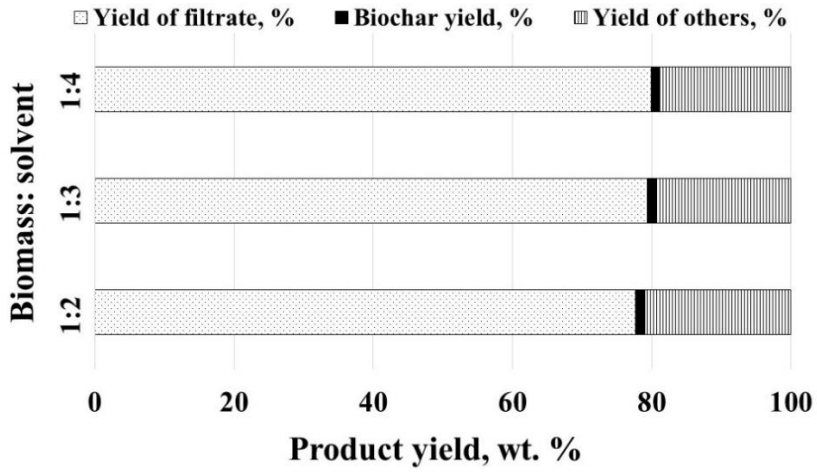

Figure 5.4.1 Distribution of product yield from CLPE and CLPU biomass co-liquefaction at 260 °C and varying biomass-to-solvent ratios.

5.4.2 Liquid product analysis

5.4.2.1 Physical and fuel characteristics

Table 5.4.1 shows the physical characteristics and energy content of the filtrate and MSR post solvent removal from co-liquefaction products of CLPE and CLPU which shall be denoted as CLPE-PU henceforth, at co-feed ratio of 1.2 and 260 °C temperature with methanol at biomass-to-solvent ratios of 1:2, 1:3 and 1:4. It was observed that at vapor pressures near to methanol in its pure form, the filtrate contained some lighter hydrocarbons. The results obtained also gave a possible indication of transfer of few lighter hydrocarbon fractions of filtrates and/or their methanol soluble fractions to MSR during the process of evaporation since the density and viscosity of MSR was evidently more than that of pure methanol solvent. Therefore, this rendered them to be unsuitable in terms of usage as solvent but showed their

utility as lighter portion of fuel. However, both the densities and viscosities of filtrate and MSR from co-liquefaction were seen to be rising with rise in biomass-to-solvent ratios unlike their individual counterparts where they showed a decreasing trend with biomass-to-solvent ratio rise**.**

Table 5.4.1 Physical characteristics of MSR and filtrate from co-liquefaction of CLPE and CLPU at 260 °C temperature and varying biomass-to-solvent ratios.

Product	1:2	1:3	1:4
		Density, g mL^{-1}	
CLPE-PU (Filtrate)	0.865	0.856	0.847
CLPE-PU (MSR)	0.833	0.824	0.823
Density of pure methanol (reagent grade), g mL^{-1}= 0.782			
		Viscosity, mPa.s	
CLPE-PU (Filtrate)	1.219	1.089	1.044
CLPE-PU (MSR)	0.928	0.906	0.897
Viscosity of pure methanol (reagent grade), mPa.s = 0.677			
		HHV, MJ kg^{-1}	
CLPE-PU (Filtrate)	14.54	15.26	15.96
CLPE-PU (MSR)	15.83	16.78	16.74
HHV of pure methanol (reagent grade), MJ kg^{-1} = 19.62			

HHV of filtrate from CLPE and CLPU co-liquefaction was observed to be decreasing with increasing biomass-to-solvent ratio and approximately similar trends were observed for their corresponding MSR also except at 1:3 biomass-to-solvent ratio. Also HHV of MSRs were greater than filtrates just like individual liquefaction results and that might be accredited to rise in penetration of solvent into biomass with increasing biomass-to-solvent ratios during the initial stage of co-liquefaction [85,275]. HHV of biocrude from co-liquefaction of CLPE and CLPU (final liquid product after recovery of MSR from raw filtrate) followed mixed trend with increase in biomass-to-solvent ratios as represented in Table 5.4.2, Table A5 and Figure A5 of the Annexure. These HHV values were much larger than that of untreated and raw biomasses. A maximum value of HHV of 25.72 MJ kg^{-1} for biocrude was seen at 1:3 biomass-to-solvent ratio. These HHV values were comparable to biocrude from co-liquefaction of lignocellulosic biomasses with various feedstocks [87,88,303]. As already discussed in

Subsection 5.2.2.1, for liquefaction under similar conditions for individual CLPE and CLPU at 1:3 biomass-to-solvent ratio, HHV of biocrude from pulp was found to be 26.7 MJ kg^{-1} while that from peel was 24.2 MJ kg^{-1}.

Table 5.4.2 Biocrude and biochar fuel potential attained by co-liquefaction at 260 °C temperature and varying biomass-to-solvent ratios.

	HHV of biocrude, MJ kg^{-1}			HHV of biochar, MJ kg^{-1}		
Biomass feedstock	1:2	1:3	1:4	1:2	1:3	1:4
CLPE-PU	23.64	25.72	25	15.09	16.11	16.6

It was seen that the HHV of biocrude from co-liquefaction was evidently upgraded from CLPE with decline in biomass-to-solvent ratios due to co-liquefaction effect of peel and pulp biomasses. Due to this effect, the HHV of mixed feed liquefaction was close to that of individual biomass liquefaction. Similar findings were reported in literatures as well [304,305], from which it could be inferred that under present test conditions biocrude from co-liquefaction of CLPE and CLPU resulted in higher HHV than biocrude from CLPE but slightly less than that of CLPU. The decarboxylation, decarbonylation and dehydration reactions during co-liquefaction were responsible for rise in HHV of biocrude due to the decline in its oxygen content. The synthesis of active hydrogen by integration of methanol in supercritical state in biocrude also resulted in rise of its hydrogen content. However, in order to obtain optimum biocrude yield with desirable heating values, the biomass-to-solvent ratio must be selected after careful adjustments [85,248].

5.4.2.2 Chemical analysis

The co-liquefaction of CLPE and CLPU at 1.2 biomass co-feed ratio and 1:2, 1:3 and 1:4 biomass-to-solvent ratios gave rise to biocrude as their final product and this was denoted in the form CLPE-PU 260_2, CLPE-PU 260_3 and CLPE-PU 260_4 respectively. From Figure 5.4.2 we obtain information on functional groups existing in the biocrude from its FTIR spectra. The existence of vibrations due to O-H stretching of hydroxyl groups is visible from the wide peaks amid 3200-3400 cm^{-1} wavenumber of the spectra. The C-H stretching vibration as depicted from absorption peaks in 3000-2800 cm^{-1} and 1461-1350 cm^{-1} range might have arisen due to methylene and methyl groups which also showed the prospect of occurrence of long chain alkanes [155,250].

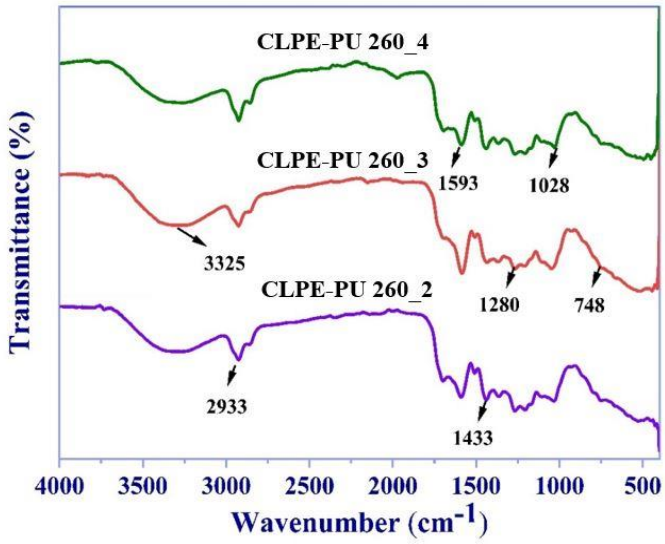

Figure 5.4.2 FTIR spectra results of biocrude from co-liquefaction of CLPE and CLPU at diverse biomass-to-solvent ratios.

C=O vibrational stretching in esters, aldehydes, carboxylic acids and ketones were designated by absorption peaks within 1800-1586 cm^{-1} [275]. The occurrence of aromatic C-C stretching vibrations were confirmed by absorption peaks in between 1500-1620 cm^{-1}. The intensity of these peaks were higher for co-liquefaction biocrude in comparison to individual peel and pulp biocrude [306]. O-H bending and C-O stretching of alcohols in their primary, secondary, tertiary forms, phenol, ether and esters stood apparent from peak at around 1020 cm^{-1} [252]. Additionally peaks around 800-740 cm^{-1} stated the incidence of substituted, single and polycyclic groups of aromatics [170]. Even though FTIR of biocrude from co-liquefaction showed higher functional group peaks in comparison to biocrude from liquefaction of individual biomasses CLPE and CLPU [275], almost near functional groups distribution was observed. However, there was a slight rise in peak intensity corresponding to C-C stretching whereas decline in intensities of C-O, C=O and O-H peaks from co-liquefaction biocrude compared to CLPE and CLPU biocrude. This was an indication of deterioration in oxygen groups thereby leading to higher HHV of co-liquefied biocrude than peel biocrude.

GC-MS analysis was done to obtain information on chemical composition of biocrude found after co-liquefaction of CLPE and CLPU. The NIST library was used for identification of compounds corresponding to major peaks and these have been represented in Table 5.4.3 and Figure 5.4.3. The major compounds in co-liquefaction biocrude were observed to be found within the range of C_5 to C_{37} groups which was alike the biocrude from individual liquefaction

of biomasses [275]. The biocrude mostly consisted of esters, ketones, alcohols, phenols, fatty acids, N-containing compounds and hydrocarbons as depicted by their FTIR spectrum and shown in Table 5.4.4. The biocrude configuration depended on the feedstock nature and the operational settings of the co-liquefaction [255]. The fragmentation of biomass is achieved by hydration, solvolysis and pyrolysis reactions of the solvent. This in turn lead to enhancement in disintegration of reaction intermediates [288]. The esters formation could be accredited to the hemicellulose and cellulose breakdown in lignocelluloses. The influence of hydrogen-donating methanol solvent in co-liquefaction via methanolysis/esterification can be evident from the occurrence of methylated esters [254]. The lower oxygen content of the co-liquefaction biocrude could be attributed to their deoxygenation caused by H_2O removal from them by dehydration and CO_2 removal by decarboxylation. This in turn might have resulted in the formation of hydrocarbons in them [307]. The hydrogen donation by methanol [223] leading to hydrolysis of lipids were also a reason behind this. The low N-containing compounds in this work confirm with liquefaction of individual citrus wastes as found from literature [72] and pave their path for upgrading as well as downstream applications. The depolymerization and reformation reaction of biomass constituents such as carbohydrates under high alteration pressures lead to the formation of phenols [288]. The higher percentage of phenols in co-liquefaction biocrude in comparison to individual feed liquefaction biocrude as discussed in Subsection 5.2.2.2 might have occurred due to the rise in degree of hydrolysis of lignin in co-liquefaction samples causing aromaticity by cyclization and repolymerization [308]. Ketones were produced due to moisture removal from hemicellulose caused by high temperature solvent atmosphere. The biocrude quality has been improved significantly due to co-liquefaction under the experimental settings in comparison to liquefaction of individual biomasses as shown in Subsection 5.2.2.2. Hence, on the basis of the experimental information available till now, it could be inferred that co-liquefaction held the potential to boost the quality of biocrude. However, due to limited data availability, further study on this conclusion needs to be done.

Table 5.4.3 Main compounds found from GC-MS analysis of biocrude from co-liquefaction of CLPE and CLPU at 260 °C and 1:2, 1:3 & 1:4 biomass-to-solvent ratios.

Compounds	Molecular formula	Chemical class	CLPE-PU 260_2		CLPE-PU 260_3		CLPE-PU 260_4	
			RT (min)	Area (%)	RT (min)	Area (%)	RT (min)	Area (%)
5-hepten-2-amine, n,6-dimethyl-	$C_9H_{19}N$	Amine	5.013	6.210	-	-	-	-
2-undecene, 4-methyl-	$C_{12}H_{24}$	Unsaturated aliphatic hydrocarbons	-	-	5.013	5.411	-	-
Z,z-6,28-heptatriactontadien-2-one	$C_{37}H_{70}O$	Ketones	-	-	-	-	5.013	9.218
1-dodecanone, 1-cyclopropyl-	$C_{15}H_{28}O$	Ketones	-	-	5.279	3.899	-	-
Cyclopentane-1,2-diol	$C_5H_{10}O_2$	Cyclopentanols	5.279	2.386	-	-	-	-
Furan, 2-methoxy-	$C_5H_6O_2$	Alkyl aryl ethers	6.909	7.828	6.914	7.281	6.909	8.852
2-octanol, 2,6-dimethyl-	$C_{10}H_{22}O$	Fatty alcohols	-	-	-	-	7.674	5.367
Ethanol, pentamethyl-	$C_7H_{16}O$	Alcohol	-	-	7.669	4.951	-	-
Methyl 11-methyl-dodecanoate	$C_{14}H_{28}O_2$	Fatty acid methyl esters	28.893	2.182	28.898	5.286	28.893	2.632
11,14-octadecadienoic acid, methyl ester	$C_{19}H_{34}O_2$	Fatty acid methyl esters (FAME)	31.224	1.981	31.224	5.016	31.214	2.044
Methyl 9-eicosenoate	$C_{21}H_{40}O_2$	Fatty acid methyl esters	-	-	-	-	31.284	3.742

N-propyl 11-octadecenoate	$C_{21}H_{40}O_2$	Lipid derivative	-	-	31.294	5.887	-	-
13-octadecenoic acid, methyl ester	$C_{19}H_{36}O_2$	Fatty acid methyl esters	31.299	2.163	31.359	3.199	-	-
Phenol, p-(2-methylallyl)-	$C_{10}H_{12}O$	Phenols	-	-	32.370	1.209	-	-
2,4-pentadien-1-ol, 3-propyl-, (2z)-	$C_8H_{14}O$	Alcohol	31.359	1.220	-	-	-	-

Table 5.4.4 Percentage distribution of major compounds in biocrude from co-liquefaction of CLPE and CLPU at 260 °C and 1:2, 1:3 & 1:4 biomass-to-solvent ratios on the basis of GC-MS results.

Class	CLPE-PU 260_2 (Area %)	CLPE-PU 260_3 (Area %)	CLPE-PU 260_4 (Area %)
Ester/Acid	6.326	13.501	8.418
Alcohol	3.606	4.951	5.367
Amine	6.21	-	-
Phenol	-	1.209	-
Aliphatic	-	5.411	-
Ether	7.828	7.281	8.852
Ketone/ Aldehyde	-	3.899	9.218
Other	-	5.887	-

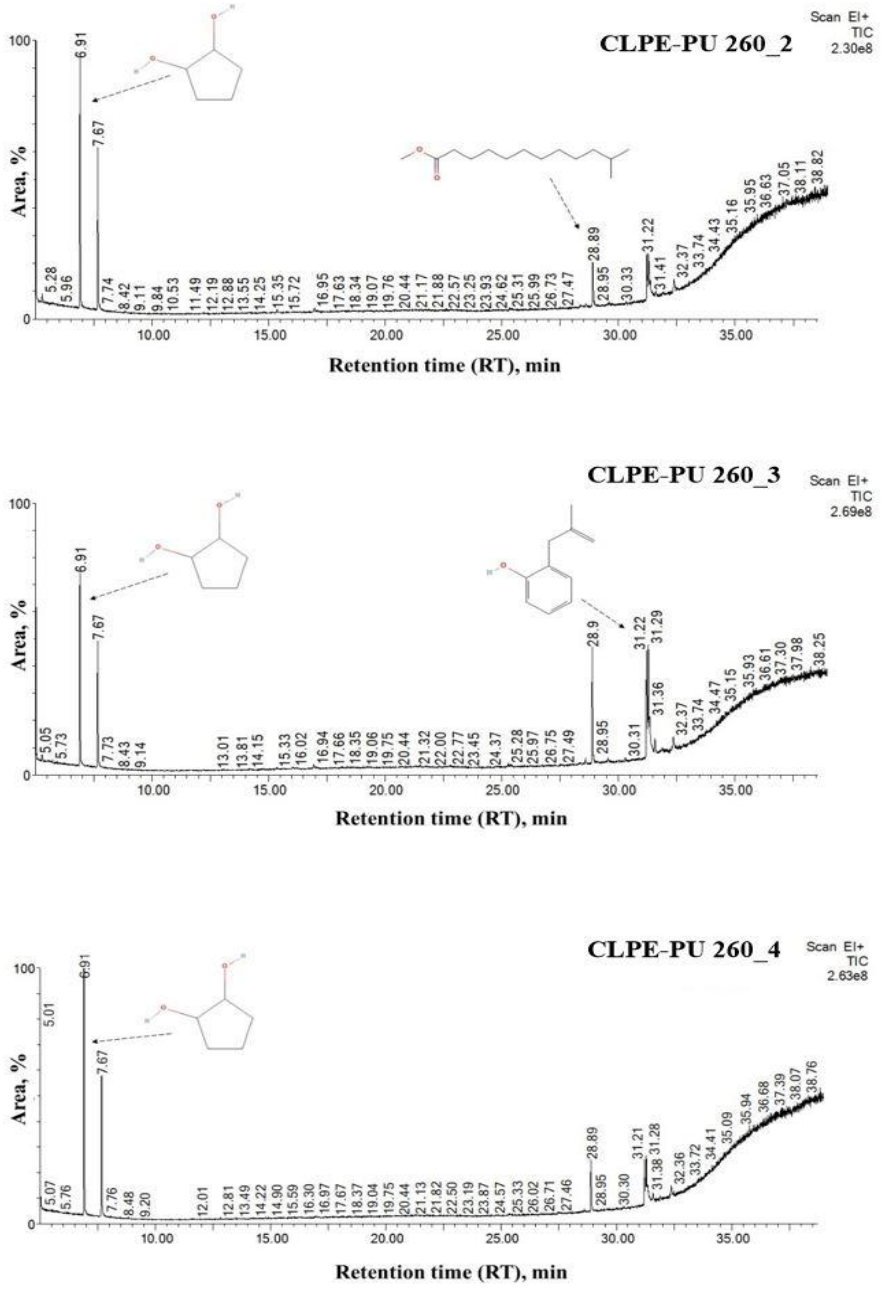

Figure 5.4.3 Chromatogram from GC-MS of biocrude samples from co-liquefaction of CLPE and CLPU at different biomass-to-solvent ratios.

NMR technique was used to examine the structural chemistry and functional groups in biocrude. It helped in obtaining these assignments by chemical shifts in ppm [259]**.** Figure 5.4.4 illustrated the ^{1}H NMR of biocrude from co-liquefaction of CLPE and CLPU and were in close conformity with biocrude from individual liquefaction of peel and pulp biomasses, with certain differences that have been highlighted below. The peak corresponding to 7.26

ppm indicated chemical shift due to solvent chloroform-D used in the NMR studies. The default tetramethylsilane (TMS) that is a standard used in NMR systems was depicted by the peak at 0 ppm [215]**.** The peaks between 0-1.5 ppm were an indication of aliphatic proton attachment to carbon atoms of alkanes [261].

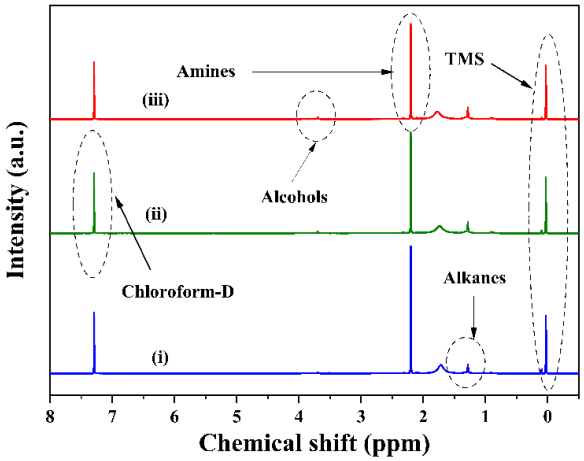

Figure 5.4.4 ^{1}H NMR of biocrude samples (i) CLPE-PU 260_2 (ii) CLPE-PU 260_3 (iii) CLPE-PU 260_4 from co-liquefaction of CLPE and CLPU at 260 ° C & diverse biomass-to-solvent ratios.

Hence, this justified the existence of fatty acids as well as hydrocarbons (alkanes) in the biocrude. Occurrence of amines is shown through peaks between 1.5-3 ppm [307]. The methoxy protons connected by double aromatic rings and proton attachment to carbon lying next to alcohol of aliphatic nature were signified by peaks at 3-4.5 ppm [245]**.** The peaks between 4.5-6 ppm indicated occurrence of protons due to aromatic ethers in co-liquefaction biocrude [307].

5.4.3 Solid product analysis

Table 5.4.2, Table A5 and Figure A5 of the Annexure gives the HHV of co-liquefaction biochar which ranged in between 15.09 MJ kg^{-1} and 16.6 MJ kg^{-1}. These values were comparable to biochar obtained from individual liquefaction of CLPE and CLPU which was found to be between 14.94 MJ kg^{-1} and 16.98 MJ kg^{-1} as reported in Table 5.2.2. The biochar HHV for co-liquefaction was found to be decreasing with the increase in ratio of biomass-to-solvent just like individual pulp liquefaction biochar but unlike peel biochar. Thus they showed their potentiality to be used as a possible bio-refinery feedstock [245]**.**

The thermogravimetric and differential thermogravimetric analysis plots of biochars obtained from co-liquefaction of CLPE and CLPU as illustrated in Figure 5.4.5 showed that the initial temperature of decomposition for biochar was more than that of raw biomass thereby clearly giving an indication that both compositional and structural differences have occurred in biomass due to their co-liquefaction [309]. Weight loss of water from bio-molecules was observed between 50-200 °C. Decomposition of carbohydrates was observed between 300-600 °C. Loss of mass even above 600 °C indicated complete decomposition and oxidation of organic matters [263].

The fluctuations in cellulose crystalline structure by disruption of cellulose chain hydrogen bonding occurring due to co-liquefaction were investigated by powder X-ray diffraction (XRD) procedure to examine crystalline nature of dry biochar and biomass samples [268]. The XRD pattern for CLPE and CLPU biomass along with conforming co-liquefaction biochar obtained at biomass-to-solvent ratios of 1:2, 1:3 and 1:4 has been represented in Figure 5.4.6. The diffraction peaks were equated with database by the Joint Committee on Powder Diffraction Standards (JCPDS). Presence of two diverse peaks at 2θ = 15° and 22° for XRD pattern of both peel and pulp biomass corresponded to the presence of cellulose in them. These attributed to peak pattern of cellulose II (JCPDS No. 00-056-1717).

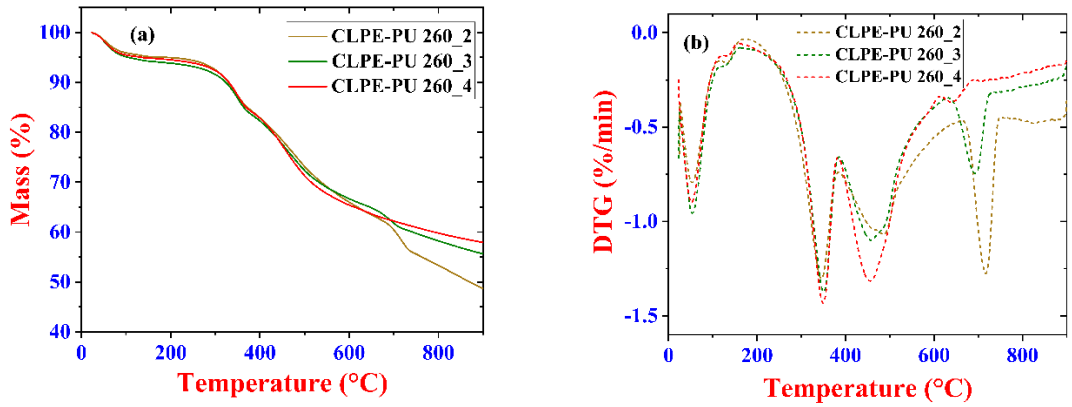

Figure 5.4.5 Plots obtained from (a) thermogravimetric analysis (TGA) and (b) differential thermogravimetry (DTGA) of biochar from co-liquefaction of CLPE and CLPU at diverse biomass-to-solvent ratios.

However, these peaks tended to lower in intensity for the co-liquefaction biochar thereby establishing the demolition of the fiber structure of biomass [292]. The disintegration of cellulose and lignin in the process was shown by peaks at 2θ = 24° and 26° (JCPDS No. 00-056-1717). It also was an implication of turbostratic and amorphous carbon peaks [74] leading to biochar formation by decomposition of these biomass components during co-liquefaction [271]. Despite of the breakdown of multifaceted structure of biomass by thermochemical conversion to biochar, these samples of biochar were still successful in partial retainment of their crystalline properties as visible from their corresponding XRD plots [245,272,275].

Table 5.4.5 provided the surface parameters of biochar from liquefaction of CLPE and CLPU along with biochar from subsequent co-liquefaction of aforementioned biomasses. The surface areas of biochar were seen to be within the range of 11.16 to 25.08 m^2g^{-1}. These values were in conformity with biochar from contemporary studies on liquefaction of biomass [295,299,300]. The low values of both surface area and pore volume maybe due to the blockage of pores caused by the occurrence of organic matters in them [301].

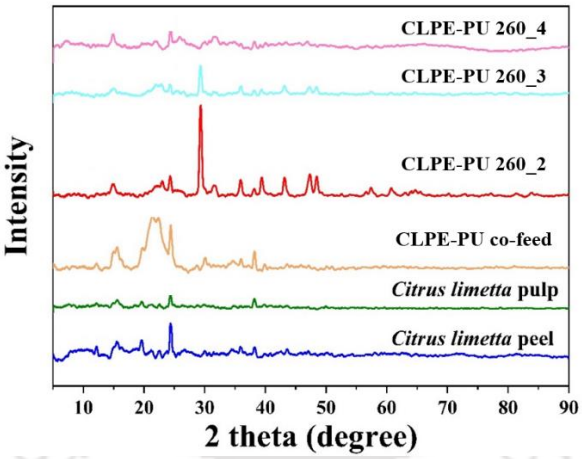

Figure 5.4.6 X-ray diffractogram of biochar and biomass from co-liquefaction of CLPE and CLPU at diverse biomass-to-solvent ratios.

CLPU biochar was observed to be having higher surface area and pore volume in comparison to both CLPE and co-liquefaction CLPE-PU biochars. Nonetheless, their average pore diameters (13.27-16.01 nm) indicated them as mesoporous material as per IUPAC classification of pore sizes where below 2 nm indicated micro-pores, 2-50 nm indicated mesopores and above 50 nm attributed to macro-pores [310,311]. The biochars belonged to

Type IV adsorption isotherm as depicted in Figure 5.4.7 and their hysteresis loop were related to capillary condensation in mesoporous structure of the biochars [295,299,300].

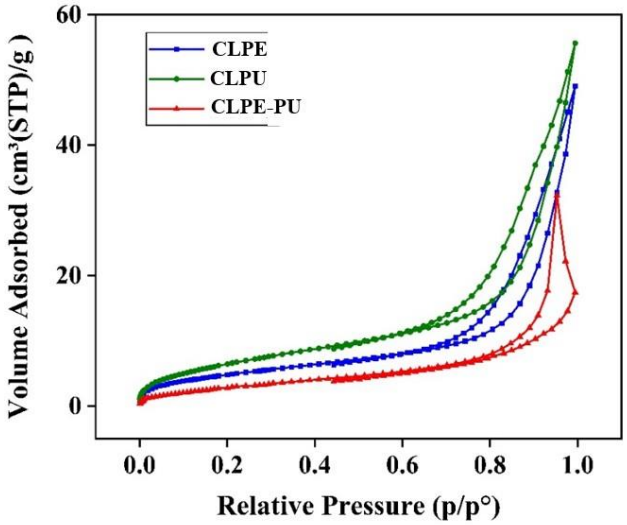

Figure 5.4.7 N_2 adsorption-desorption isotherms at 77K for biochars obtained from liquefaction and co-liquefaction of CLPE and CLPU.

Table 5.4.5 Surface parameters of biochar from liquefaction and co-liquefaction of CLPE and CLPU.

Biochar	Surface structure		
	Surface area, $m^2\ g^{-1}$	Average pore size/ diameter, nm	Total pore volume (P/P_o = 0.99), $cm^3\ g^{-1}$
CLPE	18.11	16	0.073
CLPU	25.08	13.27	0.083
CLPE-PU	11.16	16.01	0.045

5.4.4 Summary

The substantial results from this objective where solvothermal co-liquefaction of *Citrus limetta* pulp and peel had been carried out at co-feed ratio of 1.2 and variable biomass-to-solvent ratios of 1:2, 1:3 and 1:4 have been summarized below:

- A notable biocrude yield of 11.25 wt. %, peaking at 1:2 biomass-to-solvent ratio was obtained which surpassed that of single feed *Citrus limetta* pulp biomass but was lower compared to single feed *Citrus limetta* peel biomass liquefaction.

- Physical characteristics of remaining methanol solvent (MSR) and filtrate indicated the possible transfer of lighter fuel fractions during evaporation, suggesting the potential to obtain cleaner fractions.
- Higher heating value (HHV) of biocrude from co-liquefaction was significantly upgraded to 25.72 MJ kg^{-1} at a 1:3 biomass-to-solvent ratio, demonstrating synergistic effects compared to *Citrus limetta* peel biocrude at the same ratio. This finding aligned with co-liquefaction studies on various lignocellulosic biomasses.
- High intensities of aromatic C-C stretching vibrations in FTIR of co-liquefaction biocrude, confirmed by ^{1}H NMR studies, distinguished it from individual peel and pulp biocrude.
- GC-MS analysis identified esters, ketones, alcohols, hydrocarbons and fatty acids in the co-liquefaction biocrude, highlighting its diverse composition.
- Presence of N-containing compounds and high phenols were observed, attributed to depolymerization and reformation reactions of biomass constituents.

5.5 Solvothermal co-liquefaction of pulp and peel of *Citrus limetta* fruits at variable temperatures and biomass-to-solvent ratios

5.5.1 Product yield distribution

Product distribution from co-liquefaction of *Citrus limetta* peel (CLPE) and pulp (CLPU) at co-feed ratio of 1.2 and temperatures between 240 °C and 280 °C with biomass-to-solvent ratios of 1:2, 1:3 and 1:4 has been shown in Figure 5.5.1. The filtrate yield from co-liquefaction showed variation in trends with increase in temperature from 240 °C to 280 °C. This yield was found to be increasing with rise in temperature for all three biomass-to-solvent ratios and was comparable to yields from single biomass liquefaction of CLPE and CLPU. The low biochar yields as depicted might be due to the nature of the fruit wastes being used. The extremely viscous biocrude yield was calculated with reference to the co-liquefaction feed employed in each iteration of this study. It was observed to be maximum at 240 °C for all three biomass-to-solvent ratios. The yield of biocrude from co-liquefaction was found to reduce significantly with rise in temperature to 260 °C, followed by similar decline in yield at 280 °C. In fact, at 240 °C temperature the yield of biocrude from co-liquefaction was larger than that of individual liquefaction of CLPE and CLPU biomasses, except for CLPE liquefaction at 1:3 biomass-to-solvent ratio. The contrary was seen in the case of 280 °C

temperature where the yield of co-liquefaction biocrude was less than that from single biomass liquefaction. The combination of analogous lignocellulosic biomass components, such as hemicellulose, cellulose and lignin might have led to the difference in yield between co-liquefaction and independent feedstock liquefaction [121]. The possible reason behind this might have been that majority of the organic materials might have converted into gaseous and solid phases, thereby increasing the rate of cracking and repolymerization and lowering the biocrude yield from them [302]. The maximum biocrude yield of 13.47 wt. % was observed at 240 °C and 1:2 biomass-to-solvent ratio. With the exception of certain co-feed ratio of biomass, the yield of biocrude obtained from the co-liquefaction in this study demonstrated comparability to and exceeded the biocrude yield achieved through the hydrothermal co-liquefaction studies of analogous citrus waste (specifically lemon peel) and microalgae *Spirulina platensis* [68]. The biocrude yield has been less significantly influenced by the modification in biomass-to-solvent ratio resulting from changing biomass approach in the current case. Despite initiatives, it is still difficult to get certainty about the most suitable biomass-to-solvent ratio for optimizing biocrude output. This might be attributed to the fact that several crucial reaction factors also significantly affect the production of biocrude [85].

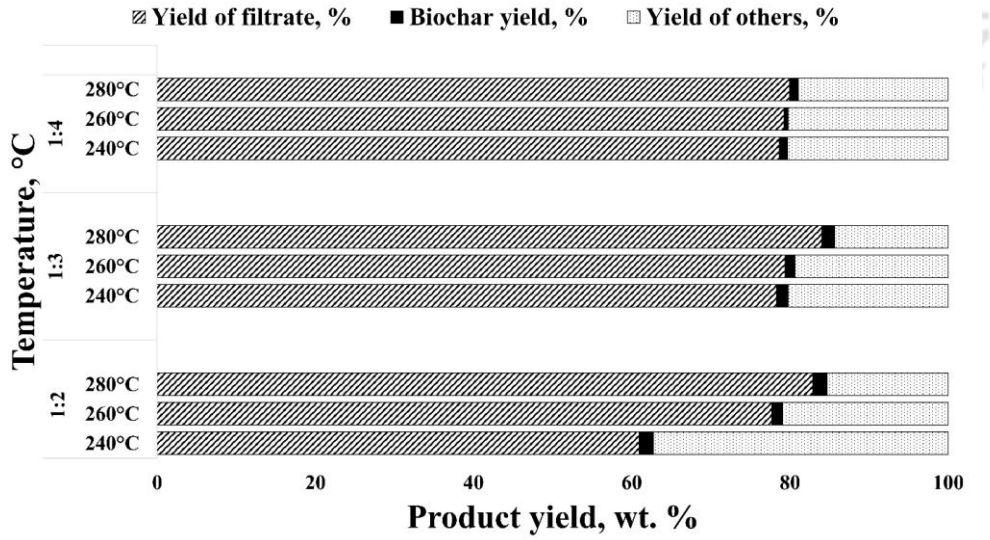

Figure 5.5.1 Yield distribution of products via co-liquefaction of CLPE & CLPU between 240 °C and 280 °C and variable biomass-to-solvent ratios.

5.5.2 Analysis of liquid products

5.5.2.1 Physical and fuel attributes

The abbreviations CLPE-PU 240, CLPE-PU 260 and CLPE-PU 280 signify the products (filtrate, MSR, biocrude and biochar) generated by the co-liquefaction of CLPE and CLPU at 240 °C, 260 °C and 280 °C respectively. Table 5.5.1 provides a summary of the investigation of the physical and fuel attributes of the CLPE and CLPU biomass co-liquefaction products at 240 °C, 260 °C and 280 °C for 1:2, 1:3 and 1:4 biomass-to-solvent ratios. It was observed that at all temperatures and biomass-to-solvent ratios, the filtrate and MSR densities and viscosities were evidently higher than pure reagent grade methanol that was used in these studies. So, just like single feed liquefaction, the co-liquefaction MSR also had lighter hydrocarbons and methanol soluble components formed due to co-liquefaction.

Table 5.5.1 Fuel and physical characteristic properties of products (filtrate & MSR) via co-liquefaction specific to CLPE and CLPU between 240 °C and 280 °C temperature & variable biomass-to-solvent ratio.

Liquid product	1:2	1:3	1:4
	Density, g mL^{-1}		
CLPE-PU 240 (Filtrate)	0.855	0.868	0.839
CLPE-PU 240 (MSR)	0.822	0.821	0.812
CLPE-PU 260 (Filtrate)	0.865	0.856	0.847
CLPE-PU 260 (MSR)	0.833	0.824	0.823
CLPE-PU 280 (Filtrate)	0.857	0.842	0.836
CLPE-PU 280 (MSR)	0..823	0.819	0.814
Density, Methanol (pure reagent), g mL^{-1}= 0.782			
	Viscosity, mPa.s		
CLPE-PU 240 (Filtrate)	1.174	1.143	1.086
CLPE-PU 240 (MSR)	0.865	0.846	0.861
CLPE-PU 260 (Filtrate)	1.219	1.089	1.044
CLPE-PU 260 (MSR)	0.928	0.906	0.897
CLPE-PU 280 (Filtrate)	1.228	1.081	0.973
CLPE-PU 280 (MSR)	0.878	0.856	0.838
Viscosity, Methanol (pure reagent), mPa.s = 0.677			

	HHV, MJ kg^{-1}		
CLPE-PU 240 (Filtrate)	15	15.34	15.92
CLPE-PU 240 (MSR)	17.49	20.35	16.75
CLPE-PU 260 (Filtrate)	14.54	15.26	15.96
CLPE-PU 260 (MSR)	15.83	16.78	16.74
CLPE-PU 280 (Filtrate)	15.21	15.85	16.26
CLPE-PU 280 (MSR)	15.47	18.65	17.91
HHV, Methanol (pure reagent), MJ kg^{-1}= 19.62			

Incidentally, this occurred during the process of solvent extraction from filtrate in rotary evaporator. The increase in temperature from 240 °C to 280 °C led to the decrease in densities and viscosities of filtrates for all conditions of biomass-to-solvent ratio except for 1:2 followed by an increase in density for 1:4 biomass-to-solvent ratio at 260 °C. However, decrease in biomass-to-solvent ratio led to decrease in densities of filtrates except for 1:3 biomass-to-solvent ratio. For MSRs also same decreasing trend was observed for density and viscosity values except for 1:4 biomass-to-solvent ratio for viscosity value. For co-liquefaction studies of CLPE and CLPU biomass, the energy content of the MSR was found to be larger than filtrates. This could possibly be explained by the fact that the solvent penetrated the biomass co-feed more thoroughly during the first co-liquefaction phase, which was regulated by the biomass-to-solvent ratio [85]. For temperature rise, HHV of filtrates showed a rising trend except for biomass-to-solvent ratio of 1:2 and 1:3 at 260 °C. However, HHV of MSRs showed mixed trends. The energy content of co-liquefaction biocrude from CLPE and CLPU biomasses depicted a mixed trend with decrease in biomass-to-solvent ratio as depicted in Table 5.5.2. At 240 °C, the HHV values were found to be decreasing while for 260 °C and 280 °C, it was found to be first increasing then decreasing with reduction in biomass-to-solvent ratio. Nevertheless, these HHV levels were substantially greater compared to that of raw and un-processed biomasses and exhibited consistency with the biocrude derived from co-liquefaction of several other lignocellulosic feedstocks as reported in open literature [87,88,303]. It was observed that with temperature rise the energy content (HHV) of biocrude increased for 1:3 biomass-to-solvent ratio depicting maximum value of 27.6 MJ kg^{-1} at 280 °C. This was reportedly higher than liquefaction biocrude of single CLPE and CLPU biomass under same reaction conditions. The reason behind this upgrade might be the synergistic effects of co-liquefaction of both biomasses at this ratio. Due to high temperature, followed

by high pressure of the reaction, the feedstocks reacted rapidly causing degradation of their structure by dehydration and decarboxylation leading to oxygen removal in the form of H_2O and CO_2 and hence increase in the energy content of the biocrude. Additionally, the supercritical integration of methanol throughout the procedure resulted in the creation of active hydrogen, increasing the hydrogen content of the biocrude [277].

Table 5.5.2 Fuel potential of biocrude and biochar from co-liquefaction of CLPE and CLPU between 240 °C and 280 °C temperature and changing biomass-to-solvent ratios.

	HHV of biocrude, MJ kg^{-1}			HHV of biochar, MJ kg^{-1}		
Feedstock	1:2	1:3	1:4	1:2	1:3	1:4
CLPE-PU 240	25.55	24.79	22.49	16.12	17.56	19.96
CLPE-PU 260	23.64	25.72	25	15.09	16.11	16.6
CLPE-PU 280	26.26	27.6	24.5	14.45	16.66	15.41

5.5.2.2 Chemical characteristics

The chemical characterization of the co-liquefaction biocrude obtained from CLPE and CLPU at co-feed proportion of 1.2 and between 240 °C and 280 °C at varying biomass-to-solvent ratios of 1:2, 1:3 and 1:4 has been discussed here. It aids in identifying the key components and compounds present in the complex biocrude mixture. This information helps in refinement and adjusting the process parameters to enhance the yield, quality and desired properties of the biocrude. The abbreviations CLPE-PU 240_2, CLPE-PU 240_3 and CLPE-PU 240_4 indicate biocrude from co-liquefaction of CLPE and CLPU at 240 °C, for biomass-to-solvent ratios of 1:2, 1:3 and 1:4 respectively. Similar depictions have been used to indicate biocrude obtained at 260 °C and 280 °C for biomass-to-solvent ratios of 1:2, 1:3 and 1:4 as well. Figure 5.5.2 displayed the FTIR spectra of biocrude where the absorption bands at specific wavelengths exhibited presence of a unique functional group allowing for their identification and characterization.

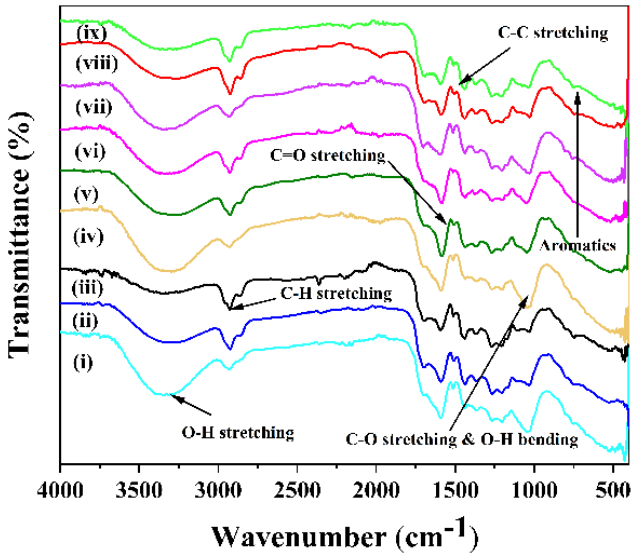

Figure 5.5.2 FTIR of biocrude via co-liquefaction of CLPE & CLPU: (i) CLPE-PU 240_2 (ii) CLPE-PU 260_2 (iii) CLPE-PU 280_2 (iv) CLPE-PU 240_3 (v) CLPE-PU 260_3 (vi) CLPE-PU 280_3 (vii) CLPE-PU 240_4 (viii) CLPE-PU 260_4 (ix) CLPE-PU 280_4.

The decrease in intensities of peaks conforming to O-H stretching of hydroxyl groups (3200-3400 cm^{-1} wavenumber range), C=O stretching vibrations of ketones, aldehydes, esters and carboxylic acids (1800-1586 cm^{-1} wavenumber range) & C-O corresponding to alcohols (stretching) against their respective primary, secondary, tertiary structures, phenol, esters & ethers (1020 cm^{-1} wavenumber) [252] with rise in temperature of co-liquefaction from 240 °C to 280 °C at their corresponding biomass-to-solvent ratios were a sign of degradation in oxygen assemblages causing larger HHV values. The increase in peak intensities of C-H stretching vibration (3000-2801 cm^{-1} and 1461-1351 cm^{-1} wavenumber range) with temperature rise could have possibly occurred subject to methyl and methylene groups indicating presence of extended-chain alkanes [155,250]. The C-C stretching vibrations (1500-1620 cm^{-1} wavenumber range) depicted presence of aromatics in the co-liquefaction biocrude. It was evident that almost near chemical groups distribution was detected in biocrude from single feed liquefaction of CLPE and CLPU as well as their co-liquefaction under similar conditions at 260 °C as described in Subsection 5.2.2.2.

The chemical makeup of the biocrude samples (on molecular level) from co-liquefaction studies of CLPE and CLPU were obtained from GC-MS studies. Main chemical

species detected by GC-MS have been compared to National Institute of Standards and Technology (NIST) library and presented in Table 5.5.3. However, there could have been a possibility of loss of low boiling point fractions and un-identification of high boiling point fractions, during solvent separation and due to temperature limitations of GC-MS, respectively. The biocrude from co-liquefaction between 240 °C and 280 °C temperatures were within C_3 to C_{24} range and depicted similarity in assemblage of compounds identified by GC-MS in biocrude from single biomass liquefaction of CLPE and CLPU. The majority of compounds detected belonged to classes as shown in Table 5.5.4. The fatty acids and ester compounds in biocrude occurred due to hydrolysis of lipids in biomass [312]. In fact, the significant amount of esters portrayed that the biocrude had enhanced ignition characteristics [257]. It was possible that the conversion of the biomass's cell wall and membrane led to the high concentration of phenol and its derivatives in biocrude [252]. The decarboxylation of fatty acids, hydrolysis of lipids and use of alcoholic solvent could have likely led to the occurrence of alcohols and hydrocarbons in the biocrude [257]. The formation of ketones and aldehydes (particularly cyclic ketones) might have originated from the monosaccharide depolymerization occurring due to cyclization and dehydration reactions [313]. The aromatic content in the co-liquefaction biocrude at 280 °C was produced due to aromatization and dehydration of hemicellulose and cellulose structural units.

Table 5.5.3 Major compounds obtained via GC-MS study of co-liquefaction biocrude of CLPE and CLPU at 240 °C and 280 °C temperature and biomass-to-solvent ratio of 1:3.

Compounds	Molecular formula	Chemical class	CLPE-PU 240		CLPE-PU 280	
			RT (min)	Area (%)	RT (min)	Area (%)
1-nonylcycloheptane	$C_{16}H_{32}$	Alkane	7.018	4.320	-	-
3-methyl-2-(2-oxopropyl) furan	$C_8H_{10}O_2$	Heteroaromatic compounds/Furan	-	-	7.018	4.923
3-methylbut-2-enoic acid, 4-methoxy-2-methylbutyl ester	$C_{11}H_{20}O_3$	FAME	7.123	3.321	-	-
Cyclobutanone, 2-(1,1-dimethylethyl)-	$C_8H_{14}O$	Cyclic ketones/Cyclo oxegenates	-	-	7.133	2.920
Cyclopentane, methyl-	C_6H_{12}	Cycloalkanes	-	-	7.314	22.398
Cyclopentanone, 2-(1-methylpropyl)-	$C_9H_{16}O$	Cyclic ketones/Cyclo oxegenates	-	-	8.084	0.782
Furan, 2-methoxy-	$C_5H_6O_2$	Alkyl aryl ethers	10.975	9.485	10.980	7.473
Ethanol, pentamethyl-	$C_7H_{16}O$	Alcohol	-	-	12.095	2.972
2-octanol, 2,6-dimethyl-	$C_{10}H_{22}O$	Tertiary alcohols	12.085	4.395	-	-
Catechol	$C_6H_6O_2$	Phenol/Phenolics	20.634	0.831	-	-
Benzene-1,4-diol	$C_{12}H_{16}O_2$	Phenol	22.280	1.116	-	-
Carbamic acid, hydroxy-, ethyl ester	$C_3H_7NO_3$	FAME	24.921	0.890	-	-

Octadecanoic acid, hexyl ester	$C_{24}H_{48}O_2$	FAME	25.206	0.695	-	-
3-ethyl-3-methylnonadecane	$C_{22}H_{46}$	Alkane	32.274	1.573	-	-
Arsenous acid, tris(trimethylsilyl) ester	$C_9H_{27}AsO_3Si_3$	Arsenic ester	34.114	1.050	35.070	0.480
Thymol, tms derivative	$C_{10}H_{14}O$	Phenol	34.369	1.039	34.390	1.600
Hexestrol, 2tms derivative	$C_{18}H_{22}O_2$	Phenol	36.650	2.287	35.555	0.606
4-(4-hydroxyphenyl)-4-methyl-2-pentanone, tms derivative	$C_{12}H_{16}O_2$	Phenylpropanes	-	-	36.676	1.857
4-tert-amylphenol, tms derivative	$C_{16}H_{29}OSi(CH_3)_3$	Phenol	-	-	36.246	0.583
4-tert-octylphenol, tms derivative	$C_{14}H_{22}O$	Phenol	37.861	0.775	36.726	1.081
Cyclotrisiloxane, hexamethyl-	$C_6H_{18}O_3Si_3$	Column bleeding, Chemical	37.961	0.754	36.791	1.382
Benzestrol, 2tms derivative	$C_{26}H_{42}O_2Si_2$	TMS derivative	-	-	36.991	0.548

Table 5.5.4 Percentage distribution of major compounds in biocrude via co-liquefaction of CLPE and CLPU between 240 °C and 280 °C at biomass-to-solvent ratio of 1:3 on the basis of GC-MS results.

Compound Class	CLPE-PU 240 (Area %)	CLPE-PU 260 (Area %)	CLPE-PU 280 (Area %)
Acid & Ester	5.956	13.501	0.48
Alcohol	4.395	4.951	2.972
Phenol	6.048	1.209	3.87
Alkane	5.893	5.411	24.255
Alkene	-	-	-
Ether	9.485	7.281	7.473
Ketone/Aldehyde	-	3.899	3.702
Aromatic	-	-	4.923
Nitrogen containing	-	-	-
Other	0.754	5.887	1.93

Figure 5.5.3 illustrated the proton NMR analysis pertaining to biocrude from co-liquefaction of CLPE and CLPU between 240 °C and 280 °C with variation in biomass-to-solvent ratios. This provided a clear depiction of its chemical structure and functional groups on the basis of chemical shifts in ppm [279]. Peaks at 0 ppm and 7.26 ppm were indicative of default tetramethylsilane (TMS) and chloroform-D solvent used in the NMR analysis [215]. Occurrence of aliphatic functional groups (alkanes) in the co-liquefaction biocrude was evident from peaks in between 0 to 1.5 ppm range.

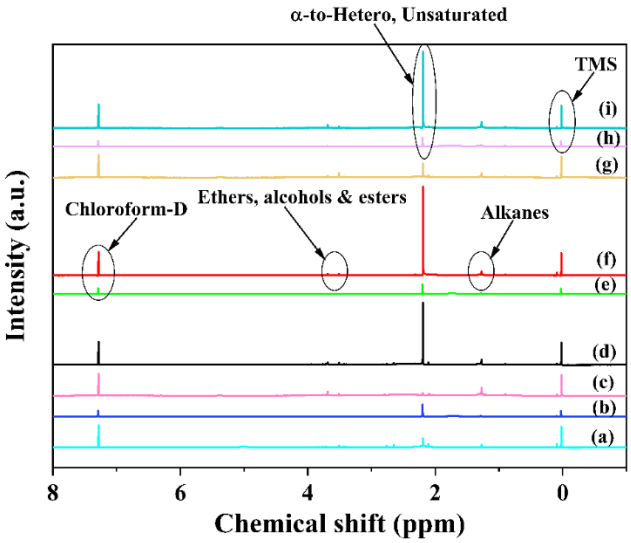

Figure 5.5.3 NMR (^{1}H) of biocrude via co-liquefaction of CLPE & CLPU: (a) CLPE-PU 240_2 (b) CLPE-PU 260_2 (c) CLPE-PU 280_2 (d) CLPE-PU 240_3 (e) CLPE-PU 260_3 (f) CLPE-PU 280_3 (g) CLPE-PU 240_4 (h) CLPE-PU 260_4 (i) CLPE-PU 280_4.

This was indicative of larger values of HHV of biocrude as they depend on these aliphatic protons that are interrelated to carbon atoms from hydrocarbons [314]. The chemical shift between 1.5 to 3 ppm ranges were related to heteroaromatic compounds in the biocrude. While protons of alcohols, ethers and esters were verified by peaks between chemical shift range of 3 to 4.5 ppm. In fact, their synthesis was intensified by usage of alcoholic methanol solvent in this process as proved by their FTIR spectra as discussed above. It is worth noting that no peaks were observed in 4.4 to 6 ppm range (methoxy/carbohydrate functional groups) for co-liquefaction biocrude. This might be due to substantial conversion of carbohydrates due to co-

liquefaction at high temperatures [282]. Overall findings from NMR portrayed that co-liquefaction biocrude contained more alkanes and aliphatics.

5.5.3 Biochar analysis

Biochar that is the solid product obtained from this co-liquefaction process is a versatile and sustainable material that offers multiple environmental and agricultural benefits. The decrease in the original mass of the biochar and the exclusion of volatiles having low energy through hydrolysis, decarboxylation and dehydration processes might be accountable for increase in its carbon content [289] as evident from its HHV depicted in Table 5.5.2. These values ranged between 14.45 MJ kg^{-1} and 19.96 MJ kg^{-1} for co-liquefied product of CLPE and CLPU obtained within 240 °C to 280 °C at varying biomass-to-solvent ratios 1:2, 1:3 and 1:4 with the maximum HHV of 19.96 MJ kg^{-1} found for co-liquefaction biochar at 240 °C and 1:4 biomass-to-solvent ratio. This value showed synergistic effects of liquefaction at this temperature as it was significantly higher in comparison to HHV values of biochar from single liquefaction of CLPE and CLPU which were found to be 16.28 MJ kg^{-1} & 15.43 MJ kg^{-1} respectively under same reaction conditions. For further analysis of biochars biomass-to-solvent ratio of 1:3 was chosen for this study.

From the TGA and DTG analysis of co-liquefaction biochars at 1:3 biomass-to-solvent ratio as shown in Figure 5.5.4, thermal stability and the structural as well as compositional changes brought about by co-liquefaction in CLPE and CLPU biomass was obtained. In fact, the characteristics of the biochar could possibly be studied with the help of the plots depicted [265]. The loss of weight that occurred during the co-liquefaction process might be attributed to the exhaustion of moisture from acidic functional groups. These happened in stages where water elimination, hemicellulose breakdown, cellulose degradation and lignin rupture took place in subsequent first, second, third and fourth stages respectively. Thermal study of biochar demonstrated weight loss in the range of 30 to 200 °C, which was due to the elimination of moisture. The breakdown of cellulose was initially observed between 260 and 500 °C followed by hemicellulose. The study also discovered that mass loss beyond 600 °C indicated total oxidation and decomposition of organic components with low boiling and melting temperatures with only carbon residue as remainder [290]. It was seen that the largest weight loss occurred in between 340-370 °C, thereby implying that total degradation of cellulose and hemicellulose in co-liquefaction of CLPE and CLPU have not taken place [264].

As observed from their DTG profiles, the co-liquefaction effect was able to bring about higher thermal stability of biochars at 240 °C temperature compared to biochars from single feed liquefaction for which higher temperature of 280 °C was required to ensure greater thermal stability of biochars.

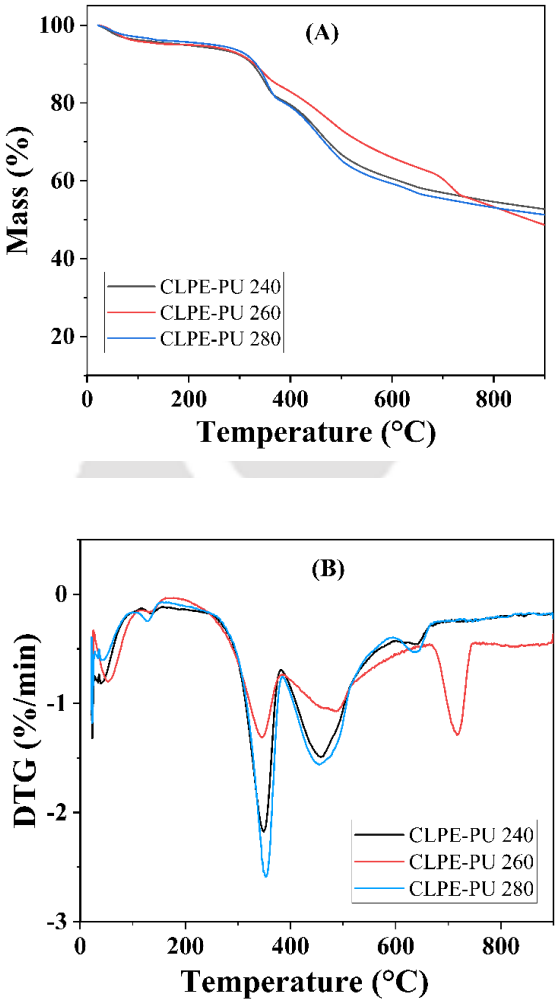

Figure 5.5.4 (A) Thermogravimetric analysis (TGA) & (B) Differential thermogravimetry analysis (DTGA) depiction of biochar via co-liquefaction studies of CLPE & CLPU between 240 °C & 280 °C and biomass-to-solvent ratio of 1:3.

The ultimate analysis of biochars from co-liquefaction of CLPE and CLPU in between 240 °C & 280 °C and at 1:3 biomass-to-solvent ratio have been presented in Table 5.5.5. It was visible that temperature rise from 240 °C to 260 °C led to decrease in H/C ratio which might have possibly taken place due to removal of hydrogen from biomass during initial stage of co-liquefaction as evident from H/C ratio of single feed liquefaction biochar of CLPE.

Table 5.5.5 Ultimate analysis of biochars from CLPE and CLPU co-liquefaction between 240 °C & 280 °C and biomass-to-solvent ratio of 1:3.

CHNS Analysis, wt. %							
Biochar	C	H	N	S	O[b]	H/C	O/C
CLPE-PU 240	65.39	6.59	2.37	-	25.65	1.209	0.294
CLPE-PU 260	52.67	4.54	2.18	-	40.61	1.034	0.578
CLPE-PU 280	48.07	5.74	2.25	-	43.94	1.433	0.686

[b] calculated by difference

However, higher temperatures might have caused hydrogenating reaction leading to further increase in H/C ratio at 280 °C depicting the influence of H/C ratio of CLPU single feed liquefaction biochar on their co-liquefaction products. O/C ratio for both biochars were increasing slightly, which suggested that demethanation might have been a dominant pathway for biochar formation by co-liquefaction [291].

XRD patterns of biochars from co-liquefaction of CLPE and CLPU between 240 °C & 280 °C and at 1:3 biomass-to-solvent ratio have been represented in Figure 5.5.5 to adjudge the interference in cellulose chain hydrogen bonding related to cellulose crystalline structure change occurring during co-liquefaction reactions [292]. The diffraction peaks were cross-referenced with database by JCPDS (Joint Committee on Powder Diffraction Standards).

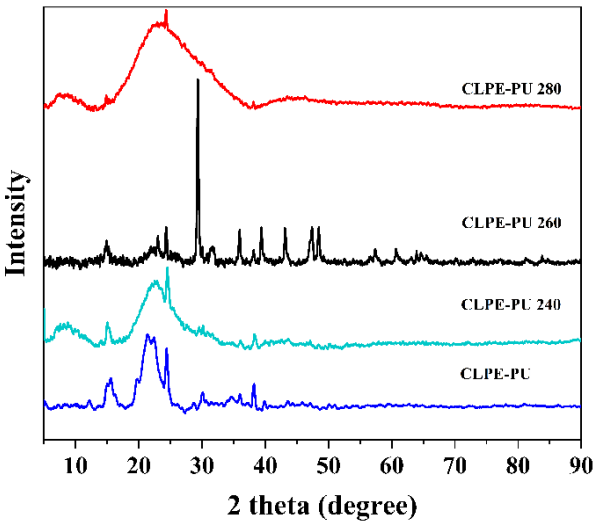

Figure 5.5.5 X-ray diffractogram of CLPE-PU biomass and biochar via co-liquefaction studies of CLPE & CLPU between 240 °C and 280 °C and biomass-to-solvent ratio of 1:3.

The peak values at 2θ = 15° and 22° (JCPDS Card No. 00-003-0192) indicated the presence of cellulose [293] in both co-liquefaction biochars. Peaks values obtained at 2θ = 24° and 26° (JCPDS Card No. 00-003-0192) pertaining to amorphous and turbostratic carbon in biochar were evidence of cellulose and lignin degradation during co-liquefaction [74]. However, only partial degradation might have occurred as the existence of these peaks depicted retainment of cellulose crystalline structure, thereby showing its thermal stability to some extent [294]. It was evident that the additional heating to high temperature of 280 °C as well as co-liquefaction effect did not affect the peak locations, although it did result in sharper and more symmetrical peaks.

The surface parameters of biochars obtained from the co-liquefaction of CLPE and CLPU between 240 °C & 280 °C and at 1:3 biomass-to-solvent ratio as well as their nitrogen adsorption/desorption isotherms at 77K have been presented in the Table 5.5.6 and Figure 5.5.6 respectively. A hysteresis loop indicating Type IV isotherm as per IUPAC classification [295] is visible for these biochars.

Table 5.5.6 Surface parameters of biochars via co-liquefaction of CLPE and CLPU between 240 °C & 280 °C and biomass-to-solvent ratio of 1:3.

Biochar	Surface morphology		
	Surface area, $m^2\ g^{-1}$	Avg. size of pore / diameter, nm	Total volume of pore (P/P_o = 0.99), $cm^3\ g^{-1}$
CLPE-PU 240	1.42	11.55	0.004
CLPE-PU 260	11.16	16.01	0.045
CLPE-PU 280	5.76	15.50	0.043

This showed that biochar composed of mostly mesoporous carbon with occasional microporous solids and at low pressures monolayer coverage was followed by multilayer occurrence just like biochar from single liquefaction of CLPE and CLPU. The pore diameter size on comparison to IUPAC classification indicated it lying between mesopore range of 2-50 nm [295]. The biochar surface areas obtained were also in conformity with results from other liquefaction studies [299,300]. Low values of the pore volumes and surface areas of biochar of co-liquefaction obtained from BET might be due to blockage of pores due to organic materials generated by co-liquefaction effect of CLPE and CLPU [301].

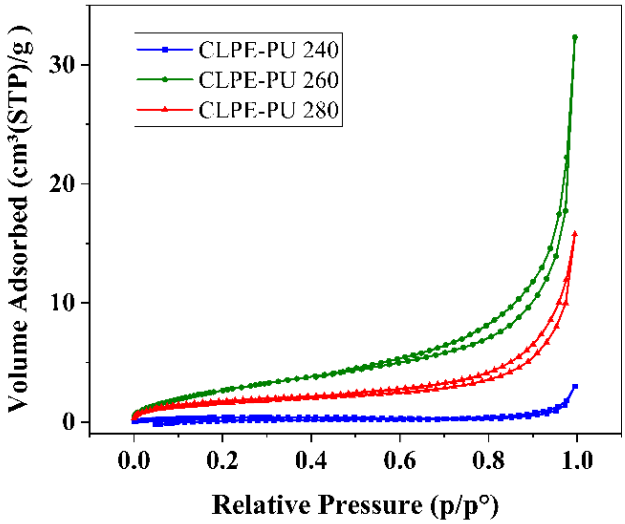

Figure 5.5.6 Adsorption-desorption isotherms of N_2 at 77K from biochar found via co-liquefaction studies of CLPE & CLPU between 240 °C & 280 °C and biomass-to-solvent ratio of 1:3.

The FESEM images of biochar obtained from co-liquefaction of CLPE and CLPU at 240 °C and 280 °C has been depicted in Figure 5.5.7. These images at 500X, 1KX and 10KX magnification illustrated their surface morphology quite vividly. The breakdown of the dense and fibrous structure of both biomasses as well as the mixture of their surface morphology is evident from this co-liquefaction biochar. The surface morphology shows a mutilated shape and distorted structure with small pores which might have occurred due to volatilization of organic compounds [299]. The biochar obtained at 280 °C showed more particle deposits along with irregular flakes owing to the condensation of organic hydrocarbons and degradation of the char formed [315]. These deposits were caused due to mineral residues formed after liquefaction [74].

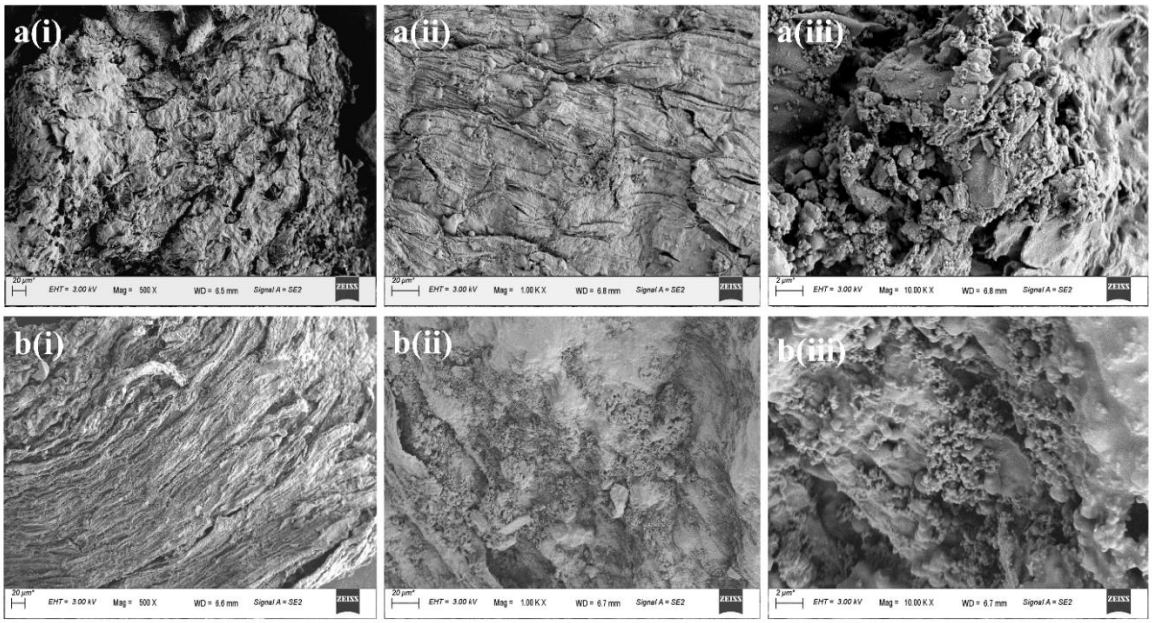

Figure 5.5.7 a(i), a(ii) & a(iii): FESEM images of biochars via co-liquefaction of CLPE & CLPU at 240 °C and b(i), b(ii) & b(iii): FESEM images of biochars from co-liquefaction of CLPE and CLPU at 280 °C (where (i) 500X, (ii) 1KX and (iii) 10KX resolutions each).

5.5.4 Summary

The consequences from this objective where solvothermal co-liquefaction of *Citrus limetta* pulp and peel had been carried out at co-feed ratio of 1.2, variable temperature between 240 °C and 280 °C along with variable biomass-to-solvent ratios of 1:2, 1:3 and 1:4 have been summarized below:

- A peak biocrude yield of 13.47 wt. % was attained at a less severe temperature of 240 °C and 1:2 biomass-to-solvent ratio, indicating the significance of these conditions for maximizing output.
- Increasing the temperature demonstrated a positive correlation with the HHV of the biocrude. The HHV reached a maximum of 27.6 MJ kg^{-1} at 280 °C and a 1:3 biomass-to-solvent ratio, implying a synergistic effect in co-liquefaction.
- The observed HHV values in co-liquefaction were higher than those in the specific liquefaction of CLPE (*Citrus limetta* peel) and CLPU (*Citrus limetta* pulp), indicating the enhanced efficacy of the co-liquefaction process.

- Nuclear magnetic resonance (NMR) analysis identified the presence of aliphatic functional groups, particularly alkanes, contributing to the elevated HHV values in the biocrude.
- The biocrude exhibited a significant amount of esters, suggesting enhanced ignition characteristics, which could be advantageous for certain applications.
- Aromatization and dehydration of hemicellulose and cellulose structural units at 280 °C during co-liquefaction led to an increased aromatic content compared to single biomass liquefaction.
- The biochar obtained from the co-liquefaction process displayed a mutilated shape and distorted structure, likely attributed to the volatilization of organic compounds during liquefaction.

5.6 Summary of the Chapter

In this chapter the experimental results of the objectives of this dissertation have been discussed in details. The following could be inferred from this chapter:

- Waste valorization of *Citrus limetta* pulp and peel fruits constructively for energy generation has been experimentally established here.
- Suitability of these fruits for solvothermal liquefaction and co-liquefaction for production of biofuels has been observed here.
- Extensive characterization of both liquid product (biocrude) and solid product (biochar) has been explained here.
- Influence of temperature and biomass-to-solvent ratio on solvothermal liquefaction and co-liquefaction product characteristics has been explored here.

CHAPTER 6

CONCLUSION & FUTURE SCOPE

6.1 Conclusion

The solvothermal liquefaction and co-liquefaction of *Citrus limetta* fruit wastes, encompassing both pulp and peel, were meticulously investigated using methanol as the solvent across a broad spectrum of parameters. Prior to the liquefaction experiments, a thorough characterization of the biomasses was conducted, focusing on their essential properties. The high volatility of the samples underscored their aptness for biofuel production through these thermochemical conversion techniques. The exploration of diverse reaction parameters, including temperatures ranging between 240 °C and 280 °C and biomass-to-solvent ratios 1:2, 1:3 & 1:4, aimed at enhancing the quality of the biocrude and biochar derived from the liquefaction processes. The biocrude exhibited a significantly higher energy content compared to the raw feedstock, with a peak higher heating value (HHV) of 26.76 MJ kg^{-1} achieved from the liquefaction of *Citrus limetta* pulp (CLPU) biomass at a 1:4 ratio and 260 °C. Moreover, a maximum biocrude yield of 12.5 wt. % was observed from the CLPE liquefaction at 240 °C, indicating an improvement compared to analogous studies on citrus fruit wastes. Co-liquefaction further influenced the biocrude yield, showing a positive synergistic effect with an increased yield of 13.47 wt. % for co-liquefaction at 240 °C and 1:2 biomass-to-solvent ratio. This investigation also revealed an augmentation in the energy content of the co-liquefaction biocrude compared to the single-feed liquefaction biocrude of *Citrus limetta* peel (CLPE), with HHV values reaching as high as 27.6 MJ kg^{-1} due to co-liquefaction at 280 °C. The quality of the co-liquefaction biocrude, as evidenced by C-C stretching corresponding to aromatics in FTIR spectra, surpassed that of the single-feed liquefaction biocrude. Moreover, higher content of phenols in co-liquefaction biocrude as reported by their GC-MS analysis suggested enhanced lignin degradation. NMR results also portrayed weak carbohydrate and methoxy functionality in co-liquefaction biocrude indicating efficient degradation of biomass. Additionally, an in-depth analysis of the biochar characteristics showcased their high energy density and porous nature, suggesting their potential utility as solid fuel feedstock and as adsorbents for soil bioremediation, respectively. XRD analysis indicated that the biomass experienced partial decomposition during liquefaction, with the cellulose component retaining some of its crystalline properties in the

resulting biochar. Surface cracks and pores observed in the biochar through FESEM analysis suggested decomposition of cellulose and hemicellulose. While, BET analysis of pore diameters indicated the formation of mesoporous biochars. In conclusion, this study provided a comprehensive and internally consistent overview of converting fruit wastes into biofuels through the liquefaction process, contributing valuable insights to biomass liquefaction research. The nuanced understanding of co-liquefaction presented here, offered for the first time to the best of our knowledge, preliminary findings regarding the properties of biocrude and biochar derived from *Citrus limetta* fruit wastes in a methanol solvent. Furthermore, the liquefaction of both pulp and peel of *Citrus limetta* fruits emerged as a superior choice for producing high-quality biocrude at enhanced yields.

6.2 Future Scope

The possibilities for further research in the field of this dissertation have been expressed as future scope of this work:

- Investigation of the techno-economic viability of liquefaction and co-liquefaction processes applied to *Citrus limetta* fruits wastes which might represent a promising avenue for future research. This entails a comprehensive analysis of the economic feasibility of these processes, considering factors such as production costs, resource utilization and potential revenue streams.
- Additionally, a focus on understanding the influence of catalysts on the liquefaction and co-liquefaction of *Citrus limetta* fruits is crucial. Examining various alkali catalysts such as K_2CO_3 and Ni, Ru, Pd, Co, Pt catalysts and their impact on reaction kinetics, product yields and overall efficiency will contribute valuable insights for optimizing these processes.
- The integration of co-solvents into the liquefaction and co-liquefaction studies offers another intriguing avenue for exploration. Investigating the effects of co-solvents on reaction pathways, product distribution and overall process efficiency can enhance the understanding of how these auxiliary substances can be utilized to improve the conversion of fruit wastes into valuable products.
- Furthermore, exploring strategies for the effective upgrading of biocrude obtained from these processes is essential. This involves identifying suitable methods for

enhancing the quality and energy density of the biocrude making it a more viable biofuel.

- Simultaneously, investigating the activation potential of biochar for applications in soil remediation might add an environmental dimension to the research, contributing to sustainable waste management practices.

6.3 Summary of the Chapter

The major conclusions drawn from this dissertation have been portrayed in this chapter. In summary, the future research scope which encompasses a holistic evaluation of the techno-economic aspects, catalytic influences, co-solvent utilization and the upgrading of biocrude and biochar for biofuel production and soil remediation from *Citrus limetta* fruits were proposed.

REFERENCES

[1] A. Jayanthi Antonisamy, S. Marimuthu, S. Malayandi, K. Rajendran, Y.C. Lin, G. Andaluri, S.L. Lee, V.K. Ponnusamy, Sustainable approaches on industrial food wastes to value-added products – A review on extraction methods, characterizations, and its biomedical applications, Environ. Res. 217 (2023) 114758. https://doi.org/10.1016/j.envres.2022.114758.

[2] Z. Maqbool, W. Khalid, H.T. Atiq, H. Koraqi, Z. Javaid, S.K. Alhag, L.A. Al-Shuraym, D.M.D. Bader, M. Almarzuq, M. Afifi, A. AL-Farga, Citrus Waste as Source of Bioactive Compounds: Extraction and Utilization in Health and Food Industry, Molecules. 28 (2023). https://doi.org/10.3390/molecules28041636.

[3] Z. Zou, W. Xi, Y. Hu, C. Nie, Z. Zhou, Antioxidant activity of Citrus fruits, Food Chem. 196 (2016) 885–896. https://doi.org/10.1016/j.foodchem.2015.09.072.

[4] E.M. Garcia-Castello, A.D. Rodriguez-Lopez, L. Mayor, R. Ballesteros, C. Conidi, A. Cassano, Optimization of conventional and ultrasound assisted extraction of flavonoids from grapefruit (Citrus paradisi L.) solid wastes, Lwt. 64 (2015) 1114–1122. https://doi.org/10.1016/j.lwt.2015.07.024.

[5] A. Ben Hsouna, C. Sadaka, I. Generalić Mekinić, S. Garzoli, J. Švarc-Gajić, F. Rodrigues, S. Morais, M.M. Moreira, E. Ferreira, G. Spigno, T. Brezo-Borjan, B. Ben Akacha, R. Ben Saad, C. Delerue-Matos, W. Mnif, The Chemical Variability, Nutraceutical Value, and Food-Industry and Cosmetic Applications of Citrus Plants: A Critical Review, Antioxidants. 12 (2023) 1–37. https://doi.org/10.3390/antiox12020481.

[6] E. Gómez-Mejía, N. Rosales-Conrado, M.E. León-González, Y. Madrid, Citrus peels waste as a source of value-added compounds: Extraction and quantification of bioactive polyphenols, Food Chem. 295 (2019) 289–299. https://doi.org/10.1016/j.foodchem.2019.05.136.

[7] C. Xia, A. Pathy, B. Paramasivan, P. Ganeshan, K. Dhamodharan, A. Juneja, D. Kumar, K. Brindhadevi, S.H. Kim, K. Rajendran, Comparative study of pyrolysis and hydrothermal liquefaction of microalgal species: Analysis of product yields with reaction temperature, Fuel. 311 (2022) 121932.

https://doi.org/10.1016/j.fuel.2021.121932.

[8] G. Ahmed, S. Acharya, H. Kawale, A. Singh, N. Kishore, S. Pal, Thermochemical conversion of Polyalthia longifolia leaves at different temperatures and characterization of their products, Fuel. 280 (2020) 118574. https://doi.org/10.1016/j.fuel.2020.118574.

[9] S. Anouti, G. Haarlemmer, M. Déniel, A. Roubaud, Analysis of Physicochemical Properties of Bio-Oil from Hydrothermal Liquefaction of Blackcurrant Pomace, Energy & Fuels. 30 (2016) 398–406. https://doi.org/10.1021/acs.energyfuels.5b02264.

[10] Z. Yuan, G. Jia, X. Cui, X. Song, C. Wang, P. Zhao, A.J. Ragauskas, Effects of temperature and time on supercritical methanol Co-Liquefaction of rice straw and linear low-density polyethylene wastes, Energy. 245 (2022) 123315. https://doi.org/10.1016/j.energy.2022.123315.

[11] IEA, Renewables 2022, IEA, Paris, (2022) 158. https://www.iea.org/reports/renewables-2022.

[12] I.U. Khan, A. Haleem, A.U. Khan, Non-edible plant seeds of Acacia farnesiana as a new and effective source for biofuel production, RSC Adv. 12 (2022) 21223–21234. https://doi.org/10.1039/d2ra03406a.

[13] Y. Wang, X. Gu, Y. Huang, Z. Ding, Y. Chen, X. Hu, Insight into biomass feedstock on formation of biochar-bound environmentally persistent free radicals under different pyrolysis temperatures, RSC Adv. 12 (2022) 19318–19326. https://doi.org/10.1039/d2ra03052g.

[14] W. Prins, F. Ronsse, W. Brilman, D. Lo, Hydrothermal liquefaction (HTL) of microalgae for biofuel production : State of the art review and future prospects, 3 (2012). https://doi.org/10.1016/j.biombioe.2012.12.029.

[15] D.G. Christian, Biomass for Renewable Energy, Fuels, and Chemicals, J. Environ. Qual. 29 (2000) 662–663. https://doi.org/10.2134/jeq2000.00472425002900020040x.

[16] A. V. Bridgwater, S.A. Bridge, A Review of Biomass Pyrolysis and Pyrolysis Technologies, in: Biomass Pyrolysis Liq. Upgrad. Util., Springer; 1991 edition (31 March 1991), 1991: pp. 11–92. https://doi.org/10.1007/978-94-011-3844-4_2.

[17] M.A. Perea-Moreno, E. Samerón-Manzano, A.J. Perea-Moreno, Biomass as renewable

energy: Worldwide research trends, Sustain. 11 (2019). https://doi.org/10.3390/su11030863.

[18] G. Amaral, J. Bushee, U.G. Cordani, Summary for Policymakers. Climate Change 2013 – The Physical Science Basis. 369 (1) 1-30 2014. https://doi.org/10.1017/CBO9781107415324.004

[19] A. Singh, K.S. Rawat, O.P. Nautiyal, T. V. Chavdal, Biomass To Fuel: Conversion Techniques, (2016) 155–194.

[20] S. Nanda, D.V.N. Vo, P.K. Sarangi, Biorefinery of alternative resources: Targeting green fuels and platform chemicals, 2020. https://doi.org/10.1007/978-981-15-1804-1.

[21] K. Tekin, S. Karagöz, S. Bektaş, A review of hydrothermal biomass processing, Renew. Sustain. Energy Rev. 40 (2014) 673–687. https://doi.org/10.1016/j.rser.2014.07.216.

[22] S. Sharma, R. Meena, A. Sharma, P. kumar Goyal, Biomass Conversion Technologies for Renewable Energy and Fuels: A Review Note., IOSR J. Mech. Civ. Eng. 11 (2014) 28–35. https://doi.org/10.9790/1684-11232835.

[23] A. Pandey, T. Bhaskar, M. Stöcker, R.K. Sukumaran, Recent Advances in Thermo-Chemical Conversion of Biomass, Elsevier, 2015. https://doi.org/10.1016/C2013-0-00403-3.

[24] J.M.M. Adams, T.A. Toop, I.S. Donnison, J.A. Gallagher, Seasonal variation in Laminaria digitata and its impact on biochemical conversion routes to biofuels, Bioresour. Technol. 102 (2011) 9976–9984. https://doi.org/10.1016/j.biortech.2011.08.032.

[25] J.E.A. Seabra, I.C. Macedo, Comparative analysis for power generation and ethanol production from sugarcane residual biomass in Brazil, Energy Policy. 39 (2011) 421–428. https://doi.org/10.1016/j.enpol.2010.10.019.

[26] S.N. Gebremariam, J.M. Marchetti, Economics of biodiesel production: Review, Energy Convers. Manag. 168 (2018) 74–84. https://doi.org/10.1016/j.enconman.2018.05.002.

[27] José Miguel Cisneros Herreros, Germán Peñalva Moreno, Article in Press Article in Press, GEF Bull. Biosci. 1 (2010) 1–6. https://doi.org/10.1016/j.jinf.2020.02.020.

[28] M.P. Robbins, G. Evans, J. Valentine, I.S. Donnison, G.G. Allison, New opportunities for the exploitation of energy crops by thermochemical conversion in northern Europe and the UK, Prog. Energy Combust. Sci. 38 (2012) 138–155. https://doi.org/10.1016/j.pecs.2011.08.001.

[29] M.M. Küçük, A. Demirbaş, Biomass conversion processes, Energy Convers. Manag. 38 (1997) 151–165. https://doi.org/10.1016/0196-8904(96)00031-3.

[30] A. V. Bridgwater, Renewable fuels and chemicals by thermal processing of biomass, Chem. Eng. J. 91 (2003) 87–102. https://doi.org/10.1016/S1385-8947(02)00142-0.

[31] P. McKendry, Energy production from biomass (part 2): Conversion technologies, Bioresour. Technol. 83 (2002) 47–54. https://doi.org/10.1016/S0960-8524(01)00119-5.

[32] P. Tanger, J.L. Field, C.E. Jahn, M.W. DeFoort, J.E. Leach, Biomass for thermochemical conversion: targets and challenges, Front. Plant Sci. 4 (2013). https://doi.org/10.3389/fpls.2013.00218.

[33] M. Balat, Gasification of biomass to produce gaseous products, Energy Sources, Part A Recover. Util. Environ. Eff. 31 (2009) 516–526. https://doi.org/10.1080/15567030802466847.

[34] A.K. Rajvanshi, Biomass gasification in: Alternative Energy in Agriculture, Altern. Energy Agric. 2 (1986) 83–102.

[35] M.R. Susta, P. Luby, S. Bin Mat, Biomass Energy Utilization & Environment Protection - Commercial Reality and Outlook, Power-Gen Asia. (2003) 1–21.

[36] A. Demirbaş, Hydrogen production from biomass by the gasification process, Energy Sources. 24 (2002) 59–68. https://doi.org/10.1080/00908310252712307.

[37] J. Piskorz, P. Majerski, D. Radlein, A. Vladars-Usas, D.S. Scott, Flash pyrolysis of cellulose for production of anhydro-oligomers, J. Anal. Appl. Pyrolysis. 56 (2000) 145–166. https://doi.org/10.1016/S0165-2370(00)00089-9.

[38] K.R. Thines, E.C. Abdullah, N.M. Mubarak, M. Ruthiraan, Synthesis of magnetic biochar from agricultural waste biomass to enhancing route for waste water and polymer application: A review, Renew. Sustain. Energy Rev. 67 (2017) 257–276.

https://doi.org/10.1016/j.rser.2016.09.057.

[39] M. Van de Velden, J. Baeyens, A. Brems, B. Janssens, R. Dewil, Fundamentals, kinetics and endothermicity of the biomass pyrolysis reaction, Renew. Energy. 35 (2010) 232–242. https://doi.org/10.1016/j.renene.2009.04.019.

[40] SERI, Specialists' Workshop on Fast Pyrolysis of Biomass, Spec. Work. Fast Pyrolysis Biomass. (1980) 428. https://ntrl.ntis.gov/NTRL/dashboard/searchResults/titleDetail/SERICP6221096.xhtml.

[41] D.S. Scott, L. Paterson, J. Piskorz, D. Radlein, Pretreatment of poplar wood for fast pyrolysis: Rate of cation removal, J. Anal. Appl. Pyrolysis. 57 (2001) 169–176. https://doi.org/10.1016/S0165-2370(00)00108-X.

[42] T.B. Reed, Combustion, Pyrolysis, Gasification and Liquefaction of Biomass., Comm. Eur. Communities, EUR. (1981) 496–508.

[43] R. Alén, E. Kuoppala, P. Oesch, Formation of the main degradation compound groups from wood and its components during pyrolysis, J. Anal. Appl. Pyrolysis. 36 (1996) 137–148. https://doi.org/10.1016/0165-2370(96)00932-1.

[44] M. Yang, X.R. Song, P.F. Deng, H.R. Yang, Pyrolysis and liquefaction of biomass, Linchan Huaxue Yu Gongye/Chemistry Ind. For. Prod. 20 (2000) 77–82.

[45] M.S. Bohn, C.B. Benham, Biomass Pyrolysis with an Entrained Flow Reactor, Ind. Eng. Chem. Process Des. Dev. 23 (1984) 355–363. https://doi.org/10.1021/i200025a030.

[46] K. Alper, K. Tekin, S. Karagöz, A.J. Ragauskas, Sustainable energy and fuels from biomass: A review focusing on hydrothermal biomass processing, Sustain. Energy Fuels. 4 (2020) 4390–4414. https://doi.org/10.1039/d0se00784f.

[47] M. Kumar, A. Olajire Oyedun, A. Kumar, A review on the current status of various hydrothermal technologies on biomass feedstock, Renew. Sustain. Energy Rev. 81 (2018) 1742–1770. https://doi.org/10.1016/j.rser.2017.05.270.

[48] A.A. Peterson, F. Vogel, R.P. Lachance, M. Fröling, M.J. Antal, J.W. Tester, Thermochemical biofuel production in hydrothermal media: A review of sub- and

supercritical water technologies, Energy Environ. Sci. 1 (2008) 32–65. https://doi.org/10.1039/b810100k.

[49] K.M. Isa, T.A.T. Abdullah, U.F.M. Ali, Hydrogen donor solvents in liquefaction of biomass: A review, Renew. Sustain. Energy Rev. 81 (2018) 1259–1268. https://doi.org/10.1016/j.rser.2017.04.006.

[50] S. Nizamuddin, H.A. Baloch, G.J. Griffin, N.M. Mubarak, A.W. Bhutto, R. Abro, S.A. Mazari, B.S. Ali, An overview of effect of process parameters on hydrothermal carbonization of biomass, Renew. Sustain. Energy Rev. 73 (2017) 1289–1299. https://doi.org/10.1016/j.rser.2016.12.122.

[51] J.A. Libra, K.S. Ro, C. Kammann, A. Funke, N.D. Berge, Y. Neubauer, M.M. Titirici, C. Fühner, O. Bens, J. Kern, K.H. Emmerich, Hydrothermal carbonization of biomass residuals: A comparative review of the chemistry, processes and applications of wet and dry pyrolysis, Biofuels. 2 (2011) 71–106. https://doi.org/10.4155/bfs.10.81.

[52] J. Mumme, L. Eckervogt, J. Pielert, M. Diakité, F. Rupp, J. Kern, Hydrothermal carbonization of anaerobically digested maize silage, Bioresour. Technol. 102 (2011) 9255–9260. https://doi.org/10.1016/j.biortech.2011.06.099.

[53] A.R.K. Gollakota, N. Kishore, S. Gu, A review on hydrothermal liquefaction of biomass, Renew. Sustain. Energy Rev. 81 (2018) 1378–1392. https://doi.org/10.1016/j.rser.2017.05.178.

[54] S.S. Toor, L. Rosendahl, A. Rudolf, Hydrothermal liquefaction of biomass: A review of subcritical water technologies, Energy. 36 (2011) 2328–2342. https://doi.org/10.1016/j.energy.2011.03.013.

[55] J. Akhtar, N.A.S. Amin, A review on process conditions for optimum bio-oil yield in hydrothermal liquefaction of biomass, Renew. Sustain. Energy Rev. 15 (2011) 1615–1624. https://doi.org/10.1016/j.rser.2010.11.054.

[56] R.D. Cortright, R.R. Davda, J.A. Dumesic, Hydrogen from catalytic reforming of biomass-derived hydrocarbons in liquid water, Mater. Sustain. Energy A Collect. Peer-Reviewed Res. Rev. Artic. from Nat. Publ. Gr. 418 (2010) 289–292. https://doi.org/10.1142/9789814317665_0043.

[57] B.W.L. Jang, R. Gläser, M. Dong, C.J. Liu, Fuels of the future, Energy Environ. Sci. 3

(2010) 253. https://doi.org/10.1039/c003390c.

[58] S. Chaudry, P.A. Bahri, N.R. Moheimani, Pathways of processing of wet microalgae for liquid fuel production: A critical review, Renew. Sustain. Energy Rev. 52 (2015) 1240–1250. https://doi.org/10.1016/j.rser.2015.08.005.

[59] U. Jena, A.T. McCurdy, A. Warren, H. Summers, R.N. Ledbetter, S.K. Hoekman, L.C. Seefeldt, J.C. Quinn, Oleaginous yeast platform for producing biofuels via co-solvent hydrothermal liquefaction, Biotechnol. Biofuels. 8 (2015) 1–19. https://doi.org/10.1186/s13068-015-0345-5.

[60] I. Moir, A. Seabridge, Fuel Systems, 2008. https://doi.org/10.1002/9780470770931.ch3.

[61] Z. Wang, S. Adhikari, P. Valdez, R. Shakya, Upgrading of hydrothermal liquefaction biocrude from algae grown in municipal wastewater, Am. Soc. Agric. Biol. Eng. Annu. Int. Meet. 2015. 6 (2015) 5124–5142. https://doi.org/10.13031/aim.20152191148.

[62] S. Karagöz, T. Bhaskar, A. Muto, Y. Sakata, T. Oshiki, T. Kishimoto, Low-temperature catalytic hydrothermal treatment of wood biomass: Analysis of liquid products, Chem. Eng. J. 108 (2005) 127–137. https://doi.org/10.1016/j.cej.2005.01.007.

[63] D. Zhou, L. Zhang, S. Zhang, H. Fu, J. Chen, Hydrothermal liquefaction of macroalgae enteromorpha prolifera to bio-oil, Energy and Fuels. 24 (2010) 4054–4061. https://doi.org/10.1021/ef100151h.

[64] Z. Zhang, I.M. O'Hara, S. Mundree, B. Gao, A.S. Ball, N. Zhu, Z. Bai, B. Jin, Biofuels from food processing wastes, Curr. Opin. Biotechnol. 38 (2016) 97–105. https://doi.org/10.1016/j.copbio.2016.01.010.

[65] K. Jõgi, R. Bhat, Valorization of food processing wastes and by-products for bioplastic production, Sustain. Chem. Pharm. 18 (2020) 100326. https://doi.org/10.1016/j.scp.2020.100326.

[66] W.H. Chen, Y.Y. Lin, H.C. Liu, S. Baroutian, Optimization of food waste hydrothermal liquefaction by a two-step process in association with a double analysis, Energy. 199 (2020) 117438. https://doi.org/10.1016/j.energy.2020.117438.

[67] M.J. Stablein, A. Aierzhati, J. Watson, B. Si, Y. Zhang, Characterization and

bioremediation potential of byproducts from hydrothermal liquefaction of food wastes, Bioresour. Technol. Reports. 12 (2020). https://doi.org/10.1016/j.biteb.2020.100555.

[68] B. Zhang, J. Chen, S. Kandasamy, Z. He, Hydrothermal liquefaction of fresh lemon-peel and Spirulina platensis blending -operation parameter and biocrude chemistry investigation, Energy. 193 (2020) 116645. https://doi.org/10.1016/j.energy.2019.116645.

[69] S. Anouti, G. Haarlemmer, M. Déniel, A. Roubaud, Analysis of Physicochemical Properties of Bio-Oil from Hydrothermal Liquefaction of Blackcurrant Pomace, Energy and Fuels. 30 (2016) 398–406. https://doi.org/10.1021/acs.energyfuels.5b02264.

[70] S.O. Dahunsi, Liquefaction of pineapple peel: Pretreatment and process optimization, Energy. 185 (2019) 1017–1031. https://doi.org/10.1016/j.energy.2019.07.123.

[71] Y.H. Chan, A.T. Quitain, S. Yusup, Y. Uemura, M. Sasaki, T. Kida, Liquefaction of palm kernel shell to bio-oil using sub- and supercritical water: An overall kinetic study, J. Energy Inst. 92 (2019) 535–541. https://doi.org/10.1016/j.joei.2018.04.005.

[72] B. Zhang, J. Chen, H. Chen, S. Kandasamy, Hydrothermal liquefaction of fresh lemon-peel: Parameter optimisation and product chemistry, Renew. Energy. 143 (2019) 512–519. https://doi.org/10.1016/j.renene.2019.05.003.

[73] S. Hongthong, S. Raikova, H.S. Leese, C.J. Chuck, Co-processing of common plastics with pistachio hulls via hydrothermal liquefaction, Waste Manag. 102 (2020) 351–361. https://doi.org/10.1016/j.wasman.2019.11.003.

[74] R. Kaur, P. Gera, M.K. Jha, T. Bhaskar, Reaction parameters effect on hydrothermal liquefaction of castor (Ricinus Communis) residue for energy and valuable hydrocarbons recovery, Renew. Energy. 141 (2019) 1026–1041. https://doi.org/10.1016/j.renene.2019.04.064.

[75] Risso, Citrus limetta Risso, Ann. Mus. Natl. Hist. Nat. xx. (1813) 195. t. 2. f. 1., Https://Www.Ipni.Org/n/771956-1. (1813). https://doi.org/https://www.ipni.org/n/771956-1.

[76] D. Rivera, A. Bermúdez, C. Obón, F. Alcaraz, S. Ríos, J. Sánchez-Balibrea, P. Pablo Ferrer-Gallego, R. Krueger, Analysis of 'Marrakesh limetta' (Citrus × limon var.

limetta (Risso) Ollitrault, Curk & R.Krueger) horticultural history and relationships with limes and lemons, Sci. Hortic. (Amsterdam). 293 (2022). https://doi.org/10.1016/j.scienta.2021.110688.

[77] R. Saha, K. Mukherjee, I. Saha, A. Ghosh, S.K. Ghosh, B. Saha, Removal of hexavalent chromium from water by adsorption on mosambi (Citrus limetta) peel, Res. Chem. Intermed. 39 (2013) 2245–2257. https://doi.org/10.1007/s11164-012-0754-z.

[78] S. Shakoor, A. Nasar, Removal of methylene blue dye from artificially contaminated water using citrus limetta peel waste as a very low cost adsorbent, J. Taiwan Inst. Chem. Eng. 66 (2016) 154–163. https://doi.org/10.1016/j.jtice.2016.06.009.

[79] Poonam, N. Kumar, Experimental and kinetic study of removal of lead (Pb+2) from battery effluent using sweet lemon (Citrus limetta) peel biochar adsorbent, Environ. Dev. Sustain. 22 (2020) 4379–4406. https://doi.org/10.1007/s10668-019-00389-2.

[80] M.M. Musthafa, Production of biodiesel from Citrus limetta seed oil, Energy Sources, Part A Recover. Util. Environ. Eff. 38 (2016) 2994–3000. https://doi.org/10.1080/15567036.2015.1135205.

[81] V. Sukumar, V. Manieniyan, R. Senthilkumar, S. Sivaprakasam, Production of bio oil from sweet lime empty fruit bunch by pyrolysis, Renew. Energy. 146 (2020) 309–315. https://doi.org/10.1016/j.renene.2019.06.156.

[82] A. Trabelsi, N. Mihoubi, S. ABIDI, A. Trabelsi, N. Mihoubi, Pyrolysis of Lemon Peel Waste in a Fixed-bed Reactor and Characterization of Innovative Pyrolytic Products, Journal of Material Cycles and Waste Management. 25 (1) (2023). https://doi.org/10.1007/s10163-022-01527-1.

[83] N. Ahmad, N. Ahmad, U. Ahmed, A.G. Abdul Jameel, U. e. S. Amjad, M. Hussain, M.M. Arif, Production of fuel oil from elastomer rubber waste via methanothermal liquefaction, Fuel. 338 (2023) 127330. https://doi.org/10.1016/j.fuel.2022.127330.

[84] B. Ashok, N. Hariram, S. Siengchin, A.V. Rajulu, Modification of tamarind fruit shell powder with in situ generated copper nanoparticles by single step hydrothermal method, J. Bioresour. Bioprod. 5 (2020) 180–185. https://doi.org/10.1016/j.jobab.2020.07.003.

[85] H. Zeb, A. Riaz, J. Kim, Understanding the effect of biomass-to-solvent ratio on

macroalgae (Saccharina japonica) liquefaction in supercritical ethanol, J. Supercrit. Fluids. 120 (2017) 65–74. https://doi.org/10.1016/j.supflu.2016.10.013.

[86] A. Sahoo, K. Saini, M. Jindal, T. Bhaskar, K.K. Pant, Co-Hydrothermal Liquefaction of algal and lignocellulosic biomass: Status and perspectives, Bioresour. Technol. 342 (2021) 125948. https://doi.org/10.1016/j.biortech.2021.125948.

[87] J. Yang, Q. (Sophia)He, L. Yang, A review on hydrothermal co-liquefaction of biomass, Appl. Energy. 250 (2019) 926–945. https://doi.org/10.1016/j.apenergy.2019.05.033.

[88] Q. Li, X. Yuan, X. Hu, E. Meers, H.C. Ong, W.H. Chen, P. Duan, S. Zhang, K.B. Lee, Y.S. Ok, Co-liquefaction of mixed biomass feedstocks for bio-oil production: A critical review, Renew. Sustain. Energy Rev. 154 (2022) 111814. https://doi.org/10.1016/j.rser.2021.111814.

[89] N. Ikenaga, C. Ueda, T. Matsui, M. Ohtsuki, T. Suzuki, Co-liquefaction of micro algae with coal using coal liquefaction catalysts, Energy and Fuels. 15 (2001) 350–355. https://doi.org/10.1021/ef000129u.

[90] Z. He, B. Wang, B. Zhang, H. Feng, S. Kandasamy, H. Chen, Synergistic effect of hydrothermal Co-liquefaction of Spirulina platensis and Lignin: Optimization of operating parameters by response surface methodology, Energy. 201 (2020) 117550. https://doi.org/10.1016/j.energy.2020.117550.

[91] H. Ahmed Baloch, S. Nizamuddin, M.T.H. Siddiqui, N.M. Mubarak, D.K. Dumbre, M.P. Srinivasan, G.J. Griffin, Sub-supercritical liquefaction of sugarcane bagasse for production of bio-oil and char: Effect of two solvents, J. Environ. Chem. Eng. 6 (2018) 6589–6601. https://doi.org/10.1016/j.jece.2018.10.017.

[92] M. Makabe, K. Ouchi, Effect of pressure and temperature on the reaction of coal with alcohol-alkali, Fuel. 60 (1981) 327–329. https://doi.org/10.1016/0016-2361(81)90201-5.

[93] M. Balat, Mechanisms of Thermochemical Biomass Conversion Processes. Part 3: Reactions of Liquefaction, Energy Sources, Part A Recover. Util. Environ. Eff. 30 (2008) 649–659. https://doi.org/10.1080/10407780600817592.

[94] S. Karagöz, T. Bhaskar, A. Muto, Y. Sakata, Effect of Rb and Cs carbonates for

production of phenols from liquefaction of wood biomass, Fuel. 83 (2004) 2293–2299. https://doi.org/10.1016/j.fuel.2004.06.023.

[95] Z. Liu, F.S. Zhang, Effects of various solvents on the liquefaction of biomass to produce fuels and chemical feedstocks, Energy Convers. Manag. 49 (2008) 3498–3504. https://doi.org/10.1016/j.enconman.2008.08.009.

[96] L. Lin, Y. Yao, M. Yoshioka, N. Shiraishi, Liquefaction mechanism of cellulose in the presence of phenol under acid catalysis, Carbohydr. Polym. 57 (2004) 123–129. https://doi.org/10.1016/j.carbpol.2004.01.014.

[97] H. Deng, W. Meredith, C.N. Uguna, C.E. Snape, Impact of solvent type and condition on biomass liquefaction to produce heavy oils in high yield with low oxygen contents, J. Anal. Appl. Pyrolysis. 113 (2015) 340–348. https://doi.org/10.1016/j.jaap.2015.02.015.

[98] G. Wang, W. Li, B. Li, H. Chen, Direct liquefaction of sawdust under syngas, Fuel. 86 (2007) 1587–1593. https://doi.org/10.1016/j.fuel.2006.11.010.

[99] Y. Yan, J. Xu, T. Li, Z. Ren, Liquefaction of sawdust for liquid fuel, Fuel Process. Technol. 60 (1999) 135–143. https://doi.org/10.1016/S0378-3820(99)00026-0.

[100] J. Yip, M. Chen, Y.S. Szeto, S. Yan, Comparative study of liquefaction process and liquefied products from bamboo using different organic solvents, Bioresour. Technol. 100 (2009) 6674–6678. https://doi.org/10.1016/j.biortech.2009.07.045.

[101] T. Zhang, Y. Zhou, D. Liu, L. Petrus, Qualitative analysis of products formed during the acid catalyzed liquefaction of bagasse in ethylene glycol, Bioresour. Technol. 98 (2007) 1454–1459. https://doi.org/10.1016/j.biortech.2006.03.029.

[102] M. Kunaver, S. Medved, N. Čuk, E. Jasiukaityte, I. Poljanšek, T. Strnad, Application of liquefied wood as a new particle board adhesive system, Bioresour. Technol. 101 (2010) 1361–1368. https://doi.org/10.1016/j.biortech.2009.09.066.

[103] T. Yamada, H. Ono, Characterization of the products resulting from ethylene glycol liquefaction of cellulose, J. Wood Sci. 47 (2001) 458–464. https://doi.org/10.1007/BF00767898.

[104] R.C. Neavel, Liquefaction of coal in hydrogen-donor and non-donor vehicles, Fuel. 55

(1976) 237–242. https://doi.org/10.1016/0016-2361(76)90095-8.

[105] M.B. Abdel-Baset, R.F. Yarzab, P.H. Given, Dependence of coal liquefaction behaviour on coal characteristics. 3. Statistical correlations of conversion in coal-tetralin interactions, Fuel. 57 (1978) 89–94. https://doi.org/10.1016/0016-2361(78)90104-7.

[106] E. Jakab, Thermal decomposition of wood and cellulose in the presence of solvent vapors, Ind. Eng. Chem. Res. 36 (1997) 2087–2095. https://doi.org/10.1021/ie960335i.

[107] M. Cemek, M.M. Küçük, Liquid products from Verbascum stalk by supercritical fluid extraction, Energy Convers. Manag. 42 (2001) 125–130. https://doi.org/10.1016/S0196-8904(00)00049-2.

[108] J.E. Miller, L. Evans, A. Littlewolf, D.E. Trudell, Batch microreactor studies of lignin and lignin model compound depolymerization by bases in alcohol solvents, Fuel. 78 (1999) 1363–1366. https://doi.org/10.1016/S0016-2361(99)00072-1.

[109] E. Demirkaya, O. Dal, A. Yüksel, Liquefaction of waste hazelnut shell by using sub- and supercritical solvents as a reaction medium, J. Supercrit. Fluids. 150 (2019) 11–20. https://doi.org/10.1016/j.supflu.2019.03.019.

[110] I. Domingos, J. Ferreira, L.P. Cruz-Lopes, B. Esteves, Liquefaction and chemical composition of walnut shells, Open Agric. 7 (2022) 249–256. https://doi.org/10.1515/opag-2022-0072.

[111] S.-P. Fan, S. Zakaria, C.-H. Chia, F. Jamaluddin, S. Nabihah, T.-K. Liew, F.-L. Pua, Comparative studies of products obtained from solvolysis liquefaction of oil palm empty fruit bunch fibres using different solvents, Bioresour. Technol. 102 (2011) 3521–3526. https://doi.org/10.1016/j.biortech.2010.11.046.

[112] A. Koriakin, S. Moon, D.-W. Kim, C.-H. Lee, Liquefaction of oil palm empty fruit bunch using sub- and supercritical tetralin, n-dodecane, and their mixture, Fuel. 208 (2017) 184–192. https://doi.org/10.1016/j.fuel.2017.07.010.

[113] S. Karagöz, T. Bhaskar, A. Muto, Y. Sakata, Comparative studies of oil compositions produced from sawdust, rice husk, lignin and cellulose by hydrothermal treatment, Fuel. 84 (2005) 875–884. https://doi.org/10.1016/j.fuel.2005.01.004.

[114] Y. Guo, T. Yeh, W. Song, D. Xu, S. Wang, A review of bio-oil production from hydrothermal liquefaction of algae, Renew. Sustain. Energy Rev. 48 (2015) 776–790. https://doi.org/10.1016/j.rser.2015.04.049.

[115] S.S. Qureshi, S. Nizamuddin, H.A. Baloch, M.T.H. Siddiqui, N.M. Mubarak, G.J. Griffin, An overview of OPS from oil palm industry as feedstock for bio-oil production, Biomass Convers. Biorefinery. 9 (2019) 827–841. https://doi.org/10.1007/s13399-019-00381-w.

[116] L. Yang, Q. (Sophia) He, P. Havard, K. Corscadden, C. (Charles) Xu, X. Wang, Co-liquefaction of spent coffee grounds and lignocellulosic feedstocks, Bioresour. Technol. 237 (2017) 108–121. https://doi.org/10.1016/j.biortech.2017.02.087.

[117] H.A. Baloch, M.T.H. Siddiqui, S. Nizamuddin, N.M. Mubarak, M. Khalid, M.P. Srinivasan, G.J. Griffin, Catalytic co-liquefaction of sugarcane bagasse and polyethylene for bio-oil production under supercritical conditions: Effect of catalysts, J. Anal. Appl. Pyrolysis. 153 (2021) 104944. https://doi.org/10.1016/j.jaap.2020.104944.

[118] K.G. Burra, A.K. Gupta, Kinetics of synergistic effects in co-pyrolysis of biomass with plastic wastes, Appl. Energy. 220 (2018) 408–418. https://doi.org/10.1016/j.apenergy.2018.03.117.

[119] X. Pei, X. Yuan, G. Zeng, H. Huang, J. Wang, H. Li, H. Zhu, Co-liquefaction of microalgae and synthetic polymer mixture in sub- and supercritical ethanol, Fuel Process. Technol. 93 (2012) 35–44. https://doi.org/10.1016/j.fuproc.2011.09.010.

[120] M. Coma, E. Martinez-Hernandez, F. Abeln, S. Raikova, J. Donnelly, T.C. Arnot, M.J. Allen, D.D. Hong, C.J. Chuck, Organic waste as a sustainable feedstock for platform chemicals, Faraday Discuss. 202 (2017) 175–195. https://doi.org/10.1039/c7fd00070g.

[121] L. Leng, J. Li, X. Yuan, J. Li, P. Han, Y. Hong, F. Wei, W. Zhou, Beneficial synergistic effect on bio-oil production from co-liquefaction of sewage sludge and lignocellulosic biomass, Bioresour. Technol. 251 (2018) 49–56. https://doi.org/10.1016/j.biortech.2017.12.018.

[122] Y. Hu, M. Hu, H. Jiang, P. Yu, W. Yang, Co-liquefaction of livestock manure and food waste: Synergistic effects and product combustion performance, Appl. Energy. 341

(2023) 121073. https://doi.org/10.1016/j.apenergy.2023.121073.

[123] X. Chen, X. Peng, X. Ma, J. Wang, Investigation of Mannich reaction during co-liquefaction of microalgae and sweet potato waste, Bioresour. Technol. 284 (2019) 286–292. https://doi.org/10.1016/j.biortech.2019.03.136.

[124] C. Gai, Y. Li, N. Peng, A. Fan, Z. Liu, Co-liquefaction of microalgae and lignocellulosic biomass in subcritical water, Bioresour. Technol. 185 (2015) 240–245. https://doi.org/10.1016/j.biortech.2015.03.015.

[125] B. Jin, P. Duan, Y. Xu, F. Wang, Y. Fan, Co-liquefaction of micro- and macroalgae in subcritical water, Bioresour. Technol. 149 (2013) 103–110. https://doi.org/10.1016/j.biortech.2013.09.045.

[126] A. Aierzhati, M.J. Stablein, N.E. Wu, C.T. Kuo, B. Si, X. Kang, Y. Zhang, Experimental and model enhancement of food waste hydrothermal liquefaction with combined effects of biochemical composition and reaction conditions, Bioresour. Technol. 284 (2019) 139–147. https://doi.org/10.1016/j.biortech.2019.03.076.

[127] R.P. Overend, The average haul distance and transportation work factors for biomass delivered to a central plant, Biomass. 2 (1982) 75–79. https://doi.org/10.1016/0144-4565(82)90008-7.

[128] A. Mathanker, S. Das, D. Pudasainee, M. Khan, A. Kumar, R. Gupta, A review of hydrothermal liquefaction of biomass for biofuels production with a special focus on the effect of process parameters, co-solvents and extraction solvents, Energies. 14 (2021). https://doi.org/10.3390/en14164916.

[129] Y. Qu, X. Wei, C. Zhong, Experimental study on the direct liquefaction of Cunninghamia lanceolata in water, Energy. 28 (2003) 597–606. https://doi.org/10.1016/S0360-5442(02)00178-0.

[130] J. Akhtar, S.K. Kuang, N.A.S. Amin, Liquefaction of empty palm fruit bunch (EPFB) in alkaline hot compressed water, Renew. Energy. 35 (2010) 1220–1227. https://doi.org/10.1016/j.renene.2009.10.003.

[131] S. Zou, Y. Wu, M. Yang, C. Li, J. Tong, Bio-oil production from sub- and supercritical water liquefaction of microalgae Dunaliella tertiolecta and related properties, Energy Environ. Sci. 3 (2010) 1073–1078. https://doi.org/10.1039/c002550j.

[132] F. Wang, Z. Chang, P. Duan, W. Yan, Y. Xu, L. Zhang, J. Miao, Y. Fan, Hydrothermal liquefaction of Litsea cubeba seed to produce bio-oils, Bioresour. Technol. 149 (2013) 509–515. https://doi.org/10.1016/j.biortech.2013.09.108.

[133] M. Déniel, G. Haarlemmer, A. Roubaud, E. Weiss-Hortala, J. Fages, Optimisation of bio-oil production by hydrothermal liquefaction of agro-industrial residues: Blackcurrant pomace (Ribes nigrum L.) as an example, Biomass and Bioenergy. 95 (2016) 273–285. https://doi.org/10.1016/j.biombioe.2016.10.012.

[134] C. Xu, J. Lancaster, Conversion of secondary pulp/paper sludge powder to liquid oil products for energy recovery by direct liquefaction in hot-compressed water, Water Res. 42 (2008) 1571–1582. https://doi.org/10.1016/j.watres.2007.11.007.

[135] S. Brand, R.F. Susanti, S.K. Kim, H. shik Lee, J. Kim, B.I. Sang, Supercritical ethanol as an enhanced medium for lignocellulosic biomass liquefaction: Influence of physical process parameters, Energy. 59 (2013) 173–182. https://doi.org/10.1016/j.energy.2013.06.049.

[136] J. Akhtar, N.A.S. Amin, A review on process conditions for optimum bio-oil yield in hydrothermal liquefaction of biomass, Renew. Sustain. Energy Rev. 15 (2011) 1615–1624. https://doi.org/10.1016/j.rser.2010.11.054.

[137] Z. Abu El-Rub, E.A. Bramer, G. Brem, Review of catalysts for tar elimination in biomass gasification processes, Ind. Eng. Chem. Res. 43 (2004) 6911–6919. https://doi.org/10.1021/ie0498403.

[138] B. De Caprariis, P. De Filippis, A. Petrullo, M. Scarsella, Hydrothermal liquefaction of biomass : Influence of temperature and biomass composition on the bio-oil production, Fuel. 208 (2017) 618–625. https://doi.org/10.1016/j.fuel.2017.07.054.

[139] D. Vallero, Fundamentals of Air Pollution - Fourth edition, 2008. https://doi.org/10.1016/B978-0-12-373615-4.X5000-6

[140] Y. Hu, M. Gong, S. Feng, C. (Charles) Xu, A. Bassi, A review of recent developments of pre-treatment technologies and hydrothermal liquefaction of microalgae for bio-crude oil production, Renew. Sustain. Energy Rev. 101 (2019) 476–492. https://doi.org/10.1016/j.rser.2018.11.037.

[141] B.E.O. Eboibi, D.M. Lewis, P.J. Ashman, S. Chinnasamy, Hydrothermal liquefaction

of microalgae for biocrude production: Improving the biocrude properties with vacuum distillation, Bioresour. Technol. 174 (2014) 212–221. https://doi.org/10.1016/j.biortech.2014.10.029.

[142] P. Sun, M. Heng, S. Sun, J. Chen, Direct liquefaction of paulownia in hot compressed water: Influence of catalysts, Energy. 35 (2010) 5421–5429. https://doi.org/10.1016/j.energy.2010.07.005.

[143] T. Minowa, F. Zhen, T. Ogi, Cellulose decomposition in hot-compressed water with alkali or nickel catalyst, J. Supercrit. Fluids. 13 (1998) 253–259. https://doi.org/10.1016/S0896-8446(98)00059-X.

[144] A. Mathanker, D. Pudasainee, A. Kumar, R. Gupta, Hydrothermal liquefaction of lignocellulosic biomass feedstock to produce biofuels: Parametric study and products characterization, Fuel. 271 (2020). https://doi.org/10.1016/j.fuel.2020.117534.

[145] K. Khampuang, N. Boreriboon, P. Prasassarakich, Alkali catalyzed liquefaction of corncob in supercritical ethanol-water, Biomass and Bioenergy. 83 (2015) 460–466. https://doi.org/10.1016/j.biombioe.2015.10.022.

[146] F. Goudnaan, B. van de Beld, F.R. Boerefijn, G.M. Bos, J.E. Naber, S. van der Wal, J.A. Zeevalkink, Thermal Efficiency of the HTU® Process for Biomass Liquefaction, Prog. Thermochem. Biomass Convers. (2008) 1312–1325. https://doi.org/10.1002/9780470694954.ch108.

[147] B.M. Kabyemela, M. Takigawa, T. Adschiri, R.M. Malaluan, K. Arai, Mechanism and Kinetics of Cellobiose Decomposition in Sub- and Supercritical Water, Ind. Eng. Chem. Res. 37 (1998) 357–361. https://doi.org/10.1021/ie9704408.

[148] D.A. Cantero, Á. Sánchez Tapia, M.D. Bermejo, M.J. Cocero, Pressure and temperature effect on cellulose hydrolysis in pressurized water, Chem. Eng. J. 276 (2015) 145–154. https://doi.org/10.1016/j.cej.2015.04.076.

[149] K.P.R. Dandamudi, T. Muppaneni, J.S. Markovski, P. Lammers, S. Deng, Hydrothermal liquefaction of green microalga Kirchneriella sp. under sub- and super-critical water conditions, Biomass and Bioenergy. 120 (2019) 224–228. https://doi.org/10.1016/j.biombioe.2018.11.021.

[150] Y.H. Chan, S. Yusup, A.T. Quitain, R.R. Tan, M. Sasaki, H.L. Lam, Y. Uemura, Effect

of process parameters on hydrothermal liquefaction of oil palm biomass for bio-oil production and its life cycle assessment, Energy Convers. Manag. 104 (2015) 180–188. https://doi.org/10.1016/j.enconman.2015.03.075.

[151] T. Ogi, S.Y. Yokoyama, K. Koguchi, Direct Liquefaction of Wood by Catalyst (Part 1): Effects of Pressure, Temperature, Holding Time and Wood/Catalyst/Water Ratio on Oil Yield, J. Japan Pet. Inst. 28 (1985) 239–245. https://doi.org/10.1627/jpi1958.28.239.

[152] S. Sangon, S. Ratanavaraha, S. Ngamprasertsith, P. Prasassarakich, Coal liquefaction using supercritical toluene-tetralin mixture in a semi-continuous reactor, Fuel Process. Technol. 87 (2006) 201–207. https://doi.org/10.1016/j.fuproc.2005.07.007.

[153] L. Ye, J. Zhang, J. Zhao, S. Tu, Liquefaction of bamboo shoot shell for the production of polyols, Bioresour. Technol. 153 (2014) 147–153. https://doi.org/10.1016/j.biortech.2013.11.070.

[154] M. Sasaki, T. Adschiri, K. Arai, Production of cellulose II from native cellulose by near- and supercritical water solubilization, J. Agric. Food Chem. 51 (2003) 5376–5381. https://doi.org/10.1021/jf025989i.

[155] C. Xu, T. Etcheverry, Hydro-liquefaction of woody biomass in sub- and super-critical ethanol with iron-based catalysts, Fuel. 87 (2008) 335–345. https://doi.org/10.1016/j.fuel.2007.05.013.

[156] R.D. Li, B.S. Li, T.H. Yang, Y.H. Xie, Liquefaction of rice stalk in sub- and supercritical ethanol, Ranliao Huaxue Xuebao/Journal Fuel Chem. Technol. 41 (2013) 1459–1465. https://doi.org/10.1016/s1872-5813(14)60006-2.

[157] D. Özçimen, F. Karaosmanoğlu, Production and characterization of bio-oil and biochar from rapeseed cake, Renew. Energy. 29 (2004) 779–787. https://doi.org/10.1016/j.renene.2003.09.006.

[158] P.J. Valdez, M.C. Nelson, H.Y. Wang, X.N. Lin, P.E. Savage, Hydrothermal liquefaction of Nannochloropsis sp.: Systematic study of process variables and analysis of the product fractions, Biomass and Bioenergy. 46 (2012) 317–331. https://doi.org/10.1016/j.biombioe.2012.08.009.

[159] Y. Yang, A. Gilbert, C. (Charles) Xu, Production of bio-crude from forestry waste by

hydro-liquefaction in sub-/super-critical methanol, AIChE J. 55 (2009) 807–819. https://doi.org/10.1002/aic.11701.

[160] S.C. Yim, A.T. Quitain, S. Yusup, M. Sasaki, Y. Uemura, T. Kida, Metal oxide-catalyzed hydrothermal liquefaction of Malaysian oil palm biomass to bio-oil under supercritical condition, J. Supercrit. Fluids. 120 (2017) 384–394. https://doi.org/10.1016/j.supflu.2016.05.044.

[161] X. Wang, X. an Xie, J. Sun, W. Liao, Effects of liquefaction parameters of cellulose in supercritical solvents of methanol, ethanol and acetone on products yield and compositions, Bioresour. Technol. 275 (2019) 123–129. https://doi.org/10.1016/j.biortech.2018.12.047.

[162] Y. Marcus, Extraction by subcritical and supercriticalwater, methanol, ethanol and their mixtures, Separations. 5 (2018). https://doi.org/10.3390/separations5010004.

[163] N. Simsek Kus, Organic reactions in subcritical and supercritical water, Tetrahedron. 68 (2012) 949–958. https://doi.org/10.1016/j.tet.2011.10.070.

[164] J. Yamazaki, E. Minami, S. Saka, Liquefaction of beech wood in various supercritical alcohols, J. Wood Sci. 52 (2006) 527–532. https://doi.org/10.1007/s10086-005-0798-4.

[165] T. Ogi, S.Y. Yokoyama, Liquid Fuel Production from Woody Biomass by Direct Liquefaction, Sekiyu Gakkaishi (Journal Japan Pet. Institute). 36 (1993) 73–84. https://doi.org/10.1627/jpi1958.36.73.

[166] E. Minami, S. Saka, Decomposition behavior of woody biomass in water-added supercritical methanol, J. Wood Sci. 51 (2005) 395–400. https://doi.org/10.1007/s10086-004-0670-y.

[167] H.L. Yan, Z.M. Zong, W.W. Zhu, Z.K. Li, Y.G. Wang, Z.H. Wei, Y. Li, X.Y. Wei, Poplar liquefaction in water/methanol cosolvents, Energy and Fuels. 29 (2015) 3104–3110. https://doi.org/10.1021/ef502518n.

[168] R. Singh, T. Bhaskar, B. Balagurumurthy, Effect of solvent on the hydrothermal liquefaction of macro algae Ulva fasciata, Process Saf. Environ. Prot. 93 (2015) 154–160. https://doi.org/10.1016/j.psep.2014.03.002.

[169] H. Durak, T. Aysu, Effects of catalysts and solvents on liquefaction of Onopordum heteracanthum for production of bio-oils, Bioresour. Technol. 166 (2014) 309–317. https://doi.org/10.1016/j.biortech.2014.05.051.

[170] Y. Chen, Y. Wu, P. Zhang, D. Hua, M. Yang, C. Li, Z. Chen, J. Liu, Direct liquefaction of Dunaliella tertiolecta for bio-oil in sub/supercritical ethanol-water, Bioresour. Technol. 124 (2012) 190–198. https://doi.org/10.1016/j.biortech.2012.08.013.

[171] S. Cheng, I. DCruz, M. Wang, M. Leitch, C. Xu, Highly efficient liquefaction of woody biomass in hot-compressed alcohol-water co-solvents, Energy and Fuels. 24 (2010) 4659–4667. https://doi.org/10.1021/ef901218w.

[172] Y. Wang, H. Wang, H. Lin, Y. Zheng, J. Zhao, A. Pelletier, K. Li, Effects of solvents and catalysts in liquefaction of pinewood sawdust for the production of bio-oils, Biomass and Bioenergy. 59 (2013) 158–167. https://doi.org/10.1016/j.biombioe.2013.10.022.

[173] X.F. Wu, J.J. Zhang, M.F. Li, J. Bian, F. Peng, Catalytic hydrothermal liquefaction of eucalyptus to prepare bio-oils and product properties, Energy Convers. Manag. 199 (2019) 111955. https://doi.org/10.1016/j.enconman.2019.111955.

[174] S. Nagappan, R.R. Bhosale, D.D. Nguyen, N.T.L. Chi, V.K. Ponnusamy, C.S. Woong, G. Kumar, Catalytic hydrothermal liquefaction of biomass into bio-oils and other value-added products – A review, Fuel. 285 (2021) 119053. https://doi.org/10.1016/j.fuel.2020.119053.

[175] T.O. Matsui, A. Nishihara, C. Ueda, M. Ohtsuki, N.O. Ikenaga, T. Suzuki, Liquefaction of micro-algae with iron catalyst, Fuel. 76 (1997) 1043–1048. https://doi.org/10.1016/S0016-2361(97)00120-8.

[176] A.B. Ross, P. Biller, M.L. Kubacki, H. Li, A. Lea-Langton, J.M. Jones, Hydrothermal processing of microalgae using alkali and organic acids, Fuel. 89 (2010) 2234–2243. https://doi.org/10.1016/j.fuel.2010.01.025.

[177] K.R. Arturi, S. Kucheryavskiy, E.G. Søgaard, Performance of hydrothermal liquefaction (HTL) of biomass by multivariate data analysis, Fuel Process. Technol. 150 (2016) 94–103. https://doi.org/10.1016/j.fuproc.2016.05.007.

[178] Z. Shuping, W. Yulong, Y. Mingde, I. Kaleem, L. Chun, J. Tong, Production and

characterization of bio-oil from hydrothermal liquefaction of microalgae Dunaliella tertiolecta cake, Energy. 35 (2010) 5406–5411. https://doi.org/10.1016/j.energy.2010.07.013.

[179] B. Zhang, Z. He, H. Chen, S. Kandasamy, Z. Xu, X. Hu, H. Guo, Effect of acidic, neutral and alkaline conditions on product distribution and biocrude oil chemistry from hydrothermal liquefaction of microalgae, Bioresour. Technol. 270 (2018) 129–137. https://doi.org/10.1016/j.biortech.2018.08.129.

[180] Z. Zhu, S.S. Toor, L. Rosendahl, D. Yu, G. Chen, Influence of alkali catalyst on product yield and properties via hydrothermal liquefaction of barley straw, Energy. 80 (2015) 284–292. https://doi.org/10.1016/j.energy.2014.11.071.

[181] H. Mazaheri, K.T. Lee, A.R. Mohamed, Influence of temperature on liquid products yield of oil palm shell via subcritical water liquefaction in the presence of alkali catalyst, Fuel Process. Technol. 110 (2013) 197–205. https://doi.org/10.1016/j.fuproc.2012.12.015.

[182] D. Castello, M.S. Haider, L.A. Rosendahl, Catalytic upgrading of hydrothermal liquefaction biocrudes: Different challenges for different feedstocks, Renew. Energy. 141 (2019) 420–430. https://doi.org/10.1016/j.renene.2019.04.003.

[183] K. Tekin, Hydrothermal conversion of Russian olive seeds into crude bio-oil using a CaO catalyst derived from waste mussel shells, Energy and Fuels. 29 (2015) 4382–4392. https://doi.org/10.1021/acs.energyfuels.5b00724.

[184] B. Meryemoğlu, A. Hasanoğlu, S. Irmak, O. Erbatur, Biofuel production by liquefaction of kenaf (Hibiscus cannabinus L.) biomass, Bioresour. Technol. 151 (2014) 278–283. https://doi.org/10.1016/j.biortech.2013.10.085.

[185] A. Dimitriadis, S. Bezergianni, Hydrothermal liquefaction of various biomass and waste feedstocks for biocrude production_ A state of the art review, Renew. Sustain. Energy Rev. 68 (2017) 113–125. https://doi.org/10.1016/j.rser.2016.09.120.

[186] B. Zhang, M. von Keitz, K. Valentas, Thermochemical liquefaction of high-diversity grassland perennials, J. Anal. Appl. Pyrolysis. 84 (2009) 18–24. https://doi.org/10.1016/j.jaap.2008.09.005.

[187] Z. He, D. Xu, S. Wang, H. Zhang, Z. Jing, Catalytic Upgrading of Water-Soluble

Biocrude from Hydrothermal Liquefaction of Chlorella, Energy and Fuels. 32 (2018) 1893–1899. https://doi.org/10.1021/acs.energyfuels.7b03823.

[188] L. Zhang, P. Champagne, C. (Charles) Xu, Bio-crude production from secondary pulp/paper-mill sludge and waste newspaper via co-liquefaction in hot-compressed water, Energy. 36 (2011) 2142–2150. https://doi.org/10.1016/j.energy.2010.05.029.

[189] M. Saber, A. Golzary, M. Hosseinpour, F. Takahashi, K. Yoshikawa, Catalytic hydrothermal liquefaction of microalgae using nanocatalyst, Appl. Energy. 183 (2016) 566–576. https://doi.org/10.1016/j.apenergy.2016.09.017.

[190] C. Zhou, X. Zhu, F. Qian, W. Shen, H. Xu, S. Zhang, J. Chen, Catalytic hydrothermal liquefaction of rice straw in water/ethanol mixtures for high yields of monomeric phenols using reductive CuZnAl catalyst, Fuel Process. Technol. 154 (2016) 1–6. https://doi.org/10.1016/j.fuproc.2016.08.010.

[191] T. Xu, Q. Zhang, J. Cen, Y. Xiang, X. Li, Selectivity tailoring of Pd/CNTs in phenol hydrogenation by surface modification: Role of CO oxygen species, Appl. Surf. Sci. 324 (2015) 634–639. https://doi.org/10.1016/j.apsusc.2014.10.165.

[192] T.M. Brown, P. Duan, P.E. Savage, Hydrothermal Liquefaction and Gasification of Nannochloropsis sp., Energy & Fuels. 24 (2010) 3639–3646. https://doi.org/10.1021/ef100203u.

[193] U. Jena, K.C. Das, Comparative evaluation of thermochemical liquefaction and pyrolysis for bio-oil production from microalgae, Energy and Fuels. 25 (2011) 5472–5482. https://doi.org/10.1021/ef201373m.

[194] L.G. Alba, C. Torri, C. Samorì, J. Van Der Spek, D. Fabbri, S.R.A. Kersten, D.W.F.W. Brilman, Hydrothermal Treatment (HTT) of Microalgae : Evaluation of the Process As Conversion Method in an Algae Biorefinery Concept, (2012) 642–657.

[195] S. Karagöz, T. Bhaskar, A. Muto, Y. Sakata, M.A. Uddin, Low-temperature hydrothermal treatment of biomass: Effect of reaction parameters on products and boiling point distributions, Energy and Fuels. 18 (2004) 234–241. https://doi.org/10.1021/ef030133g.

[196] T.H. Pedersen, C.U. Jensen, L. Sandström, L.A. Rosendahl, Full characterization of compounds obtained from fractional distillation and upgrading of a HTL biocrude,

Appl. Energy. 202 (2017) 408–419. https://doi.org/10.1016/j.apenergy.2017.05.167.

[197] K.F. Tzanetis, J.A. Posada, A. Ramirez, Analysis of biomass hydrothermal liquefaction and biocrude-oil upgrading for renewable jet fuel production : The impact of reaction conditions on production costs and GHG emissions performance, Renew. Energy. 113 (2017) 1388–1398. https://doi.org/10.1016/j.renene.2017.06.104.

[198] M. Wang, C. (Charles) Xu, M. Leitch, Liquefaction of cornstalk in hot-compressed phenol-water medium to phenolic feedstock for the synthesis of phenol-formaldehyde resin, Bioresour. Technol. 100 (2009) 2305–2307. https://doi.org/10.1016/j.biortech.2008.10.043.

[199] E. Panisko, T. Wietsma, T. Lemmon, K. Albrecht, D. Howe, Characterization of the aqueous fractions from hydrotreatment and hydrothermal liquefaction of lignocellulosic feedstocks, Biomass and Bioenergy. 74 (2015) 162–171. https://doi.org/10.1016/j.biombioe.2015.01.011.

[200] Z. Zhu, L. Rosendahl, S.S. Toor, D. Yu, G. Chen, Hydrothermal liquefaction of barley straw to bio-crude oil: Effects of reaction temperature and aqueous phase recirculation, Appl. Energy. 137 (2015) 183–192. https://doi.org/10.1016/j.apenergy.2014.10.005.

[201] Y. Tian, F. Wang, J.O. Djandja, S.L. Zhang, Y.P. Xu, P.G. Duan, Hydrothermal liquefaction of crop straws: Effect of feedstock composition, Fuel. 265 (2020). https://doi.org/10.1016/j.fuel.2019.116946.

[202] P. Biller, R.B. Madsen, M. Klemmer, J. Becker, B.B. Iversen, M. Glasius, Effect of hydrothermal liquefaction aqueous phase recycling on bio-crude yields and composition, Bioresour. Technol. 220 (2016) 190–199. https://doi.org/10.1016/j.biortech.2016.08.053.

[203] Y. Miyata, K. Sagata, Y. Yamazaki, H. Teramura, Y. Hirano, C. Ogino, Y. Kita, Mechanism of the Fe-Assisted Hydrothermal Liquefaction of Lignocellulosic Biomass, Ind. Eng. Chem. Res. 57 (2018) 14870–14877. https://doi.org/10.1021/acs.iecr.8b03725.

[204] N. Neveux, A.K.L. Yuen, C. Jazrawi, M. Magnusson, B.S. Haynes, A.F. Masters, A. Montoya, N.A. Paul, T. Maschmeyer, R. de Nys, Biocrude yield and productivity from the hydrothermal liquefaction of marine and freshwater green macroalgae, Bioresour.

Technol. 155 (2014) 334–341. https://doi.org/10.1016/j.biortech.2013.12.083.

[205] D.C. Elliott, L.J. Sealock, Aqueous Catalyst Systems for the Water-Gas Shift Reaction. 1. Comparative Catalyst Studies, Ind. Eng. Chem. Prod. Res. Dev. 22 (1983) 426–431. https://doi.org/10.1021/i300011a008.

[206] Y. Chen, X. Cao, S. Zhu, F. Tian, Y. Xu, C. Zhu, L. Dong, Synergistic hydrothermal liquefaction of wheat stalk with homogeneous and heterogeneous catalyst at low temperature, Bioresour. Technol. 278 (2019) 92–98. https://doi.org/10.1016/j.biortech.2019.01.076.

[207] Z. Liu, F.S. Zhang, Removal of lead from water using biochars prepared from hydrothermal liquefaction of biomass, J. Hazard. Mater. 167 (2009) 933–939. https://doi.org/10.1016/j.jhazmat.2009.01.085.

[208] L.P. Xiao, Z.J. Shi, F. Xu, R.C. Sun, Hydrothermal carbonization of lignocellulosic biomass, Bioresour. Technol. 118 (2012) 619–623. https://doi.org/10.1016/j.biortech.2012.05.060.

[209] U. Jena, K.C. Das, J.R. Kastner, Effect of operating conditions of thermochemical liquefaction on biocrude production from Spirulina platensis, Bioresour. Technol. 102 (2011) 6221–6229. https://doi.org/10.1016/j.biortech.2011.02.057.

[210] A. Demirbaş, Effect of lignin content on aqueous liquefaction products of biomass, Energy Convers. Manag. 41 (2000) 1601–1607. https://doi.org/10.1016/S0196-8904(00)00013-3.

[211] Z. Liu, A. Quek, S. Kent Hoekman, R. Balasubramanian, Production of solid biochar fuel from waste biomass by hydrothermal carbonization, Fuel. 103 (2013) 943–949. https://doi.org/10.1016/j.fuel.2012.07.069.

[212] S. Baronti, G. Alberti, F. Camin, I. Criscuoli, L. Genesio, R. Mass, F.P. Vaccari, L. Ziller, F. Miglietta, Hydrochar enhances growth of poplar for bioenergy while marginally contributing to direct soil carbon sequestration, GCB Bioenergy. 9 (2017) 1618–1626. https://doi.org/10.1111/gcbb.12450.

[213] D. Kalderis, G. Papameletiou, B. Kayan, Assessment of Orange Peel Hydrochar as a Soil Amendment: Impact on Clay Soil Physical Properties and Potential Phytotoxicity, Waste and Biomass Valorization. 10 (2019) 3471–3484.

https://doi.org/10.1007/s12649-018-0364-0.

[214] Anthony V. Bridgwater, Biomass Fast Pyrolysis, Bioresour. Technol. 85 (2004) 21–49. http://www.ncbi.nlm.nih.gov/pubmed/21232946.

[215] S. Gupta, H.D. Kawale, G. Ahmed, S. Acharya, N. Kishore, Effect of temperature on catalytic pyrolysis of Polyalthia Longifolia leaves solid waste and characterization of their products, Curr. Res. Green Sustain. Chem. 4 (2021) 100062. https://doi.org/10.1016/j.crgsc.2021.100062.

[216] ASTM E871-82 (2019) Standard test method for moisture analysis of particulate wood fuels. ASTM International, Pennsylvania. https:// doi. org/ 10. 1520/ E0871- 82R19

[217] ASTM E0872-82 (2019) Standard test method for volatile matter in the analysis of coal particulate wood fuels. ASTM Interna- tional, Pennsylvania. https:// doi. org/ 10. 1520/ E0872- 82R19

[218] ASTM D1102-84 (2021) Standard test method for ash in wood. ASTM International, Pennsylvania. https:// doi. org/ 10. 1520/ D1102- 84R21

[219] C.J. Napier, R.O. Mabokela, K.L. King, Apartheid No More: Case Studies of Southern African Universities in the Process of Transformation, Can. J. African Stud. / Rev. Can. Des Études Africaines. 36 (2002) 159. https://doi.org/10.2307/4107413.

[220] C.G. Lee, C. Choi, J.C. Yoo, H.J. Kim, S.M. Yang, S.G. Kang, The combustion characteristics of self-igniting briquettes prepared with torrefied wood powder from a wood-roasting method, BioResources. 11 (2016) 9803–9810. https://doi.org/10.15376/biores.11.4.9803-9810.

[221] M.K. Jindal, M.K. Jha, Effect of process parameters on hydrothermal liquefaction of waste furniture sawdust for bio-oil production, RSC Adv. 6 (2016) 41772–41780. https://doi.org/10.1039/c6ra02868c.

[222] R. Li, B. Li, T. Yang, X. Kai, W. Wang, Y. Jie, Y. Zhang, G. Chen, Sub-supercritical liquefaction of rice stalk for the production of bio-oil: Effect of solvents, Bioresour. Technol. 198 (2015) 94–100. https://doi.org/10.1016/j.biortech.2015.08.088.

[223] B. Zhao, H. Wang, S. Xu, L. Qian, H. Li, J. Gao, G. Zhao, M.B. Ray, C.C. Xu, Influence of extraction solvents on the recovery yields and properties of bio-oils from woody

biomass liquefaction in sub-critical water, ethanol or water–ethanol mixed solvent, Fuel. 307 (2022) 121930. https://doi.org/10.1016/j.fuel.2021.121930.

[224] J. Zhang, W.T. Chen, P. Zhang, Z. Luo, Y. Zhang, Hydrothermal liquefaction of Chlorella pyrenoidosa in sub- and supercritical ethanol with heterogeneous catalysts, Bioresour. Technol. 133 (2013) 389–397. https://doi.org/10.1016/j.biortech.2013.01.076.

[225] G. Yu, Y. Zhang, L. Schideman, T. Funk, Z. Wang, Distributions of carbon and nitrogen in the products from hydrothermal liquefaction of low-lipid microalgae, Energy Environ. Sci. 4 (2011) 4587–4595. https://doi.org/10.1039/c1ee01541a.

[226] A. Mehrabadi, R. Craggs, M.M. Farid, Wastewater treatment high rate algal pond biomass for bio-crude oil production, Bioresour. Technol. 224 (2017) 255–264. https://doi.org/10.1016/j.biortech.2016.10.082.

[227] L.C. Cardenas Velandia, A.E. Fontaine, D. Loquet, R. Checa, C. Lorentz, B. Bujoli, N. Guilhaume, C. Geantet, E. Chailleux, C. Queffélec, D. Laurenti, Catalytic hydrothermal conversion of algal residue to bio-bitumen, J. Clean. Prod. 322 (2021). https://doi.org/10.1016/j.jclepro.2021.129024.

[228] B. Zhao, H. Wang, S. Xu, L. Qian, H. Li, J. Gao, G. Zhao, M.B. Ray, C.C. Xu, Influence of extraction solvents on the recovery yields and properties of bio-oils from woody biomass liquefaction in sub-critical water, ethanol or water–ethanol mixed solvent, Fuel. 307 (2022) 121930. https://doi.org/10.1016/j.fuel.2021.121930.

[229] A. V. Bridgwater, Review of fast pyrolysis of biomass and product upgrading, Biomass and Bioenergy. 38 (2012) 68–94. https://doi.org/10.1016/j.biombioe.2011.01.048.

[230] Rotavapor® R-300 Operation Manual, (2017). https://assets.fishersci.com/TFS-Assets/CCG/Buchi-Corporation/manuals/R-300_OM.pdf

[231] D.A. Granados, H.I. Velásquez, F. Chejne, Energetic and exergetic evaluation of residual biomass in a torrefaction process, Energy. 74 (2014) 181–189. https://doi.org/10.1016/j.energy.2014.05.046.

[232] Y. Leng, Related Titles Characterization of Surfaces and Nanostructures Basic Concepts of X-Ray Diffraction Characterization of Solid Materials and Heterogeneous Catalysts Advanced Characterization Techniques for Thin Film Solar Cells

Characterization Techniques f, 2013.

[233] J.J.A. Lozeman, P. Führer, W. Olthuis, M. Odijk, Spectroelectrochemistry, the future of visualizing electrode processes by hyphenating electrochemistry with spectroscopic techniques, Analyst. 145 (2020) 2482–2509. https://doi.org/10.1039/c9an02105a.

[234] N.M. Resonance, 14 14.1, (n.d.) 494–537. https://icvcollege.edu.in/sites/default/files/Nuclear%20Magnetic%20Resonance.pdf

[235] N.J. Rankin, D. Preiss, P. Welsh, K.E.V. Burgess, S.M. Nelson, D.A. Lawlor, N. Sattar, The emergence of proton nuclear magnetic resonance metabolomics in the cardiovascular arena as viewed from a clinical perspective, Atherosclerosis. 237 (2014) 287–300. https://doi.org/10.1016/j.atherosclerosis.2014.09.024.

[236] Perkin Elmer, Clarus 600/560 D GC/MS Tutorial, (2007). https://resources.perkinelmer.com/corporate/cmsresources/images/44-74535gde_clarus600560dgcmstutorial.pdf

[237] T. Surface, S. Society, Compendium of Surface and Interface Analysis, 2018. https://doi.org/10.1007/978-981-10-6156-1.

[238] N. Joudeh, D. Linke, Nanoparticle classification, physicochemical properties, characterization, and applications: a comprehensive review for biologists, J. Nanobiotechnology. 20 (2022) 1–29. https://doi.org/10.1186/s12951-022-01477-8.

[239] M. Abunowara, M.A. Bustam, S. Sufian, M. Babar, U. Eldemerdash, H. Suleman, R. Bencini, S. Ullah, Characterization of Mukah-Balingian and Merit-Pila Coals before and after Subcritical CO 2 Exposure Using Surface-Area Techniques , J. Environ. Eng. 146 (2020) 1–15. https://doi.org/10.1061/(asce)ee.1943-7870.0001761.

[240] Characterization of porous solids and powders: surface area, pore size, and density, 2005. https://doi.org/10.5860/choice.42-5288.

[241] P.D. Pathak, S.A. Mandavgane, B.D. Kulkarni, Fruit peel waste: Characterization and its potential uses, Curr. Sci. 113 (2017) 444–454. https://doi.org/10.18520/cs/v113/i03/444-454.

[242] A.C. Gowman, M.C. Picard, A. Rodriguez-Uribe, M. Misra, H. Khalil, M. Thimmanagari, A.K. Mohanty, Physicochemical analysis of Apple and Grape

Pomaces, BioResources. 14 (2019) 3210–3230. https://doi.org/10.15376/biores.14.2.3210-3230.

[243] H.D. Kawale, N. Kishore, Pyrolysis of Delonix Regia and Characterization of Its Pyrolytic Products: Effect of Pyrolysis Temperature, J. Energy Resour. Technol. Trans. ASME. 142 (2020). https://doi.org/10.1115/1.4046226.

[244] S. Gupta, N. Kishore, G. Ahmed, K. Kumari, Catalytic co-pyrolysis of leaves of Polyalthia longifolia, woods of Delonix regia and polypropylene grocery bags using zeolite Y-hydrogen catalyst, Biomass Convers. Biorefinery. (2023). https://doi.org/10.1007/s13399-022-03731-3.

[245] S. Acharya, N. Kishore, Hydro-liquefaction of Lemna minor (Duckweed) with hydrogen-donor solvent at varying hydrogen pressures, Int. J. Sustain. Energy. 41 (2022) 2169–2184. https://doi.org/10.1080/14786451.2022.2140157.

[246] Y. Lei, H. Su, F. Tian, A Novel Nitrogen Enriched Hydrochar Adsorbents Derived from Salix Biomass for Cr (VI) Adsorption, Sci. Rep. 8 (2018) 1–9. https://doi.org/10.1038/s41598-018-21238-8.

[247] J.A. Ramirez, R.J. Brown, T.J. Rainey, A review of hydrothermal liquefaction bio-crude properties and prospects for upgrading to transportation fuels, Energies. 8 (2015) 6765–6794. https://doi.org/10.3390/en8076765.

[248] Q. Li, D. Liu, L. Song, P. Wu, Z. Yan, M. Li, Investigation of solvent effect on the hydro-liquefaction of sawdust: An innovative reference approach using tetralin as chemical probe, Fuel. 164 (2016) 94–98. https://doi.org/10.1016/j.fuel.2015.09.076.

[249] G. Ahmed, N. Kishore, Fuel phase extraction from pyrolytic liquid of Azadirachta indica biomass followed by subsequent characterization of pyrolysis products, Renew. Energy. (2023) 119460. https://doi.org/10.1016/j.renene.2023.119460.

[250] R. Li, Z. Ma, T. Yang, B. Li, L. Wei, Y. Sun, Sub–supercritical liquefaction of municipal wet sewage sludge to produce bio-oil: Effect of different organic–water mixed solvents, J. Supercrit. Fluids. 138 (2018) 115–123. https://doi.org/10.1016/j.supflu.2018.04.011.

[251] S. Mishra, K. Mohanty, Co-HTL of domestic sewage sludge and wastewater treatment derived microalgal biomass – An integrated biorefinery approach for sustainable

biocrude production, Energy Convers. Manag. 204 (2020) 112312. https://doi.org/10.1016/j.enconman.2019.112312.

[252] B. Zhang, H. Feng, Z. He, S. Wang, H. Chen, Bio-oil production from hydrothermal liquefaction of ultrasonic pre-treated Spirulina platensis, Energy Convers. Manag. 159 (2018) 204–212. https://doi.org/10.1016/j.enconman.2017.12.100.

[253] R. Li, B. Li, X. Kai, T. Yang, Hydro-liquefaction of rice stalk in supercritical ethanol with in situ generated hydrogen, Fuel Process. Technol. 167 (2017) 363–370. https://doi.org/10.1016/j.fuproc.2017.07.013.

[254] Z. Bi, J. Zhang, E. Peterson, Z. Zhu, C. Xia, Y. Liang, T. Wiltowski, Biocrude from pretreated sorghum bagasse through catalytic hydrothermal liquefaction, Fuel. 188 (2017) 112–120. https://doi.org/10.1016/j.fuel.2016.10.039.

[255] A. Gollakota, P.E. Savage, Hydrothermal Liquefaction of Model Food Waste Biomolecules and Ternary Mixtures under Isothermal and Fast Conditions, ACS Sustain. Chem. Eng. 6 (2018) 9018–9027. https://doi.org/10.1021/acssuschemeng.8b01368.

[256] D. Liu, Q. Li, A. Zhao, L. Song, P. Wu, Z. Yan, Hydro-liquefaction of sawdust and its three components in supercritical ethanol with [BMIM]Cl/NiCl2 catalyst, Chem. Eng. J. 279 (2015) 921–928. https://doi.org/10.1016/j.cej.2015.05.052.

[257] S. Koley, M.S. Khadase, T. Mathimani, H. Raheman, N. Mallick, Catalytic and non-catalytic hydrothermal processing of Scenedesmus obliquus biomass for bio-crude production – A sustainable energy perspective, Energy Convers. Manag. 163 (2018) 111–121. https://doi.org/10.1016/j.enconman.2018.02.052.

[258] W.H. Chen, Y.Y. Lin, H.C. Liu, T.C. Chen, C.H. Hung, C.H. Chen, H.C. Ong, A comprehensive analysis of food waste derived liquefaction bio-oil properties for industrial application, Appl. Energy. 237 (2019) 283–291. https://doi.org/10.1016/j.apenergy.2018.12.084.

[259] H.D. Kawale, N. Kishore, Comparative study on pyrolysis of Delonix Regia, Pinewood sawdust and their co-feed for plausible bio-fuels production, Energy. 203 (2020) 117921. https://doi.org/10.1016/j.energy.2020.117921.

[260] S. Gupta, H.D. Kawale, G. Ahmed, S. Acharya, N. Kishore, Effect of temperature on

catalytic pyrolysis of Polyalthia Longifolia leaves solid waste and characterization of their products, Curr. Res. Green Sustain. Chem. 4 (2021) 100062. https://doi.org/10.1016/j.crgsc.2021.100062.

[261] C.A. Mullen, G.D. Strahan, A.A. Boateng, Characterization of various fast-pyrolysis bio-oils by NMR spectroscopy, Energy and Fuels. 23 (2009) 2707–2718. https://doi.org/10.1021/ef801048b.

[262] H.D. Kawale, N. Kishore, Thermochemical putrefaction of Delonix regia biomass and tube waste to produce high-quality pyrolytic bio-oil, J. Therm. Anal. Calorim. (2021). https://doi.org/10.1007/s10973-021-10725-2.

[263] S. Masoumi, P.E. Boahene, A.K. Dalai, Biocrude oil and hydrochar production and characterization obtained from hydrothermal liquefaction of microalgae in methanol-water system, Energy. 217 (2021) 119344. https://doi.org/10.1016/j.energy.2020.119344.

[264] Z. qian Pan, H. jun Huang, C. fei Zhou, X. feng Xiao, X. wu He, F. ying Lai, J. bo Xiong, Highly efficient conversion of camphor tree sawdust into bio-oil and biochar products by liquefaction in ethanol-water cosolvent, J. Anal. Appl. Pyrolysis. 136 (2018) 186–198. https://doi.org/10.1016/j.jaap.2018.10.006.

[265] N. Hassan, R. Abdullah, T. Khadiran, P. Elham, P. Vejan, Biochar derived from oil palm trunk as a potential precursor in the production of high-performance activated carbon, Biomass Convers. Biorefinery. (2021). https://doi.org/10.1007/s13399-021-01797-z.

[266] X. Xiong, I.K.M. Yu, L. Cao, D.C.W. Tsang, S. Zhang, Y.S. Ok, A review of biochar-based catalysts for chemical synthesis, biofuel production, and pollution control, Bioresour. Technol. 246 (2017) 254–270. https://doi.org/10.1016/j.biortech.2017.06.163.

[267] Y. Shen, J.L. Linville, M. Urgun-Demirtas, R.P. Schoene, S.W. Snyder, Producing pipeline-quality biomethane via anaerobic digestion of sludge amended with corn stover biochar with in-situ CO2 removal, Appl. Energy. 158 (2015) 300–309. https://doi.org/10.1016/j.apenergy.2015.08.016.

[268] N. Mosier, C. Wyman, B. Dale, R. Elander, Y.Y. Lee, M. Holtzapple, M. Ladisch,

Features of promising technologies for pretreatment of lignocellulosic biomass, Bioresour. Technol. 96 (2005) 673–686. https://doi.org/10.1016/j.biortech.2004.06.025.

[269] W. Wu, M. Yang, Q. Feng, K. McGrouther, H. Wang, H. Lu, Y. Chen, Chemical characterization of rice straw-derived biochar for soil amendment, Biomass and Bioenergy. 47 (2012) 268–276. https://doi.org/10.1016/j.biombioe.2012.09.034.

[270] M. Keiluweit, P.S. Nico, M. Johnson, M. Kleber, Dynamic molecular structure of plant biomass-derived black carbon (biochar), Environ. Sci. Technol. 44 (2010) 1247–1253. https://doi.org/10.1021/es9031419.

[271] A. Oya, S. Otani, Influences of particle size of metal on catalytic graphitization of non-graphitizing carbons, Carbon N. Y. 19 (1981) 391–400. https://doi.org/10.1016/0008-6223(81)90064-6.

[272] H.D. Kawale, N. Kishore, Production of hydrocarbons from a green algae (Oscillatoria)with exploration of its fuel characteristics over different reaction atmospheres, Energy. 178 (2019) 344–355. https://doi.org/10.1016/j.energy.2019.04.103.

[273] S. Nizamuddin, H.A. Baloch, N.M. Mubarak, S. Riaz, M.T.H. Siddiqui, P. Takkalkar, M.M. Tunio, S. Mazari, A.W. Bhutto, Solvothermal Liquefaction of Corn Stalk: Physico-Chemical Properties of Bio-oil and Biochar, Waste and Biomass Valorization. 10 (2019) 1957–1968. https://doi.org/10.1007/s12649-018-0206-0.

[274] R. Kaur, P. Gera, M.K. Jha, T. Bhaskar, Reaction parameters effect on hydrothermal liquefaction of castor (Ricinus Communis)residue for energy and valuable hydrocarbons recovery, Renew. Energy. 141 (2019) 1026–1041. https://doi.org/10.1016/j.renene.2019.04.064.

[275] S. Acharya, N. Kishore, Citrus limetta fruit waste management by liquefaction using hydrogen-donor solvent, RSC Adv. 12 (2022) 32708–32721. https://doi.org/10.1039/D2RA06085J.

[276] J. Fang, Z. Liu, H. Luan, F. Liu, X. Yuan, S. Long, A. Wang, Y. Ma, Z. Xiao, Thermochemical liquefaction of cattle manure using ethanol as solvent: Effects of temperature on bio-oil yields and chemical compositions, Renew. Energy. 167 (2021)

32–41. https://doi.org/10.1016/j.renene.2020.11.033.

[277] M. Wądrzyk, Ł. Korzeniowski, M. Plata, R. Janus, M. Lewandowski, G. Borówka, P. Maziarka, Solvothermal Liquefaction of Blackcurrant Pomace in the Water-Monohydroxy Alcohol Solvent System, Energies. 16 (2023) 1127. https://doi.org/10.3390/en16031127.

[278] S. Acharya, N. Kishore, Solvothermal co-liquefaction of wastes from Citrus limetta fruit processing, J. Chem. Technol. Biotechnol. 98 (2023) 1114–1124. https://doi.org/10.1002/jctb.7316.

[279] D.R. Vardon, B.K. Sharma, J. Scott, G. Yu, Z. Wang, L. Schideman, Y. Zhang, T.J. Strathmann, Chemical properties of biocrude oil from the hydrothermal liquefaction of Spirulina algae, swine manure, and digested anaerobic sludge, Bioresour. Technol. 102 (2011) 8295–8303. https://doi.org/10.1016/j.biortech.2011.06.041.

[280] S.V. Aravind, G. Ahmed, N. Kishore, Pyrolysis of Delonix regia using metal oxide catalysts and solvent effect on fuel fraction of bio-oil, Results Eng. 17 (2023) 100876. https://doi.org/10.1016/j.rineng.2023.100876.

[281] P. Biller, A.B. Ross, Potential yields and properties of oil from the hydrothermal liquefaction of microalgae with different biochemical content, Bioresour. Technol. 102 (2011) 215–225. https://doi.org/10.1016/j.biortech.2010.06.028.

[282] P. Duan, P.E. Savage, Hydrothermal liquefaction of a microalga with heterogeneous catalysts, Ind. Eng. Chem. Res. 50 (2011) 52–61. https://doi.org/10.1021/ie100758s.

[283] B. Biswas, Y. Bisht, J. Kumar, S.R. Yenumala, T. Bhaskar, Effects of temperature and solvent on hydrothermal liquefaction of the corncob for production of phenolic monomers, Biomass Convers. Biorefinery. 12 (2022) 91–101. https://doi.org/10.1007/s13399-020-01012-5.

[284] B. Biswas, A. Arun Kumar, Y. Bisht, B.B. Krishna, J. Kumar, T. Bhaskar, Role of temperatures and solvents on hydrothermal liquefaction of Azolla filiculoides, Energy. 217 (2021) 119330. https://doi.org/10.1016/j.energy.2020.119330.

[285] P.J. Arauzo, P.A. Maziarka, K.A. Schoder, J. Pfersich, F. Ronsse, A. Kruse, Influence of sequential HTC pre-treatment and pyrolysis on wet food-industry wastes: Optimisation toward nitrogen-rich hierarchical carbonaceous materials intended for use

in energy storage solutions, Sci. Total Environ. 816 (2022) 151648. https://doi.org/10.1016/j.scitotenv.2021.151648.

[286] Y. Chen, Y. Wu, D. Hua, C. Li, M.P. Harold, J. Wang, M. Yang, Thermochemical conversion of low-lipid microalgae for the production of liquid fuels: Challenges and opportunities, RSC Adv. 5 (2015) 18673–18701. https://doi.org/10.1039/c4ra13359e.

[287] M.P. Olszewski, P.J. Arauzo, M. Wądrzyk, A. Kruse, Py-GC-MS of hydrochars produced from brewer's spent grains, J. Anal. Appl. Pyrolysis. 140 (2019) 255–263. https://doi.org/10.1016/j.jaap.2019.04.002.

[288] B. Biswas, D. Sahoo, R.K. Sukumaran, B.B. Krishna, J. Kumar, Y.S. Reddy, V.P. Adarsh, A. Puthiyamadam, K.K. Mallapureddy, S.B. Ummalyma, T. Bhaskar, Co-hydrothermal liquefaction of phumdi and paragrass an aquatic biomass: Characterization of bio-oil, aqueous fraction and solid residue, J. Energy Inst. 102 (2022) 247–255. https://doi.org/10.1016/j.joei.2022.03.013.

[289] J. Nallasivam, B.E. Eboibi, A. Isdepsky, M. Lavanya, S. Bhaskar, S. Chinnasamy, Hydrothermal liquefaction of water hyacinth (Eichhornia crassipes): influence of reaction temperature on product yield, carbon and energy recovery, and hydrocarbon species distribution in biocrude, Biomass Convers. Biorefinery. 12 (2022) 3827–3841. https://doi.org/10.1007/s13399-020-01032-1.

[290] T. Khadiran, M.Z. Hussein, Z. Zainal, R. Rusli, Textural and chemical properties of activated carbon prepared from tropical peat soil by chemical activation method, BioResources. 10 (2015) 986–1007. https://doi.org/10.15376/biores.10.1.986-1007.

[291] J. Chen, S. Li, Characterization of biofuel production from hydrothermal treatment of hyperaccumulator waste (Pteris vittata L.) in sub- And supercritical water, RSC Adv. 10 (2020) 2160–2169. https://doi.org/10.1039/c9ra09410e.

[292] Z. Wu, F. Wang, L. Hu, Y. Jiang, X. Wang, J. Xu, Directional liquefaction of lignocellulose in 1,4-dioxane–ethanol–formic acid co-solvents, J. Chem. Technol. Biotechnol. 96 (2021) 971–979. https://doi.org/10.1002/jctb.6606.

[293] Z. Wang, J. Cao, J. Wang, Pyrolytic characteristics of pine wood in a slowly heating and gas sweeping fixed-bed reactor, J. Anal. Appl. Pyrolysis. 84 (2009) 179–184. https://doi.org/10.1016/j.jaap.2009.02.001.

[294] A.R.A. Usman, A. Abduljabbar, M. Vithanage, Y.S. Ok, M. Ahmad, M. Ahmad, J. Elfaki, S.S. Abdulazeem, M.I. Al-Wabel, Biochar production from date palm waste: Charring temperature induced changes in composition and surface chemistry, J. Anal. Appl. Pyrolysis. 115 (2015) 392–400. https://doi.org/10.1016/j.jaap.2015.08.016.

[295] L.J. Leng, X.Z. Yuan, H.J. Huang, H. Wang, Z. Bin Wu, L.H. Fu, X. Peng, X.H. Chen, G.M. Zeng, Characterization and application of bio-chars from liquefaction of microalgae, lignocellulosic biomass and sewage sludge, Fuel Process. Technol. 129 (2015) 8–14. https://doi.org/10.1016/j.fuproc.2014.08.016.

[296] J.M. Jabar, Y.A. Odusote, Y.T. Ayinde, M. Yılmaz, African almond (Terminalia catappa L) leaves biochar prepared through pyrolysis using H3PO4 as chemical activator for sequestration of methylene blue dye, Results Eng. 14 (2022) 100385. https://doi.org/10.1016/j.rineng.2022.100385.

[297] S.M. Yakout, G. Sharaf El-Deen, Characterization of activated carbon prepared by phosphoric acid activation of olive stones, Arab. J. Chem. 9 (2016) S1155–S1162. https://doi.org/10.1016/j.arabjc.2011.12.002.

[298] A.H. Jawad, M.H. Sauodi, M.S. Mastuli, M.A. Aouda, K.A. Radzun, Pomegranate peels collected from fresh juice shop as a renewable precursor for high surface area activated carbon with potential application for methylene blue adsorption, Desalin. Water Treat. 124 (2018) 287–296. https://doi.org/10.5004/dwt.2018.22725.

[299] L. Leng, X. Yuan, G. Zeng, J. Shao, X. Chen, Z. Wu, H. Wang, X. Peng, Surface characterization of rice husk bio-char produced by liquefaction and application for cationic dye (Malachite green) adsorption, Fuel. 155 (2015) 77–85. https://doi.org/10.1016/j.fuel.2015.04.019.

[300] L. Leng, X. Yuan, H. Huang, J. Shao, H. Wang, X. Chen, G. Zeng, Bio-char derived from sewage sludge by liquefaction: Characterization and application for dye adsorption, Appl. Surf. Sci. 346 (2015) 223–231. https://doi.org/10.1016/j.apsusc.2015.04.014.

[301] X. Zhu, Y. Liu, C. Zhou, G. Luo, S. Zhang, J. Chen, A novel porous carbon derived from hydrothermal carbon for efficient adsorption of tetracycline, Carbon N. Y. 77 (2014) 627–636. https://doi.org/10.1016/j.carbon.2014.05.067.

[302] K. Sharma, A.A. Shah, S.S. Toor, T.H. Seehar, T.H. Pedersen, L.A. Rosendahl, Co-Hydrothermal Liquefaction of Lignocellulosic Biomass in Supercritical Water, Energies. 14 (2021) 1708. https://doi.org/10.3390/en14061708.

[303] A. Sahoo, K. Saini, M. Jindal, T. Bhaskar, K.K. Pant, Co-Hydrothermal Liquefaction of algal and lignocellulosic biomass: Status and perspectives, Bioresour. Technol. 342 (2021) 125948. https://doi.org/10.1016/j.biortech.2021.125948.

[304] O.M. Adedeji, J.S. Russack, L.A. Molnar, S.K. Bauer, Co-Hydrothermal Liquefaction of Sewage Sludge and Beverage Waste for High-Quality Bio-energy Production, Fuel. 324 (2022) 124757. https://doi.org/10.1016/j.fuel.2022.124757.

[305] J. Wang, X. Peng, X. Chen, X. Ma, Co-liquefaction of low-lipid microalgae and starch-rich biomass waste: The interaction effect on product distribution and composition, J. Anal. Appl. Pyrolysis. 139 (2019) 250–257. https://doi.org/10.1016/j.jaap.2019.02.013.

[306] L. Yang, Q. (Sophia) He, P. Havard, K. Corscadden, C. (Charles) Xu, X. Wang, Co-liquefaction of spent coffee grounds and lignocellulosic feedstocks, Bioresour. Technol. 237 (2017) 108–121. https://doi.org/10.1016/j.biortech.2017.02.087.

[307] B. Biswas, A. Kumar, R. Kaur, B.B. Krishna, T. Bhaskar, Co-hydrothermal Liquefaction of Lignin and Macroalgae: Effect of Process Parameters on Product Distribution, BioEnergy Res. 16 (2023) 33–44. https://doi.org/10.1007/s12155-022-10437-x.

[308] Y. Hu, S. Wang, J. Li, Q. Wang, Z. He, Y. Feng, A.E.F. Abomohra, S. Afonaa-Mensah, C. Hui, Co-pyrolysis and co-hydrothermal liquefaction of seaweeds and rice husk: Comparative study towards enhanced biofuel production, J. Anal. Appl. Pyrolysis. 129 (2018) 162–170. https://doi.org/10.1016/j.jaap.2017.11.016.

[309] A. Shakya, A. Núñez-Delgado, T. Agarwal, Biochar synthesis from sweet lime peel for hexavalent chromium remediation from aqueous solution, J. Environ. Manage. 251 (2019) 109570. https://doi.org/10.1016/j.jenvman.2019.109570.

[310] K.S.W. Sing, Reporting physisorption data for gas/solid systems with special reference to the determination of surface area and porosity (Recommendations 1984), Pure Appl. Chem. 57 (1985) 603–619. https://doi.org/10.1351/pac198557040603.

[311] N. Kishore, S. Sachan, K.N. Rai, A. Kumar, Synthesis and characterization of a nanofiltration carbon membrane derived from phenol-formaldehyde resin, Carbon N. Y. 41 (2003) 2961–2972. https://doi.org/10.1016/S0008-6223(03)00427-5.

[312] R.K. Opu, M.R. Hossain, M.S.H. Monir, R.H. Shanto, M.S. Osman, Co-Liquefaction of Faecal Sludge and Water Hyacinth: Exploring the Fuel Characteristics of Biocrude Including Thermal Maturation and Petroleum Fractionation, SSRN Electron. J. 173 (2022) 106785. https://doi.org/10.2139/ssrn.4291501.

[313] Q. Liu, R. Xu, C. Yan, L. Han, H. Lei, R. Ruan, X. Zhang, Fast hydrothermal co-liquefaction of corn stover and cow manure for biocrude and hydrochar production, Bioresour. Technol. 340 (2021) 125630. https://doi.org/10.1016/j.biortech.2021.125630.

[314] H.A. Baloch, S. Nizamuddin, M.T.H. Siddiqui, N.M. Mubarak, S. Mazari, G.J. Griffin, M.P. Srinivasan, Co-liquefaction of synthetic polyethylene and polyethylene bags with sugarcane bagasse under supercritical conditions: A comparative study, Renew. Energy. 162 (2020) 2397–2407. https://doi.org/10.1016/j.renene.2020.10.008.

[315] K.K. Jaiswal, V. Kumar, M.S. Vlaskin, M. Nanda, M. Verma, W. Ahmad, H. Kim, Hydropyrolysis of freshwater macroalgal bloom for bio-oil and biochar production: Kinetics and isotherm for removal of multiple heavy metals, Environ. Technol. Innov. 22 (2021) 101440. https://doi.org/10.1016/j.eti.2021.101440.

RESEARCH OUTPUT

LIST OF PUBLICATIONS

Published

1. **S. Acharya** and N. Kishore, "*Citrus limetta* fruit waste management by liquefaction using hydrogen-donor solvent," *RSC Adv.*, **12**, 32708–32721, 2022. http://xlink.rsc.org/?DOI=D2RA06085J
2. **S. Acharya** and N. Kishore, "Solvothermal co-liquefaction of wastes from *Citrus limetta* fruit processing," *J. Chem. Technol. Biotechnol.*, **98**, 1114-1124, 2023. https://doi.org/10.1002/jctb.7316
3. **S. Acharya** and N. Kishore, "Investigation of the Synergistic Effects of Temperature & Feedstock-to-Solvent Ratio on Co-liquefaction of *Citrus limetta* Pulp & Peel Wastes," *Biomass Conv. Bioref.*, 1-14, 2023. https://link.springer.com/10.1007/s13399-023-05181-x

Under Review

4. **S. Acharya** and N. Kishore, "Influence of Reaction Parameters on Biofuels Derived from Solvothermal Liquefaction of *Citrus limetta* Fruit Wastes", *Biomass Bioenergy*.

LIST OF CONFERENCES ATTENDED

1. **S. Acharya** and N. Kishore, "Liquefaction of *Citrus limetta* fruit wastes in hydrogen-donor solvent for sustainable biofuels generation," for participation and oral presentation in the session "Biomass Utilization and Bioenergy" of the International Conference on "Sustainability in chemical processes through Digitalization, Artificial Intelligence and Green Chemistry", CHEMCON 2022, during December 27-30, 2022, at Harcourt Butler Technical University, Kanpur, Uttar Pradesh, India.
2. **S. Acharya** and N. Kishore, "Investigation of the effects of temperature variation on liquefaction of citrus fruit wastes," for participation and poster presentation in the session "Environmental Remediation and Waste Water Management", ChEmference 2023, during September 30-October 2, 2023, at Department of Chemical Engineering, BITS Pilani, K.K. Birla Goa campus, Goa, India.

ANNEXURE

Table A1 Yield of biocrude from liquefaction of *Citrus limetta* pulp (CLPU) and peel (CLPE) at variable biomass-to-solvent ratios.

Biomass feedstock	Biomass-to-solvent ratio	Biocrude yield, wt. %	Standard Deviation	Biomass feedstock	Biocrude yield, wt. %	Standard Deviation
CLPU	1:2	6.25	0.57	CLPE	9.20	1.00
CLPU	1:3	6.34	0.58	CLPE	11.28	0.79
CLPU	1:4	7.88	2.23	CLPE	12.50	3.87

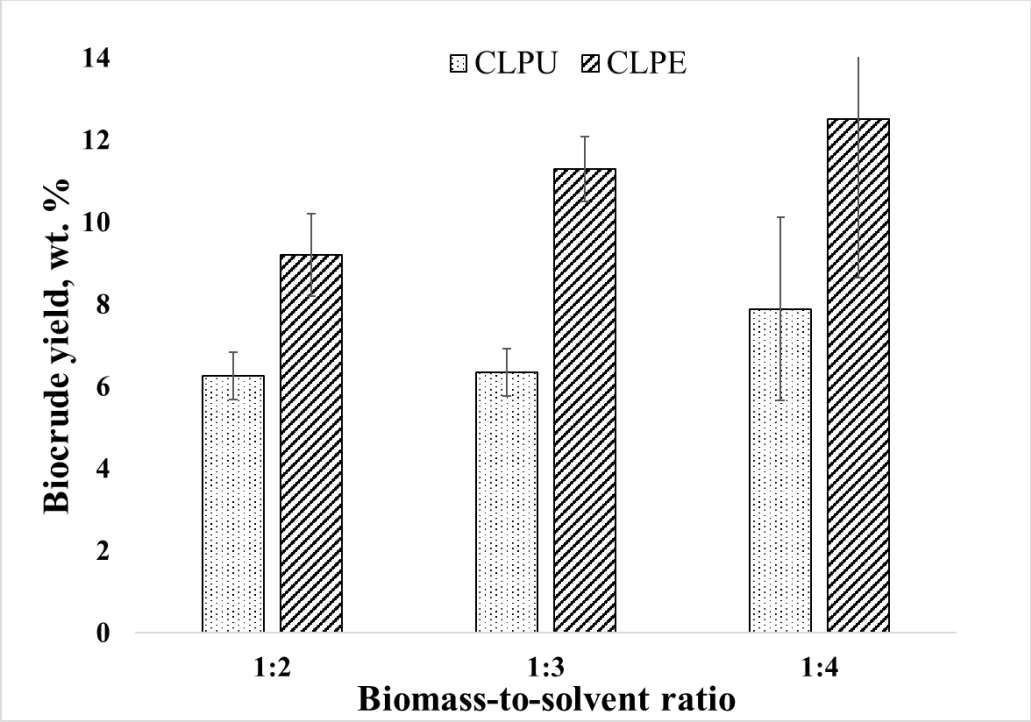

Figure A1 Yield of biocrude from liquefaction of *Citrus limetta* pulp (CLPU) and peel (CLPE) at variable biomass-to-solvent ratios.

Table A2 Yield of biocrude from co-liquefaction of *Citrus limetta* peel (CLPE) and pulp (CLPU) at variable biomass-to-solvent ratios.

Biomass feedstock	Biomass-to-solvent ratio	Biocrude yield, wt. %	Standard Deviation
CLPE-PU	1:2	8.47	1.54
CLPE-PU	1:3	9.05	1.21
CLPE-PU	1:4	11.25	0.27

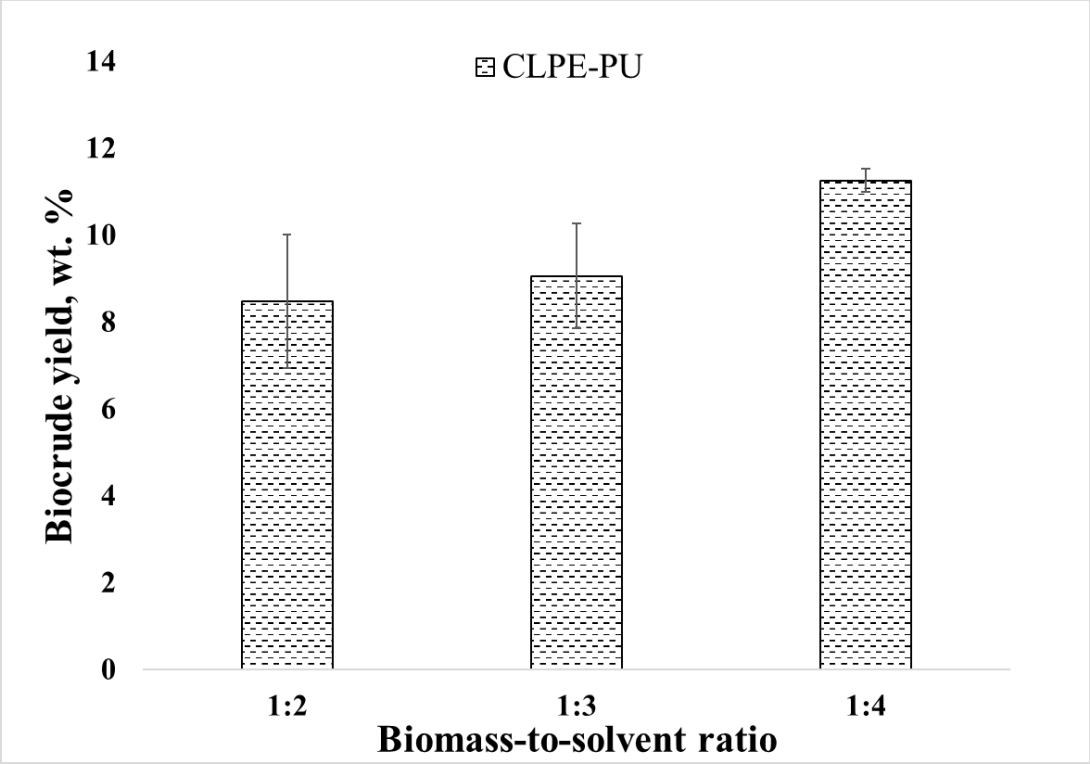

Figure A2 Yield of biocrude from co-liquefaction of *Citrus limetta* peel (CLPE) and pulp (CLPU) at variable biomass-to-solvent ratios.

Table A3 HHV of biocrude and biochar from liquefaction of *Citrus limetta* pulp (CLPU) at variable biomass-to-solvent ratios.

Biomass feedstock	Biomass-to-solvent ratio	HHV of biocrude, $MJkg^{-1}$	Standard Deviation	HHV of biochar, $MJkg^{-1}$	Standard Deviation
CLPU	1:2	26.36	1.49	16.98	0.71
CLPU	1:3	26.7	3.81	16.46	0.65
CLPU	1:4	26.76	1.06	16	0.44

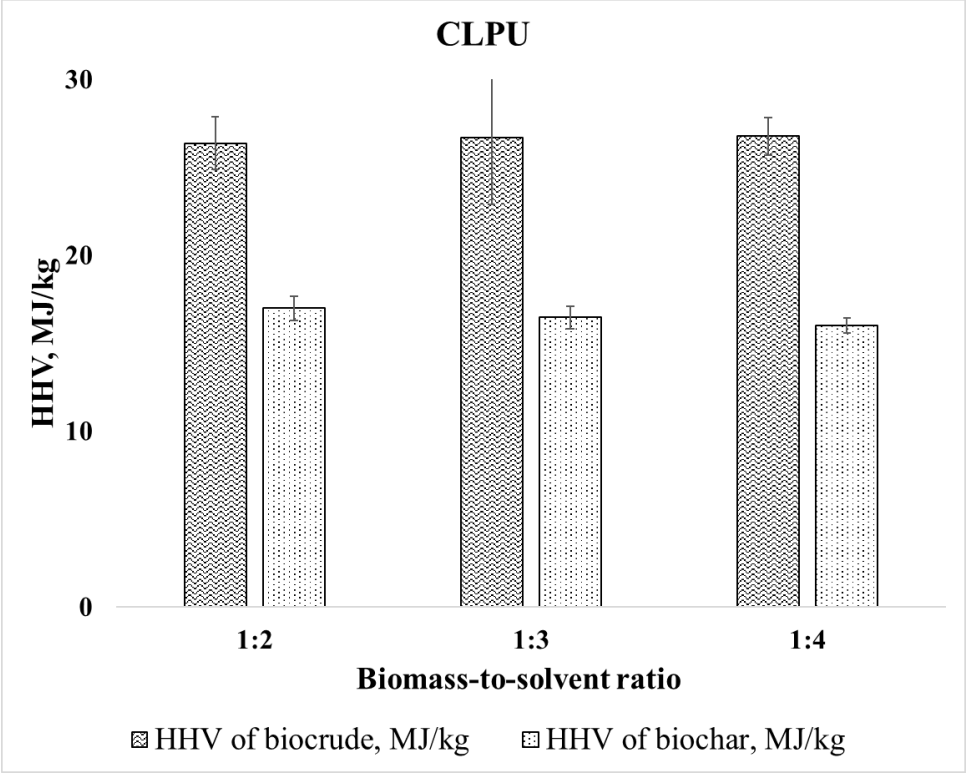

Figure A3 HHV of biocrude and biochar from liquefaction of *Citrus limetta* pulp (CLPU) at variable biomass-to-solvent ratios.

Table A4 HHV of biocrude and biochar from liquefaction of *Citrus limetta* peel (CLPE) at variable biomass-to-solvent ratios.

Biomass feedstock	Biomass-to-solvent ratio	HHV of biocrude, $MJkg^{-1}$	Standard Deviation	HHV of biochar, $MJkg^{-1}$	Standard Deviation
CLPE	1:2	24.91	1.51	14.94	1.54
CLPE	1:3	24.2	1.45	15.55	1.62
CLPE	1:4	23.7	1.62	16.5	0.36

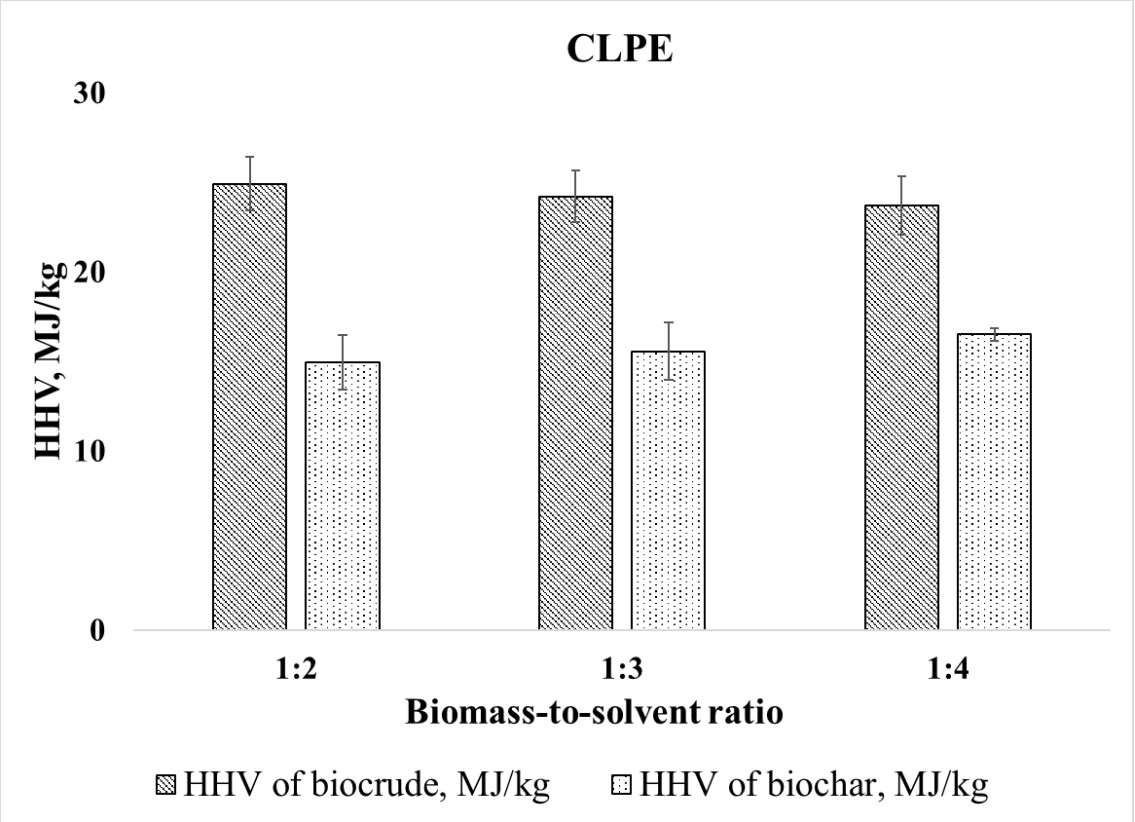

Figure A4 HHV of biocrude and biochar from liquefaction of *Citrus limetta* peel (CLPE) at variable biomass-to-solvent ratios.

Table A5 HHV of biocrude and biochar from co-liquefaction of *Citrus limetta* peel (CLPE) and pulp (CLPU) at variable biomass-to-solvent ratios.

Biomass feedstock	Biomass-to-solvent ratio	HHV of biocrude, $MJkg^{-1}$	Standard Deviation	HHV of biochar, $MJkg^{-1}$	Standard Deviation
CLPE-PU	1:2	23.64	0.44	15.09	0.91
CLPE-PU	1:3	25.72	1.48	16.11	0.77
CLPE-PU	1:4	25	0.78	16.6	1.22

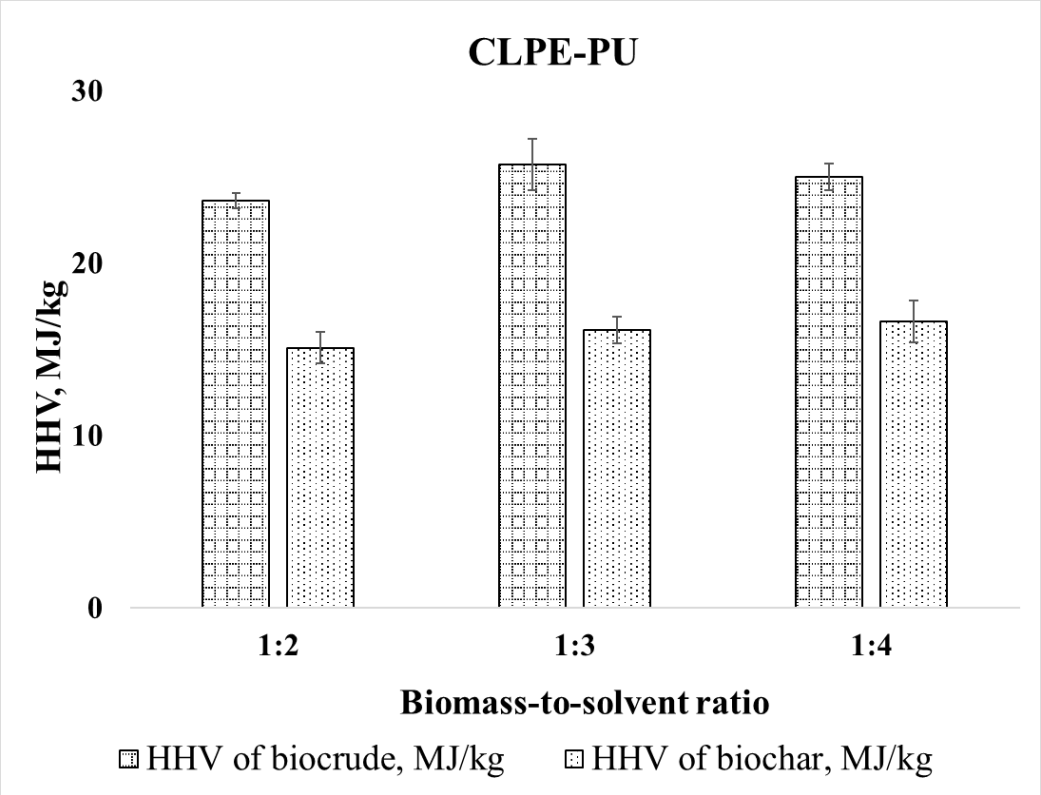

Figure A5 HHV of biocrude and biochar from co-liquefaction of *Citrus limetta* peel (CLPE) and pulp (CLPU) at variable biomass-to-solvent ratios.